International Energy Agency

Long-Term Performance of Super-Insulating Materials in Building Components and Systems

Energy in Building and Communities Programme

03 January 2020

Andreas Holm, Christoph Sprengard (Editors)

EBC is a programme of the International Energy Agency (IEA)

International Energy Agency, EBC Annex 65

Long-Term Performance of Super-Insulating Materials in Building Components and Systems

Report of Subtask:
Scientific Information for Standardization Bodies dealing with Hygro-Thermo-Mechanical Properties and Ageing

03 January 2020

Editors:

Andreas Holm,
Forschungsinstitut für Wärmeschutz e. V. München
FIW München
Lochhamer Schlag 4
82166 Gräfelfing / Germany

http://www.fiw-muenchen.de

holm@fiw-muenchen.de

Christoph Sprengard,
Forschungsinstitut für Wärmeschutz e. V. München
FIW München
Lochhamer Schlag 4
82166 Gräfelfing / Germany

http://www.fiw-muenchen.de

sprengard@fiw-muenchen.de

Chapter 1:

Authors:

Christoph Sprengard, FIW München, Germany
Sebastian Treml, FIW München, Germany

Chapter 2:

Authors:

Sebastian Treml, FIW München, Germany
Christoph Sprengard, FIW München, Germany
Alice Lorenzati, Politecnico di Torino - iNRiM - Instituto Nazionale di Ricerca Metrologica, Italy
Chiara Cucchi, Politecnico di Torino - Dipartimento Energia – DENERG, Italy

Chapter 3:

Authors:

Sebastian Treml, FIW München, Germany
Alice Lorenzati, Politecnico di Torino - iNRiM - Instituto Nazionale di Ricerca Metrologica, Italy
Chiara Cucchi, Politecnico di Torino - Dipartimento Energia – DENERG, Italy
Christoph Sprengard, FIW München, Germany

With contributions from:

Chalmers University of Technology, Sweden
CRMgroup, Belgium
Centre Scientifique et Technique du Bâtiment (CSTB), France
Deutsches Zentrum für Luft- und Raumfahrt (DLR), Germany
Électricité de France SA (EDF), France
Eidgenössische Materialprüfungs- und Forschungsanstalt (EMPA), Switzerland
Evonik Industries, Germany
Forschungsinstitut für Wärmeschutz e. V. München (FIW)
Hanita Coatings, Israel
Isover Saint Gobain, France
Kongju National University, South Korea

KTH Royal Institute of Technology, Sweden

NTUA – National Technical University of Athens, Greece

Politecnico di Torino – Dipartimento Energia – DENERG, Italy

iNRiM – Instituto Nazionale di Ricerca Metrologicam, Italy

Recticel Insulation, Belgium

Ryerson University, Canada

Fujian Super Tech Advanced Material Co., Ltd, China

University of Perugia, Italiy

University of Victoria, Canada

Chapter 4:

Authors:

Esra Kucukpinar, IVV, Germany

Oliver Miesbauer, IVV, Germany

Yoash Carmi, Hanita Coatings, Israel

Antoine Batard, EDF, France

Bernard Yrieux, EDF, France

Chapter 5:

Authors:

Esra Kucukpinar, IVV, Germany

Oliver Miesbauer, IVV, Germany

Antoine Batard, EDF, France

Bernard Yrieux, EDF, France

Sebastian Treml, FIW München, Germany

Chapter 6:

Authors:

Sebastian Treml, FIW München, Germany

Alice Lorenzati, Politecnico di Torino - iNRiM - Instituto Nazionale di Ricerca Metrologica, Italy

Chiara Cucchi, Politecnico di Torino - Dipartimento Energia – DENERG, Italy

Chapter 7:

Authors:

Sebastian Treml, FIW München, Germany

Alice Lorenzati, Politecnico di Torino - iNRiM - Instituto Nazionale di Ricerca Metrologica, Italy

Chiara Cucchi, Politecnico di Torino - Dipartimento Energia – DENERG, Italy

Lukas Berger, FIW München, Germany

External Reviewers:

Stanford Harrison: Australia

Takao Sawachi: Japan

Participating countries in EBC:

Australia, Austria, Belgium, Canada, P.R. China, Czech Republic, Denmark, Finland, France, Germany, Greece, Ireland, Italy, Japan, Republic of Korea, the Netherlands, New Zealand, Norway, Poland, Portugal, Spain, Sweden, Switzerland, Turkey, United Kingdom and the United States of America.

Additional copies of this report may be obtained from:

www.iea-ebc.org

essu@iea-ebc.org

Preface

The International Energy Agency

The International Energy Agency (IEA) was established in 1974 within the framework of the Organisation for Economic Co-operation and Development (OECD) to implement an international energy programme. A basic aim of the IEA is to foster international co-operation among the 28 IEA participating countries and to increase energy security through energy research, development and demonstration in the fields of technologies for energy efficiency and renewable energy sources.

The IEA Energy in Buildings and Communities Programme

The IEA co-ordinates research and development in a number of areas related to energy. The mission of the Energy in Buildings and Communities (EBC) Programme is to develop and facilitate the integration of technologies and processes for energy efficiency and conservation into healthy, low emission, and sustainable buildings and communities, through innovation and research. (Until March 2013, the IEA-EBC Programme was known as the Energy in Buildings and Community Systems Programme, ECBCS.)

The research and development strategies of the IEA-EBC Programme are derived from research drivers, national programmes within IEA countries, and the IEA Future Buildings Forum Think Tank Workshops. The research and development (R&D) strategies of IEA-EBC aim to exploit technological opportunities to save energy in the buildings sector, and to remove technical obstacles to market penetration of new energy efficient technologies. The R&D strategies apply to residential, commercial, office buildings and community systems, and will impact the building industry in five focus areas for R&D activities:
– Integrated planning and building design
– Building energy systems
– Building envelope
– Community scale methods
– Real building energy use

The Executive Committee

Overall control of the IEA-EBC Programme is maintained by an Executive Committee, which not only monitors existing projects, but also identifies new strategic areas in which collaborative efforts may be beneficial. As the Programme is based on a contract with the IEA, the projects are legally established as Annexes to the IEA-EBC Implementing Agreement. At the present time, the following projects have been initiated by the IEA-EBC Executive Committee, with completed projects identified by (*):
Annex 1: Load Energy Determination of Buildings (*)
Annex 2: Ekistics and Advanced Community Energy Systems (*)
Annex 3: Energy Conservation in Residential Buildings (*)
Annex 4: Glasgow Commercial Building Monitoring (*)
Annex 5: Air Infiltration and Ventilation Centre
Annex 6: Energy Systems and Design of Communities (*)
Annex 7: Local Government Energy Planning (*)
Annex 8: Inhabitants Behaviour with Regard to Ventilation (*)
Annex 9: Minimum Ventilation Rates (*)
Annex 10: Building HVAC System Simulation (*)
Annex 11: Energy Auditing (*)
Annex 12: Windows and Fenestration (*)
Annex 13: Energy Management in Hospitals (*)
Annex 14: Condensation and Energy (*)
Annex 15: Energy Efficiency in Schools (*)

Annex 16: BEMS 1- User Interfaces and System Integration (*)
Annex 17: BEMS 2- Evaluation and Emulation Techniques (*)
Annex 18: Demand Controlled Ventilation Systems (*)
Annex 19: Low Slope Roof Systems (*)
Annex 20: Air Flow Patterns within Buildings (*)
Annex 21: Thermal Modelling (*)
Annex 22: Energy Efficient Communities (*)
Annex 23: Multi Zone Air Flow Modelling (COMIS) (*)
Annex 24: Heat, Air and Moisture Transfer in Envelopes (*)
Annex 25: Real time HVAC Simulation (*)
Annex 26: Energy Efficient Ventilation of Large Enclosures (*)
Annex 27: Evaluation and Demonstration of Domestic Ventilation Systems (*)
Annex 28: Low Energy Cooling Systems (*)
Annex 29: Daylight in Buildings (*)
Annex 30: Bringing Simulation to Application (*)
Annex 31: Energy-Related Environmental Impact of Buildings (*)
Annex 32: Integral Building Envelope Performance Assessment (*)
Annex 33: Advanced Local Energy Planning (*)
Annex 34: Computer-Aided Evaluation of HVAC System Performance (*)
Annex 35: Design of Energy Efficient Hybrid Ventilation (HYBVENT) (*)
Annex 36: Retrofitting of Educational Buildings (*)
Annex 37: Low Exergy Systems for Heating and Cooling of Buildings (LowEx) (*)
Annex 38: Solar Sustainable Housing (*)
Annex 39: High Performance Thermal Insulation Systems (*)
Annex 40: Building Commissioning to Improve Energy Performance (*)
Annex 41: Whole Building Heat, Air and Moisture Response (MOIST-ENG) (*)
Annex 42: The Simulation of Building-Integrated Fuel Cell and Other Cogeneration Systems (FC+COGEN-SIM) (*)
Annex 43: Testing and Validation of Building Energy Simulation Tools (*)
Annex 44: Integrating Environmentally Responsive Elements in Buildings (*)
Annex 45: Energy Efficient Electric Lighting for Buildings (*)
Annex 46: Holistic Assessment Tool-kit on Energy Efficient Retrofit Measures for Government Buildings (EnERGo) (*)
Annex 47: Cost-Effective Commissioning for Existing and Low Energy Buildings (*)
Annex 48: Heat Pumping and Reversible Air Conditioning (*)
Annex 49: Low Exergy Systems for High Performance Buildings and Communities (*)
Annex 50: Prefabricated Systems for Low Energy Renovation of Residential Buildings (*)
Annex 51: Energy Efficient Communities (*)
Annex 52: Towards Net Zero Energy Solar Buildings (*)
Annex 53: Total Energy Use in Buildings: Analysis & Evaluation Methods (*)
Annex 54: Integration of Micro-Generation & Related Energy Technologies in Buildings (*)
Annex 55: Reliability of Energy Efficient Building Retrofitting - Probability Assessment of Performance & Cost (RAP-RETRO)
Annex 56: Cost Effective Energy & CO2 Emissions Optimization in Building Renovation
Annex 57: Evaluation of Embodied Energy & CO2 Equivalent Emissions for Building Construction
Annex 58: Reliable Building Energy Performance Characterisation Based on Full Scale Dynamic Measurements
Annex 59: High Temperature Cooling & Low Temperature Heating in Buildings
Annex 60: New Generation Computational Tools for Building & Community Energy Systems
Annex 61: Business and Technical Concepts for Deep Energy Retrofit of Public Buildings
Annex 62: Ventilative Cooling
Annex 63: Implementation of Energy Strategies in Communities
Annex 64: LowEx Communities - Optimised Performance of Energy Supply Systems with Exergy Principles
Annex 65: Long Term Performance of Super-Insulating Materials in Building Components and Systems
Annex 66: Definition and Simulation of Occupant Behavior Simulation
Annex 67: Energy Flexible Buildings

Annex 68: Design and Operational Strategies for High IAQ in Low Energy Buildings
Annex 69: Strategy and Practice of Adaptive Thermal Comfort in Low Energy Buildings

Working Group - Energy Efficiency in Educational Buildings (*)
Working Group - Indicators of Energy Efficiency in Cold Climate Buildings (*)
Working Group - Annex 36 Extension: The Energy Concept Adviser (*)

Summary

This subtask is divided in two actions:

> Action 2A: Materials Assessment & Ageing Procedures (Experiments & Simulation)

> Action 2B: Components & Systems Assessment (Experiments & Simulation)

As their structures and microstructures are completely different, Super-Insulating Materials (SIMs) cannot be compared directly to traditional insulating materials. Worldwide acceptance of these materials will be improved if the hygro-thermal and mechanical properties of SIM can be clearly articulated and reproduced. In particular, nano-structured materials used to manufacture a SIM are characterized by a high specific area (m²/g) and narrow pores (smaller than 1 µm) which make them very sensitive to gas adsorption and condensation, especially in contact with water molecules.

Therefore, methods of characterization must be adapted, or new methods developed to measure the microstructural, hygro-thermal and mechanical properties of these materials and their barrier films.

In parallel, modelling methods to describe heat, moisture and air transfer through nano-structured materials and films will have to be developed (adsorption and desorption models, diffusion models, freeze-thawing …).

Of course, a few methods will be common to all SIMs, but due to their structural differences some specific modelling methods have to be developed.

SIMs can offer considerable advantages (low thickness, low Uvalue) ; however potential drawback effects should be considered in the planning process in order to optimise the development of these extraordinary properties (very low thermal conductivity) and to prevent negative publicity which could be detrimental to this sector of emerging products. This is why ageing tests will be set according to realistic conditions (temperature, moisture, pressure, load …) as set out in SubTask 3A. One objective of artificial ageing is to understand potential degradation processes that could occur. The durability of hydrophobic treatment is one of these processes and will also be subject to discussion and investigation.

At the component scale, additional characterizations are needed as panels or rolls are sold by manufacturers. In particular, thermal bridges will be carefully investigated, as the extraordinary thermal performance of SIMs are sensitive to the influence of thermal bridges.

Table of contents

Abbreviations

Table 1:   List of frequently used abbreviations

Abbreviations	Meaning
A	Inorganic layer
AI	Aluminium
APM	Advanced porous material
ASTM	American Society for Testing and Materials International, an international standards organization
ATR	Air transmission rate
CEN	European Committee for Standardization (Comité Européen de Normalisation)
COP	Centre of panel
DHW	Domestic hot water
DIN	German Institute for Standardization (Deutsches Institute für Normung)
EE	Embodied Energy
EN	European Norm (european standard)
EOTA	European Organisation for Technical Approvals
EPBD	Energy Performance of Buildings Directive of the European Union
EPS	Expanded polystyrene
ETICS	External thermal insulation compound system
FEM	Finite element method
FG	Fibreglass
FPC	Factory production control
GHP	Guarded hot plate
GRP	Glass reinforced plastic
GUM	Guide to uncertainty of measurement
HFM	Heat flow meter
IEA-EBC	Energy in Buildings and Communities Programme of the International
ISO	International Organization for Standardization
Lab	Laboratory
LCA	Life cycle Assessment
LCI	Life cycle Impact
LCIA	Life cycle impact analysis
LDPE	Linear low density polystyrene
ME	Measurement equipment
MP	Measurement point
NZEB	Net zero energy building or net zero emissions building
OP	Operator
λ	Thermal Conductivity in W/(m K)
P	Polymeric layer
PE	Polyethylene

Abbreviations	Meaning
PET	Polyethylene terephthalate
PETM1F	Polyethylene terephthalate films metallized on one face
PU	Polyurethane
RH	Relative humidity
SIM	Super Insulating Material
ST 1	Annex 65 Subtask 1: State of the Art on Materials & Components - Case Studies
ST 2	Annex 65 Subtask 2: Characterisation of materials & components - Laboratory Scale
ST 3	Annex 65 Subtask 3: Practical Applications – Retrofitting at the Building
ST 4	Annex 65 Subtask 4: Sustainability – LCC, LCA, EE – Risk & Benefit
UEATc	Union Européenne pour l'Agrément technique dans la construction a grouping of 18 approval bodies in Europe
U-value	Thermal transmittance of a building element [W/(m²K)]
VIP	Vacuum insulation panel
VOC	Volatile organic compounds
WI	Water intake
WVTR	Water vapour transmission rate
XPS	Extruded polystyrene

Definitions

Definitions of energy performance according to EN 15603:2008 (Official Journal of the EU, 19.4. 2012, p. C 115/9) and econcept (embodied energy):

- **Thermal conductivity:** the amount of heat per unit time per unit area that can be conducted through a plate of unit thickness of a given material, the faces of the plate differing by one unit of temperature.
- **Energy need for heating or cooling:** heat to be delivered to or extracted from a conditioned space to maintain intended temperature conditions during a given period of time.
- **Energy need for domestic hot water:** heat to be delivered to the needed amount of domestic hot water to raise its temperature from the cold network temperature to the prefixed delivery temperature at the delivery point.
- **Energy use for space heating or cooling or domestic hot water:** energy input to the heating, cooling or hot water system to satisfy the energy need for heating, cooling or hot water respectively.
- **Embodied energy:** Embodied energy is the total energy required for the extraction, processing, manufacture and delivery of building materials to the building site.
- **Primary energy:** Energy found in nature that has not been subject to any conversion or transformation process. It is energy contained in raw fuels and other forms of energy received as input. It can be non-renewable or renewable.

Definitions of building life cycle according to ISO 14040:2006:

- **LCA:** Life cycle assessment: compilation and evaluation of the inputs, outputs and the potential environmental impacts of a product system throughout its life cycle.
- **LCIA:** Life cycle impact assessment: phase of life cycle assessment aimed at understanding and evaluating the magnitude and significance of the potential environmental impacts of a product system.

1 Introduction

For all kinds of insulation material the provision of reliable thermal and hygric characteristics by the manufacturer, as the essential basis for construction work and energy efficiency calculations, is the key for a successful market entrance and oconfidence in the product. Conventional insulation materials that have been established for years are well proven in this manner and therefore enjoy more confidence from the market. The reason for this is that the necessary testing methods have been developed over many years and are established in harmonised standards, so that the laboratory work of testing is comparable across a range of nations.

1.1 General context

For a defined application, normally several different material characteristics are essential. Some applications are characterised by advanced hygric stress (e.g. perimeter applications), others require enhanced mechanical stability due to long-time stress loaded situations (e.g. insulation of bottom plates).

As it is not possible to investigate the suitability of all types of testing for SIMs by this programme, the focus of this study is on the determination of thermal properties. The main properties of importance in this context are the determination of:

- thermal conductivity (VIPs and APMs),
- linear thermal bridges (especially for VIPs with different edge design),
- internal pressure (VIPs),
- ageing behaviour (VIPs and APMs).

1.2 Objectives of SUBTASK 2: Characterisation of materials & components - Laboratory scale

The methods of characterisation for SIMs must be adapted and in some cases new methods must be developed. Therefore, an inter-laboratory testing programme was developed to check for differences in thermal conductivity measurement, determination of linear thermal bridge effects, and determination of internal pressure and ageing effects. Each participating laboratory provided a detailed description of the measurement process.

The results have been screened for any differences and double-checked with the description of the measurement process, to work out the critical parts of methodology that have to be considered to provide reproducible testing.

Beside this practical approach, an extended error calculation for both the guarded hot plate (GHP) and heat flow meter (HFM) methods has been developed. Based on this model the general error of thermal conductivity measurement is calculated and compared to the level of confidence for conventional insulation materials.

To carve out the essential parameters that are crucial to achieve a sufficiently low measurement uncertainty for SIMs, a sensitivity analysis was also carried out. By varying the uncertainty of the involved measurands and calculating the combined measurement uncertainty for the thermal conductivity, useful minimum requirements on measurement accuracy for the measurands like temperature difference, thickness, heat-flux resp. heating power, etc. can be defined. This knowledge can be used for future revisions or amendments of the relevant standards to extend the range of thermal conductivity measurements defined therein, so that typical low values for SIMs are met. (EN 12664:2001, EN 12667:2001, ISO 8301:1991, ISO 8302:1991, EN 1946-2:1999, EN 1946-3:1999, ASTM C1045-07(2013), ASTM C518-15, ASTM C1667-15).

SIMs can offer considerable advantages, however potential drawback effects should be known of and considered in the planning process to optimise the development of these extraordinary properties and to prevent negative publicity detrimental to this sector of emerging products. This is why ageing tests will be determined according to realistic conditions (temperature, moisture, pressure, load, etc.) defined in Subtask 3A. One objective of artificial ageing is to understand potential degradation processes that could occur. The durability of the hydrophobic treatment is one of these processes and will also be subject to discussion and investigation.

Artificial ageing is a never-ending story and requires a comparison of natural ageing with the results of artificial ageing for each specific material, if a precise estimation of characteristics as a function of time is required. The general problem is that product development life cycles today are often very dynamic processes with fast changing raw materials, additives and production technologies. After naturally ageing for ten or more years, the products often have changed significantly. Therefore, it is difficult to develop precise life time estimation testing procedures.

Beside the question of representative ageing conditions, the reproducibility of an elevated degradation due to elevated temperature and moisture stress is dependent on the accuracy of the climate chambers in use.

Therefore, an ageing procedure defined in the draft product standard for VIPs is integrated in the inter-laboratory testing programme mentioned before. VIPs are stored in a climate of 50°C and 70% RH for 30, 60, 90 and 180 days. APMs are stored in a climate of 60°C and 80% RH for the same time frame. The chosen ageing conditions reflect the current practice for ageing these materials in the scientific community and are not necessarily designed to represent a time-lapse scenario for any real exposure. The thermal conductivity of VIPs and APMs as well as the internal pressure of VIPs by time is investigated and compared from lab to lab to check for reproducibility again.

Especially VIPs show a time-and-condition-dependent ageing behaviour due to the unavoidable permeation of dry gases and water vapour through the barrier film. Based on the results from a research project funded by the research initiative "Future of Buildings" of the German ministry "Bundesministerium für Umwelt, Naturschutz, Bau und Reaktorsicherheit (BMUB)" service life estimations are calculated for different example-applications in locations all over Europe.

The results will be compared with the ageing behaviour based on the chosen climate conditions of 50°C and 70% RH to check for an adequate time span of artificial ageing.

At the component scale, additional characterisations are needed for general panels or rolls sold by manufacturers. Thermal bridges will be particularly and carefully investigated, as the extraordinary thermal performance of SIMs is sensitive to the influence of thermal bridges.

1.3 Deliverables & target audience

The deliverables from Annex 65 will comprise a well-defined set of documentation, including:

- recommendations on how to characterise SIMs with respect to thermal properties,
- recommendations on how to perform reliable artificial ageing that provides results that are meaningful for lifetime expectations.

The target audience and annex beneficiaries are:

- ISO, CEN, UEAtc, EOTA,
- the building research community,
- the supply chain: material, component and system,
- engineering offices and consultants,
- building contractors with an interest in high performance systems.

The specific deliverables and related subtask are listed in Table 2.

Table 2: The specific deliverables and related subtasks.

Ref.	Deliverables	Related subtask	Target Audience
D1	*State of the Art and Case Studies report*	ST1	Supply Chain
D2	*Scientific Information for Standardisation Bodies dealing with Hygro-Thermo-Mechanical Properties & Ageing report*	ST2	CEN, ISO, EOTA, UEAtc, Testing laboratories Materials manufacturers
D3	*Guidelines for Design, Installation & Inspection with a special focus on Retrofitting*	ST3	Designers, Engineers, Contractors, Builders
D4	*Report on Sustainability Aspect (LCC, LCA, EE – Risk & Benefit)*	ST4	Engineers & Designers

Table 3:   The foreseen outreach activities with corresponding target groups.

	Outreach Activities	Target Group
01	Internet Site & Annex Newsletter	Building Research Community IEA-EBC program
02	Network of Excellence on Measurement Methods	Building Industry & Research Community
03	International Workshops	Building Industry Stakeholders

2 State of the art

In the following chapter state of the art methods for determination of thermal conductivity, linear thermal bridging, internal pressure measurement of VIP and ageing methods are described.

To ensure consistent reading the methods are described generally followed by individual descriptions of how these measurements are performed in different labs. The results are summarized and recommendations about best practice are given in Chapter 7.

2.1 Methodology for measurement of thermal conductivity

Thermal conductivity is the key property for thermal insulation materials. Therefore, the control of the production process regarding the performance of the produced material is essential. In this manner, factory production control is mandatory in any case, and requires a good knowledge about measurement principles for the engineers as well as for the laboratory staff. In the following the most important measurement principles are explained: more details can be found in the Sub Task (ST 1) Report, Chapter 4.5.

2.1.1 Guarded hot plate - GHP

The reference method with highest accuracy for determining thermal resistance and thermal conductivity results of building and insulating materials is the guarded hot plate measurement (GHP). The measurement is carried out by measuring the energy consumption of a hot plate, when using it to apply a defined temperature gradient to a specimen.

The method requires plane and plate-shaped specimens which are installed between heating and cooling plates. The installation is thermally decoupled to avoid outward heat flows perpendicular to the heat flow to be measured. This is achieved by an insulating guard ring, surrounding the installation with a small gap and temperature controls that zero out any differences in temperature between the specimen and the guard ring. When reaching a stationary temperature state, the heat flow becomes constant. At this point, the temperature gradient and the heat flow can be used to calculate the equivalent thermal conductivity of the specimen directly from thermal resistance using the thickness of the specimen.

The duration of the test is mainly dependent on the size and the thermal properties of the specimens and ranges between several hours and days (until steady state conditions are sufficiently met).

Compared to a HFM the GHP is more accurate because all necessary values for calculating the thermal conductivity are measured directly. On a laboratory scale the method is described in ISO 8302:1991, EN 1946-2:1999, EN 12667:2001, EN 12664:2001, ASTM C1045-07(2013) and ASTM C177-13.
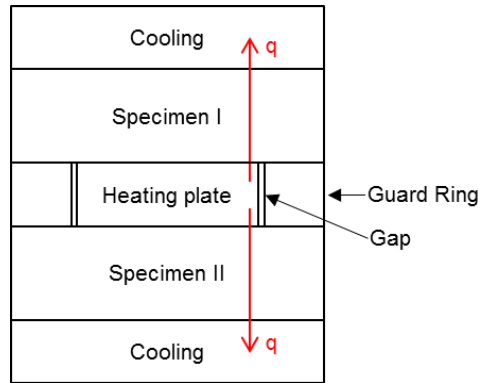
Figure 1:   Schematics of GHP apparatus with symmetric alignment and two specimens. Source: FIW München.

2.1.2   Heat flow meter – HFM

To measure the thermal conductivity of plate-shaped products the heat flow meter (HFM) can also be applied. A grid of thermocouples generates a voltage proportional to the heat flux through the element.
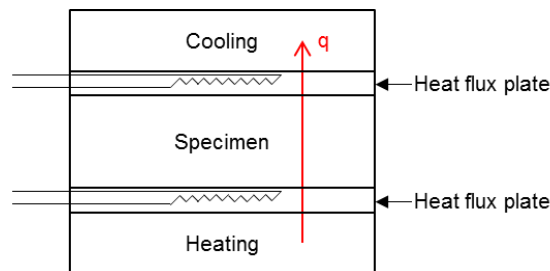
Figure 2:   Schematics of HFM apparatus with symmetric alignment and single specimen. Source: FIW München.

The HFM measurement is suitable for components consisting of homogenous layers perpendicular to the heat flow. In steady state, with a constant temperature gradient through the subject, the equivalent thermal conductivity can be derived directly from heat flux, the thickness of the specimen and the temperatures of the surfaces only (described in ISO 8301:1991, EN 12664:2001, EN 12667:2001, EN 1946-3:1999, ASTM C1045-07(2013), ASTM C518-15 and ASTM C1667-15).

HFMs are in most cases easy to maintain and will reach steady state conditions often faster than guarded hot plate (GHP) apparatus. On the other hand, the measurement uncertainty is connected to the quality of the calibration standard and in general higher than for GHP because the measurement uncertainty of the calibration standard must be factored in.

2.2 Methodology for measurement of linear thermal transmittance (ψ values) at butt joints

Linear thermal bridges occur due to geometrical (e.g. corner of the building) or material induced inhomogeneity (e.g. materials with different thermal conductivity installed side by side). In the case of VIPs, two main things must be considered. In comparison to the centre of panel (COP) measurement, at the edge of the panel the barrier film (plastic and aluminium/metal films) will enhance heat flux and the unavoidable gap between two panels is of influence on the measurement result.

For rigid boards or loose fill material (e.g. APMs) the butt joints can be designed in a more sophisticated way so as to oppress or minimize the effect of linear thermal bridges, but for VIPs this effect is of special interest.

The methodology for measurement of linear thermal bridge effects is always based on a comparative study of the heat flux through an undisturbed material in comparison to the heat flux through a set of samples that are connected. In principle, the investigation can be performed by measurement in the laboratory or by using thermal modelling with numerical simulations (according to ISO 10211:2007).

A detailed study on how to perform measurement of linear thermal bridge effects of VIPs is given in Sprengard [2016]. It is necessary in every case for the measurement of the thermal conductivity of the undisturbed material to use measurement methods as described in Chapter 2.1 of this report. For accuracy reasons, it is preferable that the same apparatus should be used as for the determination of the linear thermal bridge (GHP or HFM).

The very heart of the measurement procedure is the definition of several areas over the sample surfaces that are thermally affected by the increased heat flux through the butt joint (Figure 3).
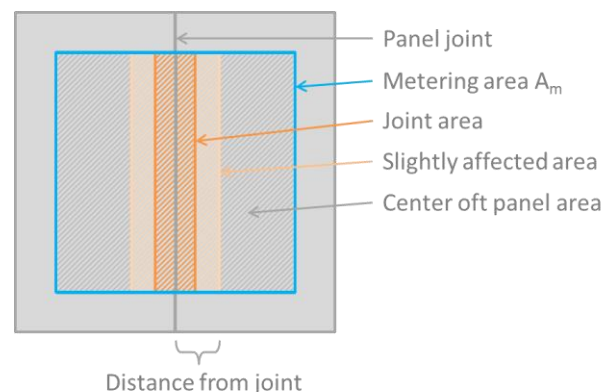
Figure 3: Highly affected (joint area), slightly affected and centre of panel area of two VIPs arranged for determination of ψ values. Source: FIW München.

The temperature distribution in the three areas defined in Figure 3 is measured with thermocouples. It is recommended to use at least two thermocouples for the joint and the slightly affected area and three thermocouples for the COP area (Figure 4).

Thermo-couples	Distance from edge [cm]	Distance from Joint [cm]
1, 2, 3	20	15
4, 5	15	1
6, 7	25	0
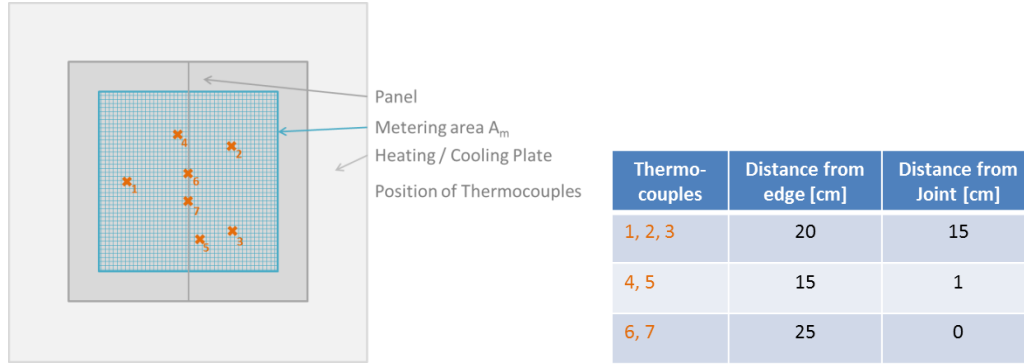
Figure 4: Exemplary distribution of thermocouples for determination of temperature differences in defined areas of the panel surface for determination of ψ values. Source: FIW München.

For calculation of the equivalent thermal conductivity (including linear thermal bridge effects), the measured temperature differences are averaged and area weighted according to equation (1).

$$\Delta T_m = \frac{A_{COP} \cdot \Delta T_{COP} + A_{SA} \cdot \Delta T_{SA} + A_{joint} \cdot \Delta T_{joint}}{A_{COP} + A_{SA} + A_{joint}} \qquad (1)$$

Where

ΔT_m area weighted temperature difference for joint assembly in K,

ΔT_{COP} temperature difference for COP area in K,

ΔT_{SA} temperature difference for slightly affected area in K,

ΔT_{joint} temperature difference for joint area in K,

A_{COP} centre of panel area in m^2,

A_{SA} slightly affected area in m^2,

A_{joint} joint area in m^2.

The equivalent thermal conductivity including the influences of the specific joint assembly ($\lambda_{eq,ja}$) is then calculated using the area weighted temperature difference ($\Delta\theta_m$). To determine the linear thermal transmittance for the joints (ψ), the thermal conductivity in the centre of panel area is subtracted and the values are converted to 1m of joint length (equation (2)).

$$\psi = \frac{A}{d \cdot l_\psi} \cdot (\lambda_{eq,ja} - \lambda_{COP}) \qquad (2)$$

Where

ψ linear thermal transmittance for the joints in the metering area in W/(m K),

A metering area of the GHP or HFM apparatus used for the measurement in m^2,

d thickness of the specimens in m,

l_ψ length of the joints within the metering area in m,

$\lambda_{eq,ja}$ equivalent thermal conductivity including edge effects in W/(m K),

λ_{COP} two specimens mean thermal conductivity for centre of panel in W/(m K).

A different approach can be followed, using commercial measurement apparatus (GHP and HFM) without any external device or thermocouples (Lorenzati et al., 2016). This method represents a more practical way to determine the thermal bridging effects, with less control over the different surface temperatures. In this way the actual overall heat flux through two adjoining VIP panels with a thermal bridge in-between is measured, and the related equivalent thermal conductivity (λ_{eq}), in W/(m K), and thermal bridge linear thermal transmittance (ψ), in W/m K, can be evaluated.

The linear thermal transmittance (ψ) can be assessed accordingly to ISO 10211-1:2007 considering the extra-flux ($\Delta\phi$ in W), or the additional heat transmission, caused by the linear thermal bridge. Because the joints between the panels cause a distortion of the temperature field, the measured heat flux (ϕ_{2D}) will be higher than the heat flux that would cross a single VIP panel alone (ϕ_{1D}): the difference, $\Delta\phi$, between these two heat flux values is the extra-flux (see Figure 5 for more details).

$$\Delta\phi = \phi_{2D} - \phi_{1D} \tag{3}$$

Where

ϕ_{1D} mono-dimensional (centre of panel) specific heat flux in W,

ϕ_{2D} measured bidimensional heat flux due to the thermal bridge in W.

The heat flux ϕ_{1D} is determined starting from the knowledge of the centre of panel thermal conductivity (λ_{COP}) of the VIP specimens. In fact, at steady state, it holds:

$$\phi_{1D} = \frac{\lambda_{COP}}{d} \cdot A_m \cdot \Delta T \tag{4}$$

where

λ_{COP} two specimens mean thermal conductivity for centre of panel in W/m K,
d panel thickness in m,
A_m metering area in m^2,
ΔT temperature difference between the plates in K.

The equation adopted for the calculation of the thermal bridge linear thermal transmittance is:

$$\psi = \frac{1}{s} \cdot \left(\frac{\phi_{2D}}{\Delta T} - 2 \cdot \frac{\lambda_{COP}}{d} \cdot A_{m-1;2} \right) \tag{5}$$

Moreover, the equivalent thermal conductivity of the assembly, λ_{eq}, is defined as:

$$\lambda_{eq} = \frac{\varphi_{2D}}{A_m \cdot \Delta T} \cdot d \tag{6}$$
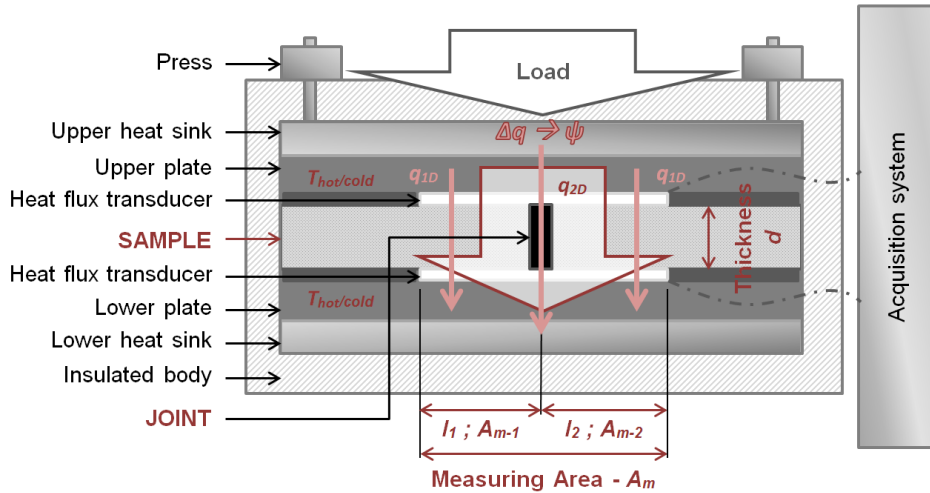
Figure 5: Schematics of HFM apparatus method for the determination of ψ values. Source: Politecnico di Torino.

2.3 Methodology for internal pressure measurement

Probably the most important process parameter in the production of VIPs is the internal pressure of the panels, as this is directly connected to the thermal conductivity of the VIP. In this context the measurement of internal pressure becomes important in several ways. First, a quality production control should cover the determination of internal pressure directly after the production to prove the correct settings of the vacuum-press and check for any significant leakage in the barrier film. Second, the internal pressure is measured to document the evolution of gas permeation due to dry gases and water vapour while ageingthe material.

The accuracy requirement of the result is normally in inverse proportion to the time effort and cost of the equipment necessary to perform the measurement. Therefore, different test methods have been established in recent years that offer a range of performance between fast and easy to maintain test procedures for factory production control (FPC) and scientific requirements for accuracy. The most important methods are presented below.

For small internal pressures in the range of 0.1-100mbar, different measurement gauges are common (Table 4) that vary with respect to the accuracy of measurement.

Table 4: Different principles of pressure measurement.

Measurement principle	Measuring range
Piezo-membrane-vacuum-gauge	$10^{-1} - 10^{3}$mbar
Capacitance-membrane-vacuum-gauge	$10^{-5} - 10^{3}$mbar
Pirani-vacuum-gauge (hot-wire method)	$10^{-4} - 10^{-1}$mbar
Spinning Rotor Gauge	$10^{-7} - 10^{-3}$mbar

A direct measurement of internal pressure with one of the mentioned methods would require a connection between the core material of the VIP and the measurement gauge. As this is only possible for scientific measurements in the lab, different methodology for determination of internal pressure on normal VIPs were developed, based on the foil lift-off method and indirect measurement of dependent physical characteristics like thermal conductivity (Table 5).

Table 5: Internal pressure measurement on VIP.

Measurement principle	Accuracy
Vacuum chamber (foil lift-off method)	medium – high
Vacuum suction-bell (foil lift-off method)	medium – high
va-Q-check (indirect measurement)	low – medium
Thermal conductivity (indirect measurement)	low – medium

The accuracy of the measurement varies due to the specific method and as mentioned above, is normally in inverse proportion to the required effort. Methods developed for FPC (e.g. the va-Q-check method) are easy to perform and offer quick results. The

measurement principle is based on the inter-connection between the thermal conductivity of a small piece of fleece installed directly below the barrier film of the VIP that can be determined very quickly, using the special measurement gauge developed by the manufacturer. As the measurement is quick and can be performed automatically directly after production, statistical data evaluation for quality control purposes is easy to derive using this system. On site a quick check of the functionality of the panels can also be performed.

However, for scientific purposes, methods with higher accuracy are required. Therefore, the foil lift-off methods are preferred. The measurement principle is based on the lift-off of the barrier film as soon as the internal pressure of the VIP becomes higher than the surrounding pressure.

In general, two different approaches are common. The panel is placed in a vacuum chamber to evacuate the surrounding atmosphere (vacuum chamber method, Figure 6), or only a limited space over the barrier film is evacuated using a suction bell (suction bell method, Figure 6)
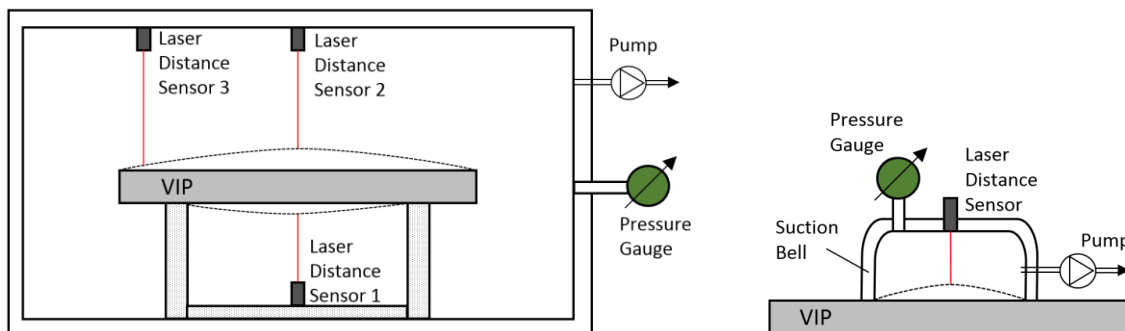
Figure 6:   Principles sketch of vacuum chamber method (left) and suction bell method (right). (Regauer, 2017)

In any case it should be mentioned that the lift-off of the barrier film observed with laser measurement gauges can be influenced by the specific VIP assembly, concerning positioning of the welding and unavoidable kinks in the panel surface as well as from the specific support situation (compare Figure 6, distance sensor 1, 2 and 3). Therefore, differences between measuring from the top of the panel and from the bottom are likely to occur.

The data evaluation can be performed with different methods. Most common is the tangent method, that defines the internal pressure (p_i) of the VIP as the intersection of two tangents defined by linear regression on the curve from the foil displacement (s) as a function from the vacuum chamber pressure ($p_{i,c}$) (Figure 7).
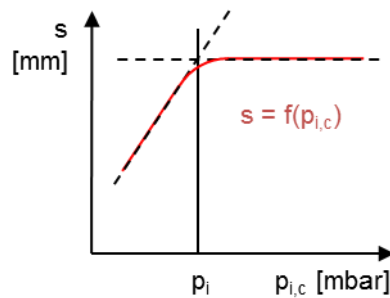
Figure 7: Raw data (red line) of the distance (s) between laser measuring gauge and the VIP surface as a function of the internal pressure of the chamber ($p_{i,c}$) and the tangents to derive the internal pressure of the VIP (p_i). Source: FIW München.

2.4 Methodology for ageing

Ageing of building materials describes the time dependent change of characteristics. For an intended use, minimum requirements regarding material characteristics are normally set that should be met by the material over the full-service life time. As natural ageing requires long term monitoring, or at least the decomposition of building elements after many years to measure characteristics, artificial ageing is applied to speed up the process of degradation.

Therefore, it is essential to evaluate the key parameters that occur in real life and make the conditions severe enough to speed up the degradation process without breaking any threshold value that will trigger physical effects that are not realistic (e.g. for polymers the application of temperatures higher than the softening temperature).

Below, the relevant ageing parameters for VIPs and APMs are introduced.

2.4.1 Ageing parameters

For VIPs the most important ageing parameter is the unavoidable increase of the internal pressure. Assuming a defect-free panel this characteristic is highly dependent on the temperature and the relative humidity of the specific application. In Germany an ageing condition developed by the Deutsches Institut für Bautechnik (DIBT), the so called DIBT procedure, was applied for years that is based on 7 days of climatic changes between -15°C and +80°C (one temperature cycle per day) followed by 2 times 90 days of storage in elevated temperature at 80°C and ca. 3% RH. According to the actual draft of the product standard for VIPs, the ageing procedure is reduced to 180 days of climatic stress with 50°C and 70% RH to include the effect of water vapour permeation through the envelope that is relevant for applications in the construction sector.

A study on the influence of climatic impact on the internal pressure increase of VIP was performed by Sprengard et al., 2016. This research project focussed on the determination of internal pressure increase as a function of temperature and relative humidity. For both impact factors, an Arrhenius behaviour that describes the reaction

13

rate as a function of the temperature (Sprengard et al., 2016) was observed and used to calculate the pressure increase of VIP under realistic climate conditions that are specific to certain exemplary construction and installation sites.

As the thermal performance of APM is highly dependent on the microstructure, changes of the porous structure are crucial with respect to ageing. Several impact factors can be determined as relevant such as heat, moisture, freezing and thawing but also the adsorption of VOC (volatile organic compounds), dust and settling phenomena for loose filled materials.

Detailed information about the ageing of APM and VIP is included in the Annex65, Sub Task (ST) 1 report Chapter 3.3 for APM and Chapter 4.5.3 for VIP.

2.4.2   Modelling

Modelling can be applied on different scales and oftenrequires simplification to achieve useful results with economical effort. Detailed modelling on the microscale, (e.g. for VIPs) the investigation of defects in the welding zone, or the thermal transport phenomena in APMs with changing porous distributions enables enhanced understanding of potential failure risks and gives the opportunity for material developments by improving production technologies or material.

On the other hand, more generalist models can also be applied; those reflect a higher degree of simplification but enable the researcher to investigate the interdependencies of varying boundary conditions on interesting material characteristics.

In this report, detailed modelling about film barrier permeation (Chapter 5**Erreur ! Source du renvoi introuvable.**), defect zones in VIP envelopes (Chapter 5.1), and different approaches to describe the gas permeation through VIP barrier films and calculate the associated changes in the thermal properties under a broad variety of climatic conditions and constructions (examples for Germany) are shown (Chapter 5.2).

3 Inter-laboratory test programme - VIP and APM

To check the variability of measurements on SIMs and to define potential improvements on the applied methods, an inter-laboratory test programme was developed.

3.1 Principle and approach

The principle of the test programme was the allocation of VIPs and APMs by several manufacturers and the testing of these materials at several laboratories. Each laboratory provided extended information about the individual methodology of measurement. To ensure a uniform data exchange several excel templates were developed to collect the necessary information about the test methods and the obtained values.

It was the purpose of the study to discuss methods and not individual material quality. To encourage the manufacturersto cooperate, confidentiality was ensured by an anonymous material distribution, performed by FIW München.

All in all, 6 different types of VIPs (4 products with fumed silica core and 2 products with fibreglass cores – that represent the two most common core materials for VIP) and 2 different types of APMs (1 loose filled granulate and 1 rigid board) were chosen to be tested.

Tested characteristics were thermal conductivity in the centre of the panel (COP), linear thermal bridge effect represented by ψ-values and internal pressure. The thermal conductivity and the internal pressure were tested both for non-aged values (values of the panel not subjected to an ageing procedure) and after different steps of ageing, while the ψ-values were tested only for the non-aged values due to a meaningless result obtained for the ageing steps.

The tests were carried out at 20 different labs (institutes, companies and universities) spread all over the world (Germany, France, Italy, Sweden, Belgium, Switzerland Greece, South Korea) that agreed to participate in the project. Due to the partial presence of specific laboratory equipment and so as not to exceed effort, not all tests were carried out at all laboratories.

3.2 Common exercise

Below, the necessary information about the material and the methods used in the inter-laboratory test programme are explained.

3.2.1 Material

Table 6 shows the material included in the test. As one can see, the material VIP 2 is not represented. This is because this material was not supplied by the manufacturer. Therefore, the number of VIPs included in the test was reduced to 5 VIPs. Due to consistency in the statistics and documents received from the labs, the numbering of the VIPs remains from VIP 1 – VIP 6. To ensure the confidentiality of the participants, the name of the lab that performed the measurement is not indicated.

Table 6:   SIMs included in the test and distribution of materials on the participating labs.

Laboratory	Material							
	APM1	APM2	VIP1	VIP2	VIP3	VIP4	VIP5	VIP6
1	X	X						
2					X			
3		X						
4		X	X				X	
5	X				X			
6		X	X					
7		X						
8	X	X	X		X	X	X	X
9			X				X	
10						X	X	
11							X	X
12						X		
13					X			X
14						X		
15		X	X			X		
16		X						
17		X						
18								X
19	X	X						
20					X			

There were many laboratories testing APM 2 with ten different labs participating. Except for VIP 6, all the VIPs in the test were tested at 5 different labs. A comparison of measurement results carried out by different labs in one group of materials points to first conclusions about the reproducibility of the measurement.

However, several things should be considered in this context.

First, the variability of measurements describes in principle the influence of the user and equipment whilst taking a measurement in a defined way. Due to variations in equipment, temperature differences, assembling of the samples meanthe measurement method is not identical in each participating lab. These influences may also vary from material to material depending on the simplicity of handling. In this connection uneven, brittle or loose filled material can require more experience in product-handling than rigid, plane and stable building materials like rigid foams or wood-based materials.

Secondly, especially for VIPs, each panel represents an individual piece of material with a specific internal pressure. The material is transported in different ways (shipping, road, etc.) which means that different climatic stresses were induced before the material was measured in the lab. Therefore, the internal pressure may vary from case to case, leading to differences in the thermal conductivity that is not connected to differing test methods but to real differences in thermal conductivity. It is not possible to separate these influences with certainty.

3.2.2 Methods

The methods were assessed according to details in Chapter 2 of this report. As remarked before not all labs were undertaking all types of measurement.

The thermal conductivity in the centre of panel (COP) was measured according to EN 12667:2001 with the guarded hot plate apparatus (GHP) and the heat flow meter apparatus (HFM). The ψ-values were determined by applying the weighted temperature to the heat flow measured in the GHP or HFM respectively. The internal pressure was measured using the lift-off foil method.

3.2.2.1 Thermal conductivity measurement in the COP

The focus of the following explanations is firstly on the handling of the material in the labs. Some of the descriptions by different labs are summarized, some are explained more in detail due to the degree of unique information included.

Loose filled granulate APM

One of the two investigated aerogels is a loose filled granulate that requires a special specimen holder to ensure a proper installation in any kind of apparatus. Some participants used accessories made by the manufacturer of thermal conductivity measurement apparatus; others used a self-made specimen holder made of wooden frames or EPS frames with plastic membranes or very thin metal plates as boundary layers to the heating and cooling plates of the apparatus.
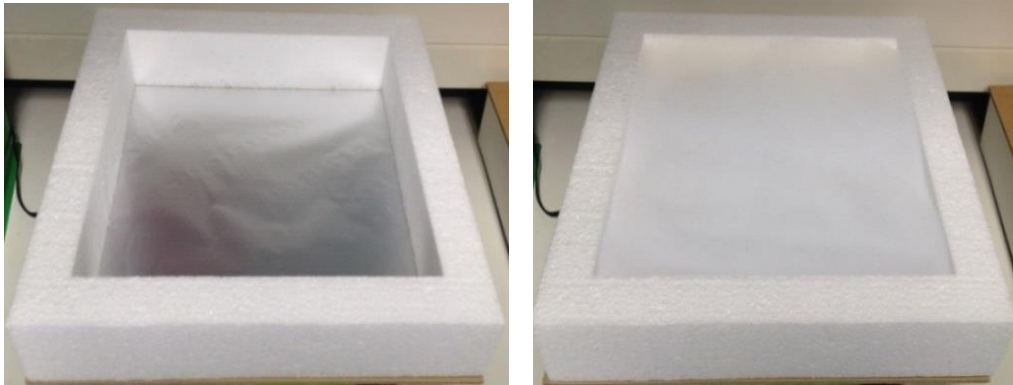
Figure 8:   Specimen holder for loose filled granulate made of EPS frame, provided as accessory from the manufacturer of thermal conductivity apparatus. Source: Deutsches Zentrum für Luft- und Raumfahrt.

Figure 9:   Self-made specimen holder for loose filled granulate made of wooden frame with thin metal plates (thickness of 0.4mm). Source: Università di Perugia.

It is assumed that the metal plates in Figure 9 have negligible thermal resistance. The construction would have ensured good thermal contact with the hot and cold plate of the apparatus. Information about thermal conductivity measurement of loose filled granulate is enclosed in ASTM C687 - 12 ("Standard Practice for Determination of Thermal Resistance of Loose-Fill Building Insulation", which includes granular types such as vermiculite, perlite and pelletized products, comparable to granular aerogels).

Figure 10: Self-made specimen holder for loose filled granulate made of EPS frame; the sample is sealed in a PE bag at ambient pressure. Source: Électricité de France.

Figure 10 shows another self-made specimen holder for loose filled granulate made of EPS. To ensure that the material was properly in place whilst handling the sample and to avoid drying or moistening during measurement the sample was sealed in a PE bag at ambient pressure.

All specimen holders used were designed to fit the specific measurement apparatus with respect to the maximum sample size that can be installed. Therefore, no additional insulation in the area of the guard ring was necessary. The sample sizes therefore varied from 0.25m edge length up to 0.5m in square. Also, the thicknesses varied. Samples with greater dimensions were installed in sample holders with higher normal thickness. Thickness varied from 25mm up to 40mm.

In any case an appropriate pressure must be applied by the measurement apparatus. The specific force is dependent on the size of the apparatus, the raw density installed (if the material tends to creep or undergoes relaxation effects) and the compressibility of the specimen holder. The forces applied by the different labs are between 2N and 265 N.

Rigid board APM

The rigid APM boards in the test were tested with several sample sizes. The variation of sample size is between 0.2 m and 0.6 m in square. The thickness was about 30mm.

Some labs were testing the rigid APM boards with extra insulation at the edge to minimize heat losses through the edge of the material (Figure 11), others only placed the sample inside the apparatus (Figure 12). Some limitations in the sample size were considered due to limited space in the conditioned apparatus for artificial ageing. In any case it seems recommended practice to use the full size of the apparatus, thus it is advisable to use extra insulation e.g. made of compressible insulation wool (mineral fibre, etc.) at the edge.
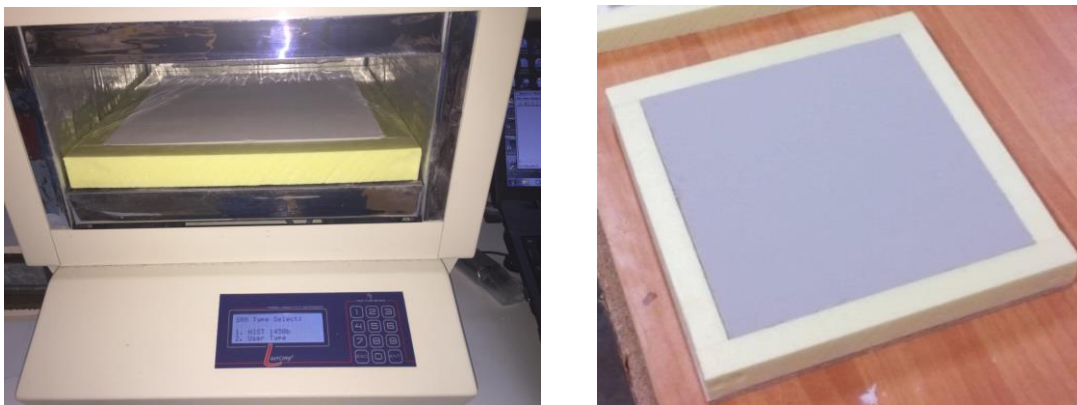
Figure 11: Rigid APM board installed in the heat flow meter apparatus with PU foam frame. Source: Università di Perugia.

Figure 12: Rigid APM board installed in the heat flow meter apparatus without insulation at the edge. Source: Deutsches Zentrum für Luft- und Raumfahrt.

Laboratory staff observed partial damage to the samples when they arrived. Damage on the edges of the boards were documented (Figure 13). As long as the damage was not situated in the measurement area this would not influence the results of thermal conductivity.

Figure 13: Obvious damage to the samples before measurement. Left: source: CRMgroup; right: source: Deutsches Zentrum für Luft- und Raumfahrt.

As with the loose filled granulate, the rigid APM boards were partly wrapped in plastic bags by some labs to prevent water vapour adsorption and drying during the measurement (Figure 14).

Figure 14: Rigid APM board wrapped in a plastic bag to prevent water vapour adsorption during measurement. Source: Politecnico di Torino.

As the material itself enables good thermal contact between the sample and the heating and cooling plates, no additional layers were used.

Vacuum insulation panels

In contrast to the APM materials in the test, the VIPs normally have more uneven surfaces and include welding seams on the surface. For this reason, the thermal contact between the heating and cooling plates and the panels is not ideal.

To guarantee good thermal contact, additional layers are commonly used that can even out the surface. Labs used, for example, polyethylene foam of 2mm thickness, thin silicone mats or cellular rubber for this purpose.

Some used very thick layers of 10mm para rubber sheets (Figure 15). This procedure was proposed to bypass some limits of the apparatus regarding the measurable thermal conductivity, thermal resistance and thickness. With two para rubber layers of 10mm thickness, the equivalent thermal conductivity of the three layers together increase enough to be (theoretically) measured by the device without exceeding the maximum available thickness ($\lambda_{para\,rubber}$ ~ 0.2W/m K). But with this configuration some different problems occurred, the main one due to the lateral heat flux dispersions through the conductive para rubber layers. However, it could be an interesting solution but needs to be deeply investigated per the suggestion in Chapter 7.1.3.

If no external thermo-couples are used to directly measure the temperature difference on the surface of the VIP, the thermal conductivity of the additional layers must be known very accurately to eliminate the influence on the result. The utilization of very thick layers is not recommended, because it influences the heat flux significantly.

Figure 15: Extra layers of 10 mm thick para rubber. Source: iNRiM.

To avoid lateral heat losses during measurement most participants used extra insulation at the edges. In most cases, flexible materials like mineral wool or other fibre-based paddings were used (Figure 16). It seems helpful to use a guard insulation that is slightly thicker than the panel. In doing so, the insulation at the edge is compressed during measurement and ensures a proper insulation without any gaps.

Figure 16: VIP in the heat flow meter apparatus with a guard of mineral wool around the specimen. Source: Centre Scientifique et Technique du Bâtiment.
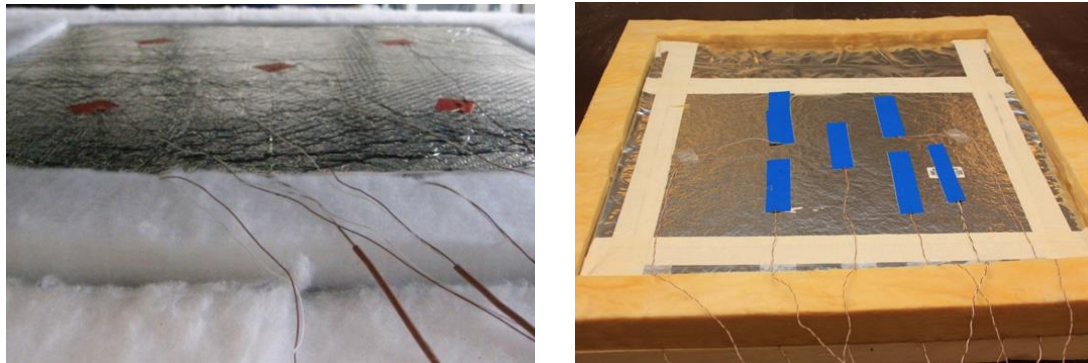
Figure 17: VIP in the heat flow meter apparatus with a guard of fibre based padding around the specimen (left) and mineral wool (right). The padding is thicker than the panel to ensure a proper insulation during measurement. Left: source: FIW München; right: source: KTH Royal Institute of Technology.

In some apparatus, no extra insulation at the edge was used due to lack of space (Figure 18, left) or the apparatus having a fixed installed EPS insulation (Figure 18, right).
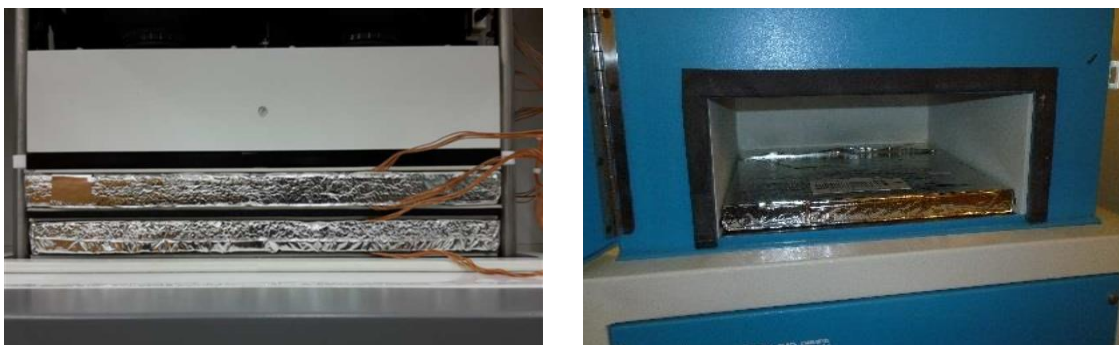
Figure 18: Left: Samples installed without extra insulation at the edge. Source: NTUA – National Technical University of Athens. Right: Sample in an apparatus with fixed installed EPS insulation. Source: Chalmers University of Technology.

Another approach to minimise lateral thermal losses is to control the temperature inside the apparatus. A thermal condition during measurement to the level of the mean

temperature over the height of the sample (e.g. 10°C or 23°C) helps to prevent lateral heat losses. According to the individual temperature of the hot and cold plate (e.g. 5°C and 15°C) a temperature gradient is introduced over the sample height that comes close to the temperature gradient inside the sample.

To ensure proper contact of the VIP panel with the adjacent hot or cold plates a variety of pressure force was applied between 375N and 875N. The reason for deviating pressure force is due to individual setup of the apparatus, which may vary with respect to the dimension of the apparatus, the insulation on the edge and the individual panel that is measured.

The direction of heat flux depends on the apparatus used. It seems that most of the one plate apparatus have the hot plate on top of the sample so that the heat flux is directed downward. The two-plate apparatus will lead to one sample with an upward and one sample with a downward heat flux.

Most of the thermocouples used are of type E (Nickel-Chromium/Constantan). The uncertainty of the measurement performed by the thermocouple depends on the type of material the thermocouple is made from. Detailed explanation of this topic is included in 6.6.2. In many cases thermocouples are installed directly on the heating/cold plate. Thermocouples are also partially attached directly to the sample surface. In this case the thermocouples are fixed using an adhesive tape (Figure 17, right) or they are glued on a thin foil. The use of a foil as support guarantees an exact and repeatable positioning, however it limits the freedom to position the thermocouples (e.g. when a welding seam is crossing the measuring area).

A very important measurement required for testing of thermal conductivity is the correct determination of thickness. Two principles are common. First, the thickness of the panel is measured outside the apparatus by means of a micrometre or other adequate measuring tools. Second, the thickness is determined in the apparatus by measuring the distance between the hot and cold plate using a calliper or adequate spacers or by the interpretation of the recognized traverse path.

Both routines have advantages and disadvantages. The measuring of the thickness outside the apparatus can be performed with a different type of measuring equipment (e.g. calliper, digital gauge and dial gauge) that is of specific accuracy depending on the thickness and individual behaviour of the panel. Also, in many product standards defined parameters e.g. with respect to the pressure force, the pressure area, and the number and distribution of measuring points on the surface are given, and they require the use of different measuring tools for different kinds of panels.

For VIPs it is crucial to guarantee that the panel is flat on the support table during measurement. Many panels show a certain torsion or concavity that must be evened out during measurement. In most cases this is done by applying a certain force by hand on the sample (Figure 19).

Figure 19: Measurement of thickness using a micrometer measuring gauge. The sample is pressed flat by hand that may cause differing pressure on the surface of the panel. Source: Chalmers University of Technology.

Differences are visible according to the dimension of the tip of the measuring tool. Some labs use small round tips (Figure 19), others use measuring plates (Figure 20, left) or even additional rectangular plates to enlarge the area that is in contact with the VIP surface. A larger surface helps to even out small slots due to kinks in the barrier foil. On the other hand, it may be more problematic if uprising kinks occur, and may lead to an overestimation of the thickness.

Figure 20: Measurement gauge for determination of panel thickness using a measuring plate (left) or additional rectangular plates (right). Source: KTH Royal Institute of Technology.

Also, different types of digital slide callipers were used which can only measure the thickness at the edge of the sample.

When the measurement was done by the HFM or GHP apparatus directly, some labs used a reference specimen in a calibration routine to increase the accuracy of measurement. A reference specimen (e.g. with 20-30mm thickness) is installed in the apparatus as substitute to the original VIP but with all the measurement equipment like thermocouples and extra layers to improve the thermal contact. The displayed thickness

of the apparatus is calibrated to the known thickness of the reference specimen. Afterwards the reference specimen is replaced by the VIP and the measured thickness is used for calculation of thermal conductivity.

For determination of panel size, measuring tapes (Figure 21, right) or a digital slide calliper (Figure 21, left) were used. Using a digital slide calliper the measurement values were dependent on the pressure applied by the measuring gauge, which are adjusted by hand and therefore might increase the error.
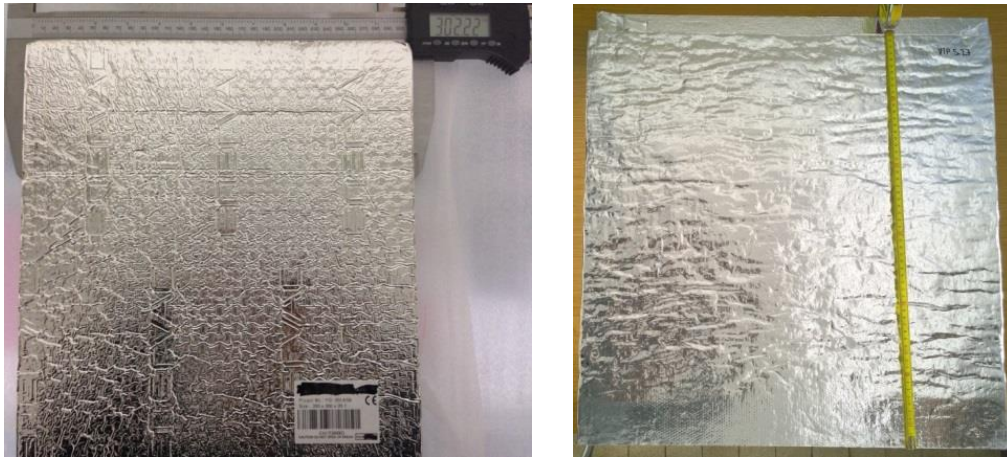
Figure 21: Determination of panel size using a digital slide calliper (left; source: Kongju National University) or a measuring tape (right; source: Centre Scientifique et Technique du Batiment).

The number and distribution of thermocouples varied depending on the size of the measuring area and the equipment used. Most labs used five thermocouples on each side of the panel with a distribution pattern according to Figure 22.
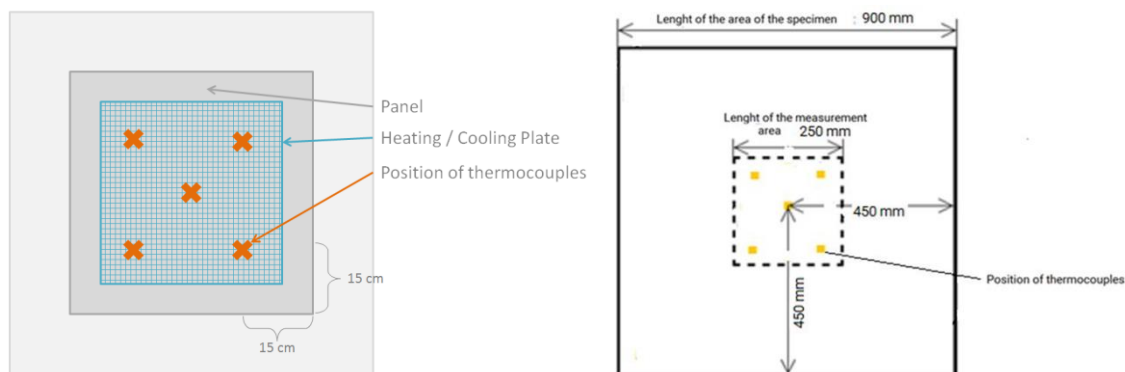
Figure 22: Positioning of thermocouples during measuring. Source: FIW München.

It is important to guarantee good thermal contact of the thermocouple with the surface of the VIP. Due to differing production technologies with varying positions of the sealing seam or glued labels on the surface, it is recommended to use free thermocouples that can be rearranged if necessary to guarantee measurement in the undisturbed zone.

3.2.2.2 Determination of ψ values

The determination of ψ values follows the system for determination of thermal conductivity in the COP with the difference that two panels are installed in the apparatus and the temperature difference is weighted to three different areas that are the joint itself, a slightly affected area around the joint and the undisturbed COP area (see Chapter 2.2).

Figure 23 shows an example of the distribution of thermocouples according to the definitions in Sprengard, 2016. Thermocouples numbered with 2 and 4 are directly positioned on the joint, thermocouples 1 and 5 are in the slightly affected area of 1cm around the joint. The size of the slightly affected area is influenced by the type of barrier foil and the individual production technology, especially due to differing welding at the edges. Thermocouple 3 represents the undisturbed temperature difference in the COP.
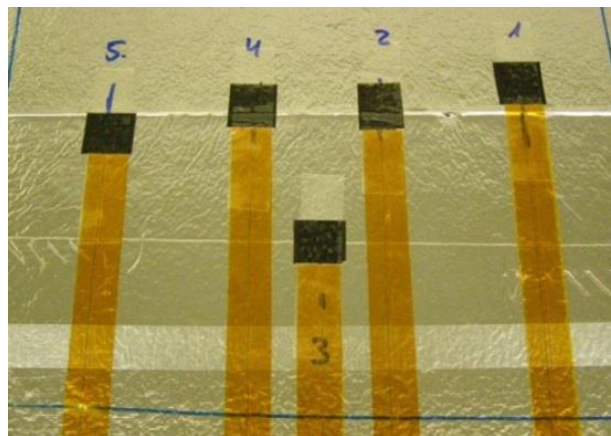
Figure 23: Distribution of thermocouples around the joint during measurement of ψ values. Source: FIW München.

An example installation of four VIP panels in the measurement apparatus is shown in Figure 24. The joint between the panels is visible in detail in the picture on the right. It is obvious that the imperfection at the edges of the VIPs can influence the results.

Figure 24: Setup for measurement of ψ values. Source: NTUA – National Technical University of Athens.

As edges are not necessarily rectangular and often include welding seams it is obvious that the obtained results will in principle show a much higher spread than the results of thermal conductivity in the COP. The individual setup of the panels is of great influence,

especially with no rectangular edges, as the width of the gap is highly influenced by the individual positioning of the panels.

Also, if the panels are pressed together using adhesive tapes or any other additional equipment, the joint becomes smaller and only a loose positioning of the samples occurs.

With a look at the results it became obvious that those obtained on aged panels are not at all representative. In some cases, negative ψ values were determined since the reference values of thermal conductivity for the calculation of ψ values are the values of the COP measurement. An appropriate determination of the ψ values in the aged condition requires measurement of COP values for all VIPs used for the measurement.

Limited space in the apparatus requires the use of small VIPs. It is then not possible (depending on the apparatus) to determine the individual COP value of the aged panels because the specimen size is too low compared to the measuring area. The trial to use COP values obtained on other panels that are aged with the same conditions did not lead to realistic results (as stated before, some negative ψ values were calculated) as the individual ageing behaviour would require a larger control sample size to include a statistical evaluation. More details are explained in Chapter 3.3.2.

3.2.2.3 Determination of internal pressure

The internal pressure of VIPs were assessed using the foil lift-off method performed in a vacuum chamber. The principal approach is described in Chapter 2.3. Differences are due to individual equipment availability at the labs.

Figure 25 shows the equipment set-up for one lab with a laser sensor positioned on the outside of the apparatus (Figure 25, bottom left). To adjust the correct height of the panel surface for the observation of the lift-off, the panel is positioned on an adjustable table that supports the panel from the bottom side (Figure 25, bottom right).
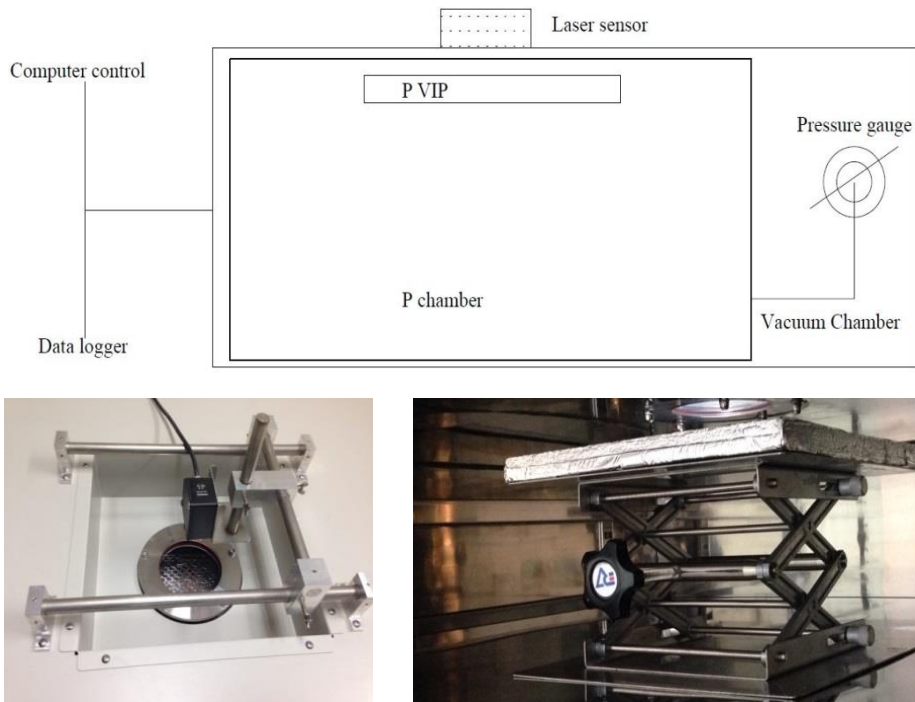
Figure 25: Equipment for determination of internal pressure measurement using the foil lift-off method in a vacuum chamber. Top: principal sketch of the measurement; bottom left: laser measuring device outside the vacuum chamber; bottom right: adjustable bearing support of the VIP inside the vacuum chamber. Source: Kongju National University.

Another approach is to place the laser measurement gauge inside the vacuum chamber. To do so, the equipment must be vacuum proof in general and any deformation of the equipment (e.g. the case of the measurement gauge) due to pressure differences during the evacuation of the chamber has to be avoided (e.g. by drilling a hole in the case or removing a screw, etc.). Figure 26 shows a possible setup with three laser measurement gauges. The VIPs are placed on a rectangular support frame with a side length of 250mm and weighted by such a frame from the top also. In this way, the area of the barrier foil that is free for lift-off is limited, and ensures equal conditions both for small and big panels. In effect this leads to a lift-off behaviour of the foil that is no longer influenced by individual positioning of the welding or the dimension of the panel.

Figure 26: Equipment for determination of internal pressure measurement using the foil lift-off method in a vacuum chamber, laser measurement gauges are placed inside the vacuum chamber, VIPs are placed on a rectangular support with 250mm side length. Source: FIW München.

An example for obtained test data is included in Figure 27. The tangents from both sides of the test data have a point of intersection defining the pressure inside the vacuum chamber that is assumed to be equal to the internal pressure of the VIP.
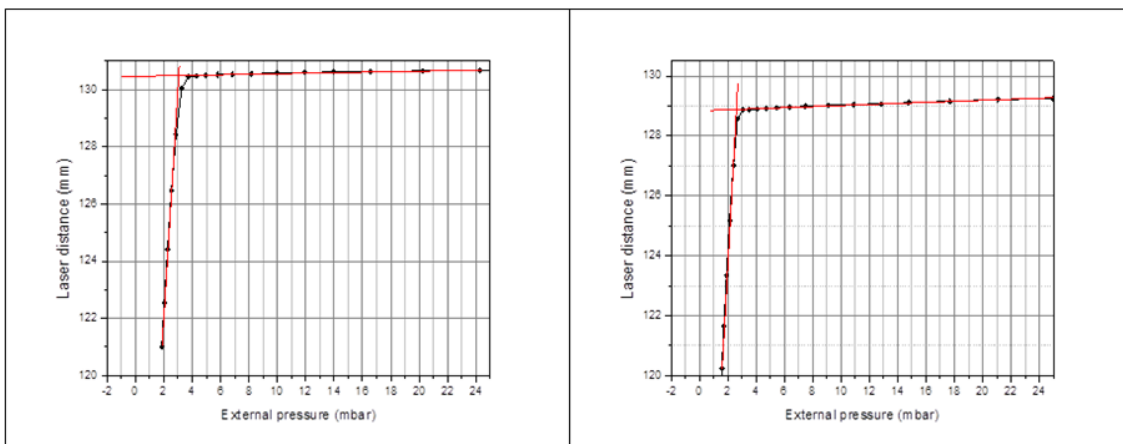
Figure 27: Test data obtained with the vacuum chamber lift-off method, laser distance as a function of the external pressure, the intersection of the red lines (tangents) represent the estimated internal pressure of the VIP. Source: Kongju National University.

3.3 Results and discussion

In the following, the results of thermal conductivity, ψ-values and internal pressure as assessed by the participating laboratories are tabled and discussed.

3.3.1 Thermal conductivity

All in all, nineteen labs participated in the measurement of centre of panel (COP) thermal conductivity. The chapter starts with some general statistics about the equipment used and the temperature conditions for measurement.

3.3.1.1 Equipment used and temperature conditions for measurement

Most participants used a heat flow meter (HFM) single-specimen apparatus, followed by a guarded hot plate (GHP) two-specimen apparatus. GHP single-specimen apparatus and HFM two-specimen apparatus were both used three times. All in all, more HFM apparatus were used than GHP apparatus (Figure 28).
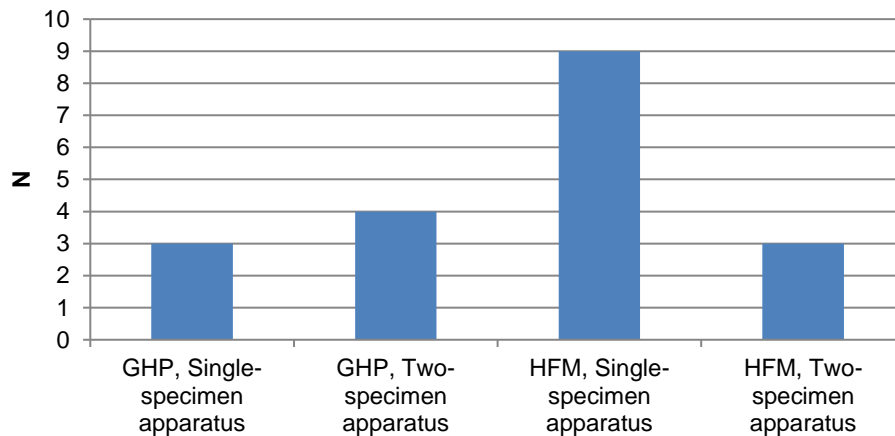
Figure 28: Apparatus for thermal conductivity measurement used by the participating labs (19 labs).

Figure 29 shows the distribution of side length of the measuring area used for the different apparatus. Mean values of side length of the measuring area are around 250-300mm for all kinds of apparatus used. The smallest measurement areas are used in the GHP two-specimen apparatus and HFM single-specimen apparatus with side lengths of 100mm. The biggest measurement areas are recognized for the GHP single-specimen apparatus and HFM two-specimen apparatus reaching up to 500mm square.
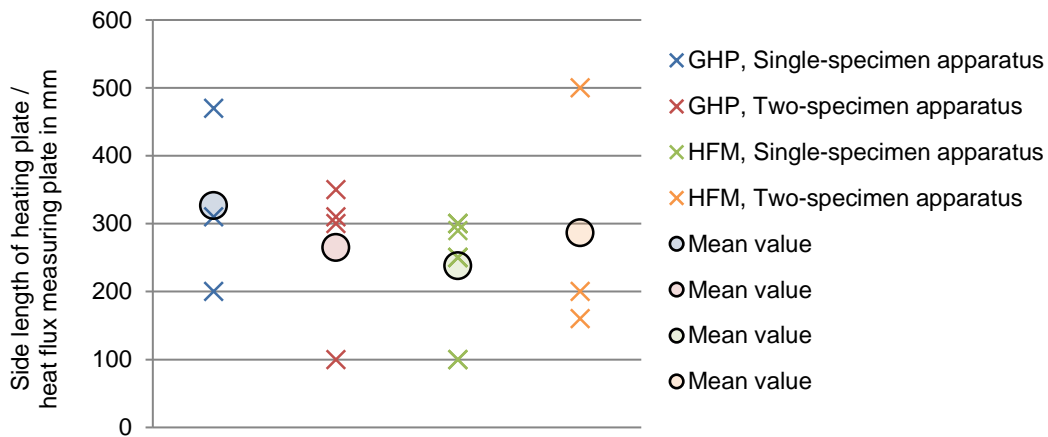
Figure 29: Side length of heating plate / heat flux measuring plate in mm of the apparatus for thermal conductivity measurement distinct to type of apparatus.

In Figure 30 the applied temperature differences for determination of thermal conductivity are summarized. The mean of the temperature difference applied was around 15K. The spreading of the data is in between 10K and 20K. Slightly higher mean values are applied for the GHP two-specimen apparatus, but these differences are not significant with respect to the spreading of the data.
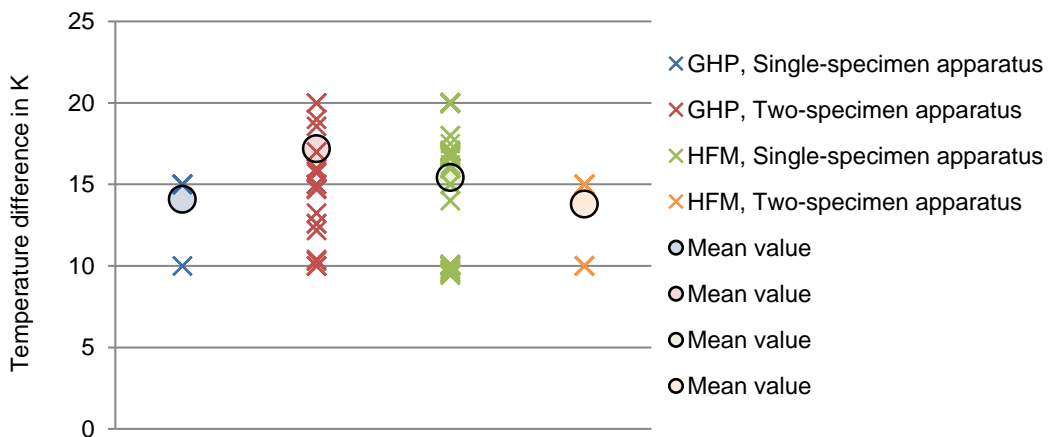
Figure 30: Applied temperature difference for thermal conductivity assessment distinct to type of apparatus.

The agreed mean temperatures for measurement were 10°C and 23°C. These target values were met by most of the participating labs as one can see in Figure 31. One lab provided additional data for 35°C mean temperature and one lab had a deviating mean temperature of 20°C instead of 23°C.

Figure 31: Applied mean temperature for thermal conductivity assessment distinct to type of apparatus.

3.3.1.2 General remarks on data evaluation

In the following section, the assessed data for all materials in the tests are shown with individual charts. One interesting question is whether the spreading of the test data for thermal resistance (R) in (m² K)/W is different from the spreading of test data for thermal conductivity (λ) in W/(m K). For the determination of λ the accuracy of the thickness determination becomes important. As described in the chapter before there are several ways to assess the thickness of VIPs and APMs. Therefore, it is likely that results for thickness determination vary amongst the participating labs, even if they were performed on the same panel.

All results were summarized under the conditions "Non-aged", "Aged 1", "Aged 2" and "Aged 3", representing storage in a certain climate for 30, 90 and 180 days. The agreed climates for APMs are 80°C and 60% RH and 50°C and 70% RH for VIPs. These conditions represent the current practice for artificial ageing of these materials in the scientific community. However, these climates and the distinct time spans were not applied in all cases. In some cases, APMs were also stored in the climate for VIPs, in other cases the time span differs for several days. As the data basis to apply statistics is low in any case it was decided not to distinguish between these cases. If we did, it would be impossible to draw any conclusion, because then most of the measurement would represent individual test combinations.

For each condition a statistic is included below the graphic with the following parameters:

Condition	Non-aged / Aged 1 / Aged 2 / Aged 3,
N_{labs}	number of labs providing data for this step,
N_{meas}	number of measurements for this step,
mdn	median
$mean$	mean value,

s	standard deviation,
V	coefficient of variation in %,
$x_L(N_{meas}; 0.5; 0.9)$	lower limit of a two-sided statistical tolerance range for $p = 0.5$ with a confidence level of 90%, according to DIN 16269-6:2009-10, Table E.3,
$x_U(N_{means}; 0.5; 0.9)$	upper limit of a two-sided statistical tolerance range for $p = 0.5$ with a confidence level of 90%, according to DIN 16269-6:2009-10, Table E.3,
$x_{L/U}(N_{meas}; 0.9; 0.9)$	lower (for determination of R) respectively upper (for determination of λ) limit of a one-sided statistical tolerance range for $p = 0.9$ with a confidence level of 90%, according to DIN 16269-6:2009-10, Table D.3.

The two-sided statistical tolerance range ($x_L(N_{meas}; 0.5; 0.9)$ *and* $x_U(N_{meas}; 0.5; 0.9)$) represents the confidence range for the mean values and the one-sided statistical tolerance range ($x_{L/U}(N_{meas}; 0.9; 0.9)$) represents the value that is true for 90%, of the basic population. The value $x_{L/U}(N_{meas}; 0.9; 0.9)$ is comparable for the so called $\lambda_{90/90}$ statistic that is applied for the calculation of nominal values. Of course the confidence ranges are comparably high, which is due to a low number of measurements and partly deviating methods and conditions, however it gives an impression about what could be statistical proven values.

The explained statistics were only assessed if three or more single values are available. If fewer values are given, only the mean value is calculated and included in the graphics.

For the sake of brevity, only the results obtained with 10°C of mean temperature are shown in detail.

Also included is information about the increase of thermal conductivity and thermal resistance for a mean temperature of 10°C and 23°C by time, using linear regression. The associated graphics show the increase of thermal properties by day; however, to give more meaningful information the linear regression refers to the increase during one year.

R	thermal resistance in (m² K)/W,
λ	thermal conductivity in mW/(m K),
m	slope of the regression straight line in (m² K)/(W a), respectively mW/(m K a),
t	time in years [a],
b	intercept of the ordinate axis in (m² K)/W or mW/(m K) for R and λ respectively.

3.3.1.3 Thermal resistance and thermal conductivity for material APM 1

Condition	Non-aged	Aged 1	Aged 2	-	
N_{labs}	3	2	2	-	
N_{meas}	4	2	3	-	
mdn	1.95	-	2.03	-	in (m² K)/W
mean	1.89	1.83	1.99	-	in (m² K)/W
s	0.15	-	0.07	-	in (m² K)/W
V	7.8	-	3.4	-	in %
$x_L(N_{labs};0.5;0.9)$	1.63	-	1.82	-	in (m² K)/W
$x_U(N_{labs};0.5;0.9)$	2.16	-	2.16	-	in (m² K)/W
$x_L(N_{labs};0.9;0.9)$	1.42	-	1.70	-	in (m² K)/W
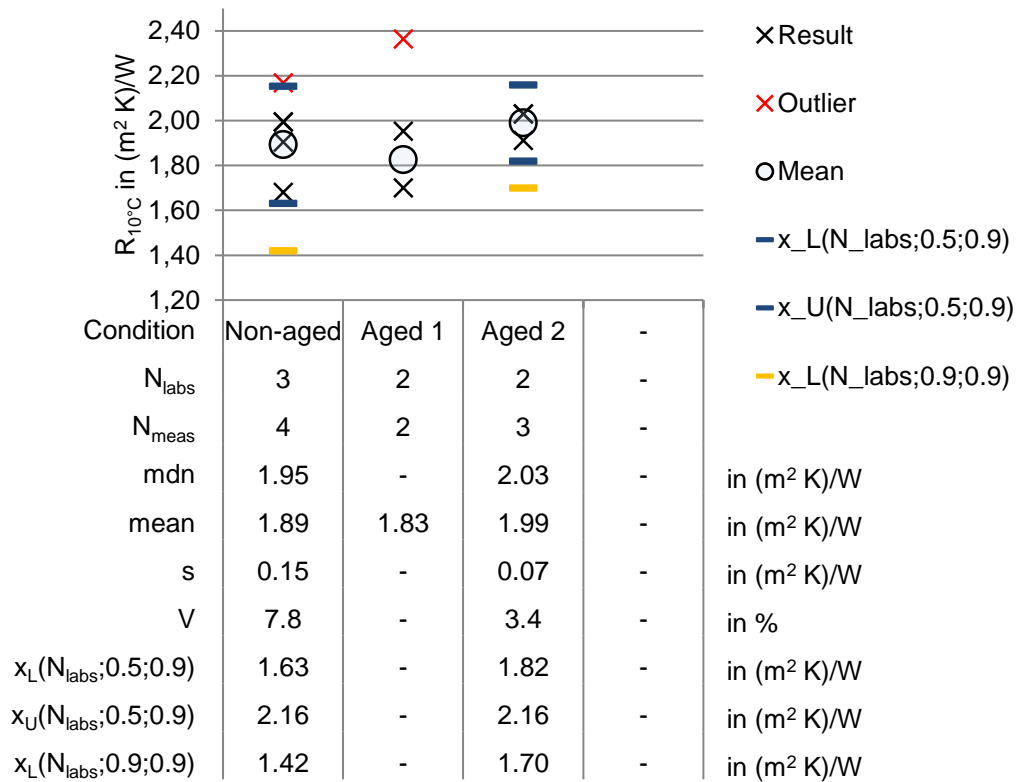
Figure 32: Results of thermal resistance (R) at 10°C mean temperature in (m² K)/W for material APM 1.

Condition	Non-aged	Aged 1	Aged 2	-	
N_{labs}	3	2	2	-	
N_{meas}	4	2	3	-	
mdn	20.1	-	19.7	-	in mW/(m K)
m	20.1	19.8	20.2	-	in mW/(m K)
s	0.78	-	0.81	-	in mW/(m K)
V	3.9	-	4.0	-	in %
$x_L(N_{labs};0.5;0.9)$	18.8	-	18.2	-	in mW/(m K)
$x_U(N_{labs};0.5;0.9)$	21.5	-	22.2	-	in mW/(m K)
$x_U(N_{labs};0.9;0.9)$	22.6	-	23.6	-	in mW/(m K)
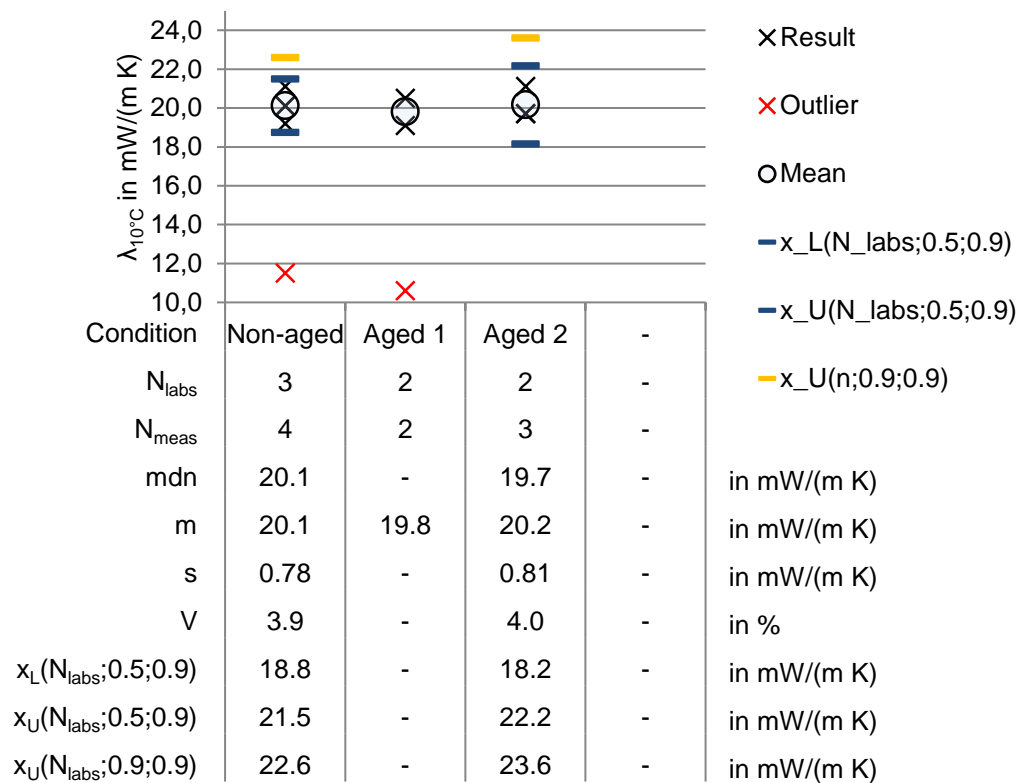
Figure 33: Results of thermal conductivity (λ) at 10°C mean temperature in W/(m K) for material APM 1.

The obtained results for the material APM 1 are characterised by well-defined values of thermal resistance as well as for the thermal conductivity. One lab obtained values that are statistically significantly different from the others. The decision to mark them as outliers is due to the fact that the measurements were taken out at a higher raw density of the loose fill bulk material, and therefore they are not comparable with the other specimens, so they were excluded from the analysis.

With respect to the differences between thermal resistance and thermal conductivity, the coefficient of variation (V) is lower for the non-aged values of thermal conductivity and slightly higher for the values in the step Aged 2. The reason may be seen in the variability of applied thickness for the loose fill material, which is varying in between the used sample holder.

The differences between the mean temperature of 10°C and 23°C are, as expected, with slightly higher values of thermal conductivity for the higher mean temperature.

Regarding the stability of the thermal properties by time, only a slow increase even at the severe ageing factors is visible (Table 7, Figure 34). From the obtained results no statistically proven ageing behaviour can be derived.

Table 7:   Parameters of linear regression of thermal resistance (R) and thermal conductivity (λ) as a function of ageing time for material APM 1.

T_m in °C	$R = m \cdot t + b$			$\lambda = m \cdot t + b$		
	m in (m² K)/(W a)	b in (m² K)/W	R²	m in mW/(m K a)	b in mW/(m K)	R²
10	0.481	1.85	0.54	0.463	20.0	0.08
23	0.445	1.73	0.65	0.536	21.4	0.04
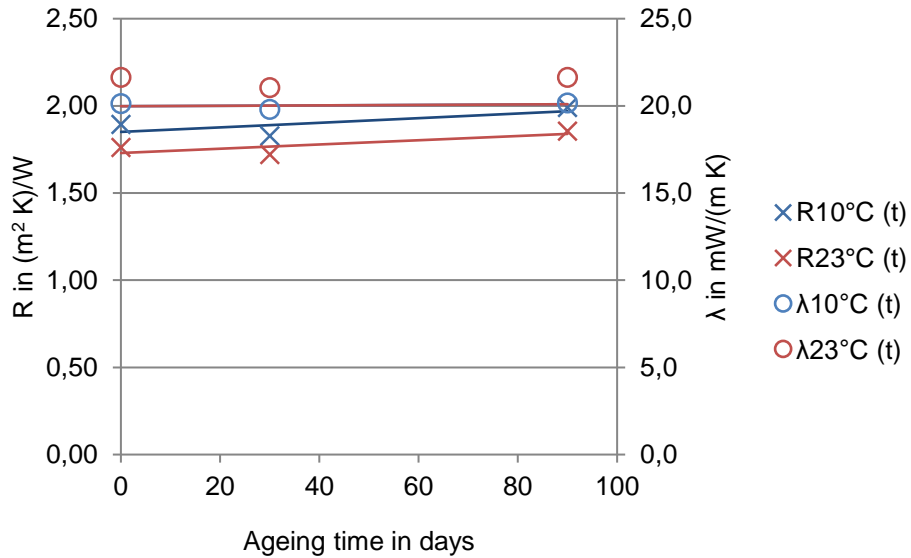
Figure 34: Results of thermal resistance (R) and thermal conductivity (λ) at 10°C and 23°C as a function of ageing time for material APM 1.

3.3.1.4 *Thermal resistance and thermal conductivity for material APM 2*

Condition	Non-aged	Aged 1	Aged 2	-	
N_{labs}	9	5	2	-	
N_{meas}	12	9	4	-	
mdn	1.63	1.62	1.65	-	in $(m^2 K)/W$
mean	1.64	1.64	1.65	-	in $(m^2 K)/W$
s	0.03	0.03	0.04	-	in $(m^2 K)/W$
V	1.6	1.8	2.6	-	in %
$x_L(N_{labs};0.5;0.9)$	1.61	1.60	1.57	-	in $(m^2 K)/W$
$x_U(N_{labs};0.5;0.9)$	1.67	1.67	1.72	-	in $(m^2 K)/W$
$x_L(N_{labs};0.9;0.9)$	1.59	1.57	1.51	-	in $(m^2 K)/W$

Figure 35: Results of thermal resistance (R) at 10°C mean temperature in $(m^2 K)/W$ for material APM 2.

Condition	Non-aged	Aged 1	Aged 2	-	
N_{labs}	9	5	2	-	
N_{meas}	9	9	4	-	
mdn	18.6	18.9	18.9	-	in mW/(m K)
mean	18.6	18.9	18.9	-	in mW/(m K)
s	0.40	0.32	0.40	-	in mW/(m K)
V	2.2	1.7	2.1	-	in %
$x_L(N_{labs};0.5;0.9)$	18.2	18.5	18.1	-	in mW/(m K)
$x_U(N_{labs};0.5;0.9)$	19.1	19.2	19.6	-	in mW/(m K)
$x_U(N_{labs};0.9;0.9)$	19.5	19.6	20.1	-	in mW/(m K)
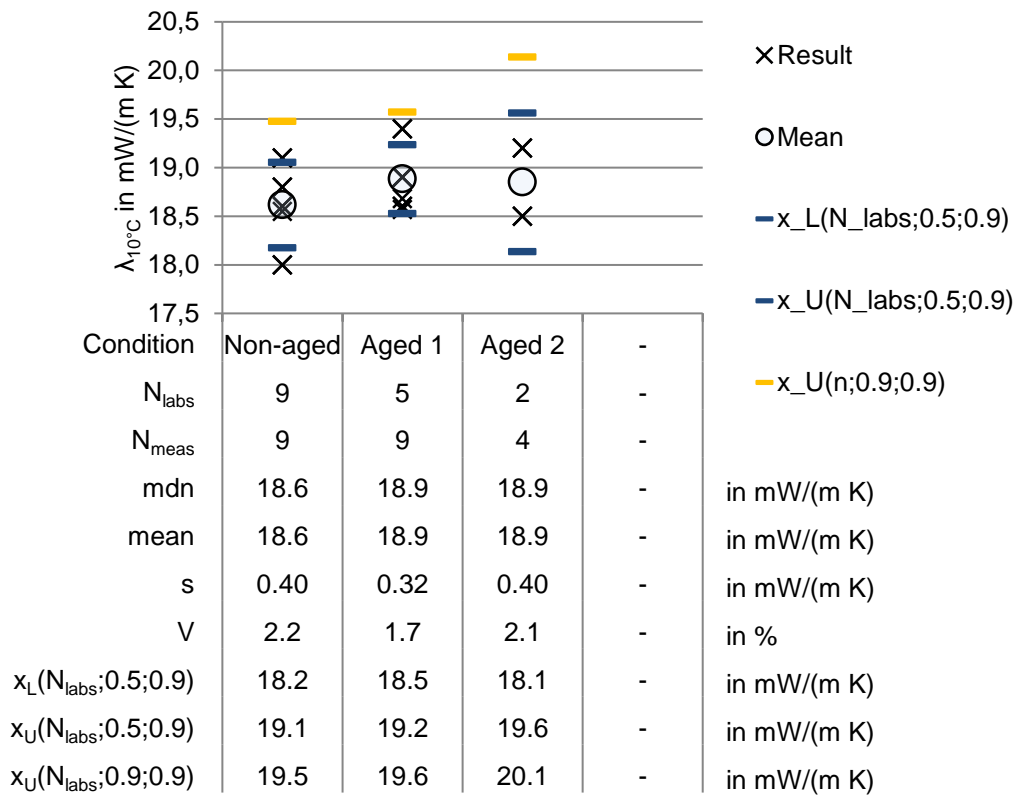
Figure 36: Results of thermal conductivity (λ) at 10°C mean temperature in W/(m K) for material APM 2.

The second APM material in the test shows a consistency between the results obtained in the inter-laboratory tests. Compared to the material APM 1, the deviation of the measurement results is lower with coefficients of variation (V) in between 1.6-2.6%. This can be explained by the fact that APM 2 is a rigid board material that comprises less variation in thickness and raw density during testing.

All in all, nine labs measured the APM 2 material in the non-aged stage. The coefficient of deviation in the range of 1.6-2.2% (thermal resistance and thermal conductivity respectively) for this value shows the consistant measurement procedures in the participating labs, as the obtained uncertainty is in the range of uncertainty of the measurement itself. Of course, other types of material that may be more demanding in terms of lab handling may cause higher deviations (e.g. the loose fill material APM 1 or VIP with uneven surfaces, etc).

As observed for APM 1, APM 2 offers a very good stability of thermal properties in the observed time frame of artificial ageing, despite the different ageing conditions (Table 8, Figure 37). The slope of the regression for thermal resistance and thermal conductivity by time is again on a very low level. Consequently, from the statistical point no proven ageing behaviour can be derived from the obtained results.

Table 8: Parameters of linear regression of thermal resistance (R) and thermal conductivity (λ) as a function of ageing time for material APM 2.

T_m in °C	$R = m \cdot t + b$			$\lambda = m \cdot t + b$		
	m in (m² K)/(W a)	b in (m² K)/W	R^2	m in mW/(m K a)	b in mW/(m K)	R^2
10	0.042	1.64	0.72	0.782	18.7	0.46
23	0.038	1.63	0.20	-1.159	19.3	0.70
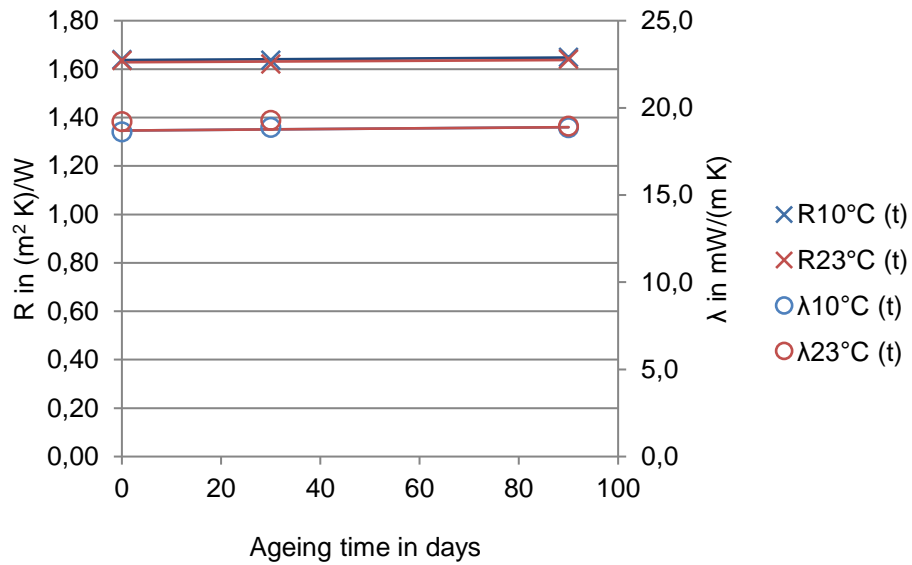
Figure 37: Results of thermal resistance (R) and thermal conductivity (λ) at 10°C and 23°C as a function of ageing time for material APM 2.

3.3.1.5 Thermal resistance and thermal conductivity COP for material VIP 1

Condition	Non-aged	Aged 1	Aged 2	Aged 3	
N_{labs}	4	3	1	2	
N_{meas}	9	5	2	4	
mdn	4.73	4.54	-	3.74	in (m² K)/W
mean	4.66	4.51	4.32	3.74	in (m² K)/W
s	0.31	0.20	-	0.53	in (m² K)/W
V	6.5	4.4	-	14.3	in %
$x_L(N_{labs};0.5;0.9)$	4.33	4.22	-	2.79	in (m² K)/W
$x_U(N_{labs};0.5;0.9)$	4.99	4.80	-	4.68	in (m² K)/W
$x_L(N_{labs};0.9;0.9)$	4.01	3.96	-	2.03	in (m² K)/W

Figure 38: Results of thermal resistance (R) at 10°C mean temperature in COP in (m² K)/W for material VIP 1.

Condition	Non-aged	Aged 1	Aged 2	Aged 3	
N_{labs}	4	3	1	2	
N_{meas}	9	5	2	4	
mdn	4.51	4.69	-	5.70	in mW/(m K)
mean	4.71	4.76	4.96	5.70	in mW/(m K)
s	0.37	0.20	-	0.81	in mW/(m K)
V	7.9	4.1	-	14.2	in %
$x_L(N_{labs};0.5;0.9)$	4.31	4.47	-	4.27	in mW/(m K)
$x_U(N_{labs};0.5;0.9)$	5.12	5.05	-	7.13	in mW/(m K)
$x_U(N_{labs};0.9;0.9)$	5.50	5.30	-	8.28	in mW/(m K)
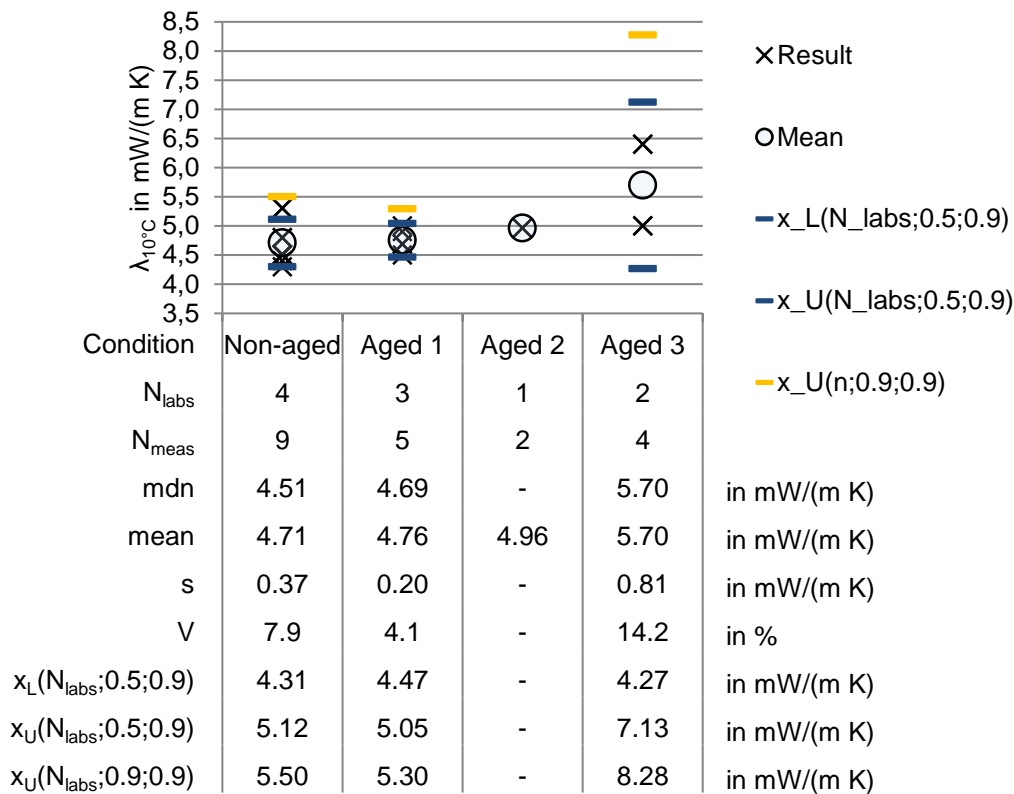
Figure 39: Results of thermal conductivity (λ) at 10°C mean temperature in COP in W/(m K) for material VIP 1.

Compared to the APM materials, the observed values for the VIP 1 material show a higher spread of data. The coefficients of variation (V) are in the range of 6.5-7.9% for the non-aged values and will rise by trend if the material is tested after ageing.

Differences between the spread of data for thermal conductivity and thermal resistance are low. Coefficient of variation (V) is higher for thermal conductivity data in the non-aged stage, but comparable for the steps Aged 1 and Aged 3. Therefore, if one or the other value is preferable no recommendation can be derived.

In general, it is difficult to distinguish whether varying measurement results are caused by differing test procedures, increased measurement uncertainty due to low heat fluxes of SIMs or whether they reflect a real variation of material properties. Especially for the observed VIP one has to take into account, even if the material was produced in one batch, that each panel may vary in internal pressure. Also, the long transport from Asia to Germany and back to Asia before measurement with unknown climatic and mechanical stress may cause differences in the observed values.

In contrast to the APM materials, the VIP 1 material shows a clear increase of thermal conductivity over the observed time frame of artificial ageing at 50°C and 70% RH (Table 9, Figure 40). The obtained regression shows a well-defined slope in the range of 2.0-3.9 mW/(m K a). The increase of thermal conductivity at 23°C mean temperature is higher in this case.

Table 9:   Parameters of linear regression of thermal resistance (R) and thermal conductivity (λ) as a function of ageing time for material VIP 1.

| T_m in °C	$R = m \cdot t + b$			$\lambda = m \cdot t + b$		
	m in (m² K)/(W a)	b in (m² K)/W	R²	m in mW/(m K a)	b in mW/(m K)	R²
10	-1.842	4.69	0.98	2.037	4.6	0.93
23	-2.748	4.58	0.93	3.860	4.6	0.91
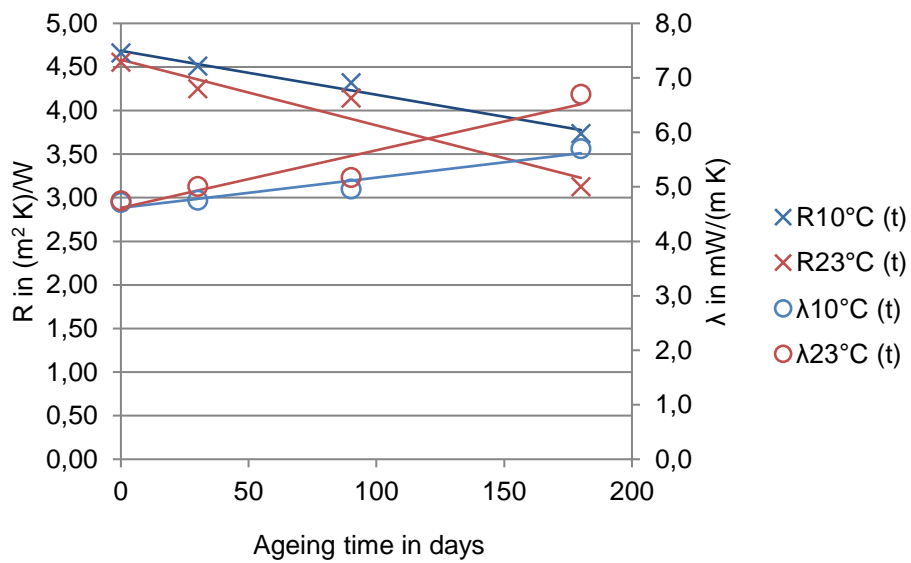
Figure 40: Results of thermal resistance (R) and thermal conductivity (λ) at 10°C and 23°C as a function of ageing time for material VIP 1.

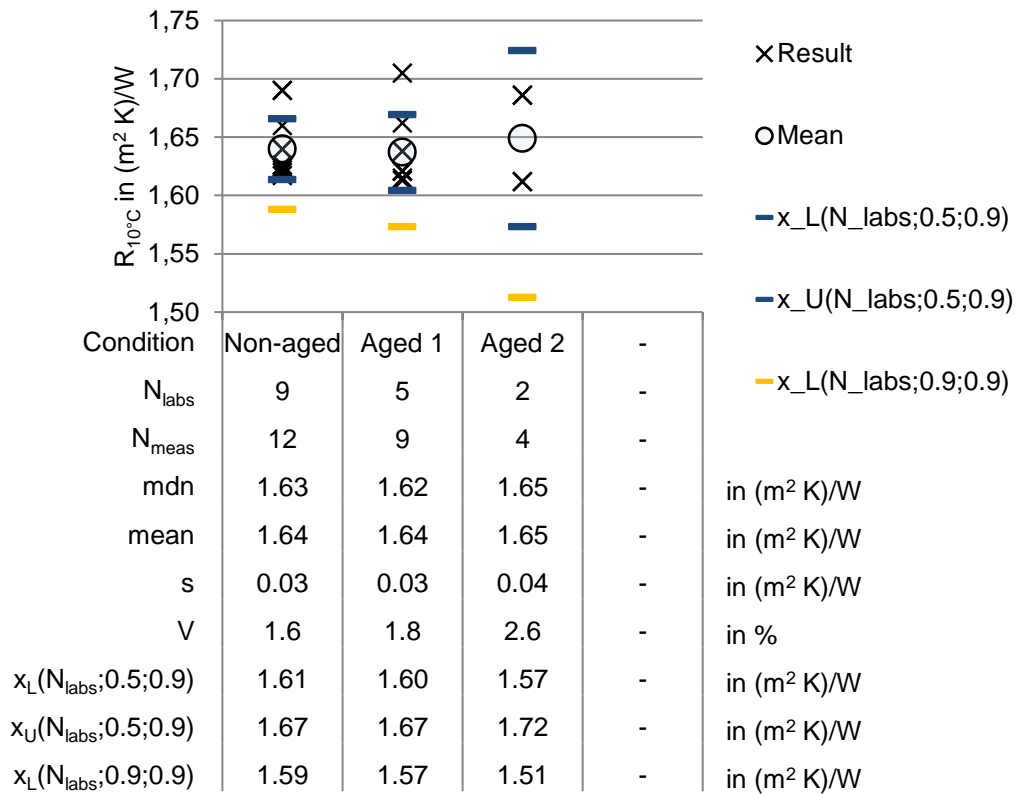### 3.3.1.6 *Thermal resistance and thermal conductivity COP for material VIP 3*

Condition	Non-aged	Aged 1	Aged 2	Aged 3	
N_{labs}	5	3	2	1	
N_{meas}	10	6	4	2	
mdn	5.12	5.22	4.70	-	in $(m^2\,K)/W$
mean	5.21	5.13	4.69	4.57	in $(m^2\,K)/W$
s	0.22	0.26	0.05	-	in $(m^2\,K)/W$
V	4.2	5.1	1.1	-	in %
$x_L(N_{labs};0.5;0.9)$	4.98	4.79	4.60	-	in $(m^2\,K)/W$
$x_U(N_{labs};0.5;0.9)$	5.44	5.48	4.79	-	in $(m^2\,K)/W$
$x_L(N_{labs};0.9;0.9)$	4.76	4.48	4.52	-	in $(m^2\,K)/W$

Figure 41: Results of thermal resistance (R) at 10°C mean temperature in COP in (m^2 K)/W for material VIP 3.

Condition	Non-aged	Aged 1	Aged 2	Aged 3	
N_{labs}	5	3	2	1	
N_{meas}	10	6	4	2	
mdn	3.98	4.00	4.30	-	in mW/(m K)
mean	3.95	4.03	4.30	4.35	in mW/(m K)
s	0.12	0.14	0.02	-	in mW/(m K)
V	3.2	3.4	0.5	-	in %
$x_L(N_{labs};0.5;0.9)$	3.82	3.85	4.26	-	in mW/(m K)
$x_U(N_{labs};0.5;0.9)$	4.08	4.21	4.34	-	in mW/(m K)
$x_U(N_{labs};0.9;0.9)$	4.21	4.37	4.37	-	in mW/(m K)
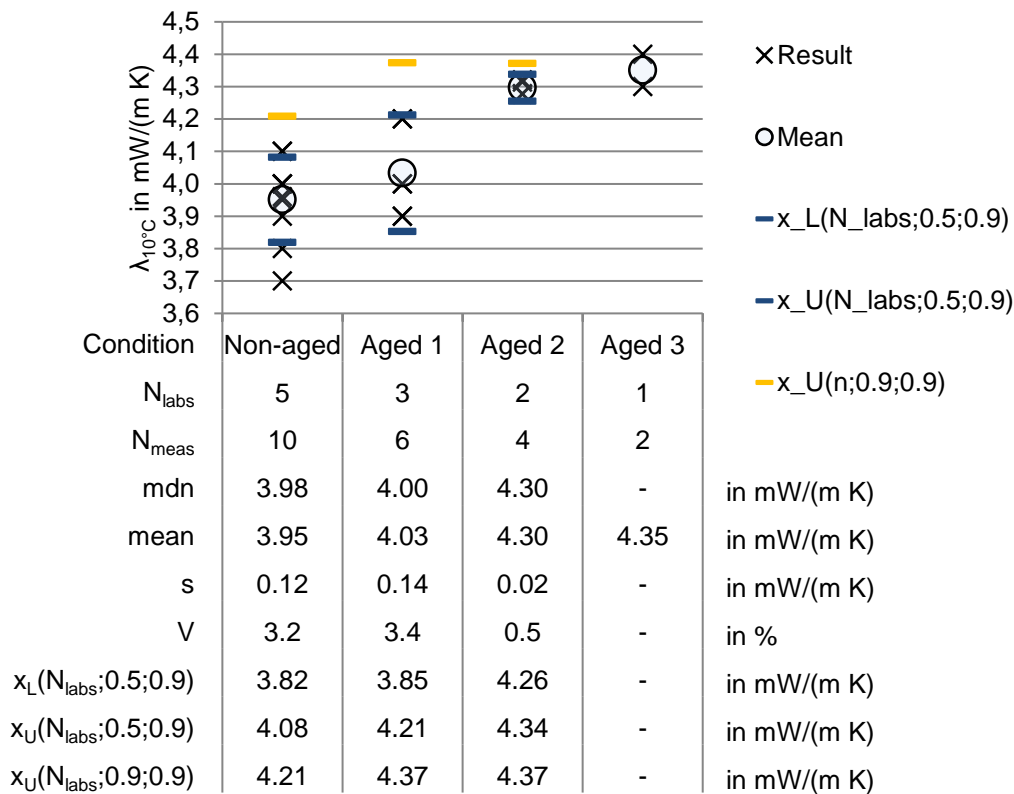
Figure 42: Results of thermal conductivity (λ) at 10°C mean temperature in COP in W/(m K) for material VIP 3.

Compared to VIP 1, VIP 3 shows a slightly lower spread of the obtained values.

Differences between the coefficients of variation (V) for thermal conductivity compared to thermal resistance are visible. The spread of data for thermal conductivity is lower. In general, it has to be considered that all tested VIP panels are individual specimens and therefore will differ in thickness and that will affect the results, the thickness being a very influential variable in the measurement of the thermal conductivity and difficult to determination for VIPs due to their curved shape. More details about VIP thickness determination are in Chapter 6.6.1.

The slope of the regression of thermal properties by time shows an increase of thermal conductivity in the range of 0.84-0.9mW/(m K a) (Table 10, Figure 43). In contrast to the results of material VIP 1 the difference between the increase rates between 10°C and 23°C are lower.

Table 10: Parameters of linear regression of thermal resistance (R) and thermal conductivity (λ) as a function of ageing time for material VIP 3.

T_m in °C	$R = m \cdot t + b$			$\lambda = m \cdot t + b$		
	m in (m² K)/(W a)	b in (m² K)/W	R²	m in mW/(m K a)	b in mW/(m K)	R²
10	-1.390	5.19	0.90	0.838	4.0	0.87
23	-1.389	4.99	0.90	0.899	4.2	0.88
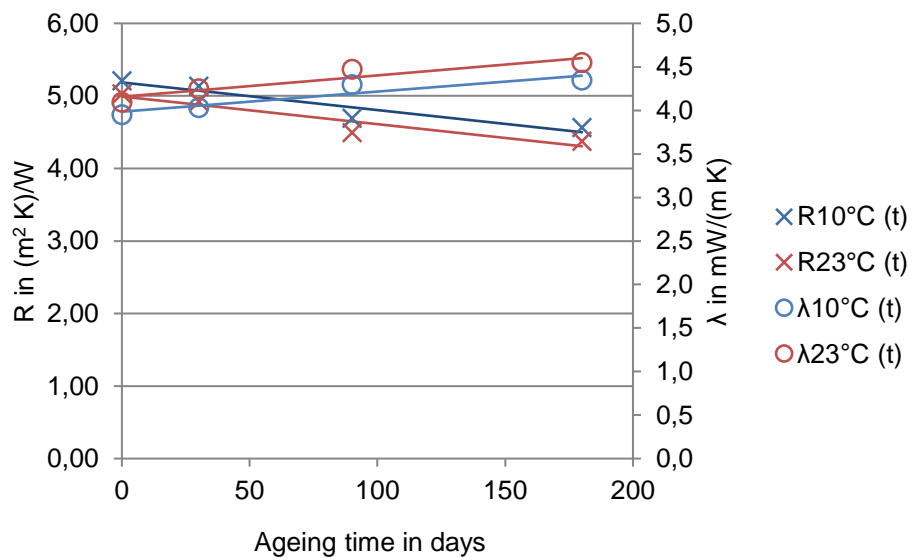
Figure 43: Results of thermal resistance (R) and thermal conductivity (λ) at 10°C and 23°C as a function of ageing time for material VIP 3.

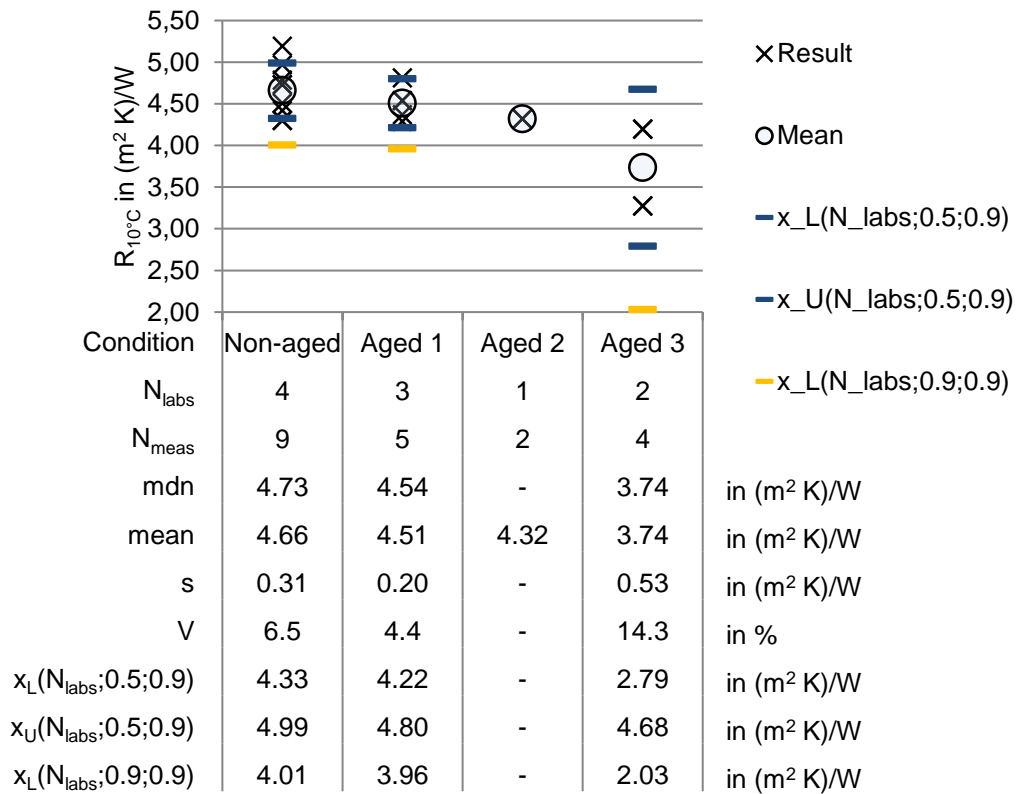### 3.3.1.7   Thermal resistance and thermal conductivity COP for material VIP 4

Condition	Non-aged	Aged 1	Aged 2	Aged 3	
N_{labs}	5	3	2	1	
N_{meas}	10	5	4	1	
mdn	5.96	5.74	5.17	-	in (m² K)/W
mean	5.95	5.69	5.08	4.59	in (m² K)/W
s	0.25	0.16	0.42	-	in (m² K)/W
V	4.3	2.8	8.3	-	in %
$x_L(N_{labs};0.5;0.9)$	5.68	5.46	4.34	-	in (m² K)/W
$x_U(N_{labs};0.5;0.9)$	6.21	5.93	5.83	-	in (m² K)/W
$x_L(N_{labs};0.9;0.9)$	5.42	5.26	3.73	-	in (m² K)/W

Figure 44: Results of thermal resistance (R) at 10°C mean temperature in COP in (m² K)/W for material VIP 4.

Condition	Non-aged	Aged 1	Aged 2	Aged 3	
N_{labs}	5	3	2	1	
N_{meas}	10	5	4	1	
mdn	3.50	3.70	4.05	-	in mW/(m K)
mean	3.54	3.69	4.05	4.60	in mW/(m K)
s	0.18	0.08	0.06	-	in mW/(m K)
V	5.0	2.2	1.4	-	in %
$x_L(N_{labs};0.5;0.9)$	3.35	3.57	3.95	-	in mW/(m K)
$x_U(N_{labs};0.5;0.9)$	3.72	3.81	4.15	-	in mW/(m K)
$x_U(N_{labs};0.9;0.9)$	3.90	3.92	4.23	-	in mW/(m K)
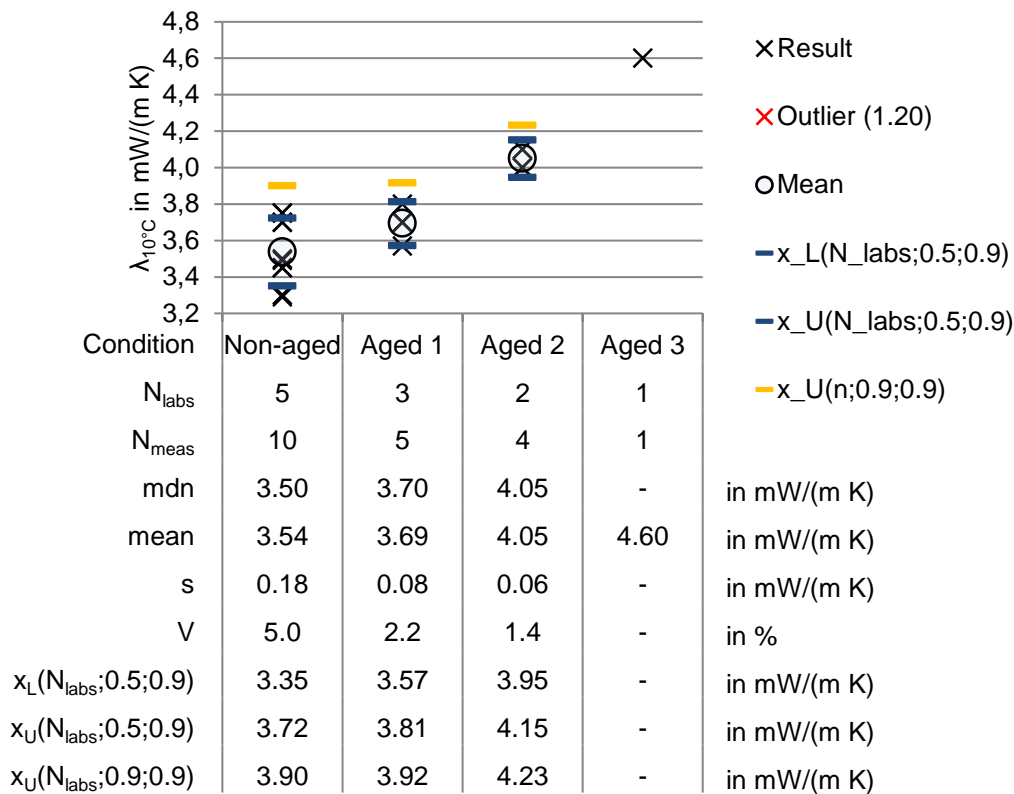
Figure 45: Results of thermal conductivity (λ) at 10°C mean temperature in COP in W/(m K) for material VIP 4.

The results for VIP 4 show values of thermal conductivity and thermal resistance with a comparable spread to VIP 1 and VIP 3. An interesting difference in the coefficient of variation (V) between thermal resistance and thermal conductivity is visible in the step Aged 2. The coefficient of variation for thermal conductivity is much lower in this case.

The outlier is expected to be caused by a VIP with a core material punctured under atmospheric pressure. This data was excluded from the analysis.

The linear regression of thermal resistance and thermal conductivity (Table 11, Figure 46) shows well defined slopes with increase rates of 2.2mW/(m K a) at 10°C mean temperature. If the measurement at 23°C mean temperature is evaluated the slope goes down to 0.9mW/(m K a) but with less confidence expressed by the coefficient of determination.

Table 11: Parameters of linear regression of thermal resistance (R) and thermal conductivity (λ) as a function of ageing time for material VIP 4.

| T_m in °C	$R = m \cdot t + b$			$\lambda = m \cdot t + b$		
	m in (m² K)/(W a)	b in (m² K)/W	R²	m in mW/(m K a)	b in mW/(m K)	R²
10	-2.772	5.90	0.98	2.166	3.5	1.00
23	-1.389	4.99	0.90	0.899	4.2	0.88
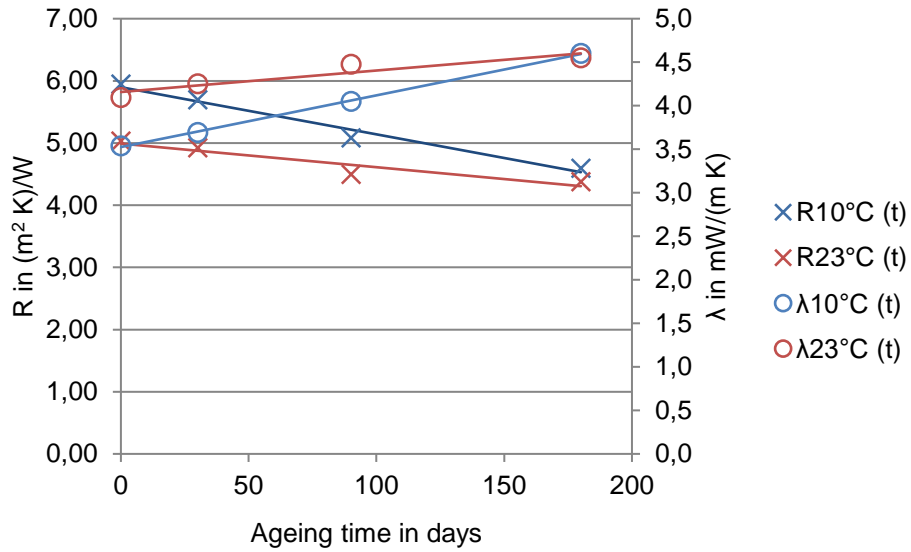
Figure 46: Results of thermal resistance (R) and thermal conductivity (λ) at 10°C and 23°C as a function of ageing time for material VIP 4.

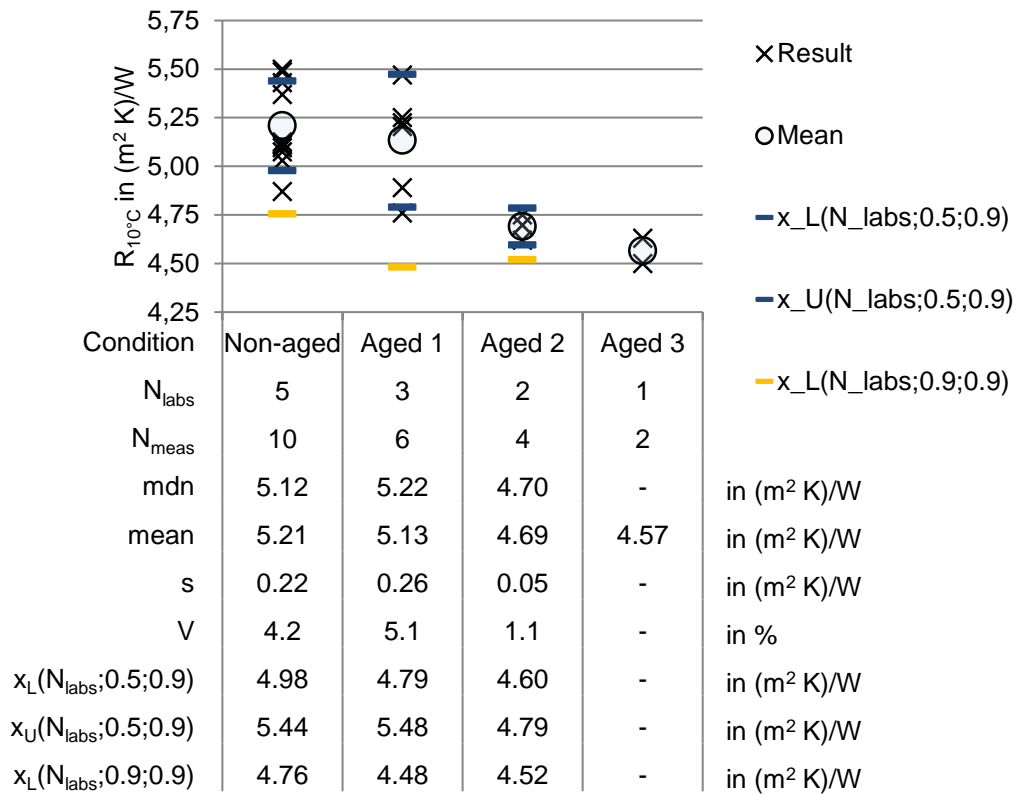### 3.3.1.8 Thermal resistance and thermal conductivity COP for material VIP 5

Condition	Non-aged	Aged 1	Aged 2	-	
N_{labs}	4	1	1	-	
N_{meas}	9	3	2	-	
mdn	11.3	9.32	-	-	in (m² K)/W
mean	11.8	9.23	6.04	-	in (m² K)/W
s	1.35	0.26	-	-	in (m² K)/W
V	11.4	2.8	-	-	in %
$x_L(N_{labs};0.5;0.9)$	10.3	8.57	-	-	in (m² K)/W
$x_U(N_{labs};0.5;0.9)$	13.3	9.88	-	-	in (m² K)/W
$x_L(N_{labs};0.9;0.9)$	8.92	8.11	-	-	in (m² K)/W
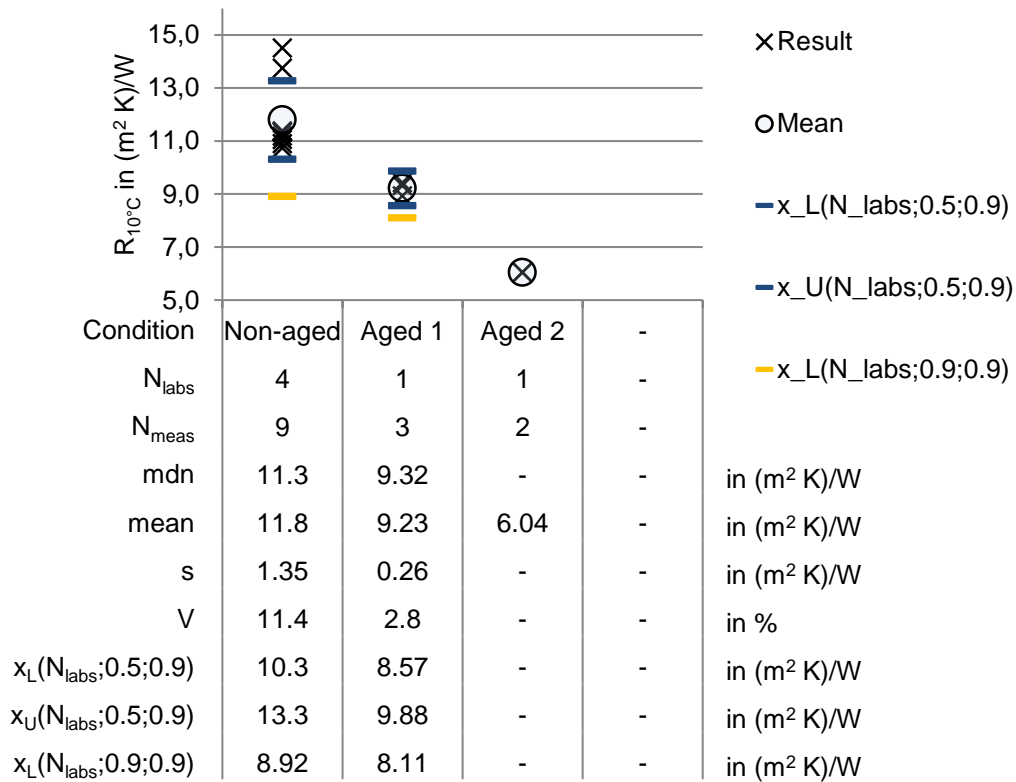
Figure 47: Results of thermal resistance (R) at 10°C mean temperature in COP in (m² K)/W for material VIP 5.

Condition	Non-aged	Aged 1	Aged 2	-	
N_{labs}	4	1	1	-	
N_{meas}	9	3	2	-	
mdn	1.90	2.30	-	-	in mW/(m K)
mean	1.85	2.33	3.50	-	in mW/(m K)
s	0.22	0.06	-	-	in mW/(m K)
V	11.9	2.5	-	-	in %
$x_L(N_{labs};0.5;0.9)$	1.61	2.19	-	-	in mW/(m K)
$x_U(N_{labs};0.5;0.9)$	2.09	2.48	-	-	in mW/(m K)
$x_U(N_{labs};0.9;0.9)$	2.32	2.58	-	-	in mW/(m K)
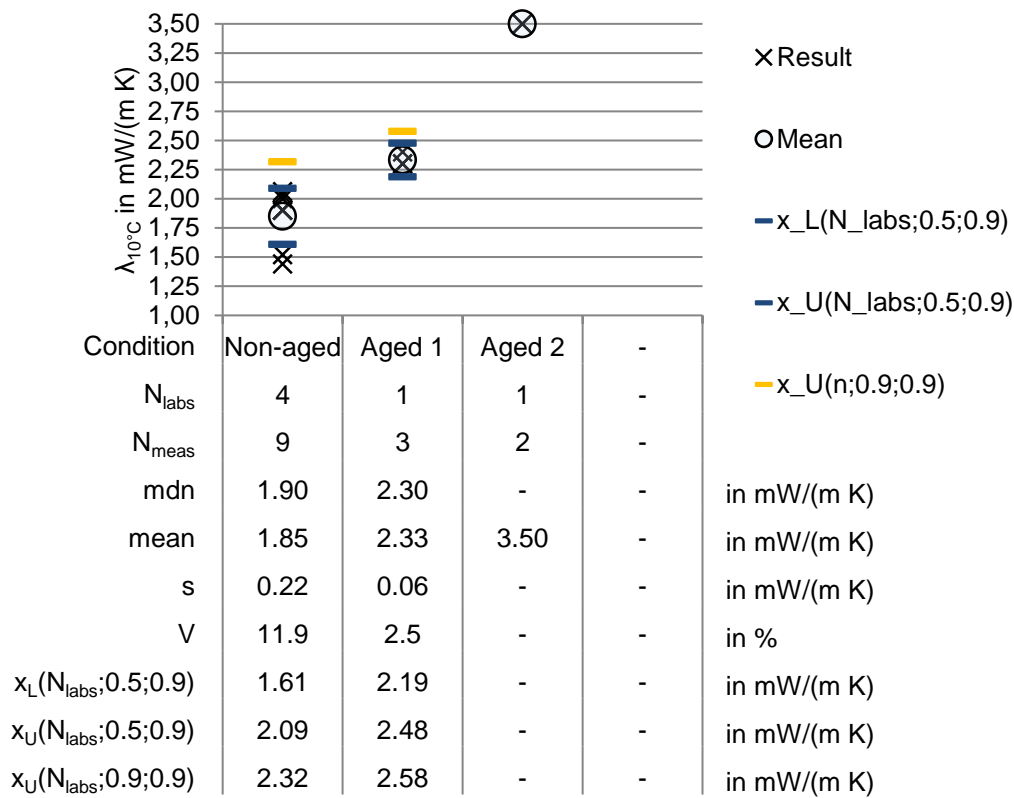
Figure 48: Results of thermal conductivity (λ) at 10°C mean temperature in COP in W/(m K) for material VIP 5.

The material VIP 5 offers significantly lower values of thermal conductivity in the non-aged stage, starting with around 2mW/(m K a). On the other hand the slope of the regression curve is significantly higher with increase rates of around 6.8mW/(m K a) (Table 12, Figure 49).

In opposite to the other materials no measurement at 23°C mean temperature was carried out and only one lab measured thermal properties at Aged 1 and Aged 2.

Concerning the non-aged values, with 4 labs making 9 measurements, the coefficient of variation of 12% is higher than materials VIP 1, VIP 3 and VIP 4.

Table 12: Parameters of linear regression of thermal resistance (R) and thermal conductivity (λ) as a function of ageing time for material VIP 5.

| T_m in °C	$R = m \cdot t + b$			$\lambda = m \cdot t + b$		
	m in (m² K)/(W a)	b in (m² K)/W	R²	m in mW/(m K a)	b in mW/(m K)	R²
10	-22.789	11.52	0.98	6.750	1.8	1.00
23	-	-	-	-	-	-
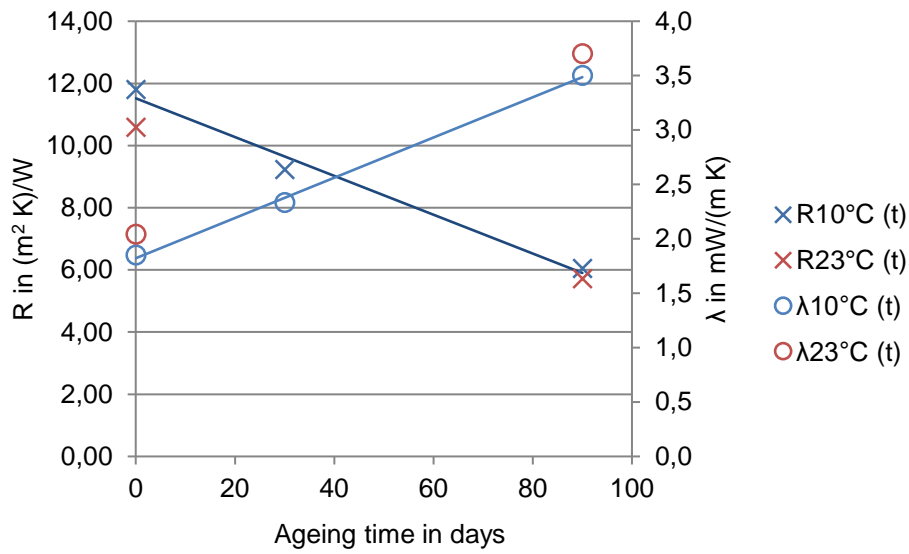
Figure 49: Results of thermal resistance (R) and thermal conductivity (λ) at 10°C and 23°C as a function of ageing time for material VIP 5.

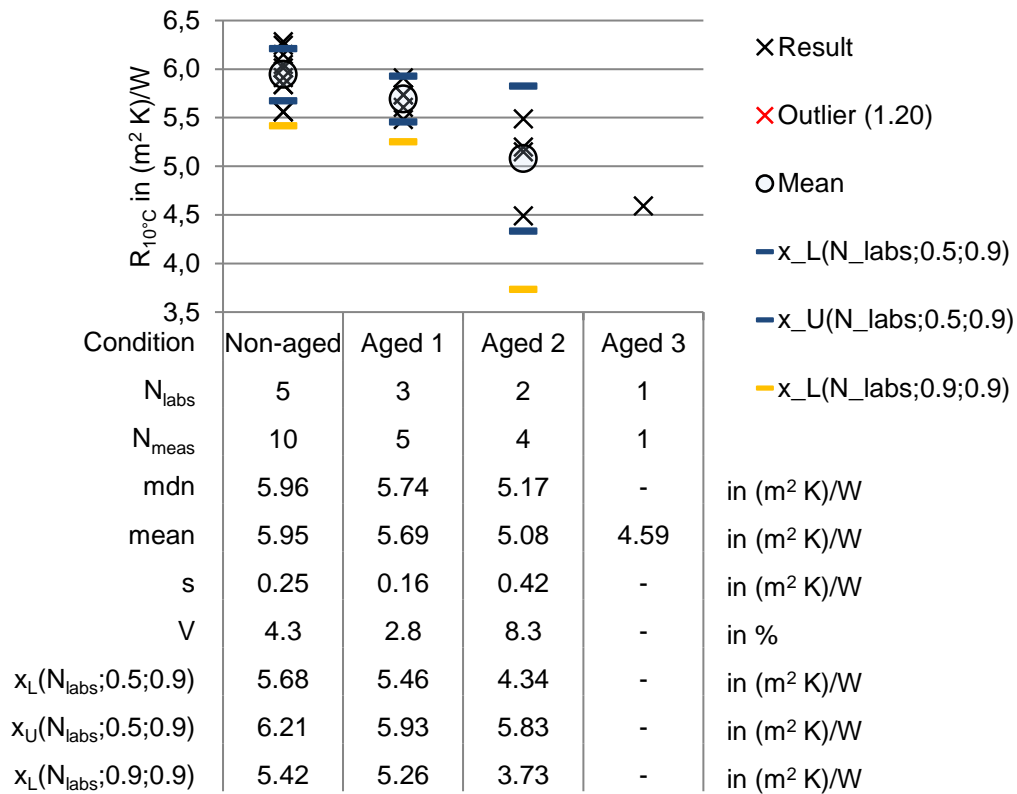### 3.3.1.9 *Thermal resistance and thermal conductivity COP for material VIP 6*

Condition	Non-aged	Aged 1	Aged 2	Aged 3	
N_{labs}	3	2	2	1	
N_{meas}	6	4	4	2	
mdn	14.9	8.93	9.08	-	in (m² K)/W
mean	11.7	7.9	8.8	8.2	in (m² K)/W
s	5.86	5.140	6.694	-	in (m² K)/W
V	50.0	65.0	76.3	-	in %
$x_L(N_{labs};0.5;0.9)$	4.0	-1.16	-3.04	-	in (m² K)/W
$x_U(N_{labs};0.5;0.9)$	19.4	16.99	20.60	-	in (m² K)/W
$x_L(N_{labs};0.9;0.9)$	-2.9	-8.47	-12.56	-	in (m² K)/W
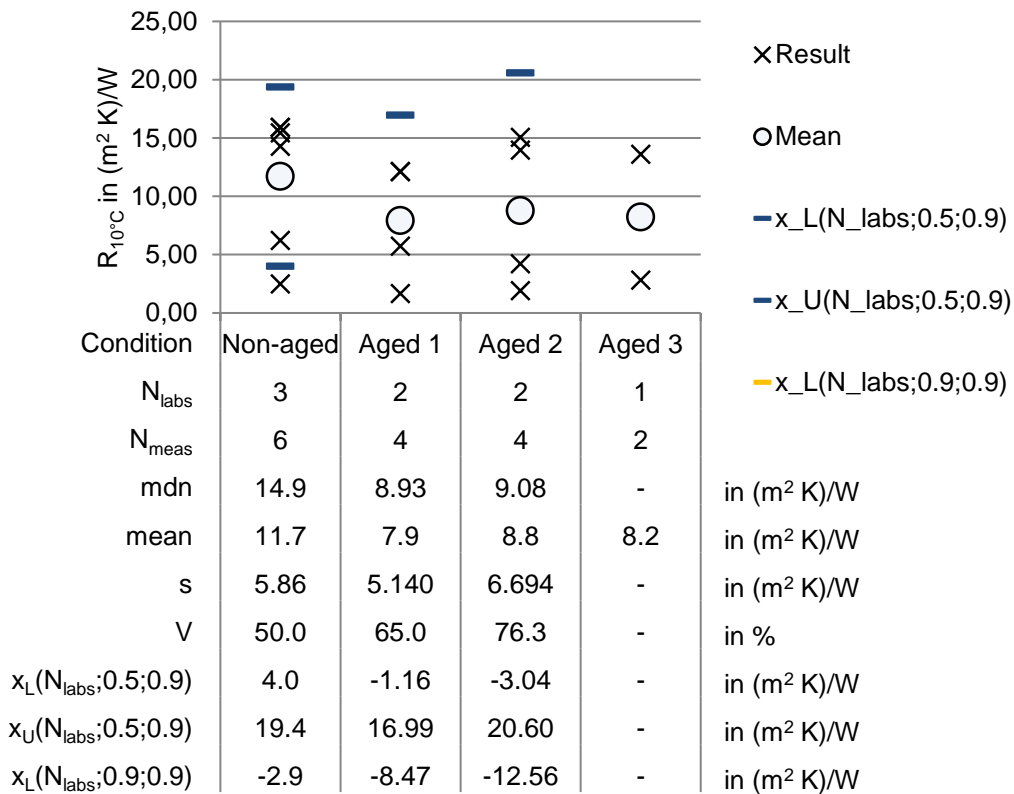
Figure 50: Results of thermal resistance (R) at 10°C mean temperature in COP in (m² K)/W for material VIP 6.

Condition	Non-aged	Aged 1	Aged 2	Aged 3	
N_{labs}	3	2	2	1	
N_{meas}	6	4	4	2	
mdn	1.45	2.60	3.35	-	in mW/(m K)
mean	2.83	4.75	4.65	4.15	in mW/(m K)
s	2.71	4.89	4.31	-	in mW/(m K)
V	95.9	103.0	92.7	-	in %
$x_L(N_{labs};0.5;0.9)$	-0.74	-3.89	-2.96	-	in mW/(m K)
$x_U(N_{labs};0.5;0.9)$	6.40	13.39	12.26	-	in mW/(m K)
$x_U(N_{labs};0.9;0.9)$	9.60	20.35	18.40	-	in mW/(m K)
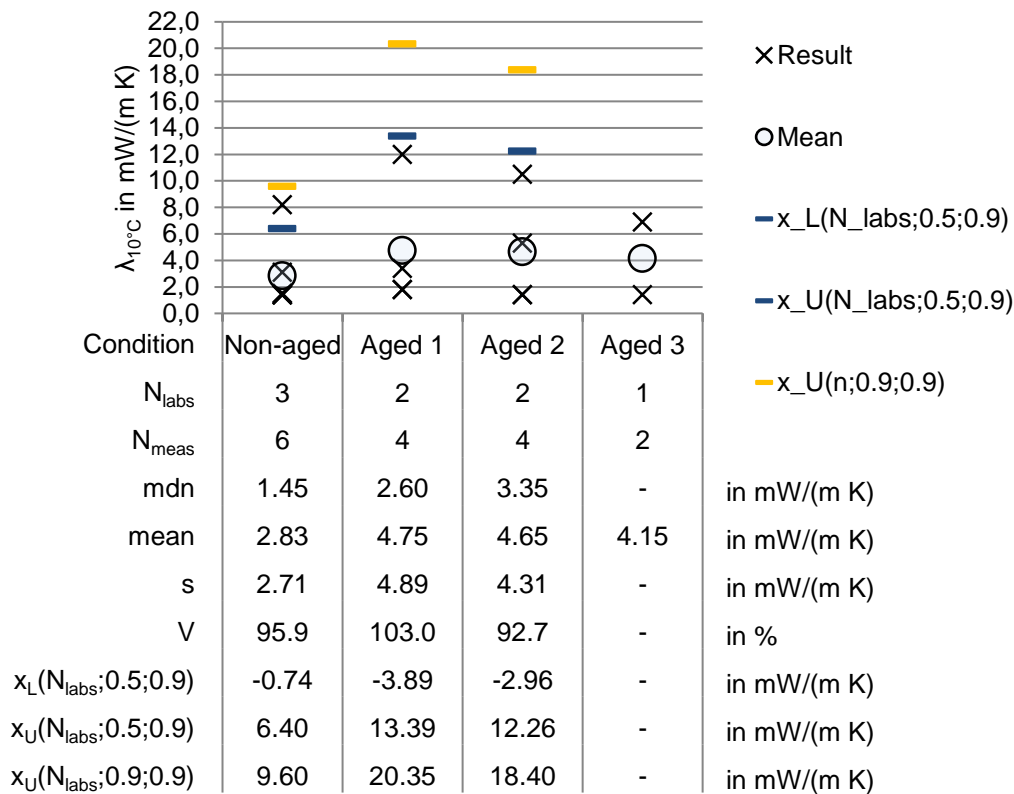
Figure 51: Results of thermal conductivity (λ) at 10°C mean temperature in COP in W/(m K) for material VIP 6.

As for VIP 5, the material VIP 6 starts with lower values of thermal conductivity. Due to high spreading, the median of around 1.5 mW/(m K) is more meaningful than the mean value. The coefficient of variation reaches 96% for thermal conductivity in the Non-Aged stage, which is the highest value found in the test series.

Also in the following steps Aged 1 – Aged 3 the high spreading is constant with values for the coefficient of variation around 93-103%. The high spreading is because some panels stay on a constant level of thermal conductivity and others show increased values. This behaviour can be explained by the presence of getter materials that guarantee a constant internal pressure as long as the capacity is not limited. If the getter material fails or the capacity of the getter material is reached, the internal pressure increases and leads to rising values of thermal conductivity.

To this effect an evaluation of regression curves is not meaningful. As given in Table 13 the resulting coefficients of determination are at a low level.

Table 13: Parameters of linear regression of thermal resistance (R) and thermal conductivity (λ) as a function of ageing time for material VIP 6.

| T_m in °C	R = m · t + b			λ = m · t + b		
	m in (m² K)/(W a)	**b** in (m² K)/W	**R²**	**m** in mW/(m K a)	**b** in mW/(m K)	**R²**
10	-4.637	10.11	0.34	1.533	3.8	0.14
23	-2.190	8.52	0.37	0.442	4.4	0.04
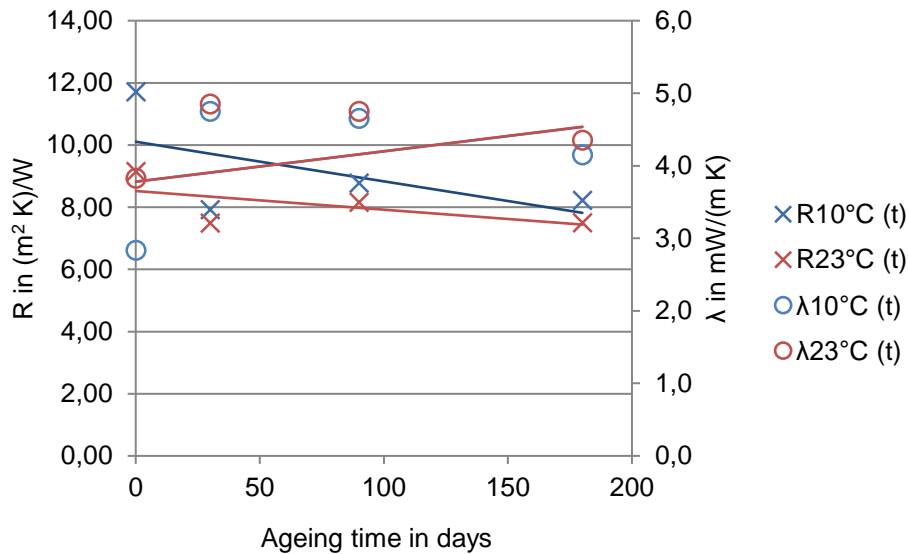
Figure 52: Results of thermal resistance (R) and thermal conductivity (λ) at 10°C and 23°C as a function of ageing time for material VIP 6.

3.3.2 ψ values

The obtained ψ values for characterisation of linear thermal bridging effects are measured according to Chapter 2.2. All values show a relatively high spreading, even in the Non-Aged stage.

Reasons for this behaviour are due to different effects. First of all the additional heat flux through the joint in between two panels is highly influenced by the quality of assembling. If any sealing band is installed between the two panels the type of elastomeric foam, the thickness of the sealing band, the compression rate, as well as the quality of gluing in between the VIP edge and the sealing band is of influence on the heat flow. If no sealing band is installed, the width of the gap in between the panels influences the results.

As already mentioned, the setup of the panels is of great importance (Figure 53).

Figure 53: Setup of panels with non-rectangular edge resulting in a small gap (left), and panels with non-rectangular edge resulting in a wide gap (right). Source: FIW München.

On the other hand, the ψ value reflects the proportion between the undisturbed case that is represented by the value in the centre of panel (COP) and the case with the joint in between two VIPs. It is necessary to refer to a measured COP that should be characterised for all panels involved in the measurement.

For practical reasons this is not possible. First of all the measurement area of the apparatus requires a certain minimum area of the specimen. On the other hand, most apparatus do not allow the specimen to overlap the heating plate due to periphery of the apparatus (e.g. the insulation case of the apparatus and table tracks, etc). Also, to limit the time effort for one measurement all four panels are not characterised.

To solve these problems the measurement effort can be split to different apparatus, using a smaller apparatus for determination of COP values and a larger one for determination of ψ values. In doing so, the uncertainty of two involved apparatus is to be considered, meaning the systematic errors are not limited in the relative point of view. If no adequate measureing equipment is available it is also common to refer to a COP measurement of material derived from the same batch of production. This is even more problematic as explained before, as each panel is an individual piece of insulation consisting of several parts (including the barrier foil and the core material) and of individual production quality with respect to defect zones in the welding and internal pressure. Otherwise if only one measuring device is available, it is important to verify (for example by means of numerical simulations) whether the measurement area will be affected by lateral heat losses due to the small dimensions of a single VIP panel. If so, the assessment of the COP thermal conductivity can be performed with the same apparatus.

The described phenomena become even more problematic in the Aged steps. This is visible in even higher spreading compared to the Non-Aged stage and some meaningless negative ψ values.

In the following sub-chapters the obtained results are displayed without further comments. The gained body of experience is used for an improved description of methodology in the Chapter 7.1.5.

3.3.2.1 ψ values for material VIP 1

	10°C	23°C	10°C	23°C	
Temperature	10°C	23°C	10°C	23°C	Temperature
N_{labs}	3	2	3	2	N_{labs}
N_{meas}	3	2	3	2	N_{meas}
mdn in (m² K)/W	3.92	-	14.4	-	mdn in mW/(m K)
mean in (m² K)/W	3.97	3.97	14.8	13.8	mean in mW/(m K)
s in (m² K)/W	0.35	-	1.06	-	s in mW/(m K)
V in %	8.8	-	7.2	-	V in %
$x_L(N_{labs};0.5;0.9)$ in (m² K)/W	3.10	-	12.2	-	$x_L(N_{labs};0.5;0.9)$ in mW/(m K)
$x_U(N_{labs};0.5;0.9)$ in (m² K)/W	4.83	-	17.4	-	$x_U(N_{labs};0.5;0.9)$ in mW/(m K)
$x_L(N_{labs};0.9;0.9)$ in (m² K)/W	4.26	-	4.26	-	$x_L(N_{labs};0.9;0.9)$ in mW/(m K)

Figure 54:   Results of measurement for determination of ψ values at 10°C and 23°C for material VIP 1, left: R_{eq} in (m² K)/W; right: ψ in W/(m K).

3.3.2.2 ψ values for material VIP 3

	10°C	23°C	10°C	23°C	
Temperature	10°C	23°C	10°C	23°C	Temperature
N_{labs}	2	2	2	2	N_{labs}
N_{meas}	2	2	2	2	N_{meas}
mdn in (m² K)/W	-	-	-	-	mdn in mW/(m K)
mean in (m² K)/W	4.63	4.61	11.0	12.0	mean in mW/(m K)
s in (m² K)/W	-	-	-	-	s in mW/(m K)
V in %	-	-	-	-	V in %
$x_L(N_{labs};0.5;0.9)$ in (m² K)/W	-	-	-	-	$x_L(N_{labs};0.5;0.9)$ in mW/(m K)
$x_U(N_{labs};0.5;0.9)$ in (m² K)/W	-	-	-	-	$x_U(N_{labs};0.5;0.9)$ in mW/(m K)
$x_L(N_{labs};0.9;0.9)$ in (m² K)/W	-	-	-	-	$x_L(N_{labs};0.9;0.9)$ in mW/(m K)

Figure 55: Results of measurement for determination of ψ values at 10°C and 23°C for material VIP 3, left: R_{eq} in (m² K)/W; right: ψ in W/(m K).

3.3.2.3 *ψ values for material VIP 4*

	10°C	23°C	10°C	23°C	
Temperature	10°C	23°C	10°C	23°C	Temperature
N_{labs}	3	3	3	3	N_{labs}
N_{meas}	3	3	3	3	N_{meas}
mdn in (m² K)/W	4.62	4.49	12.0	12.1	mdn in mW/(m K)
mean in (m² K)/W	4.33	4.23	10.6	10.7	mean in mW/(m K)
s in (m² K)/W	0.91	0.89	3.86	3.95	s in mW/(m K)
V in %	21.0	21.2	36.5	37.0	V in %
$x_L(N_{labs};0.5;0.9)$ in (m² K)/W	2.06	2.00	0.96	0.82	$x_L(N_{labs};0.5;0.9)$ in mW/(m K)
$x_U(N_{labs};0.5;0.9)$ in (m² K)/W	6.60	6.46	20.2	20.5	$x_U(N_{labs};0.5;0.9)$ in mW/(m K)
$x_L(N_{labs};0.9;0.9)$ in (m² K)/W	4.26	4.26	4.26	4.26	$x_L(N_{labs};0.9;0.9)$ in mW/(m K)

Figure 56: Results of measurement for determination of ψ values at 10°C and 23°C for material VIP 4, left: R_{eq} in (m² K)/W; right: ψ in W/(m K).

3.3.2.4 *ψ values for material VIP 5*

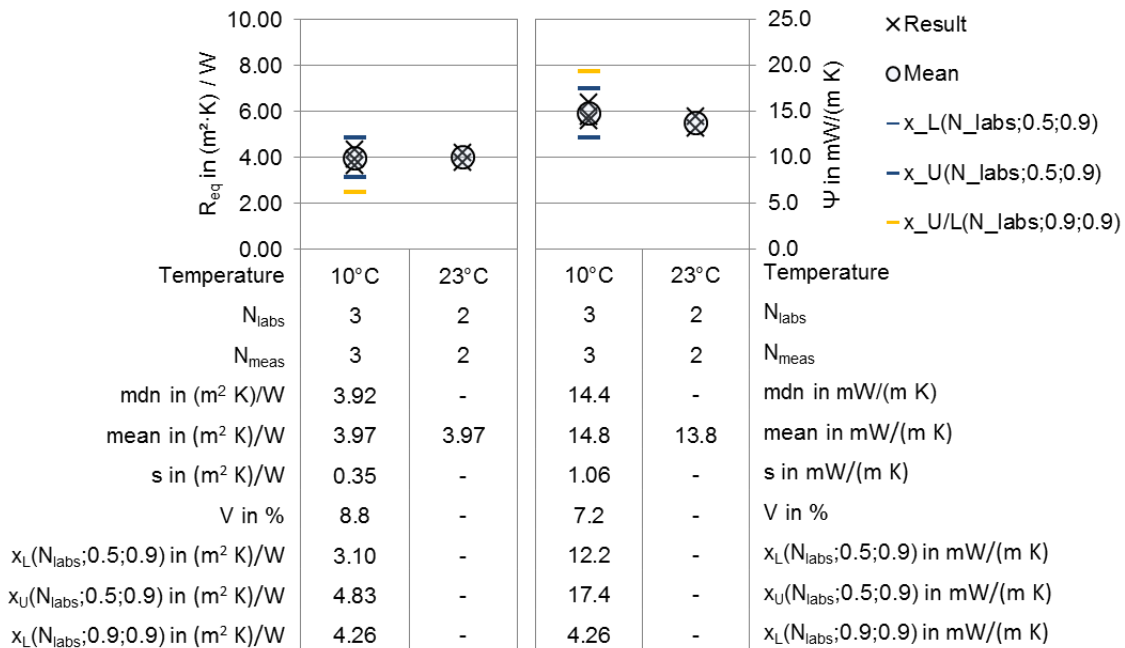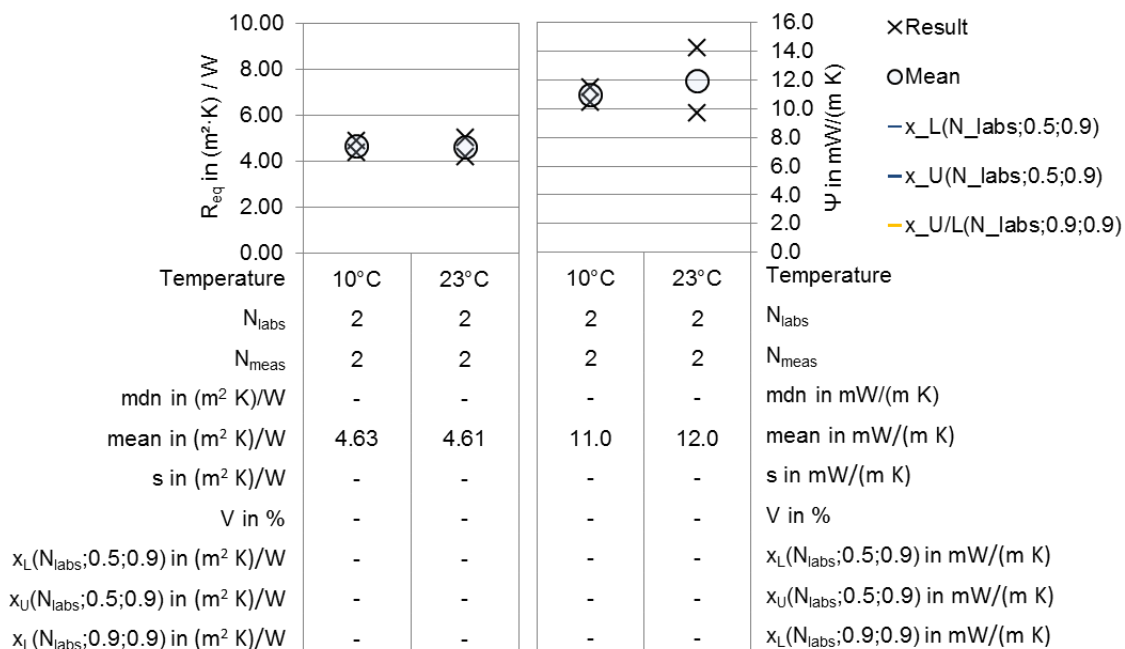|	10°C	23°C	10°C	23°C	
Temperature	10°C	23°C	10°C	23°C	Temperature
N_{labs}	2	1	3	1	N_{labs}
N_{meas}	2	1	3	1	N_{meas}
mdn in (m² K)/W	-	-	21.2	-	mdn in mW/(m K)
mean in (m² K)/W	5.46	5.82	21.6	18.9	mean in mW/(m K)
s in (m² K)/W	-	-	9.20	-	s in mW/(m K)
V in %	-	-	42.6	-	V in %
$x_L(N_{labs};0.5;0.9)$ in (m² K)/W	-	-	-1.31	-	$x_L(N_{labs};0.5;0.9)$ in mW/(m K)
$x_U(N_{labs};0.5;0.9)$ in (m² K)/W	-	-	44.5	-	$x_U(N_{labs};0.5;0.9)$ in mW/(m K)
$x_L(N_{labs};0.9;0.9)$ in (m² K)/W	-	-	4.26	-	$x_L(N_{labs};0.9;0.9)$ in mW/(m K)

Figure 57: Results of measurement for determination of ψ values at 10°C and 23°C for material VIP 5, left: R_{eq} in (m² K)/W; right: ψ in W/(m K).

3.3.2.5 ψ values for material VIP 6

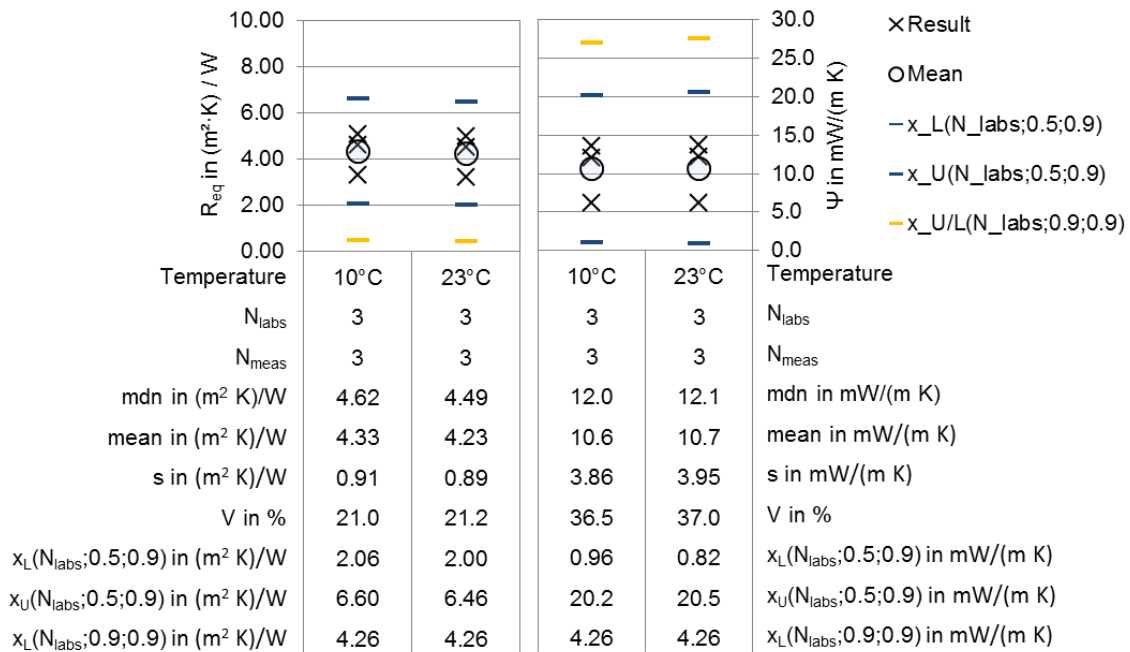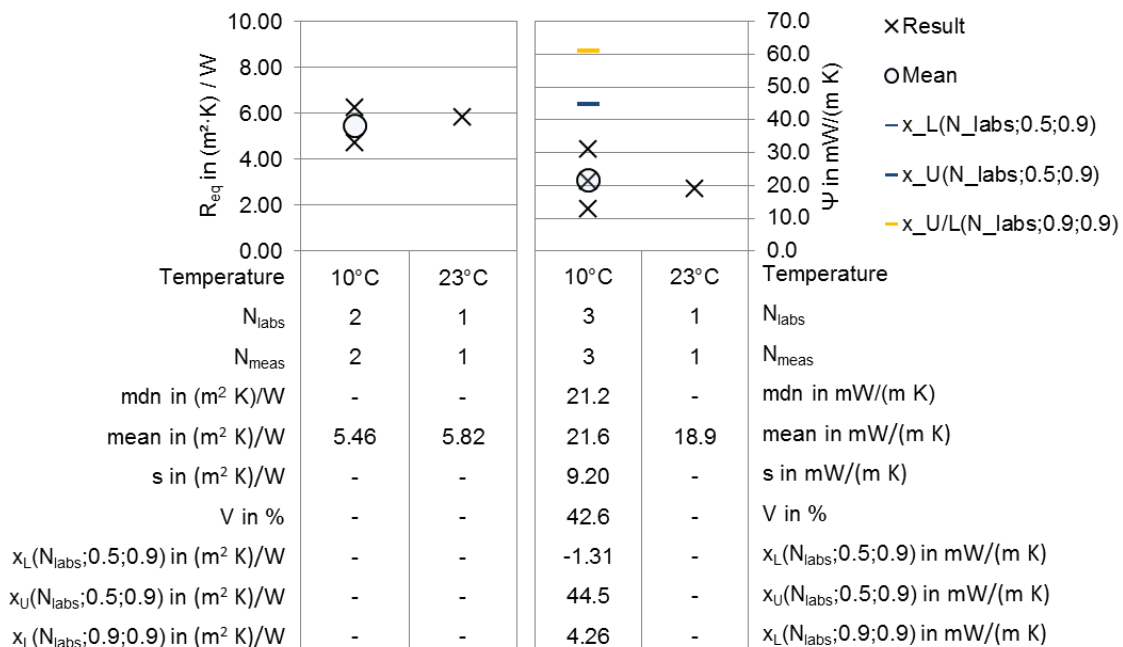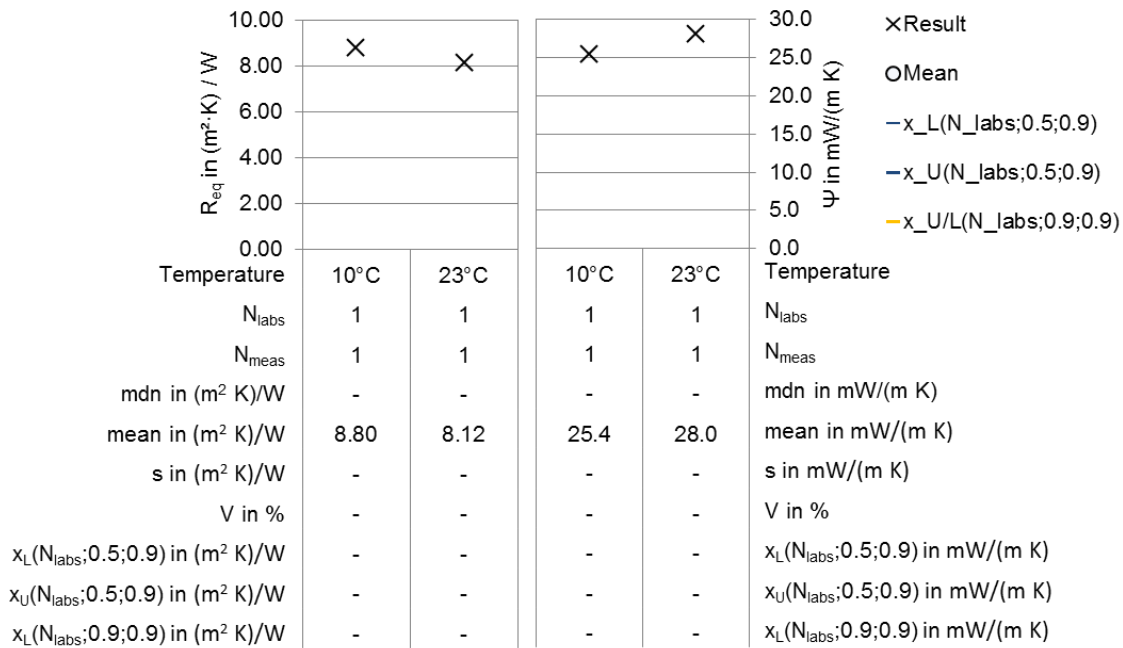| Temperature	10°C	23°C	10°C	23°C	Temperature
N_{labs}	1	1	1	1	N_{labs}
N_{meas}	1	1	1	1	N_{meas}
mdn in (m² K)/W	-	-	-	-	mdn in mW/(m K)
mean in (m² K)/W	8.80	8.12	25.4	28.0	mean in mW/(m K)
s in (m² K)/W	-	-	-	-	s in mW/(m K)
V in %	-	-	-	-	V in %
$x_L(N_{labs};0.5;0.9)$ in (m² K)/W	-	-	-	-	$x_L(N_{labs};0.5;0.9)$ in mW/(m K)
$x_U(N_{labs};0.5;0.9)$ in (m² K)/W	-	-	-	-	$x_U(N_{labs};0.5;0.9)$ in mW/(m K)
$x_L(N_{labs};0.9;0.9)$ in (m² K)/W	-	-	-	-	$x_L(N_{labs};0.9;0.9)$ in mW/(m K)

Figure 58: Results of measurement for determination of ψ values at 10°C and 23°C for material VIP 6, left: R_{eq} in (m² K)/W; right: ψ in W/(m K).

3.3.3 Internal pressure

The internal pressure was measured according to the descriptions in Chapter 2.3. The foil lift-off method is only applicable for VIPs with silica-based core material. Fibre based core materials show significant relaxation behaviour when the surrounding atmospheric pressure decreases during the measurement. This makes it impossible to precisely determine the foil lift-off from the core.

Below, the results of internal pressure measurement for VIP 1, VIP 3 and VIP 4 are described with several graphics. First a statistical data evaluation for the thermal conductivity and ψ-value measurement was conducted to show the spreading of results for the different ageing steps. Only a few labs performed internal pressure analysis. To enhance the statistical database every single measurement value was integrated in the analysis.

In addition, linear regression analysis for internal pressure as a function of time and thermal conductivity as a function of internal pressure were conducted. For this analysis the mean values from internal pressure and thermal conductivity have been selected.

3.3.3.1 Results of internal pressure for material VIP 1

The material VIP 1 was measured by two labs in the Non-Aged stage and only one lab in the Aged steps (Figure 59). The panels show a distinct and well-defined increase of internal pressure by time (Table 14). In the climatic conditions of artificial ageing (50°C and 70% RH) the increase of internal pressure would be around 12.4mbar/a. Referred

to the thermal conductivity, this leads to an increase of thermal conductivity of 0.17mW/(m K a) (Table 15). Both regressions are well defined with R^2 values of 0.95-1.00.

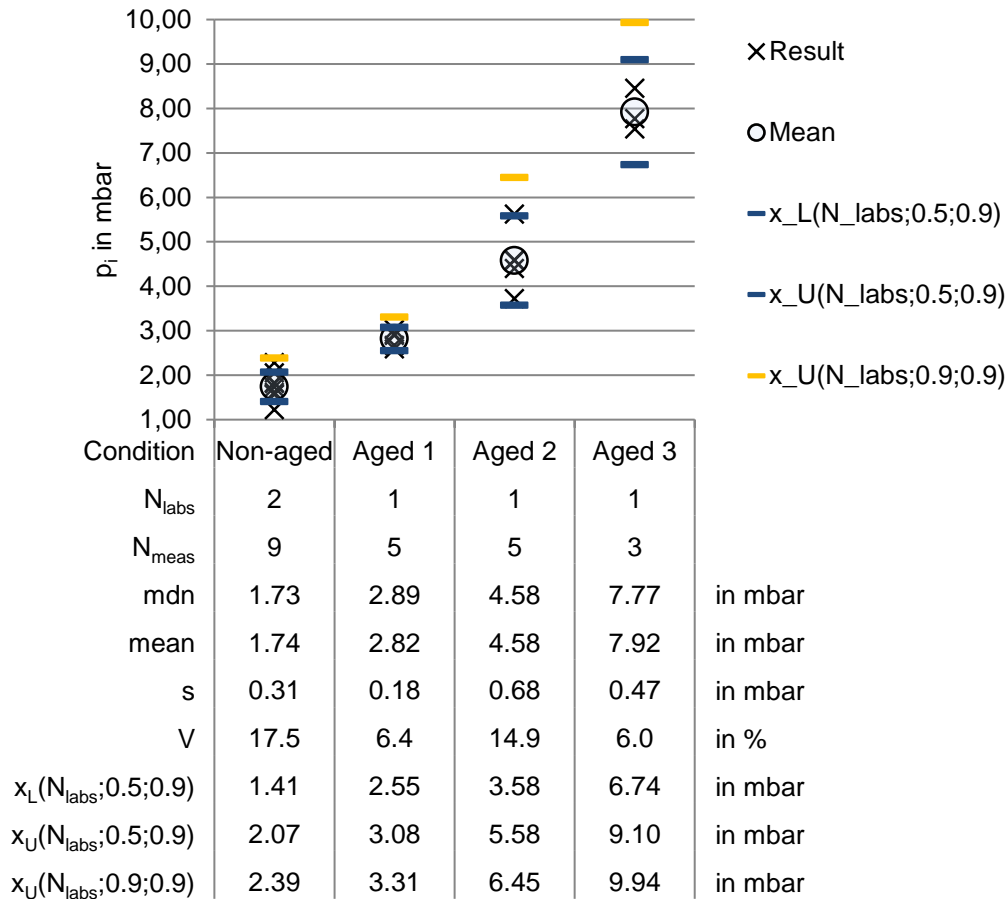| Condition	Non-aged	Aged 1	Aged 2	Aged 3	
N_{labs}	2	1	1	1	
N_{meas}	9	5	5	3	
mdn	1.73	2.89	4.58	7.77	in mbar
mean	1.74	2.82	4.58	7.92	in mbar
s	0.31	0.18	0.68	0.47	in mbar
V	17.5	6.4	14.9	6.0	in %
$x_L(N_{labs};0.5;0.9)$	1.41	2.55	3.58	6.74	in mbar
$x_U(N_{labs};0.5;0.9)$	2.07	3.08	5.58	9.10	in mbar
$x_U(N_{labs};0.9;0.9)$	2.39	3.31	6.45	9.94	in mbar

Figure 59: Results of internal pressure determination of material VIP 1.

Table 14: Parameters of linear regression of internal pressure (p_i) as a function of ageing time for material VIP 1.

$p_i = m \cdot t + b$		
m in mbar/a	**b** in mbar	**R²**
12.417	1.71	1.00

Table 15: Parameters of linear regression of thermal conductivity (λ) as a function of internal pressure p_i for material VIP 1.

$\lambda_{10°C} = m \cdot p_i + b$		
m in mW/(m K mbar)	**b** in mW/(m K)	**R²**
0.165	4.3	0.95

3.3.3.2 Results of internal pressure for material VIP 3

The material VIP 3 was measured by three labs, both for the Non-Aged and Aged steps (Figure 60). The standard deviation with values in between 0.2-0.5mbar is comparable to the spreading of data for VIP 1 (Table 16 and Table 14). In the climatic conditions of artificial ageing (50°C and 70% RH) the increase of internal pressure would be around 4.04mbar/a, around one third of the value of VIP 1 showing a well-defined regression with R^2 = 0.94. The thermal conductivity increase is 0.18mW/(m K a) (Table 17), comparable to VIP 1, however the R^2 value is lower in this case.

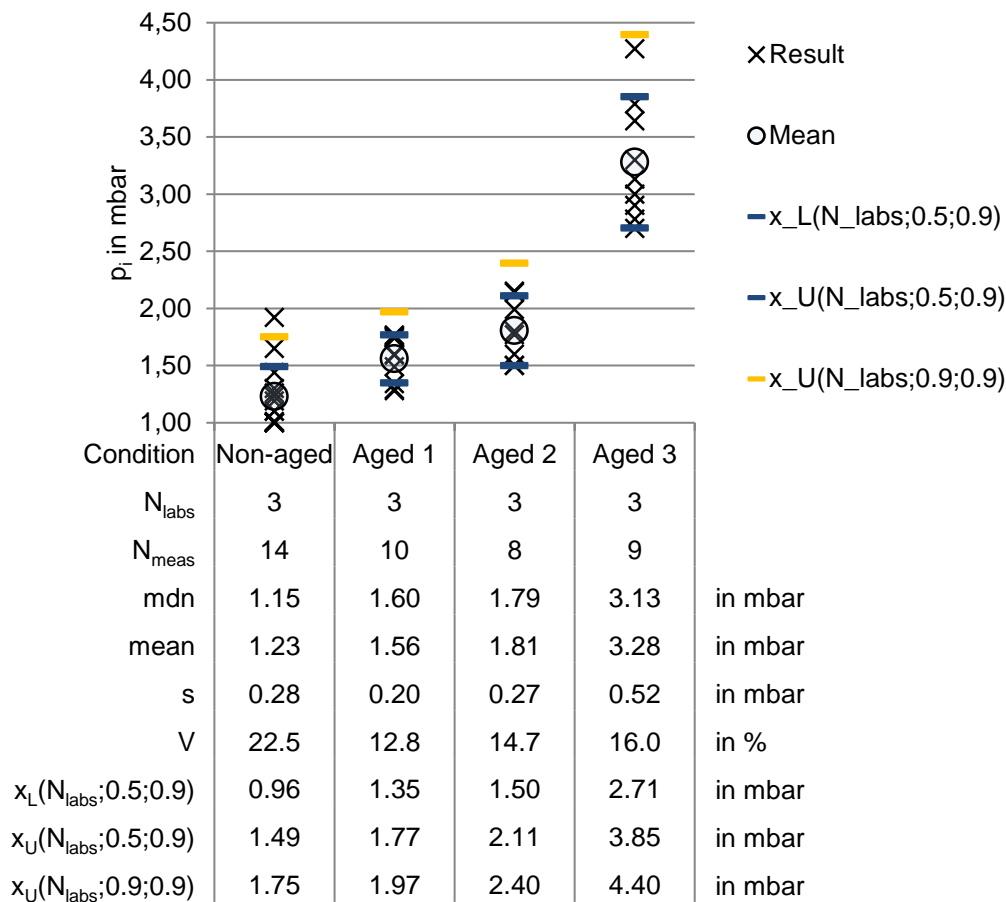| Condition	Non-aged	Aged 1	Aged 2	Aged 3	
N_{labs}	3	3	3	3	
N_{meas}	14	10	8	9	
mdn	1.15	1.60	1.79	3.13	in mbar
mean	1.23	1.56	1.81	3.28	in mbar
s	0.28	0.20	0.27	0.52	in mbar
V	22.5	12.8	14.7	16.0	in %
$x_L(N_{labs};0.5;0.9)$	0.96	1.35	1.50	2.71	in mbar
$x_U(N_{labs};0.5;0.9)$	1.49	1.77	2.11	3.85	in mbar
$x_U(N_{labs};0.9;0.9)$	1.75	1.97	2.40	4.40	in mbar

Figure 60: Results of internal pressure determination of material VIP 3.

Table 16: Parameters of linear regression of internal pressure (p_i) as a function of ageing time for material VIP 3.

$p_i = m \cdot t + b$		
m in mbar/a	**b** in mbar	**R²**
4.036	1.14	0.94

Table 17: Parameters of linear regression of thermal conductivity (λ) as a function of internal pressure (p_i) for material VIP 3.

$\lambda_{10°C} = m \cdot p_i + b$		
m in mW/(m K mbar)	**b** in mW/(m K)	**R²**
0.176	3.8	0.67

3.3.3.3   Results of internal pressure for material VIP 4

The material VIP 4 was measured by two labs in the Non-Aged stage and in subsequent Aged steps by only one lab. The spreading of test data is on a good level for the Non-aged, Aged 1 and Aged 2 step, but shows high spreading for the Aged 3 step. It is conjecturable that a mechanical damage is responsible for the high internal pressure values.

However, the obtained mean value of internal pressure for the step Aged 3 is in line with the foregoing results obtained in the Non-Aged and Aged steps, which is visible in the well-defined regression with R^2 values of 0.99 of pressure increase by time. The pressure increase by time is on a slightly higher level than for VIP 1, showing 15.5mbar/a if the panels are stored in the climatic condition of 50°C and 70% RH.

Concerning the correlation between thermal conductivity and pressure increase a well-defined linear function was obtained showing 0.14mw/(m K mbar) with an R^2 value of 0.99. Compared to VIP 1 and VIP 3 this value is on a lower level.
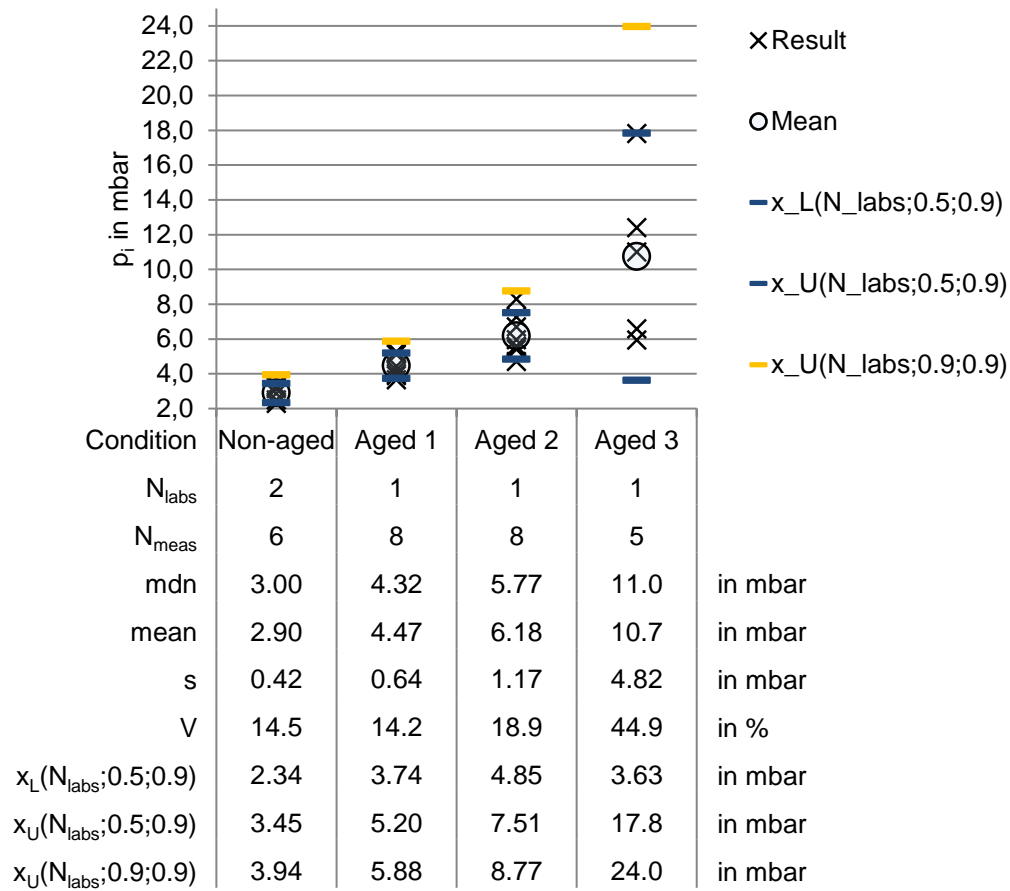
Figure 61: Results of internal pressure determination of material VIP 4.

Condition	Non-aged	Aged 1	Aged 2	Aged 3	
N_{labs}	2	1	1	1	
N_{meas}	6	8	8	5	
mdn	3.00	4.32	5.77	11.0	in mbar
mean	2.90	4.47	6.18	10.7	in mbar
s	0.42	0.64	1.17	4.82	in mbar
V	14.5	14.2	18.9	44.9	in %
$x_L(N_{labs};0.5;0.9)$	2.34	3.74	4.85	3.63	in mbar
$x_U(N_{labs};0.5;0.9)$	3.45	5.20	7.51	17.8	in mbar
$x_U(N_{labs};0.9;0.9)$	3.94	5.88	8.77	24.0	in mbar

Table 18: Parameters of linear regression of internal pressure (p_i) as a function of ageing time for material VIP 4.

$p_i = m \cdot t + b$		
m in mbar/a	**b** in mbar	**R²**
15.492	2.89	0.99

Table 19: Parameters of linear regression of thermal conductivity (λ) as a function of internal pressure (p_i) for material VIP 4.

$\lambda_{10°C} = m \cdot p_i + b$		
m in mW/(m K mbar)	**b** in mW/(m K)	**R²**
0.138	3.1	0.99

4 Characterisation of VIP Envelopes: Barrier Performance

4.1 Background of the Common Exercise with VIP Envelopes

One of the major reasons for the VIPs losing their thermal insulation performance during their lifetime is the permeation of air and water vapour through the VIP envelope (or through the barrier film) as described within the previous chapters. The lifetime and performance of the VIPs depend on the barrier properties of the laminate used as a VIP envelope. The permeation of air and water vapour into the VIP occurs through the surface of the VIP and also through the sealed region as shown in Figure 62.
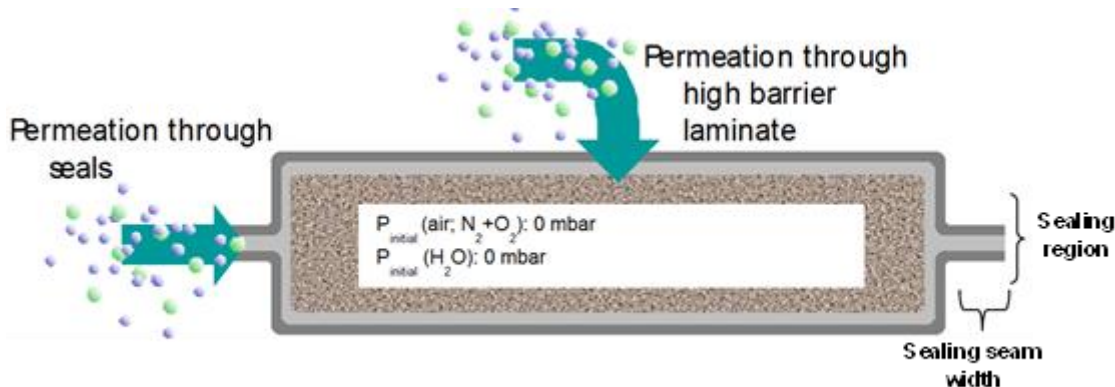
Figure 62: Schematic cross-sectional view of a "cut" VIP showing the air and water vapour permeation pathways.

The VIP envelopes are generally characterised in terms of their air and water vapour transmission rates. The film producers providing the high barrier laminates to be used as VIP envelopes by the VIP manufacturers usually report the air, or oxygen transmission rate values measured at 23°C and 50% RH and the water vapour transmission rate (WVTR) values measured at ambient conditions of 23°C and 50% RH, or at tropical conditions of 38°C and 100% RH. The reported values given in the technical data sheets of the VIP laminate manufacturers are usually the transmission rate values of the flat films. However, the barrier performances reported for flat films do not represent the transmission rates after the VIP production. Due to the evacuation processes during the VIP production, based on how the mechanical stability of the high barrier laminates is, there might be damage, especially at the corners and edges of the panel leading to the loss of the barrier performance.

In addition, the permeation through the sealing seam is not included within the transmission rate values reported for the flat films. Based on this background, a common exercise for the gas permeability and water vapour transmission rate characterisation of

VIP envelopes are performed in the framework of this Annex. The reasons for performing such a common exercise are:

- the barrier performance of VIP envelopes before and after VIP production is not comparable. It is important to understand the possible effect of the VIP production process on the gas permeability of the high barrier laminate.
- The gas permeability and WVTR values are not comparable unless all the measurement conditions are the same, such as the temperature, humidity, and the measurement duration.
- Measurement limits of the commercially available state-of-the-art devices used for the permeability measurement of the flat films are not sufficient to report the exact values, in some cases the transmission rates of the flat films are below the measurement limit of the commercially available devices. Also outgassing mechanisms can lead to incorrect values of the steady state permeation rate.
- There is also a limitation of the measurement capacity, when using commercially available devices for permeation measurements of flat films, each device can in general only measure two samples at the same time and in addition, it may take up to 2–3 weeks to reach the steady state transmission rate values. The determination of air and/or WVTR through the VIP envelopes into the VIPs eliminates this problem, since many VIPs can be tested at the same time.
- This kind of a common exercise shows the importance of having common standardised measurement methods and measurement conditions for the gas/water vapour permeability characterisation of VIP envelopes, after a VIP is produced.

4.2 Selected VIP Envelope Structures for Characterisation

The aim of this exercise is to show the importance of the VIP envelope characterisation before and after VIP production and the reliability of the different test procedures used at different laboratories. It is not the aim of this exercise to compare the barrier performance of various VIP envelopes. Three different VIP-laminates have been selected for this work and named as Laminate-1, Laminate-2 and Laminate-3. These laminates are commercially available ultra-high barrier laminates used for VIP applications.

The structure of Laminate-1 consists of an Aluminium film (about 6µm thick), laminated to the polyethylene terephthalate substrate and a sealing layer. Laminate-2 and Laminate-3 structures consist of either two, or three metallized polymeric substrates, laminated to each other by adhesive lamination. The adhesive is typically a two-component poly(urethane) based formulation. All three laminate structures consist of a polyolefin based sealing layer. Figure 63 shows the structure of one of these three laminates consisting of three metallized PET films (Laminate-3).

LLDPE	Al	PET	Al	PET	Al	PET
Seal layer 50µ	0.1µ	12µ	0.1µ	12µ	0.1µ	12µ

Figure 63: Structure of Laminate-3 used within this common exercise - A tri-laminate.

4.3 Experimental Characterisation

The gas permeability and the water vapour transmission rate of the selected high-barrier laminate films are characterised:

1) before the VIP production: the permeability measurements are performed using the flat films,

2) after the VIP production: the air and water vapour transmission rates through the ultra-high barrier laminate into the VIP are measured using the VIPs.

Four independent laboratories have participated to this common exercise with their measurement capabilities. Lab-1 has performed the flat film permeability measurements as discussed below in Chapter 4.3.1. Lab-2, Lab-3 and Lab-4 contributed to this exercise by characterising the laminates in VIP form and measured the air and water vapour transmission through the laminate into the VIP.

The measurement methods used for the determination of gas and water vapour permeation through the flat film and also for the gas and water vapour permeation into the panel are described in the chapters below.

4.3.1   Permeance measurements of flat films

The water vapour transmission and oxygen permeability of flat films can be determined by using the coulometric or manometric methods. Manometric methods can be used for the determination of the air and water vapour transmission rates of flat films and a detailed description of a manometric measurement method can be found in Pons et al, 2014. The measurement limit of the manometric device is 2.4×10^{-6} to 1.5×10^{-4} g/(m$^2 \cdot$d) for water vapour and 0.24 to 2.42cm^3(STP)/(m$^2 \cdot$d$\cdot$bar) for dry air[1]. However, due to several problems and breakdowns occurred during the manometric measurements for water vapour, it was not possible to provide any results for flat films with sufficient confidence during the course of this common exercise. In addition, the measurement limit of the manometric device is not sufficient for the determination of the air permeability of the laminates selected in this common exercise. Therefore, the permeabilities of the flat film laminates have been measured only using the coulometric methods in this common exercise as discussed below.

---

[1] A range is given mainly due to the variations of the upstream pressure and the possibility of the extrapolation to lower temperatures.

4.3.1.1 Water vapour transmission rate measurements by coulometric method

The coulometric measurements are performed according to DIN EN ISO 15106-3:2005 for water vapour on flat film (as produced, without any mechanical stress). AQUATRAN™ Model 2 is a commercially available measurement device used for these measurements, available from the company Mocon®. The detection limit is $5 \times 10^{-5} g/(m^2 \cdot d)$. Temperature range is up to 40°C, controlled relative humidity testing is up to 90%. The detection limit of the device is sufficient for the determination of moisture permeation through the flat VIP-laminates.

In the device, the measurement cell is divided by the sample into two chambers. In one chamber, constant relative humidity and temperature are maintained. The second chamber is purged using a carrier gas (dry nitrogen), which guides the permeated water molecules to a coulometric sensor (Figure 64). The sensor itself is based on phosphorous pentoxide (P_2O_5) coated electrodes. The P_2O_5 absorbs all incoming water molecules, which are then electrolyzed by a voltage across the electrodes. Therewith, an electrical current between the electrodes is induced that is measured and used to calculate the WVTR (Mocon, 2014).
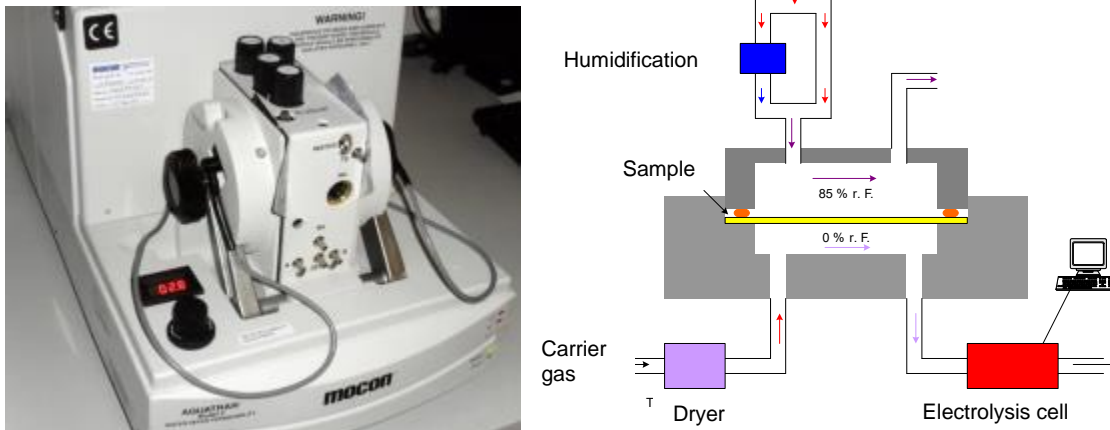

Figure 64: Left: Mocon® AQUATRAN™ Model 2; right: schematic view of measurement principle.

In this common exercise, the water vapour transmission rate (WVTR) measurement by the Mocon® Aquatran™ Model 2 (AQUATRAN) was performed at 40°C and 90% RH. The samples were pre-conditioned in a climate chamber for about 2 days at 60°C and at 0.5mbar before inserting them into the measurement cells. At least 2 samples were measured for each laminate type.

The measurement can be stopped once the measurement value varies less than 1% of the mean of the last five measurement values. In this exercise, the measurement times used for the laminates were about 500 hours at 40°C and 90% RH.

4.3.1.2 Oxygen permeability measurements by coulometric method

The measurements are performed according to DIN 53 380, T3 for oxygen permeability. Mocon® Oxtran® Model 2/21 (Oxtran) is a commercially available instrument from the company Mocon®. A photo and a schema are depicted in Figure 65. The detection limit of the measurement device is $5 \times 10^{-3} cm^3(STP)/(m^2 \cdot d \cdot bar)$. Temperature range is up to 40°C, controlled relative humidity testing is up to 90%. The measurement principle is similar to the AQUATRAN's principle as discussed above. The sensor consists of a graphite cathode and a porous cadmium anode. The permeated oxygen is transported by the nitrogen carrier gas to the sensor and absorbed in the cadmium anode, where it reacts with the Cadmium. The oxidation of the cadmium anode creates an electrical current, which can directly be converted into the oxygen permeability.

In this common exercise, the oxygen permeability of the flat films was measured at the ambient conditions of 23°C and 50% RH. The measurement was stopped once the measurement value variation from the mean of the last five measurements was less than 1%.
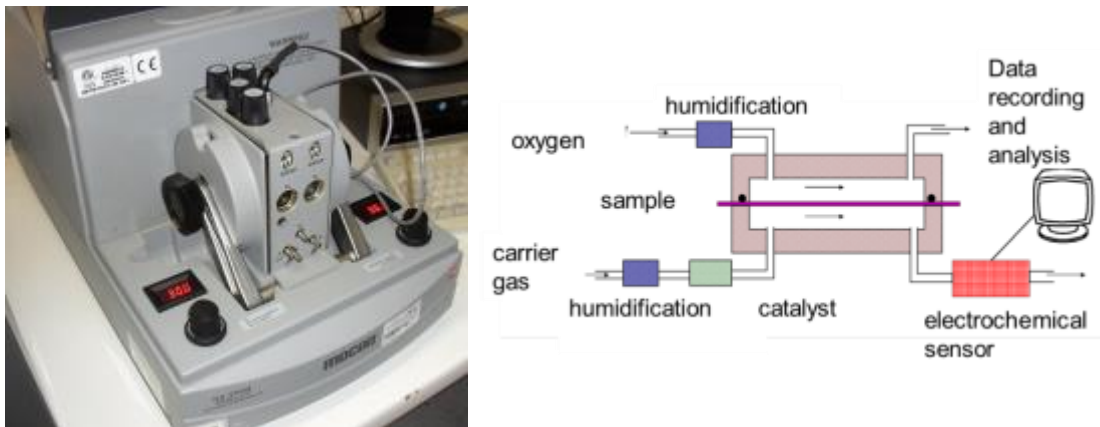

Figure 65: Left: Oxtran® Model 2/21; right: schematic view of measurement principle.

It has to be mentioned here that the Oxtran measures the oxygen permeability of a flat laminate. For the VIP applications, the air permeation or nitrogen permeation measurements would be a more relevant value for the barrier performance of the films since the air contains mainly nitrogen. Detailed test descriptions for air transmission rate measurements are discussed in the next sections.

4.3.2 Permeation measurements through the VIP envelope

The permeation measurements of water vapour and air through the VIP envelope are described in Sections 4.3.1.1 and 0, respectively. The measurement principles and procedures for all these techniques are described also in (Shufer, 2017). The procedure used for the air transmission rate measurements using the so-called lift-off measurement technique is described in Section 4.3.2.3 (Simmler and Brunner, 2005).

4.3.2.1 *Water vapour transmission rate measurements by water intake (gravimetric) technique*

This technique determines the water vapour transmission rate (WVTR) through the VIP envelope after the VIP production. The procedure starts with the preparation of small fibre glass (FG) core based panels (~15 cm x 12 cm x 5 mm) with desiccant inside (Lab-2) or larger panels (≥ 30 cm x 30 cm x 10 mm) (Lab 3) using the inspected film (Figure 66, left). The panels are weighed using an analytical or micro-balance (Figure 66, right), and then held in a humidity oven.

Figure 66: Small panel (~15 cm x 12 cm) with glass fibre and desiccant (left); weighing the panel with an analytic balance (right) (Shufer, 2017).

The storage conditions in the humidity oven used during this common exercise are listed in Table 20 **Erreur ! Source du renvoi introuvable.**- Lab-2 and Lab-4 performed the measurements at two different conditions. Lab-3 performed the measurements at five different conditions, which enables the calculation of the Arrhenius parameters of the laminates to be able to predict the WVTR at any temperature and humidity conditions needed.

Table 20: The VIP storage conditions (temperature (T) and humidity (% RH)) of the oven used by the laboratories during the water intake measurements.

Measurement Conditions: T and (% RH)	Laboratories		
	Lab-2	Lab-3	Lab-4
23 ºC / 50 % RH		x	
40 ºC / 90 % RH	x	x	x
50 ºC / 70 % RH	x	x	x
70 ºC / 50 % RH		x	
70 ºC / 3 % RH		x	

The panels are weighed once a week for about 1 to 2 months by Lab-2 and every month[2] or more for 1 to 12 months by Lab-3. The mass gain during this period is caused by the water molecules permeating. Additionally, the moisture vapour pressure inside is kept very low along the entire duration of the tests, because the water molecules are absorbed by the desiccant. The water permeation rate is about 1000 times faster than the permeation rate of air. Therefore, the contribution of the weight gain of air permeation is negligible. At the end of the test period, the WVTR of the panel is calculated by dividing the mass gain by the duration time at steady state conditions and the area of permeation.

The main advantages of the Water Intake (WI) technique are its low detection limit (due to longer test duration) and the realistic values achieved due to testing at an application level. The detection level of the WI test is around 0.002 $g/(m^2 \cdot d)$ depending on the panel dimensions and on the duration of the test.[3]

The results obtained include the contribution of the water vapour transmission through the film surface and the sealing seam. Since the relative importance of the water side permeation through the sealing seam is quite negligible with metallized laminates (Laminate-2 and Laminate-3 of this work), it can be considered that the measured WVTR is mainly due to the water vapour permeation through the surface perpendicular to the laminate. The permeation rate through the Al foil-based laminates is too small to be detected by the WI technique (Laminate-1).

---

[2] Test frequency is chosen ≥ 1 month to minimise the drying time used for temperature stabilisation when the VIP samples are taken out of the chamber for weight measurements.

[3] Typically 0.002 and 0.0005 $g/(m^2 \cdot d)$ for 3 and 12 months of measurements, respectively.

4.3.2.2 Air transmission rate measurements using VIP thermal conductivity change as a function of time

The air transmission rate (ATR) through the VIP envelope is measured using the evacuated fibreglass (FG) core-based panels according to the following procedure:

1) A 30 cm x 30 cm, 3-seal bag using the sealing machine shown in Figure 67 **Erreur ! Source du renvoi introuvable.**is produced.

Figure 67: Heat-sealing machine.

2) An FG core with a known dependency of thermal conductivity on gas pressure plus desiccant is inserted into the bag (after being baked at 150°C for more than 2 hours) (Figure 68).

Figure 68: VIP before evacuation.

3) The panel is evacuated to a pressure lower than 0.01 mbar, and the open (fourth) edge is sealed (see Figure 69).
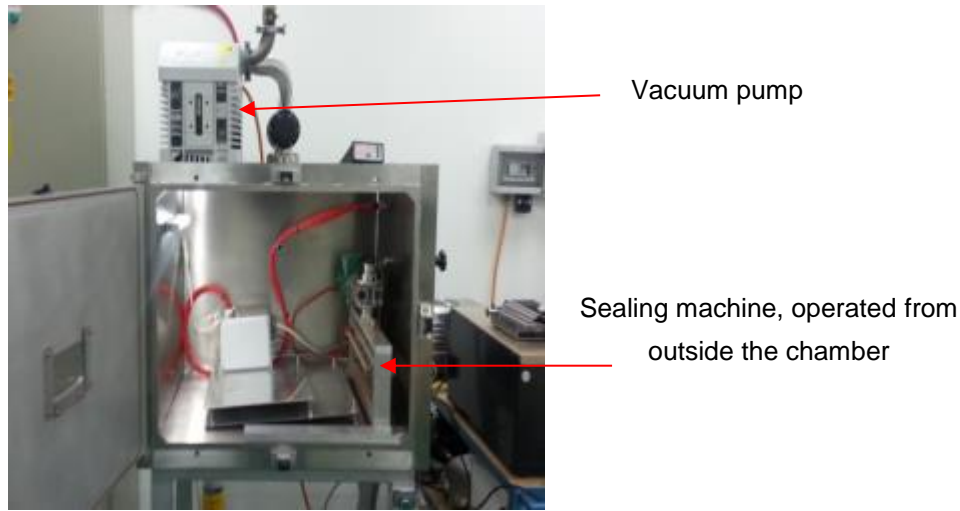

Figure 69: Vacuum chamber.

4) After preparation, the panels are stored at different temperatures and relative humidity levels, and their thermal conductivity is measured frequently using a Laser Comp thermal conductivity measurement device (Laser Comp FOX314), over a long period of time. The temperatures of the plates used for the measurements were 10 °C, and 35 °C in this study. The storage conditions of the panels in this common exercise are listed in Table 21. The thermal conductivity of each panel is measured over at least 3 months.

Table 21: The VIP storage conditions (temperature (T) and humidity (RH %)) of the oven used by the laboratories during the air transmission rate measurements.

T and RH%	Laboratories	
	Lab-2	Lab-4
23°C / 50%RH	x	x

The pressure is then calculated from the measured values of thermal conductivity using the known thermal conductivity versus pressure curve of the FG core (Reichenauer et al., 2007), enabling a very accurate assessment of internal pressure increase along the storage time (Shufer, 2017). The procedure for finding the known thermal conductivity versus pressure curve for the FG core is described in Section 4.4.3 in detail. The internal pressure increase is only due to the air, because the desiccant keeps the water pressure increase negligible.

5) In the final stage, the air transmission rate (cm^3(STP)/(m^2·year)) of the laminate for a given temperature is calculated using the calculated pressure increase rate and the panel dimensions (width, length and thickness). The calculation gives the amount of air (cm^3(STP)) permeating through the envelope of a 1 m^2 panel within a year.

It needs to be considered that a VIP panel is always encapsulated by a VIP laminate material at least twice of its area (VIP area is calculated by multiplication of its length by its width). It is important here to pay attention to the unit given for the air transmission rates. The commonly given oxygen permeability (permeance) values in the technical data specification sheets for VIP laminates are usually for flat films, and the given values have the unit of $cm^3(STP)/(m^2 \cdot day \cdot bar)$. This value is not for a 1 m^2 sized VIP, but for the 1 m^2 of the VIP laminate.

4.3.2.3 Air transmission rate measurements using lift-off method

Assessing the air[4] permeance, Q_{air} (or Π_{air}) into VIPs requires to determine the air amount inside the VIP (n) after an exposure time ensuring the steady state:

$$Q_{air} = \frac{dn}{dt} \cdot \frac{1}{\left(P_{a,ext} - P_{a,int}\right) \cdot A} \qquad (7)$$

n a mass, a volume or a number of moles,

$P_{a,int}$ air pressure within the VIP

$P_{a,ext}$ external air pressure

A surface area of the VIP laminate

t time

One of the methods to determine n is the direct measurement method by chemical or physical analysis, such as mass spectrometry, which is not so common and easy. Another method is based on the measurement of the internal pressure of the VIP, $P_{t\ int}$, which is equal to the sum of the partial pressures of air $P_{a\ int}$ and water $P_{w\ int}$, and on the assessment of the partial pressure of water $P_{w\ int}$. Therefore, the air pressure is:

$$P_{a,int} = P_{t,int} - P_{w,int} \qquad (8)$$

1) To measure the total internal pressure; the well-known method of the lift-off of the envelope (Figure 70) is the most popular, while internal sensors could also be used.
2) To determine the water pressure; the usual way is to measure the weight gain, Δm_w, assumed to be only due to water and then to report this value on the water vapour adsorption isotherm of the core in order to find the equilibrium pressure $P_{w,int}$ (Figure 71).

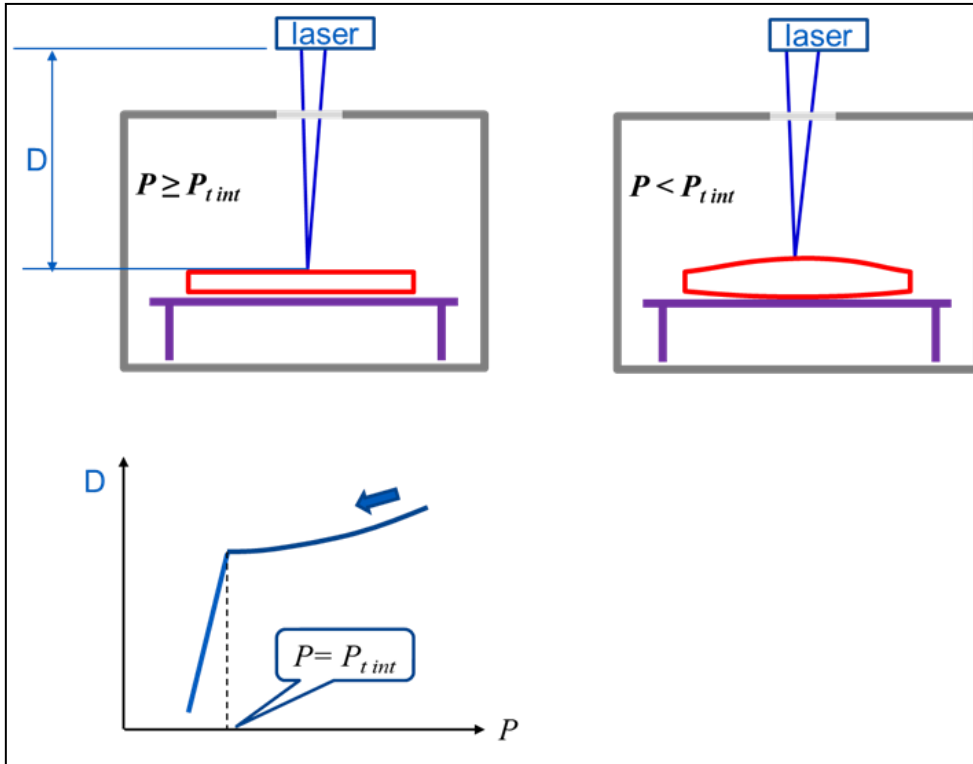[4] In this chapter "air" means dry air

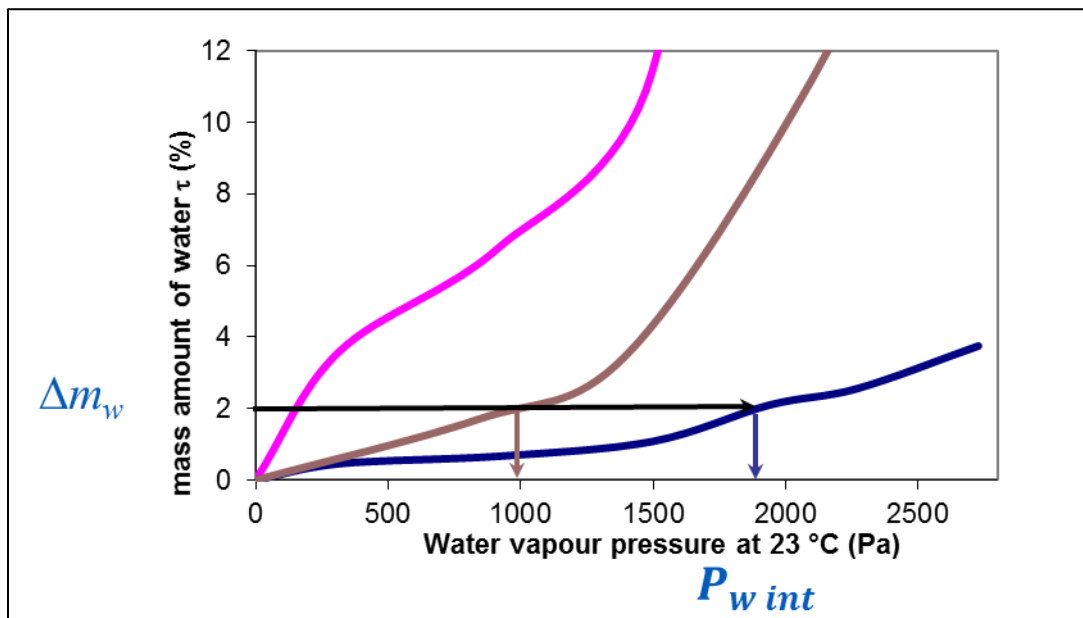Figure 70: Principle of the lift-off method. Description of the lift-off method can be found in Annex 39.

Figure 71: Examples of the determination of the water vapour pressure inside a VIP knowing the weight gain and the isotherms of different cores.

Finally, the air permeance, Q_{air} (or Π_{air}), is calculated by:

$$Q_{air} = \frac{dP_{a\,int}}{dt} \cdot \frac{V_{pores}}{R \cdot T \left(P_{a,ext} - P_{a,int}\right) \cdot A} \tag{9}$$

expressed in mol·m^{-2}·s^{-1}·Pa^{-1} , or the same expression multiplied by the molar mass of air, having the unit in kg·m^{-2}·s^{-1}·Pa^{-1}, or by the molar volume having the unit cm^3 (STP)·m^{-2}·s^{-1}·Pa^{-1}.

The difficulties of this test methodology are:

- Even if the measurement of the weight gain is quite easy at the laboratory scale, it could not be realistic with panels from the field, because of glue or facings on them.
- Knowing the water vapour adsorption isotherm for different cores is not so simple (see the difficulties listed in Yrieix et al., 2014).
- Most of the time, the accuracy is not very good, due to the low slope of the water isotherm in Henry's domain (typically for a classical new fumed silica-based core, the slope is low: $7\mu g_W/(g_{SiO2}\cdot Pa)$, as shown by the blue curve in Figure 71.
- Furthermore, for any core type which ages, like silica, we need to know the isotherm, corresponding to the real state of the core, because the hydrophilicity and thus the pressure changes a lot (Yrieix et al., 2014).

These numerous difficulties lead EDF Research and Development Department to develop a new method for the determination of the air pressure inside the VIP, which is called as "cold lift-off method". This method is as described below:

The cold lift-off method

The principle is to perform the lift-off at very **low temperature** that is the temperature where the saturation pressure of water, P_{sat}, is lower than the needed accuracy on the pressure (Figure 72). In this case, the partial pressure of air can be approximated by the total internal pressure. The air pressure must then be converted at room temperature and Equation (9) is used to determine the air permeance (air permeability) through the VIP envelope into the VIP.

Single measurement option

A single measurement at low temperature, T, gives the air pressure.

Typically at $T < -20$ °C, P_{sat} for water vapour is less than 1 mbar, then $P_{a\,int}$ is about $P_{t\,int\,@\,T<-20°C}$.

As for the classical lift-off method the true volume of pores must be used:

$$V_{pores} = V_{total\,@\,Pt} - \frac{m_{core}}{\rho_s} \tag{10}$$

m_{core} and ρ_s are the mass and the skeleton density of the core ($\sum \frac{m_i}{\rho_{0i}}$, if the core contains several constituents).
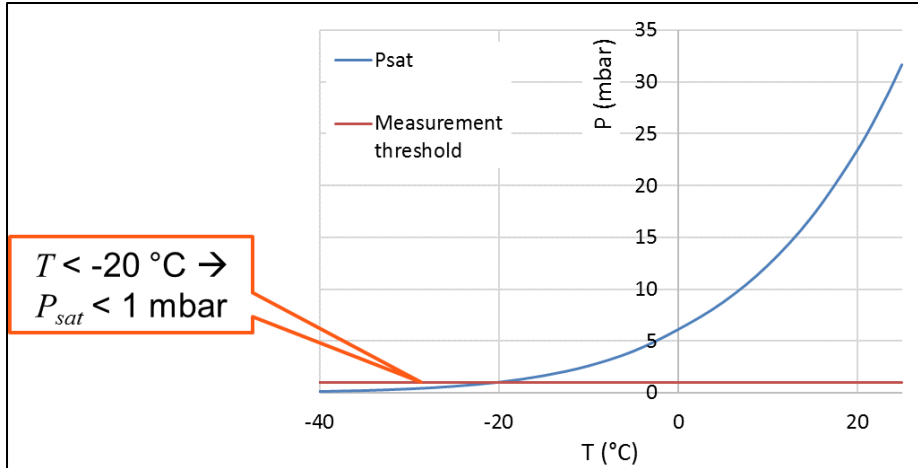

Figure 72: Principle of the cold lift-off method.

$V_{total\,@\,Pt}$ is the total volume of the VIP at the equilibrium pressure classically obtained by the dimensions of the VIP core at atmospheric pressure. In this present method, the mechanical behaviour of the core and the expansion of the volume due to the decrease of the pressure are considered:

For the silica based cores a linear elastic behaviour is observed (Figure 73),

$$V_{total\,@\,Pt} = V_{total\,@\,Patm} \cdot \left(1 + \frac{P_{atm} - P_{t\,int}}{E}\right)^3 \tag{11}$$

where E *is* the Young modulus of the core.

For other cores, which show elastic non-linear behaviour like fiberglass core (Figure 74), one can try without guaranty of success;

$$V_{total\,@\,Pt} = V_{total\,@\,Patm} + L.\,l.\,\Delta d/3 \tag{12}$$

where L, l, and Δd are the length, the width and the height of the lift-off, respectively. A suitable identification of the mechanical behaviour is encouraged. The aim of such identification is to link the total volume inside the envelope to the mechanical load of the core due to the pressure change.

It is important to note that the lift-off method can be used without any problems for the VIPs with silica cores (Figure 73**Erreur ! Source du renvoi introuvable.**), which exhibit a linear elastic quasi isotropic behaviour. More or less the same behaviour is observed for cellular foam. On the other hand, there are still problems for the VIPs with fiberglass

cores (**Erreur ! Source du renvoi introuvable.**); this seems to be due to the spring back of the fibres, which tends to lift-off the film continuously all across the pressure range; practically this hides the detachment of the film from the core.

Unlike the standard method, as the pressure is measured at low temperature, a final correction is needed to obtain the air pressure at room temperature:

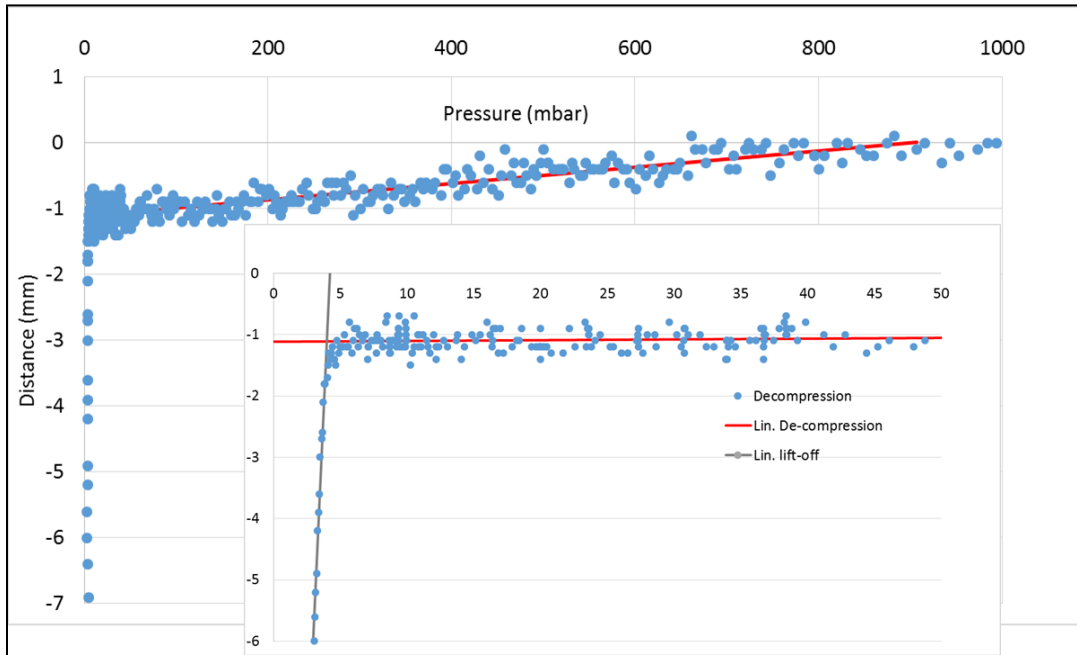$$P_{a\,int@23\,°C} = P_{t\,int@\,T<-20°C}\,\frac{(23+273)}{(T+273)} \tag{13}$$

Figure 73: Lift-off behaviour of a silica core VIP.
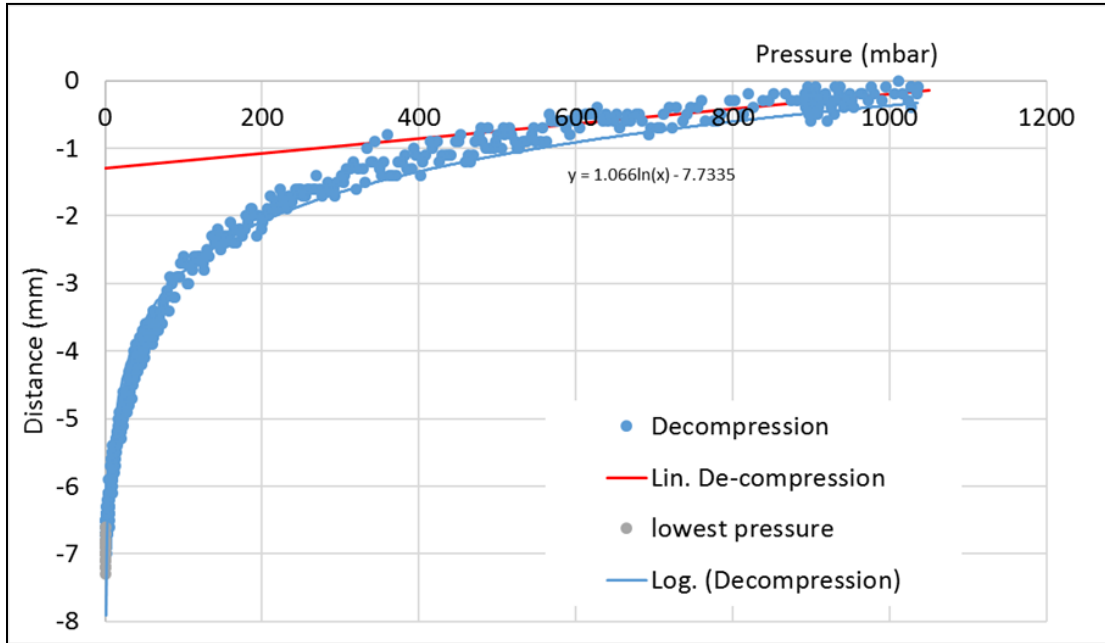
Figure 74: Lift-off behaviour of a fiberglass core VIP (corresponding to Laminate-1 of this common exercise, aged for 197 days at 70 °C and 50 % RH, measured at -38 °C).

Multiple measurements option

Another way to use this concept is to consider the whole behaviour of the pressure inside the VIP through a wide range of temperature (as shown in Figure 75).

$$P_{t\ int\ (T)} = P_{w\ int\ (T)} + P_{a\ int\ (T)} \tag{14a}$$

$$P_{a\ int\ (T)} = \frac{n_a . R . T}{V_{Pores}} \tag{14b}$$

where $P_{w\ int\ (T)}$ and $P_{a\ int\ (T)}$ are the partial pressure of the water and air, and R the perfect gas constant, and V_{Pores} is given by equations 10, 11, and 12.

$$P_{t\ int} = P_{a\ int} + P_{w\ int}$$

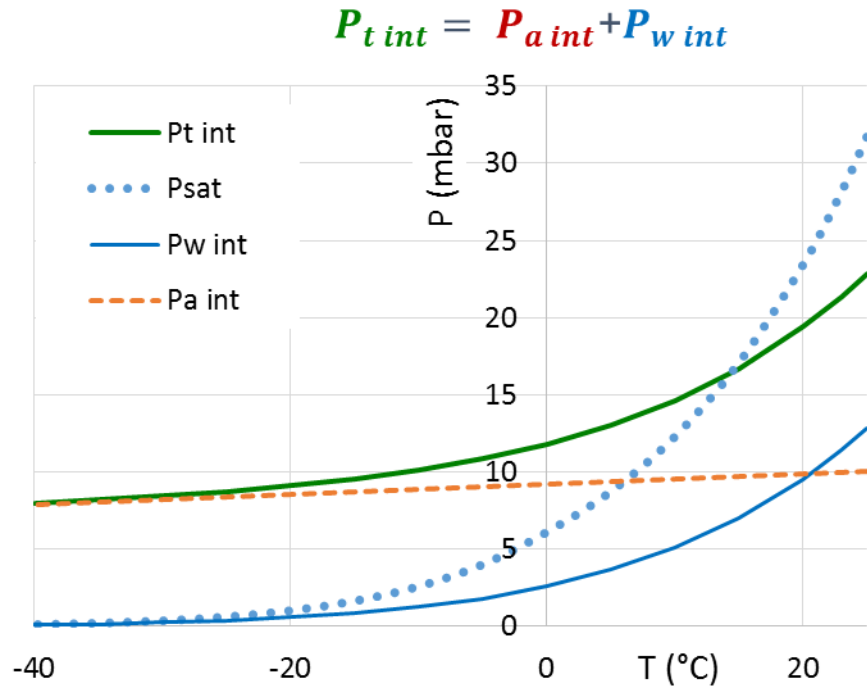Figure 75: Schematic behaviour of the internal pressure as a function of the temperature for a VIP where the partial pressures at room temperature for air and water are respectively 10 and 12 mbar.

The air pressure decreases with the temperature according to the perfect gas law.

The water pressure evolution with the temperature depends on the hygric behaviour of the core. In the general case the partial pressure of water depends not only on the temperature but also on the water sorption isotherm which describes the equilibrium between the two kinds of water inside the VIP: vapour and adsorbed water. The total amount of water $n_{W\ total}$ inside the VIP is the sum of chemisorbed ($n_{W\ Chemi}$), physisorbed ($n_{W\ Physi}$) and vapour (n_{WV}) amounts (equation 14c):

$$n_{W\ total} = n_{W\ Chemi} + n_{W\ Physi} + n_{WV} \tag{14c}$$

If large chemisorption occurred, or if the VIP includes a desiccant, or if the core is non-hygroscopic (negligible amount of water adsorbed) only the water vapour amount n_{WV} should be considered for pressure purpose.

$$P_{w\ int\ (T)} = min\left(\frac{n_{WV}.R.T}{V_{Pores}}; P_{sat\ (T)}\right) \tag{14d}$$

If the core has negligible chemisorbed water the total amount of water is split between the adsorbed water and the vapour (Equation 14e);

$$n_{W\ total} = F_{Isotherm\ (P_w,T)} + n_{WV\ (P_w,T)} \tag{14e}$$

with $F_{Isotherm\ (P_V,T)=n_{W\ Physi}}$ the water vapour isotherm function which gives the amount of water as a function of the partial water vapour pressure P_W and the temperature T, for example the GAB model (Guggenheim-Anderson-de Boer). As the two terms of Equation 14e are only dependent of P_W and T, one can find the total amount of water inside the VIP.

The function F has to be simple enough to allow hypotheses without fine characterization of the core, and accurate enough to describe the temperature dependant partitioning of water, namely the condensation due to the decrease of the saturation pressure with the decreasing temperature. A Henry function (Equation 15a) was found to be convenient, of course very simple but close enough to give a good approximation of the water content obtained on known cases as shown below.

$$\theta = K.P_w \quad or \quad \theta = K_0.e^{\frac{Q_{st}}{R.T}}.P_w \tag{15a}$$

Where

$\theta = \frac{\tau}{\tau_{max}}$ is the fractional advancement of adsorption with τ the adsorbed water content $\tau = \frac{n_c.M}{m_{core}}$ with M the water molar mass and m_{core} the core mass; τ_{max} the water content at saturation.

K (Pa^{-1}) is the adsorption equilibrium constant, which characterize the adsorbate-adsorbent system: $K = K_0.e^{\frac{Q_{st}}{R.T}}$ with Q_{st} the isosteric heat of adsorption and R the perfect gas constant (8.314 J/(mol.K)).

So Equation 14e becomes Equation 15b and gives the water pressure inside the VIP as a function of the temperature (Equation 15c).

$$n_{wt} = \frac{P_w.V_{pores}}{R.T} + \frac{P_w.m_{core}.\tau_{max}.K_0.e^{\frac{Q_{st}}{R.T}}}{M} \qquad \text{(mol)} \tag{15b}$$

$$P_{w@T} = \frac{n_{wt}}{\left(\frac{V_{pores}}{R.T} + \frac{m_{core}.\tau_{max}.K_0}{M} e^{\frac{Q_{st}}{R.T}}\right)} \qquad \text{(Pa)} \tag{15c}$$

Values of K_0 and Q_{st} can be found from literature. For water – silica gel: $\tau_{max}.K_0 = 2$ to $5 \cdot 10^{-12}$ Pa^{-1} ; $Q_{st} = 2490\ kJ/kg$ = 45 kJ/mol. For fumed silica our own measurements on the Aerosil®200 give Q_{st} = 34.5 kJ/mol, while fitting the saturation pressure with Equation 15 gives $K_0 = 8.18 \cdot 10^{-12}$ Pa^{-1} ; Q_{st} = 43.3 kJ/mol.

Finally, the input data in this model are partly the same as for single measurement option: dimensions, mass, skeleton density and Young's modulus of the core, and partly describing the adsorption isotherm: the water content at saturation, the slope of the normalized isotherm and the isosteric heat of adsorption. Afterwards it's easy to numerically identify the two unknown parameters n_a and n_{wt} (equation 15) by minimising

the error function between the model and the measurements performed at different temperatures. So, thanks to equation 9 the dry air permeation is obtained.

Compared to the single temperature measurement option, the multiple temperatures option is more robust, because it allows verifying each measurement regarding the whole behaviour. Measurements between -20 °C and room temperature are also useful. This is especially a nice possibility if the used vacuum chamber doesn't have the capability to reach enough cold temperatures. An example on a fumed silica core is given in Figure 76
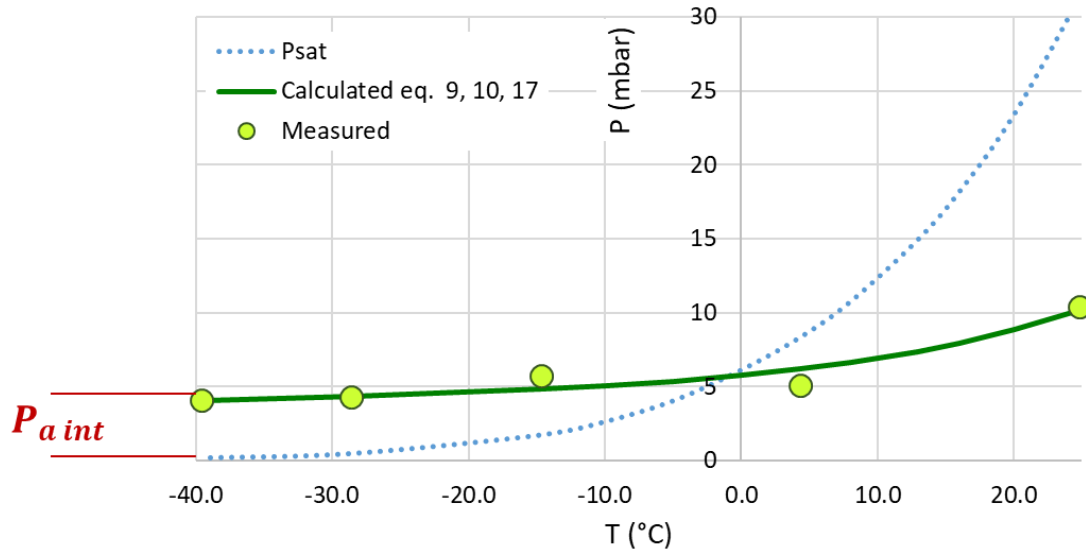

Figure 76: Example of the multiple measurements option of the cold lift-off method, comparison between matched calculation and measurements

4.4 Results and Discussion

4.4.1 Test methods used for transmission rate measurements during this common exercise – A summary

The test methods and conditions used by the four laboratories for the determination of the water vapour transmission rate (WVTR) through the flat films and through the VIP envelopes into the VIPs are listed in Table 22 and

Table 23, respectively.

Table 22: WVTR measurement conditions used for the flat films by coulometric method.

Laboratory	Test Method	Measurement conditions
Lab-1	MOCON® Aquatran™ Model 2 Water vapour transmission rate measurement limit: $5x10^{-5}g/(m^2 \cdot d)$	40°C / 90% RH

Table 23: WVTR measurement conditions used for VIPs by water intake (gravimetric) technique.

Laboratory	VIP core material & VIP dimensions	Measurement conditions
Lab-2	Fibreglass (FG) core and desiccant (~150mmx120mmx5mm)	40°C / 90% RH 50°C / 70% RH
Lab-3	Fibreglass (FG) core and desiccant (~400mmx400mmx13mm)	23°C / 50% RH 50°C / 70% RH 70°C / 50% RH 70°C / 3% RH
Lab-4	Fibreglass core (FG) and desiccant (~400mmx400mmx20mm)	50°C / 70% RH

The test methods and conditions used for the determination of the O_2 permeability of the flat films are given in Table 24 and for the air transmission rate (ATR) through the VIP envelopes into the VIP are listed in Table 25.

Table 24: Oxygen permeability measurement conditions used for the flat films by coulometric method.

Laboratory	Test Method	Measurement conditions
Lab-1	MOCON® OX-TRAN® O_2 permeability Measurement limit: $5x10^{-3}cm^3$ (STP)/($m^2 \cdot d \cdot bar$)	23°C / 50% RH

Table 25: ATR measurement conditions used for VIPs (transmission through the VIP envelope into the VIP).

Laboratory	Test Method	VIP core material & VIP dimensions	Measurement conditions
Lab-2	VIP thermal conductivity change as a function of time	Fibreglass core (FG) and desiccant (~300mm x 300mm x 6.5mm)	23°C / 50% RH
Lab-3	Cold lift-off	Fibreglass core (FG) and desiccant (~400mm x 400mm x 13mm)	23°C / 50% RH 50°C / 70% RH 70°C / 50% RH 70°C / 3% RH
Lab-4	VIP thermal conductivity change as a function of time	Fibreglass core (FG) and desiccant (~400mm x 400mm x 20mm)	23°C / 50% RH

4.4.2 WVTR results for flat films and VIP envelope

4.4.2.1 Flat films

Figure 77 shows the WVTR values measured at 40°C and 90% RH by Lab-1 for Laminate-2 and Laminate-3 using the AQUATRAN measurement device. The average steady state values were $1.5 \times 10^{-2} g/(m^2 \cdot d)$ and $2.1 \times 10^{-2} g/(m^2 \cdot d)$ after 450 hours of measurement time for Laminate-2 and Laminate-3, respectively. It was not possible to detect the WVTR of Laminate-1 as flat film, because its WVTR value is below the measurement limit of the AQUATRAN measurement device, which is $5 \times 10^{-5} g/(m^2 \cdot d)$.
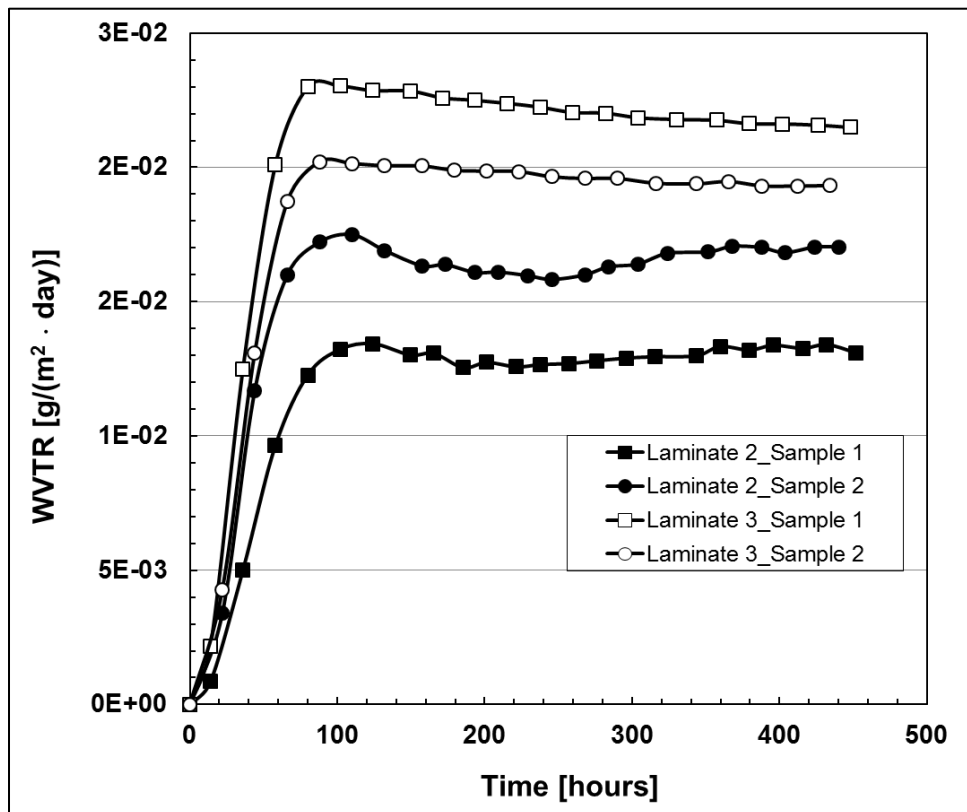
Figure 77: WVTR in g/(m²·d) as a function of the measurement time in hours for flat films of Laminate-2 and Laminate-3 at 40°C and 90% RH by AQUATRAN at Lab-1.

4.4.2.2 VIPs

Figure 78 shows the WVTR values measured at 40°C and 90% RH by Lab-2 for Laminate-2 and Laminate-3 using the water intake (gravimetric) technique. The mass increase rate (Δm in g/day) is calculated from the slope of the measured mass increase versus time curves as shown in Figure 78. The calculated slope (Δm) is then divided by the VIP total surface area to calculate the WVTR of the envelope. The average calculated values for Laminate-2 and Laminate-3 are given in Table 26.

Figure 78: Water intake tests for the VIPs prepared using Laminate-2 and Laminate-3 as VIP envelope, measured at 40°C and 90% RH by Lab-2.

Table 26: WVTR values calculated from water intake measurements on VIPs (Lab-2 results).

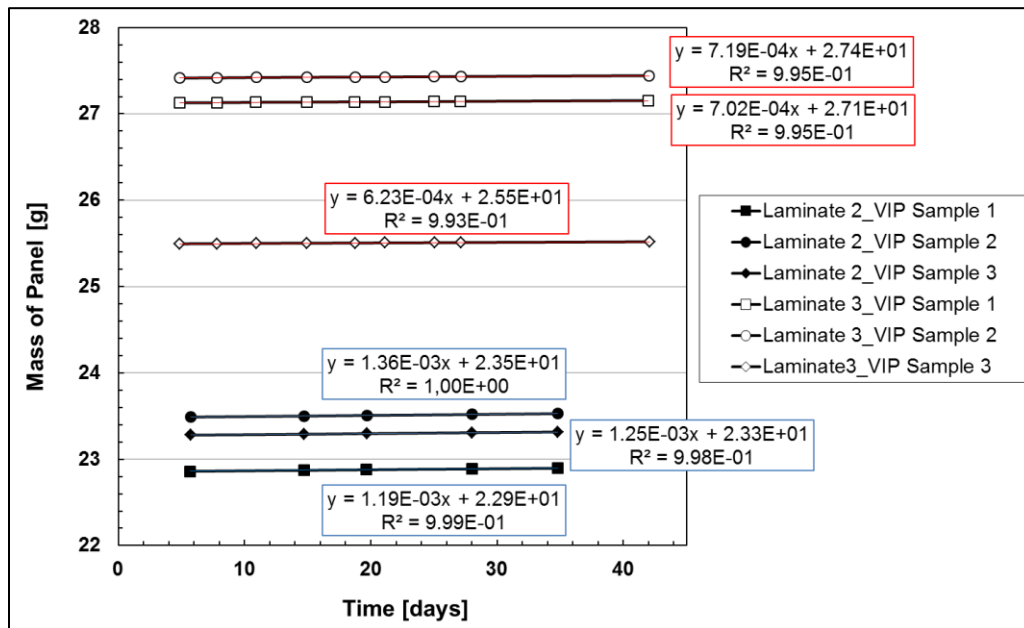| Sample Type	VIP Surface Area in m²	Mass increase (Δm) in g/day	WVTR in g/(m²·d)
Laminate-2: VIP Sample 1	3.30×10^{-2}	1.19×10^{-3}	3.6×10^{-2}
Laminate-2: VIP Sample 2	3.34×10^{-2}	1.36×10^{-3}	4.1×10^{-2}
Laminate-2: VIP Sample 3	3.34×10^{-2}	1.25×10^{-3}	3.7×10^{-2}
Average WVTR in g/(m²·d) for Laminate-2			3.8×10^{-2}
Laminate-3: VIP Sample 1	4.03×10^{-2}	7.02×10^{-4}	1.7×10^{-2}
Laminate-3: VIP Sample 2	4.16×10^{-2}	7.20×10^{-4}	1.7×10^{-2}
Laminate-3: VIP Sample 3	3.60×10^{-2}	6.23×10^{-4}	1.7×10^{-2}
Average WVTR in g/(m²·d) for Laminate-3			1.7×10^{-2}

Three VIP samples were prepared from each type of the laminate as shown in Table 26. The deviation between the measured WVTR values for the three VIP samples is negligible. It has been shown in this common exercise that the water intake (gravimetric) technique is an accurate and repeatable test for the determination of WVTR properties of the laminates under the given conditions (temperature and humidity).

Table 27: Comparison of WVTR in g/(m²·d) results obtained by four independent laboratories.

Sample Type	WVTR in g/(m²·d) (*)					
	40°C / 90% RH			50°C / 70% RH		
	Flat films	VIP				
	Lab-1 (Flat films)	Lab-2	Lab-3 Arrhenius (**)	Lab-2	Lab-3 (***)	Lab-4
Laminate-1	$< 5.0 \times 10^{-5}$	-	Ongoing calc. of Q_P	-	2.0×10^{-3}	3.3×10^{-3}
Laminate-2	1.5×10^{-2}	3.8×10^{-2}	1.2×10^{-2}	5.3×10^{-2}	2.6×10^{-2}	-
Laminate-3	2.1×10^{-2}	1.7×10^{-2}	1.4×10^{-2}	2.5×10^{-2}	2.1×10^{-2}	3.3×10^{-2}
(*) Average value of at least two measurements (**) The values are calculated by using the Arrhenius equation (16) (***) The data are obtained after test duration of 360 days at 50°C and 70% RH by Lab-3.						

Table 27 shows the WVTR measurement results obtained by all the laboratories involved. Lab-1 measurements are obtained for the flat films, while Lab-2, Lab-3 and Lab-4 investigated the WVTR of the laminates after VIP panel producing.

As described in the state-of-the-art report of Annex65 and in many documents in the literature, the permeation is considered as a thermo-activated process based on solubility and diffusion. Since in this study the conditions to which the VIPs were exposed, were different from a laboratory to another, it was necessary to evaluate the activation energy. The activation energies were then used to calculate the transmission rate at the conditions (temperature and humidity) of another laboratory. This was done by Lab-3 to compare its results to Lab-1, Lab-2 and Lab-4 (see Table 27). The classical relation type of Arrhenius is used for these calculations:

$$\mathrm{WVTR}\,(T, \mathrm{P_v}) = \mathrm{WVTR}_0 \cdot \frac{\mathrm{P}_v}{\mathrm{P}_{v0}} \cdot e^{-\left(\frac{E_\delta}{R} \cdot \left(\frac{1}{T} - \frac{1}{T_0}\right)\right)} \tag{16}$$

Where

WVTR_0 is the known WVTR at the specific given conditions of P_{v0}, and T_0,

E_δ is the activation energy of permeation and is experimentally determined as shown in Figure 79 using the permeance values obtained from the tests performed at the three different temperatures (the measurement conditions of Lab-3 are given in

Table 23).

The measured permeance values are given in Table 28.

Table 28: Permeance in kg/(m²·s·Pa) and WVTR in g/(m²·d) results obtained by Lab-3 on VIPs.

| **Permeance** in $\left(\frac{kg}{m^2 \cdot s \cdot Pa}\right)$ and **WVTR** in $\left(\frac{g}{m^2 \cdot d}\right)$				
	23°C / 50% RH	50°C / 70% RH	70°C / 50% RH	70°C / 3% RH
Duration (days)	553	360	279 ([1])	365
Laminate-1	5.5×10^{-15} / 6.7×10^{-4}	2.7×10^{-15} / 2.0×10^{-3}	2.1×10^{-15} / 2.8×10^{-3}	2.0×10^{-14} / 1.6×10^{-3}
Laminate-2	1.2×10^{-14} / 1.5×10^{-3}	3.5×10^{-14} / 2.6×10^{-2}	3.6×10^{-14} / 4.9×10^{-2} ([2])	5.4×10^{-14} / 4.4×10^{-3}
Laminate-3	2.0×10^{-14} / 2.4×10^{-3}	2.8×10^{-14} / 2.1×10^{-2}	3.5×10^{-14} / 4.7×10^{-2} ([2])	6.7×10^{-14} / 5.3×10^{-3}
([1]) The climatic chamber underwent 84 days of outage				
([2]) Value after 205 days (because 2 out 3 VIPs were out of service after 279 days)				
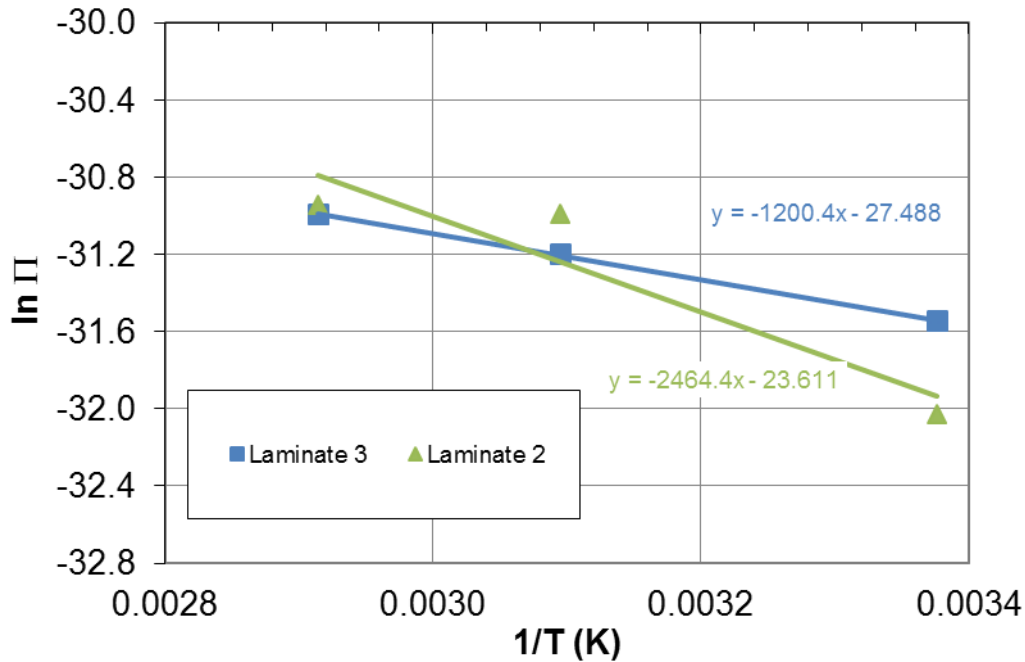
Figure 79: Determination of the activation energy of permeance (Π in kg/(m²·s·Pa)) from the data shown in Table 28.

The activation energy value (E_δ), for Laminate-2, is calculated as 20kJ/mol, and is close to the value obtained in the previous work for the tri-laminates (Pons et al, 2014). The value calculated for Laminate-3 is 10kJ/mol and it is lower than the values obtained in previous work (Pons et al, 2014). More accurate results for activation energy could be obtained by performing the tests at more than three different temperature conditions. Based on these activation energy values (E_δ), the WVTR values for Laminate-2 and Laminate-3 at 40°C and 90% RH were calculated using equation (16) and the values are given in Table 27. The WVTR values obtained by the different laboratories are quite consistent.

The detection level of the water intake measurement test is around 2x10⁻³g/m²·d (Shufer, 2017). The values reported for Laminate-1 by Lab-3 and Lab-4, are very close to the measurement limit of the water intake technique. This is also in consistency with the results of Lab-1, where the WVTR value measured for the same Laminate-1 structure as flat film was also below the measurement limit of AQUATRAN, which is 5x10⁻⁵g/(m²·d).

The WVTR values measured for flat films and also measured through the envelope into the VIP by four independent laboratories as given in Table 27 agree closely. The results of flat films obtained by AQUATRAN measurements do not differ significantly from the measurements obtained by the water intake measurement technique.

During the flat film measurements by AQUATRAN, the permeation through the sealing seam is not included in the measured permeability. Still, the flat film WVTR results do not show large deviations from the values obtained by the water intake measurements. The sealing seam of the three selected laminates used within this common exercise is a

poly(ethylene) based polymer with low WVTR values. Therefore, in comparison to the permeation perpendicular to the film surface, the water vapour permeation through the polyolefin based sealing seams becomes negligible, if the sealing seam length and width are sufficiently short and wide (seam width $\geq$ 1cm, see Figure 62), respectively.

In addition, the water vapour permeation through the metallized aluminium layers occurs mainly through the nano-sized defects existing within these layers. Depending on the structure and mechanical properties of the laminate, macro-sized defects or cracks can occur during the VIP production. These new macro-sized defects or cracks create new gas permeation pathways, in addition to those of the nano-sized defects already formed during the deposition of the aluminium layers. The effect of these new formed macro-sized defects during the VIP production on the WVTR value is found to be almost negligible, since the water vapour permeation through the aluminium layers of this common exercise seems to be dominated by the nano-sized defects, which have sizes less than 1nm (Affinito and Hilliard (2004)), rather than the macro-sized defects.

In this common exercise, the difference between the WVTR results obtained by flat film measurements and water intake of VIP measurements is found to be negligible, based on the following reasons:

1) the water vapour permeation in these laminate structures occur through the nano-sized defects and the number of the nano-sized defects for these laminates, do not seem to be significantly increased by the VIP production process,

2) the water vapour permeation through the poly(olefin) based sealing seams does not contribute significantly to the final measured WVTR for VIPs, due to the low WVTR of the poly(ethylene) based sealing seams.

It is very important to test the WVTR through the VIP envelopes using the water intake technique as described in Chapter 4.3.2.1, because the VIP production process can influence and reduce the high barrier properties of the VIP laminates.

Depending on: the properties of the metallised and organic layers used within the VIP laminate film, the VIP geometry and the dimensions, and the sealing seam type and its dimensions; the WVTR values obtained by VIP water intake technique can be 2 to 2.5 times higher than the WVTR values obtained for the flat films. This difference can be effectively detected by the water intake measurements.

4.4.3 O_2 permeation results for flat films and air transmission rate results through the VIP envelope

The O_2 permeability measurements of the flat films are performed according to the procedures as described in Chapter 4.3.1.2 by Lab-1. The measurements for the calculation of the air transmission rate (ATR) through the VIP envelopes are performed according to the measurement procedures as described in Chapter 4.3.2.2 by Lab-2 and Lab-4, and as described in Chapter 4.3.2.3 by Lab-3.

ATR results using VIP thermal conductivity change as a function of time

The method to calculate the ATR values by Lab-2 using the VIP thermal conductivity change as a function of time (as discussed in Chapter 4.3.2.2), is described in detail in Figure 80 and Figure 81.

For this method, it is required to have the VIP thermal conductivity (λ) change of the selected core as a function of the panel pressure (p). The selected core for the long-time thermal conductivity measurements in this exercise was fibreglass.

Figure 80 shows the fibreglass core-based VIPs during the λ versus p measurements. First, the thermal conductivity (λ) is measured immediately after evacuation of the system by a turbo molecular pump through a leak tight connector on the right side of Figure 80, right.

After the evacuation, the vacuum level inside the envelope is about 1x10^{-3} mbar and the initial thermal conductivity (λ_0) is determined. Afterwards, controlled amounts of gas are injected into the VIP envelope through the leak tight connector. The thermal conductivity (λ) is measured after each air injection together with the corresponding pressure measurement. Figure 81 shows the thermal conductivity change of the two typical fibreglass cores as a function of the internal panel pressure.

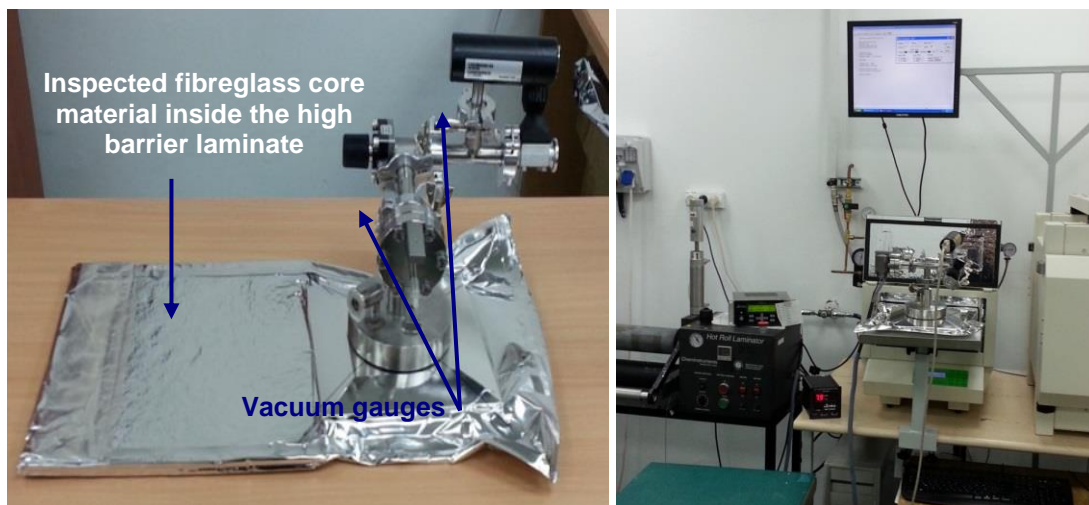Figure 80: Right: thermal conductivity (λ) versus pressure (p) measurements of fibreglass core-based VIP; left: thermal conductivity (λ) versus pressure (p) measurements inside the thermal conductivity measurement device (LaserComp FOX314).

Equation (17) is used to fit a curve to the experimentally measured curve. It is an empirical model with three parameters, which allows fitting the measured values. The three parameters used for fitting equation (17) to the curves as shown in Figure 81 in this exercise are given in

Table 29.

$$\lambda(p) = \lambda_0 + \frac{\lambda_{gas}}{1 + \frac{p_{1/2}}{p}} + \frac{\lambda_{coupl}}{1 + \frac{p_{1/2}^{coupl}}{p}} \tag{17}$$

λ_0:   initial VIP thermal conductivity at the very low pressure of from 1×10^{-3} to 1×10^{-2} mbar; it is the sum of the two contributions of heat conducted by the solid porous core and the infrared (IR) radiation,

λ_{gas}:   thermal conductivity of air (25.5mW/(m·K)),

λ_{coupl}:   thermal conductivity due to coupling effects between the skeleton of the core material and the gas molecules (11mW/(m·K)),

$p_{1/2}$ and $p_{1/2}^{coupl}$ are the two specific pressure parameters that depend on the average pore size ($d(\mu m)$, diameter) of the porous core material with the relationship:

$$d(\mu m) = \frac{230}{p_{1/2}(mbar)} \tag{18}$$

Table 29: The parameters used to plot the fit curves for fibreglass (shown in Figure 81).

	Laminate-2	**Laminate-3**
Core Type	Fibreglass-1	Fibreglass-2
λ_0 in mW/(m·K)	1.5	2
$p_{1/2}$ in mbar	5	7
$p_{1/2}^{coupl}$ in mbar	500	900
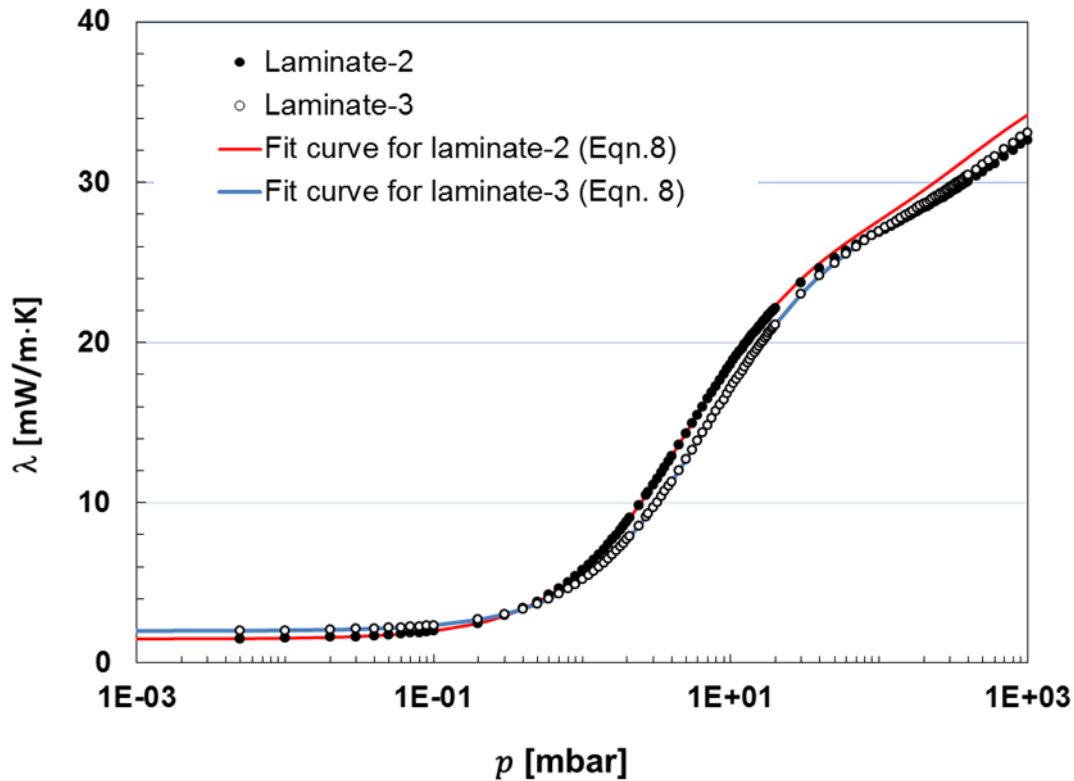
Figure 81: Thermal conductivity (λ) of two different types of fibreglass cores as a function of the internal VIP pressure in mbar, $p_{1/2}$ is at 5mbar for the fibreglass-1 core and is at 7mbar for the fibreglass-2 core.

After having the relationship between the thermal conductivity (λ) and the vacuum level for the selected core type, the procedure described in Chapter 4.3.2.2 is followed to determine the ATR through the VIP envelope into the VIP. As discussed, the VIPs at the given core dimensions of 300x300mm^2 are prepared using the Laminate-2 and Laminate-3. The thermal conductivity (λ) of each panel was measured over at least 3 months. Since the VIPs consist of desiccant, the measured pressure inside is only air pressure, the desiccant keeps the water vapour pressure negligible.

The pressure inside was then calculated using equation (17) with the given parameters in

Table 29 for each panel type. By this way, the pressure versus time curve is generated from the measured thermal conductivity versus time curve. Figure 82, top (a) and bottom (b), shows the measurement results for the thermal conductivity change as a function of time and the calculated pressure versus time curve, respectively. The measurement conditions in this study were 23°C and 50% RH.

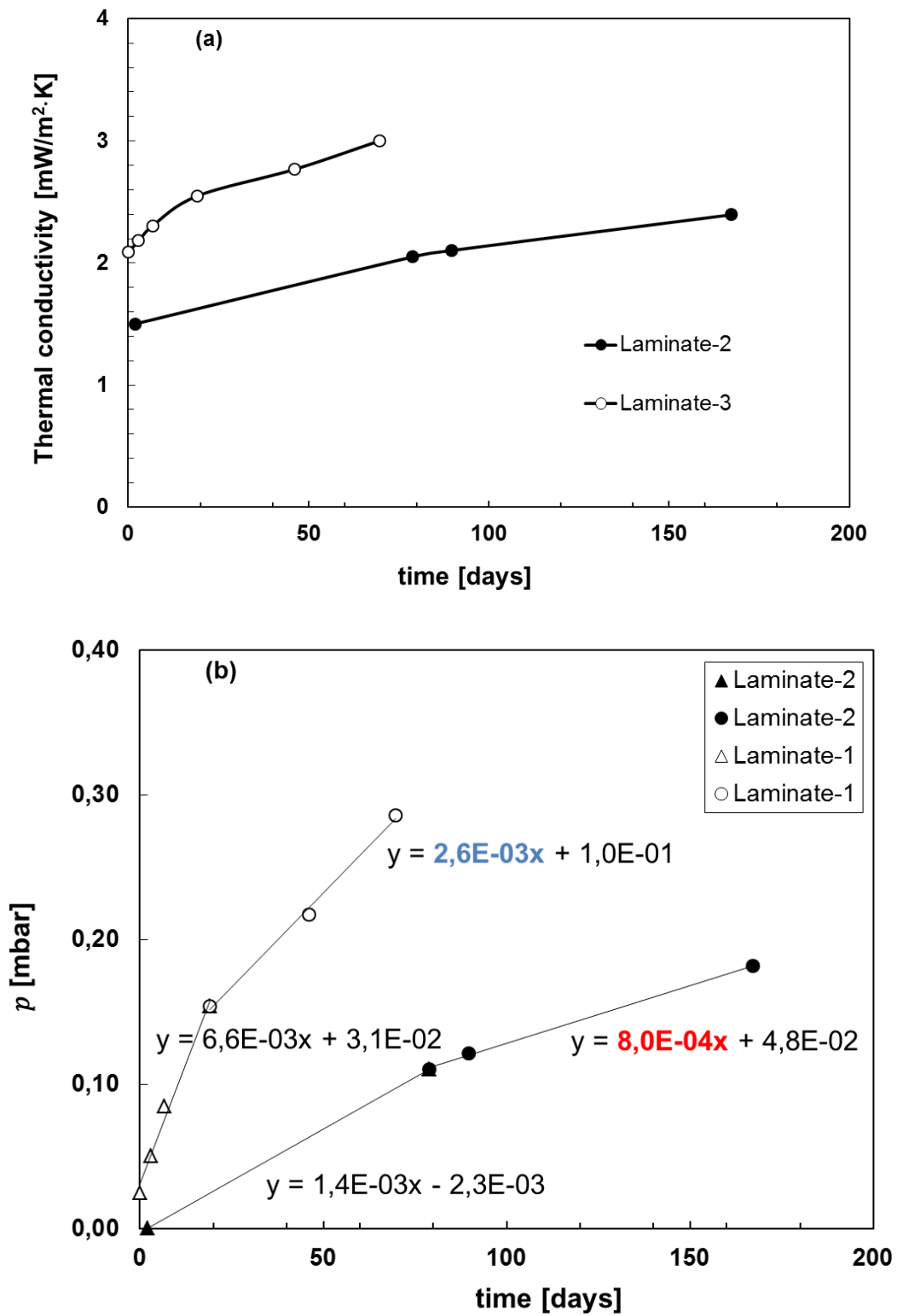Figure 82: Top (a): VIP (fibreglass core), thermal conductivity (λ) vs. time in day measurements; bottom (b): calculated VIP (fibreglass core) pressure in mbar vs. time in day curve. Equation (17) and
Table 29 were used. Measurements performed by Lab-2.

The pressure versus time graphs in Figure 82 (bottom (b)) show two different linear segments, with an initial segment showing a 2-2.5 times faster pressure increase rate than the later segment. Lab-2 relates this phenomenon to the outgassing of the films as also discussed in ST 1 Report, Chapter 4.3.3.5.

The outgassing contributes substantially to the pressure increase rate in the first few weeks after the panel production. Therefore, the initial period should be excluded from the ATR calculation. Outgassing occurs at all temperatures and its duration becomes longer at a lower storage temperature. The ATR in this study is calculated using only the pressure increase after steady state has been reached. The origin of the outgassing can be analysed using the residual gas analyser as discussed in ST 1 Report, Chapter 4.3.3.6.

The ATR, through a 1m^2 sized VIP, is then calculated from the slope of the VIP internal pressure (p) versus time curve, as given in equation (19):

$$ATR\text{-}through1\ m^2\ VIP\text{-}\left(\frac{cc(STP)}{year \cdot m^2}\right)$$
$$= \frac{dp\ (mbar)}{dt\ (days)} \times \frac{VIP\ Volume\ (cm^3) \times 365 \times 273K}{VIP\ Area\ (m^2) \times 1000 \times T(K)} \tag{19}$$

To calculate the ATR through a 1m^2 of the laminate, the VIP area in m^2 in equation (19), should be replaced by the total area of the laminate used (total VIP surface area in m^2) for VIP production. The values calculated for both cases are summarised in Table 30.

Table 30: ATR values for Laminate-2 and Laminate-3 as measured by Lab-2.

Lab-2 (23°C, 50% RH)	Units	Laminate-2	Laminate-3
dp/dt	mbar / day	8.0E-04	2.6E-03
VIP-core dimensions	mm	300x300x6.5	300x300x9
VIP dimensions	mm	335x335	335x335
ATR through 1 m^2 of the VIP	$\frac{cc\ (STP)}{year \cdot (m^2\text{- VIP})}$	1.4	6.3
ATR through 1 m^2 of the VIP envelope	$\frac{cc\ (STP)}{year \cdot (m^2\text{- laminate})}$	0.7	3.2

It is very important to pay attention to the measurement units. As it can be seen in Table 30, the ATR value reported for 1m^2 of the VIP is double the value reported for 1m^2 of the laminate. The VIP producers, in general report, the ATR with the unit in cm^3(STP)/((m^2-VIP)·year). The gas permeability of the flat film laminates are reported with the unit in cm^3(STP)/((m^2-laminate)·day·bar).

ATR results using lift-off method

Since the fibreglass core did not allow the air pressure measurement with enough accuracy as discussed in Chapter 4.3.2.3, the direct determination of the ATR at 23°C and 50% RH for Lab-3 was not possible. Nevertheless, the same procedure was applied

that is already described for WVTR in Chapter 4.4.2.2. This procedure is based on the determination of the activation energy of the air permeance and the calculation of the ATR using equation (16). The tests were performed for 227 to 248 days at 50°C and 70°C as mentioned in Table 25 and are reported in Table 31. The calculated activation energies are 39 and 50kJ/mol, for Laminate-2 and Laminate-3, respectively. The ATR values calculated at 23°C are reported in Table 32 by Lab-3. Note that the uncertainty is quite high despite the testing of three samples per temperature.

Table 31: ATR in $cm^3(STP)/(m^2$ laminate·year) measured by Lab-3.

	23°C / 50%RH	**50°C / 70%RH**	**70°C / 50%RH**
Laminate-2	Too low pressure to be measured experimentally by lift-off using fibreglass core.	36	76
Laminate-3		5.6	15.4

Comparison of results

The results obtained by Lab-2, Lab-3 and Lab-4 as seen in Table 32, show a good level of agreement for Laminate-3, it needs to be kept in mind that a difference of a factor of 2 on the ATR value is something very common. On the other hand, there is no agreement between the results measured by Lab-2 and Lab-3 for Laminate-2. There is no explanation at the moment for this difference, besides the difficulties faced by Lab-3 during the lift-off measurements as mentioned in Chapter 4.3.2.3 due to the FG core of the samples. Further research is ongoing to underpin the remaining issues for measuring the internal pressure of fibreglass core based VIPs using the lift-off technique.

The O_2 permeability values of the flat films measured at 23°C and 50% RH by Lab-1 (using Oxtran, as discussed in Chapter 4.3.1.2) are given in Table 32. The measurement device gives the O_2 permeability (O_2 permeance) values with the unit of $cm^3(STP)/(m^2 \cdot day \cdot bar)$ and has a measurement limit of $5x10^{-3} cm^3(STP)/(m^2 \cdot day \cdot bar)$. The O_2 permeability of the laminates as flat film are very close to the measurement limit of the device, and therefore, the values are reported here as $<5.0x10^{-3} cm^3(STP)/(m^2 \cdot day \cdot bar)$ at 23°C, 50% RH.

Table 32: O_2 permeability results for flat films, and ATR results through the VIP envelopes.

Sample Type	Flat films		VIP		
	O_2 permeability (*) 23ºC / 50 % RH		Air Transmission Rate, ATR (*) 23ºC / 50 % RH		
	[cm^3 (STP) / (m^2·day·bar)]	[cm^3 (STP) / (m^2·year)]	[cm^3 (STP) / (m^2 laminate·year)]		
	Lab-1 (**)	Lab-1 (***)	Lab-2 (****)	Lab-3 (*****)	Lab-4 (****)
Laminate-2	< 5.0 × 10^{-3}	< 3.7 × 10^{-1}	0.7	10	-
Laminate-3	< 5.0 × 10^{-3}	< 3.7 × 10^{-1}	3.2	1.1	3.2
(*) Average value of at least two measurements (**) Measurement unit obtained by Oxtran device (***) The Oxtran measurement unit is converted from cm^3 (STP) / (m^2·day·bar) to cm^3 (STP) / (m^2·year), multiplication by (365 days/year) × 0.2 bar, 0.2 bar is the O_2 partial pressure in atmosphere. (****) The laboratory reports the ATR in cm^3 (STP) / (m^2-panel·year). The value reported in this Table gives the ATR through 1m^2 of the laminate, but not through 1m^2 of the insulation panel. The difference is about a factor of 2, since the VIP has the laminate on both sides. (*****) Calculated at 23°C using the results given in Table 31 using equation (16).					

It is not possible to compare the O_2 permeability values measured for the flat films (Table 32) directly to those of the air permeability values measured through the VIP envelope into the VIP. The reasons are: the flat film measurements do not give any indication regarding the effect of the mechanical damages on the barrier performance occurring due to the VIP production process; the flat film measurements represent the gas permeability performance perpendicular to the VIP surface, but do not take the gas permeation through the sealing seam into consideration; the atmosphere contains about 78% of nitrogen and the ratio between the permeation rate of oxygen and nitrogen for high barrier laminates is not always known.

Although the flat film measurements for Laminate-2 and Laminate-3 show that the O_2 permeability of the laminates are both below the measurement limit of the Oxtran device, i.e. 5x10^{-3}cc(STP)/(m^2·d·bar), the ATR measurements through the VIP envelope into the VIP show a difference between the two laminates. The ATR value measured by Lab-2 as an example (using VIP thermal conductivity change as a function of time technique) for Laminate-2 is about 4.6 times lower than that of the Laminate-3.

The air permeation occurs mainly through the defects, which are larger than about 1nm as explained in Affinito and Hilliard (2004). Therefore, the cracks occurring during the VIP production have a direct influence on the final measured ATR values. The gas permeants pass relatively unrestricted through these defects that are much larger in diameters than the permeating gas molecules.

This common exercise, where the O_2 permeability of the flat films were measured in comparison to the ATR measurements through the VIP envelope into the VIPs showed once again the importance of testing the barrier performance of the laminate structures after VIP production. Although the flat film measurements do not show a difference in

the O_2 permeability values for Laminate-2 and Laminate-3, the ATR values differed after the VIP production. The ATR measurement technique as described in Chapter 4.3.2.2 was able to detect these differences reproducibly.

The measured ATR for Laminate-2, which is 1.4cc(STP)/(m^2-VIP·year) contributes to the internal air pressure increase by about 0.16cc(STP)/year (for this VIP geometry). It would not be possible to detect the O_2 permeability of such a flat film using the commercially available O_2 permeability measurement devices. On the other hand, the measured ATR for Laminate-3 being 6.3cc(STP)/(m^2-VIP·year), contributes to the internal air pressure increase by about 0.7cc(STP)/year (for this VIP geometry). The flat film O_2 permeability of such a structure is calculated and found to be at around 7x10^{-3}cc(STP)/(m^2·day·bar). This common exercise clearly demonstrated the importance of testing the air barrier performance of the laminate after the VIP production.

4.5 Conclusions and Outlook

The reason of this common exercise was, as also already reported in an already finalised European funded FP7 Project (Nanoinsulate, 2013), the difficulty to compare the air permeability and water vapour transmission rate (WVTR) results of laboratories working with VIP-laminates and with various permeation methods, either using commercially available measurement devices or self-developed measurement techniques. The tests comprised a number of different measurement techniques as well as test geometries, evaluated in different environmental conditions in different laboratories and on different VIP laminate structures. This generates quite naturally several misinterpretations and inconsistencies.

The material specification data sheets provided by the metallised laminate (VIP envelope) producers report in most of the cases the O_2 permeability and the WVTR of the flat films. However, the barrier performance of the VIP-laminates can vary after the VIP production. Consequently, there seems to be a remarkable amount of unnecessary duplication of work in this community in the absence of clear guidelines and specific test standards for the gas and water vapour barrier performance evaluation of the VIP-laminates and/or VIP envelopes. We have shown in the framework of this common exercise, including four independent laboratories by using at least two, or three different laminate structures that the tests performed in different laboratories show most of the times a remarkable quantitative agreement with one another and with a range of state of the art permeation methods, including coulometric measurement method.

The water intake (gravimetric) technique performed by the three independent laboratories delivered very consistent and comparable WVTR results. Reducing the testing conditions to two well-defined sets (40°C, 90% RH and 50°C, 70% RH) was a trivial but important step for an effective comparison. The WVTR values obtained by the coulometric measurement method using Mocon® AQUATRAN^{TM} Model 2 for the flat films

did not differ significantly from the values obtained by the water intake (gravimetric) technique on the VIPs. The VIP production did not show a significant influence on the water vapour barrier performance of the two VIP laminate structures, which were selected for this common exercise. It needs to be mentioned that the water vapour barrier performance can be affected by a factor of 2 to 2.5 due to the VIP production process depending on the laminate type.

The O_2 permeability of the flat laminates were measured by the coulometric measurement method and all found to be below the measurement limit of the Mocon® Oxtran® Model 2/21 ($5x10^{-3}cc(STP)/m^2 \cdot d \cdot bar$). It was not possible to realize any difference in the O_2 barrier performance of these laminates (before the VIP production) with the coulometric measurement method. On the other hand, the air transmission rate (ATR) measurements through the VIP envelope using the VIP thermal conductivity change as a function of time can detect the air barrier performance differences between the laminates occurring due to the VIP production. One of the two laminates, for instance, was found to have a factor of 4.6 better barrier performance than the other one. This exercise demonstrated the importance of testing the effect of the VIP production process on the final air barrier (towards O_2-, N_2- gases) performance of the VIP envelopes.

Finally, it has been demonstrated that the air transmission rate measurement using the VIP thermal conductivity change as a function of time is a very promising method for the determination of the air permeability through the VIP envelopes into the VIP. The two laboratories working with this measurement technique delivered comparable results for the investigated laminates at the well-defined test conditions of 23°C, 50% RH. During the comparison of the measured ATR values, it is very important to pay attention to the measurement units. The units should be comparable to each other, it needs to be carefully checked, whether it is the transmission rate through the $1m^2$ of VIP, or through the $1m^2$ of the VIP laminate.

The ATR measurements through the VIP envelope using the lift-off method, here at low temperature, were unfortunately in difficulties due to the mechanical behaviour of the fibreglass core of the samples. The agreement with other methods is good for one laminate and bad for another. Clearly such core should be avoided to assess the ATR, and lattice, cellular or silica cores should be preferred. The advantage of this method is to test the real production of VIPs with all the influences: handling, core strain, folds, seams, edges and angles. So, this method is useful for those that do not produce VIPs. That is why this method is proposed in the EN ISO standard and the work is in progress.

Although there are many international film testing standards used as a basis, the VIP industry is still in need to adopt specific standards for the evaluation of the VIP envelopes. The methodologies described in this chapter for testing the gas and water vapour barrier performance of the VIP laminates are already successfully utilized by some of the research institutes, laboratories, material providers and VIP producers. Furthermore, the

European Committee for Standardization (CEN) is currently working on the adoption of some of these techniques as well.

The results of this work are encouraging to further investigate and propose characterisation methods to relate the lifetime of VIPs to barrier properties, related to intrinsic degradation modes of VIPs for building applications. As an example, the effect of the moisture absorption of the VIP core on its thermal conductivity is another important data for accurate prediction of the panel performance throughout its lifetime. The results are relevant to the real degradation rate of fumed silica panels in building applications. Such a test technique has not been included in this study, nevertheless, one of the laboratories involved in this exercise has upgraded and modified the VIP measurement techniques described in this study and developed a technique for the measurement of the relation between the moisture content of the fumed silica-based VIPs and their thermal conductivity.

Another bottleneck was that we observed variations between methods, which may be reduced by applying a common set of recommendation and guidelines, especially to compare VIP envelopes to VIP laminates. The determination of the air transmission rate using the VIP thermal conductivity measurements is a reliable and a reproducible technique. On the other hand, the lift-off technique for measuring the internal pressure of the fibreglass core based VIP was found to be not enough reliable. There are ongoing projects for the validation of the lift-off technique for measuring the internal pressure of fumed silica VIPs, providing very accurate results. These are the topics of the current work and future publications.

5 Modelling of air- and moisture transfer through VIP

As already mentioned the measurement of ageing effects normally requires great effort for climatisation capacities (artificial ageing) or monitoring, respectively deconstruction work (natural ageing). For natural ageing only, a limited number of samples and adjacent climate conditions can be evaluated. Therefore, modelling approaches are desirable to investigate a larger number of cases based on theoretical assumptions on permeation behaviour of the foil barrier and climatic impact in a certain application.

In principle two different approaches are possible. First a complete theoretical model, as described in Chapter 5.1, is based on assumptions about material properties like permeation behaviour of the barrier foil in the undisturbed area, the permeation behaviour of the welding and the connected hygric and thermal response of the core material that is responsible for the performance of the VIP in the specific application. This approach requires detailed modelling on different scales, starting with the permeation behaviour of the welding, assumptions about imperfections due to production technologies and ending up with the correct consideration of the behaviour of adjacent building components and their influence on the climatic severity that impacts the VIP panel or APM product.

Second, in Chapter 5.2 is presented life expectancy estimation for VIP based on a combined lab-based and theoretical approach. Conversely to real modelling, the pressure-increase is determined for a specific type of VIP via artificial ageing of panels in several climates and subsequent determination of internal pressure increase and thermal conductivity measurement. The derived functionalities are then applied to climatic data obtained by hygro-thermal modelling for a number of exemplary applications.

5.1 Modelling

The aim of this study is to explain the relationship between the coating layer defect characteristics and its permeation performance. Monolayer film configurations are studied first. It is composed of three materials: the polymer substrate, the aluminium coating and the material which might fill the defects. The polymer substrate layer is meshed. The aluminium is considered as perfectly impermeable to gases. All defects on the coating layer are filled either with dry air, pure water vapour or glue. So the mesh of the films can be simplified. The aluminium does not need to be meshed and the defects are represented by filled cylinders.
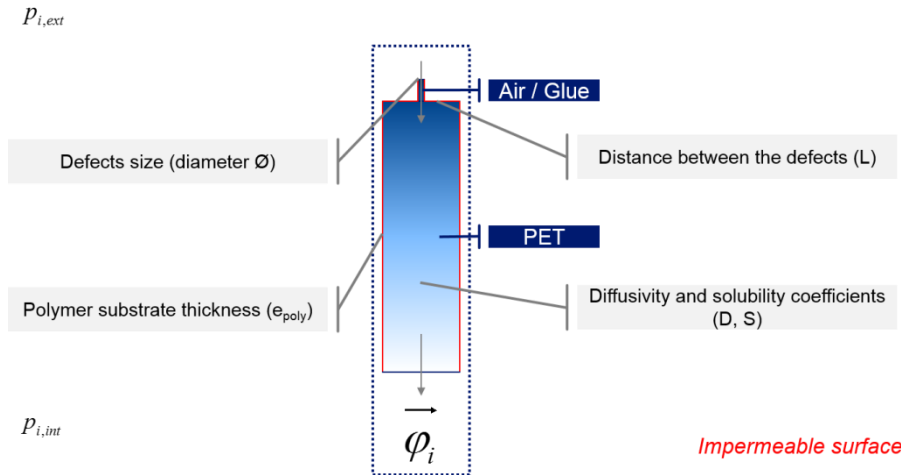
Figure 83: Schematic of the meshed pattern of PETM1F (section view), with identical and homogeneously distributed defects. Source: EDF.

5.1.1   Gas dissolution and diffusion into the polymers

The gaseous flux results from a gas pressure difference imposed between the sides of the polymer. This flow is the result of three phenomena: gas dissolution on one side of the membrane, gas diffusion through the polymer layer and desorption on the other side. The sorption phenomenon (adsorption and desorption) is described by Henry's law. At the equilibrium, the concentration (c_i) of a gas (i) in a polymer (j) is linked to the gas partial pressure (p_i) on its surface by the solubility coefficient ($S_{i,j}$).

$$c_i = S_{i,j} p_i \qquad (20)$$

In polymers, the gas flow can be represented with the Fick's law (Stannett, 1968, Hopfenberg, 1973, Klopffer, 2001). The gas flow depends on the concentration gradient and the diffusion coefficient ($D_{i,j}$).

$$\vec{\varphi}_i = -D_{i,j} \vec{\nabla} c_i \qquad (21)$$

In the case of a two layers polymer assembly, it is possible to observe that the concentration gradient of the gas is not continuous when the nature of the polymer changes, because their solubility coefficients are different. It is possible to obtain a continuous potential by combining both Henry's and Fick's laws. Preferably the potential $c_i/S_{i,j}$ can be studied.

$$p_i = \frac{c_i}{S_{i,j}} \qquad (22)$$

This potential is defined as the ratio between the gas concentration (c_i) at a point of the polymer and the solubility coefficient ($S_{i,j}$) of this gas into the polymer j. It is continuous throughout the sample and dimensionally homogeneous with a pressure. Fick's law can be written as below:

$$\vec{\varphi}_i = -D_{i,j} S_{i,j} \vec{\nabla} \frac{c_i}{S_{i,j}} \qquad (23)$$

98

5.1.2 Gas dissolution and diffusion into the defects

Defects in the coating layer can be considered as pinholes which are filled either with dry air, pure water vapour or glue. When they are filled with glue, the gas transfer phenomena are exactly the same as those presented above. When they are filled with gas (dry air or pure water vapour), the sorption and diffusion phenomena are quite different.

First, the relationship between the gas concentration and the gas partial pressure is no more given by Henry's law but by the perfect gas law. The solubility coefficient has to be replaced by the inverse of the product of the specific gas constant (r_i) and the temperature (T).

$$p_i = c_i r_i T = \frac{c_i}{\dfrac{1}{r_i T}} \tag{24}$$

Second, in small size defects, collisions between gas molecules and defects edges can be more frequent than collision between gas molecules. This happens when the defects diameter (Ø) is smaller than the mean free path of gas molecules. In such conditions the diffusion takes place according to the Knudsen process (He 2014). This phenomena strongly reduces the diffusion and also explains the low thermal properties in VIPs and APMs. The diffusion coefficient in gas is replaced by the Knudsen coefficient which can be written as a function of the temperature (T), the Boltzmann constant (k_B), the molecular mass (m_i) and the defect diameter (Ø).

$$D_K = \frac{Ø}{3}\sqrt{\frac{8 k_B T}{\pi m_i}} \tag{25}$$

5.1.3 Apparent gas permeance of a membrane

Experimental data rarely use diffusion and solubility coefficients but represent gas permeation through a macroscopic quantity which is the apparent permeance ($\pi_{i,app}$).

$$\Pi_{i,app} = \frac{\Phi_i}{A \Delta p_i} \tag{26}$$

In the following results, the thermo-activation of the permeance is neglected and simulations are made at constant temperature.

5.1.4 Simulation results: homogeneous configurations with identical and equidistant defects

Several series of simulation have been carried out on PET films metallized on one face (PETM1F) with various density of defects, for different defect diameters (Ø) and distances between defects (L). First, there is no glue into defects. The ranges of values chosen include the experimental data values from the bibliography (Garnier, 2010, Hanika, 2004). In Figure 84 each continuous colour curve is an isovalue of distance between defects.

Figure 84: Calculated apparent permeance on PETM1F as a function of the defects size for 10 distances between defects (L). Source: EDF.

The results show that a decrease by a factor of 2 of the defect diameter and the distance between them causes a higher increase of the permeance than an increase by a factor of 2 of the defect diameter for a constant distance between them. In both cases the total surface of defects is the same, but defects are not similarly distributed. In addition, when the defects become very small and close, the permeance of the PETM1F film tends to that of an uncoated PET film (represented by the red line at $7.92 \cdot 10^{-11} kg \cdot m^{-2} \cdot s^{-1} \cdot Pa^{-1}$). In other words, in a constant surface of defects, the smaller and the more numerous the defects are, the higher the permeance is. Below a certain defect diameter (around 1nm), the mass flow is slowed so much by the Knudsen effect in the defects that the permeance does not increase anymore, but decreases.

Adhesive polyurethane is used to make multilayer film. The diffusion coefficient of water vapour in polyurethane adhesive is much lower than the self-diffusion of water vapour. If PETM1F films are modelled with adhesive in defects, the first impression is that the permeance would be lower. The simulations produced the expected results. The Figure 85 shows that for defects diameters greater than 20nm, the permeance values in case of adhesive in defects are very close to those without adhesive. However for defects diameters well below 20nm, the permeance values seem to tend toward a limit below the permeance of an uncoated PET film.
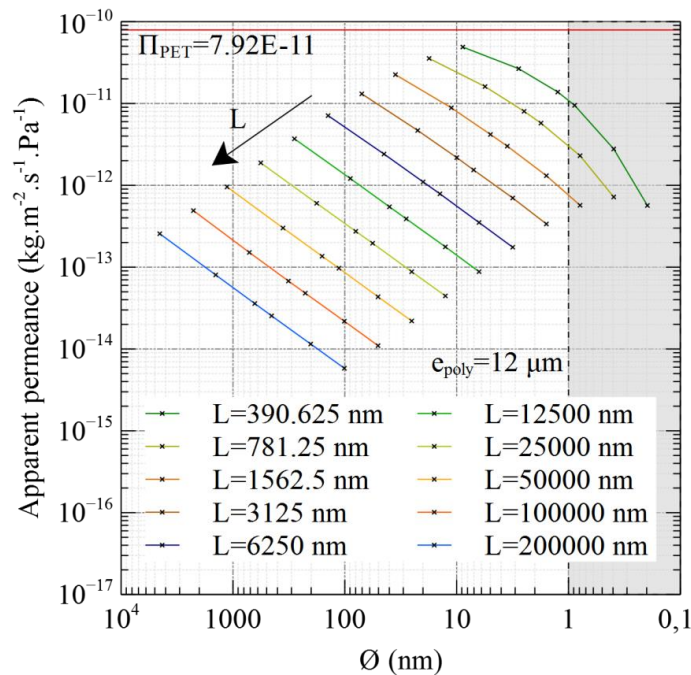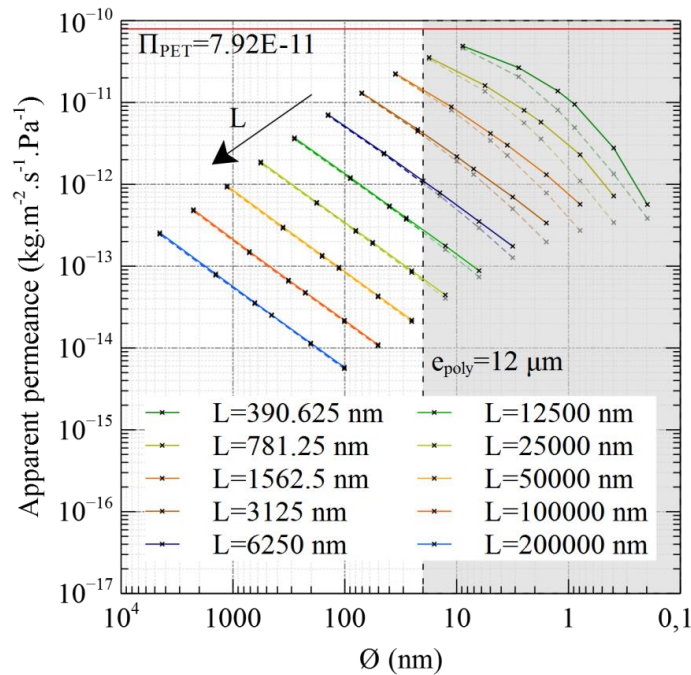
Figure 85: Calculated apparent permeance on PETM1F as a function of the defects size for 10 distances between defects. Source: EDF.

The simulations have demonstrated that the permeance of a PETM1F depends both on the defects in the coating layer and on the gas transfer properties of the polymer substrate. The simulations carried out with homogeneous defect distributions on PETM1F, confirmed that the permeance depends more on the number of defects than on the cumulated surface of defects. This can be explained by the fact that with narrow pinholes, the mean distance that gas molecules have to go through the polymer is close to the polymer thickness. At the limit, the permeance tends to be that of the uncoated film. However, if defects are smaller than 1nm, the permeance is limited by the Knudsen effect in the defects. When defects are filled with glue, for defects diameters well below 20nm, the permeance values seem to tend toward a limit below the permeance of an uncoated PET film.

Nevertheless, due to the high viscosity of glue, it is unlikely that it can enter into defects of a few tens of nanometre size. So, the permeance values from simulations without adhesive in defects are potentially closer to real values.

Validation attempts show that calculated permeances are significantly over-estimated. Even for the more favourable configurations the calculated permeances are more than 10 times higher than the experimental values. Several hypotheses could explain that difference and are detailed by Batard et al., 2017.

5.1.5   Time-dependent permeation through VIP barrier laminates (IVV)

The VIP envelope prevents the ingress of the atmospheric gases, oxygen, nitrogen and water-vapour, into the VIP core to a large extent which would otherwise cause the increase of pressure within a short time. The high barrier properties required for VIP lifetimes up to 50 years are commonly reached by laminates of two or three metallized polymeric films. An example is the structure PET / Al / PU / PET / Al / PU / PET / Al / PU / LDPE (Brunner et al., 2006).

Aiming for an accurate prediction of the VIP lifetime, a precise understanding of the mechanisms of gas and water vapour permeation through barrier laminates is mandatory. As a first approximation, VIP laminates can be considered as structures P / A / P / A / ... / A / P of continuously (…) alternating inorganic layers (abbreviated by A) and polymeric layers (P) if adjacent polymeric materials like PET and PU are combined to one-layer P. It is well-known for such structures that it can take several weeks or even months until steady-state permeation is established (Graff et al., 2004).

In order to accurately predict the time-dependent pressure-increase, within VIPs having a relatively short intended lifetime of only some years (e.g. for application in cooling devices) the potentially long lag time of permeation through barrier laminates should be taken into consideration. For such applications it might even be possible to reduce the number of barrier layers and the cost of the laminate, if the resulting higher permeation rate can be compensated by an extended lag time.

This discussion makes it clear why the development of a theoretical model for time dependent permeation through structures of alternating barrier layers and especially for barrier laminates is important. Furthermore, such a model can improve the evaluation of permeation measurement results for barrier laminates: the model is a basis for establishing a criterion when it is possible to stop the measurement and helps to extrapolate the measured values of transient permeation to the steady-state value, shortening the measurement time (Kiese et al., 2017).

Two models for permeation through multilayer structures will be presented: the ideal laminate model and the geometric defect model. Using the finite elements method, the transient diffusion equation is solved numerically for the modelled barrier structures. These results form the basis for the development of a quasi-steady-state model, which gives a simplified analytical description of the time dependent permeation through structures of alternating inorganic and polymer layers. The developed models and results are taken from Miesbauer, 2017.

The permeation of substances through polymeric materials (e.g. polymeric substrates or adhesives) is described by the solution-diffusion-model which splits the permeation process into absorption, diffusion and desorption (Rogers, 1985). For the models to be developed the concentration (c) of a substance dissolved in a polymer is assumed to be proportional to its partial pressure (p) (Henry's law) (Rogers, 1985)

$$c = Sp \tag{27}$$

and diffusion is described by Fick's law (Crank, 1975)

$$\frac{\partial c}{\partial t} = D \left(\frac{\partial^2 c}{\partial x^2} + \frac{\partial^2 c}{\partial y^2} + \frac{\partial^2 c}{\partial z^2} \right) \tag{28}$$

where S and D denote the solubility and diffusivity of the substance within the polymer. These assumptions are generally fulfilled for gases in polymers, while for water vapour non-linear sorption isotherms and diffusion mechanisms with rates being fast or comparable to relaxation rates of the polymer (Non-Fickian diffusion) can play a significant role (Crank, 1975; Rogers, 1985).

In contrast to the relatively homogeneous polymers, permeation through inorganic layers (e.g. aluminium) deposited on top of polymer substrates by evaporation processes, is restricted to defects within the materials (Langowski, 2008). For gases like oxygen and nitrogen only localised macro-defects with diameter of some nanometres up to micrometres are important, while for water vapour also the quasi-homogeneously nano-defects in sub-nanometre region are accessible and have the dominating influence.

As a consequence of this behaviour, two different models of multilayer structures are considered. Considering water vapour permeation, inorganic and polymeric layers are defined as quasi-homogeneous materials and characterised by effective solubilities and diffusivities assuming validity of Henry's and Fick's laws (Chapter 5.1.1 equation (20), (21), (22) and (23) (ideal laminate model, Figure 86 left). In the case of gas permeation, however, the only effect of inorganic layers is assumed to be the restriction of the gas transport through the interface of an adjacent polymeric layer to geometrically defined macro-defects (geometric defect model, Figure 86 right).
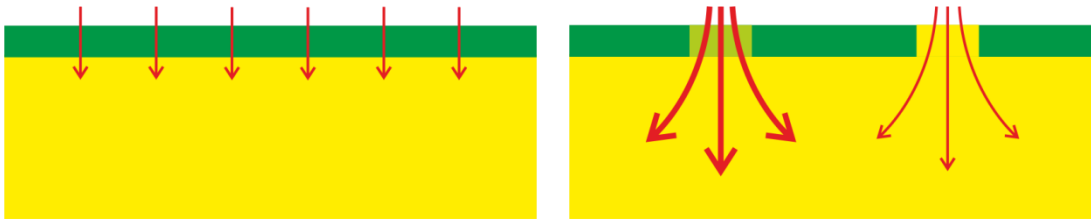
Figure 86: Models for permeation through structures of inorganic (green) and polymeric (yellow) layers. Left: ideal laminate model; right: geometric defect model (Miesbauer, 2017).

The transient permeation through structures A / P / A defined in the ideal laminate model was numerically calculated using the finite element method (FEM). The boundary partial pressures were set equal to $p_0 > 0$ and zero, respectively, and the initial concentration within the structure was zero.

Figure 87 shows the calculated normalised flux density $j\, h_A / (D_A\, S_A\, p_0)$ at the boundary with partial pressure equal to zero as a function of the normalized time $t\, D_A / h_A^2$. The curves represent different ratios S_P / S_A between the solubilities for the layers P and A while the corresponding ratios between the layer thicknesses (h) and between the diffusivities were set equal to 1 or 10, respectively.
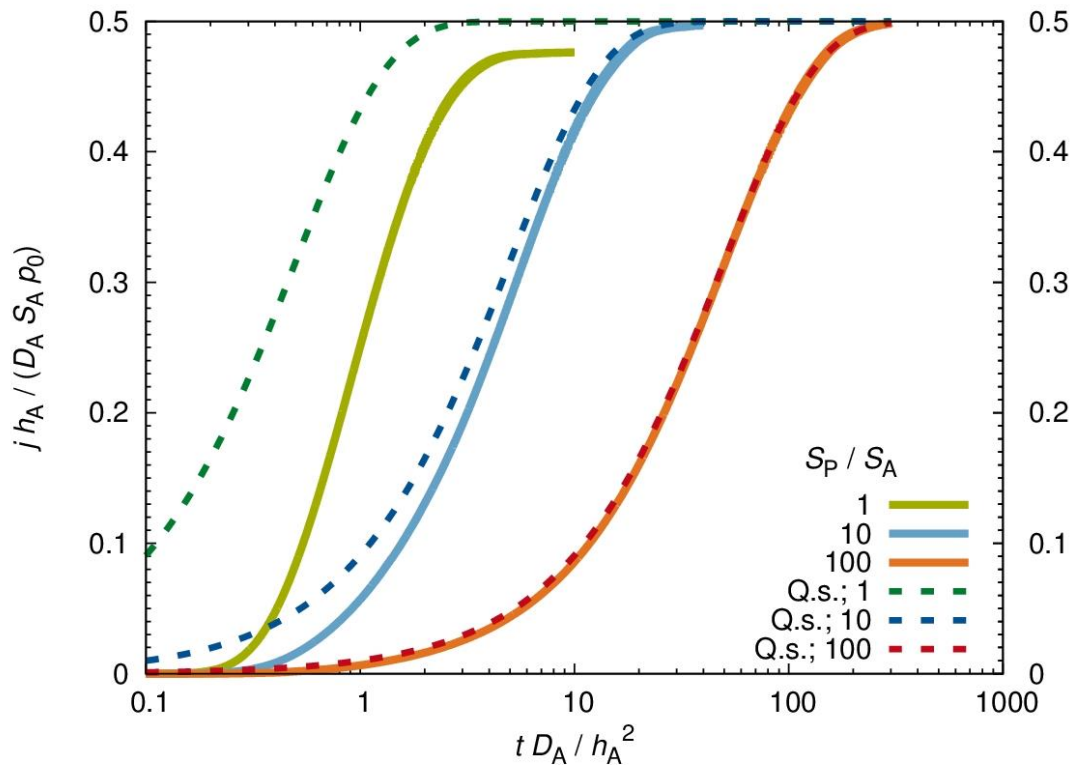
Figure 87: Structure A / P / A in the ideal laminate model: normalized flux density at the boundary with partial pressure equal to zero as a function of the normalized time. Solid lines: calculated by FEM; dotted lines: quasi-steady-state approximation (Q.s.) (Miesbauer, 2017).

The comparison of the curves shows that the rise of the flux with time is significantly reduced for increased ratio S_P/S_A. Equivalently, the lag time (Crank, 1975) which is considered as a measure for the approach to steady-state permeation is extended in this case.

An interpretation of this result is possible by plotting the time dependent profile of partial pressure which is in local equilibrium with concentration via Henry's law. Figure 88 shows the normalized partial pressure p/p_0 as a function of the normalised coordinate x/h_A and the normalised time $t\,D_A/h_A^2$ for $S_P/S_A = 5$ and $h_P/h_A = D_P/D_A = 1$.
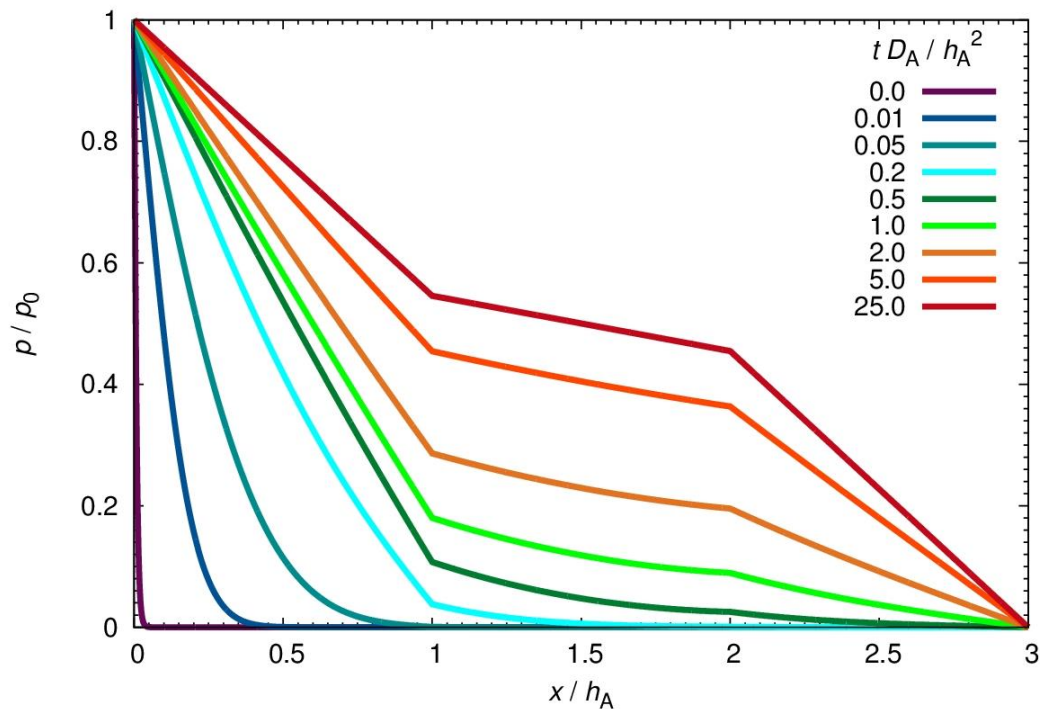
Figure 88: Structure A / P / A in the ideal laminate model: normalised partial pressure as a function of the normalized coordinate and normalized time. The layers A correspond to x/h_A values in the intervals $[0,1]$ and $[2,3]$, the layer P to the interval $[1,2]$ (Miesbauer, 2017).

Two stages of the permeation process can be identified in the shown time dependent partial pressure profile (Figure 88). In the first stage, the diffusion front moves through the first layer A to the interface with the layer P. The second stage begins at about $t\,D_A/h_A^2 = 0.1$ and is characterised by the increase of the partial pressure within the layer P with time until steady state is reached. During the second stage, the partial pressure profile in each layer is nearly linear, similar to the case of steady state permeation, but it changes with time.

This allows for interpretation of the influence of the ratio $S_P/\,S_A$ on the time dependent flux as follows: The capacity of the layer P for the permeating substance increases in parallel to the ratio $S_P/\,S_A$ while the permeation resistances of the layers A are constant. Consequently, the time required for the exchange of the substance between the layer P and the environment through the layers A is extended, resulting in an extended, resulting in an extended lag time.

As a consequence of this discussion the permeation through the structures A / P / A / ... / P / A of alternating layers, containing a number N_P of layers P, is considered in quasi-steady-state approximation assuming that the permeation resistance (Q_A^{-1}) of a layer A is large compared to a layer P. The dependence of the partial pressure (p_i) on the position within a layer P_i can then be neglected and the change of the partial pressure with time is due to the quasi-stationary permeation fluxes j_{i-1} and j_i through the adjacent layers A per area. This leads to the mass balances

$$h_P S_P \frac{\partial p_i}{\partial t} = j_{i-1} - j_i = Q_A \left(p_{i-1} - 2\, p_i + p_{i+1} \right) \tag{29}$$

for the layers P$_i$ where $p_0 > 0$ and $p_{N_P+1} = 0$ are the corresponding boundary values.

The solution of this system of linear differential equations is given by

$$p_i(t) = p_0 \left(\sum_{k=1}^{N_P} \mu_k\, exp \left(\frac{\alpha_k\, Q_A\, t}{h_P S_P} \right) v_{k,i} + p_{s,i} \right) \tag{30}$$

with $1 \leq i \leq N_P$, where $\alpha_k = 2 \left(\cos \left(\frac{k\,\pi}{N_P + 1} \right) - 1 \right)$ are the eigenvalues of the matrix of the differential equation system, $v_{k,i} = \sin \left(\frac{i\,k\,\pi}{N_P + 1} \right)$ are the components of the corresponding eigenvectors, $p_{s,i} = p_0 \left(1 - \frac{i}{N_P + 1} \right)$ are the components of the steady-state solution and μ_k are coefficients which are determined by the initial condition $p_i(0) = 0$.

Consequently, the solution for $N_P = 1$, i.e. for the structure A / P / A, is given by

$$p(t) = \frac{p_0}{2} \left(1 - exp \left(\frac{2\, Q_A\, t}{h_P S_P} \right) \right). \tag{31}$$

The resulting flux density $j = Q_A\, p$ at the boundary where the partial pressure is zero is shown in Figure 87 by the dotted curves. In the case of high S_P / S_A ratios the solutions obtained by the finite element method and in quasi-steady-state approximation agree very well. This justifies the approximation for structures of alternating layers under the given assumptions.

The solution for arbitrary number N_P shows that for structures of alternating layers in the ideal laminate model, the time required for approach to the steady state is proportional to $h_P S_P / Q_A = h_A h_P S_P / (D_A S_A)$. The further discussion shows that the time increases with the number of layers. The lag time (ϑ) is given by

$$\vartheta = \frac{N_P (N_P + 2)\, h_A\, h_P\, S_P}{6 D_A S_A}. \tag{32}$$

Similar results are obtained if structures of alternating inorganic and polymeric layers are considered in the geometric defect model. The inorganic layers, A are assumed to be impermeable outside of circular defects with diameter (d) which are placed on a quadratic lattice with distance (a) between nearest neighbours. The defects in consecutive layers A are shifted against each other (Figure 89).
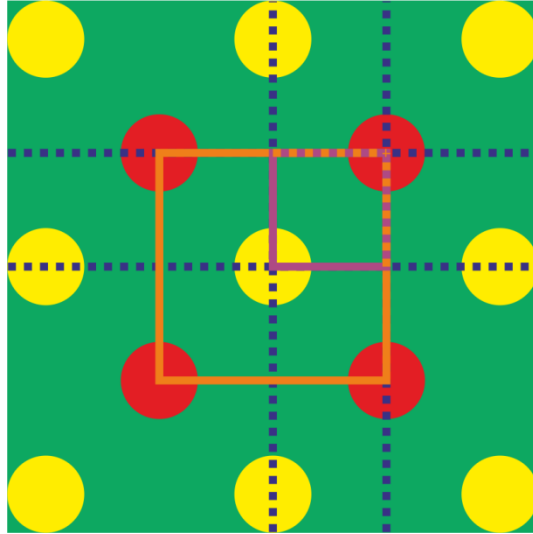
Figure 89: Structure A / P / A in the geometric defect model: the defects of one-layer A (yellow) are shifted against the defects of the other layer A (red). The blue lines show symmetry planes of the structure; the orange square confines that volume within P where the substance entering through the defect shown in the middle spreads (Miesbauer, 2017).

The FEM simulation of the transient permeation through the structure A / P / A in the geometric defect model shows that the substance which enters the layer P through one defect of the first layer A shown in the middle of Figure 89 spreads over the whole volume of P confined by the orange square. The increase of the partial pressure within this volume with time correlates with the increase of the flux at the boundary with partial pressure equal to zero.

This allows an assumption that the time dependent permeation through structures of alternating layers can be described in quasi-steady-state approximation for the geometric defect model. In case of the structure A / P / A the flux as a function of time calculated in this approximation agrees with the result of FEM simulation.

The general solution obtained for the structure A / P / A / ... / P / A in the ideal laminate model can be transferred to the geometric defect model, if one P layer is added at each boundary. The resulting structure P / A / P / A / ... / P / A / P is close to the structures of VIP barrier laminates.

The discussion finally gives a lag time

$$\vartheta = \frac{(N_P - 2)\, N_P\, h_P\, a^2}{3\, d\, D_P}$$

(33)

where N_P denotes the resulting number of layers P, having the polymer thickness, h_P is assumed to be large compared to the defect diameter d.

The theoretical discussion shows that a large lag time of permeation of oxygen and nitrogen through barrier laminates can be expected if thick polymeric materials are placed between inorganic layers. This is fulfilled for typical VIP barrier laminates (e.g. for the structure PET / Al / PU / PET / Al / PU / PET / Al / PU / LDPE). It can also be concluded

that a back-to-face laminate like PET / Al / PU / PET / Al / PU / LDPE will have a significantly extended lag time compared to the face-to-face laminate PET / Al / PU / Al / PET / PU / LDPE. This effect of lag time extension is especially large if the inorganic layers have a very low permeability, i.e. if they are characterised by a small defect diameter and a large defect distance.

In case of water-vapour-permeation a long lag time is expected when the inorganic layers have a low solubility to water vapour in comparison to the polymeric materials enclosed between them. A further extension of lag time is possible if the solubility for the polymeric materials is increased by dispersing water absorbers like zeolites or hygroscopic salts within them.

Systematically using these concepts can contribute to the overall barrier performance of VIP laminates and therefore to a long VIP lifetime. However, these lag time effects have to be taken into consideration for permeation measurements and their evaluation as discussed in Chapter 4.

5.2 Life expectancy estimation for VIP in different climates

5.2.1 Principle and Approach

The basic research approach is a combination of laboratory scale measurements to determine the relevant ageing parameter in quantities and to apply these functions on modelling data (e.g. obtained with hygro-thermal modelling software like WUFI® or DELPHIN®).

The investigation considers five different exemplary constructions that are flat roof / roof terrace (horizontal), pitched roof (30° slope of roof), external thermal insulation compound system (ETICS) (vertical), internal insulation (vertical) and a ventilated façade (vertical) (Figure 90).
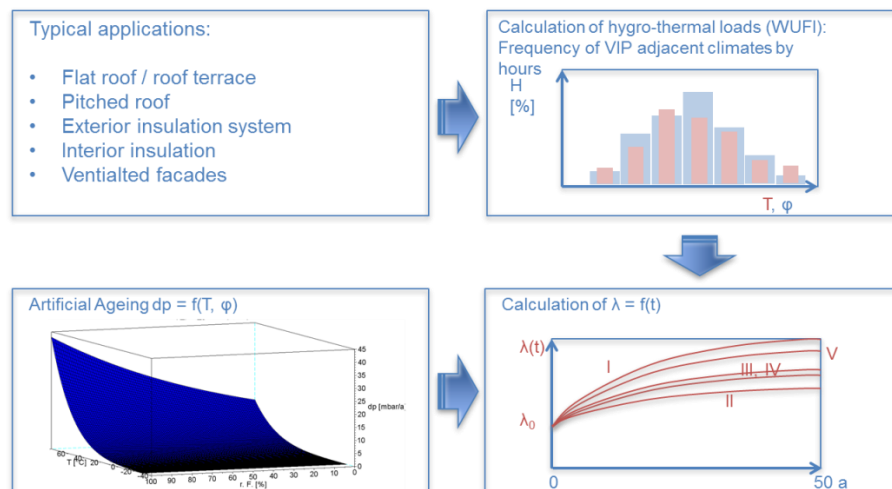
Figure 90: Principle research approach for modelling of thermal conductivity as a function of time (e.g. for VIP). Source: FIW München.

5.2.2   Investigated examples of constructions in Germany

The constructions are described in detail in the ST 3 report in Chapter 4 and Annex B. To ensure a consistent reading, the material data for the layers of the investigated constructions are given also in Table 33.

Table 33 includes a number for each material that can be used to describe the construction by a sequence of numbers, starting with the exterior layer and ending with the interior layer of the construction (Table 34). Each construction contains three different configurations of the VIP with VIP only and variations on cladding made of rigid foam (exemplary extruded polystyrene foam, XPS) and a rigid layer made of glass reinforced plastic (GRP). This "block" is identical for all observed constructions and is characterised by a numerical sequence (3-2)/1/(2-3).

Table 33: Material data for the layers of the constructions C1 – C5.

Nr.	Material	d in mm	ρ in kg/m³	porosity in m³/m³	c in J/(kg K)	λ in W/(m K)	μ -
1	VIP	20/30/40	200	0.99	850	0.004	∞
2	XPS	5	40	0.95	1500	0.03	100
3	GRP	3	1800	0.95	1500	0.3	83600
4	Vapour control layer	1	130	0.001	2300	2.3	50000
5	Underlay membrane	1	130	0.001	2300	2.3	200
6	Wood (spruce)	20	455	0.73	1500	0.09	130
7	Gypsum fibre board	12.5	850	0.65	850	0.2	8.3
8	Sand-lime brick	115	1900	0.29	850	1	28
9	Internal plaster, Gypsum	15	850	0.65	850	0.2	8.3
10	Exterior plaster	20	from WUFI® database as a sytem consisting of four layers				
11	Concrete, C35/45	175	2200	0.18	850	1.6	248
12	Concrete, C12/C15	20	2200	0.118	850	1.6	92
13	Watertight membrane V13	20	2400	0.001	1000	0.5	100000
14	Gravel	50	1400	0.3	1000	0.7	1
15	Air layer	50	1.3	0.999	1000	0.28	0.32

For all constructions C1 – C5 several variations (Table 34) are examined that consider different thickness of the VIP panels, the orientation of the building element, the internal moisture load (Table 35) and the location of the building in Freiburg (Table 36) and Holzkirchen (Table 39).

Table 34: Construction C1 – C5 with specialities of the hygro-thermal model.

C1 Flat roof / roof terrace	Outside climate - 12/14/13/(3-2)/1/(2-3)/11/9 – Interior climate	
Characteristics	Moisture spring with 1% of driving rain on the inner 5mm of layer 14	
U-value In W/(m² K)	VIP 20mm	0.173
	VIP 30mm	0.121
	VIP 40mm	0.093
C2 Pitched roof	Outside climate - 6/(3-2)/1/(2-3)/4/7 - Interior climate	
Characteristics	Moisture spring based on air infiltration on the inner 5mm of layer 6	
U-value In W/(m² K)	VIP 20mm	0.174
	VIP 30mm	0.121
	VIP 40mm	0.093
C3 ETICS	Outside climate - 10/(3-2)/1/(2-3)/8/9– Interior climate	
Characteristics	Moisture spring with 1% of driving rain on the outer 5mm of layer 8	
U-value In W/(m² K)	VIP 20mm	0.174
	VIP 30mm	0.121
	VIP 40mm	0.093
C4 Internal insulation	Outside climate - 10/8/9/(3-2)/1/(2-3)/4/7– Interior climate	
Characteristics	-	
U-value In W/(m² K)	VIP 20mm	0.172
	VIP 30mm	0.120
	VIP 40mm	0.092
C5 Ventilated façade	Outside climate - 6/15/5/3/(3-2)/1/(2-3)/0/8/9 - Interior climate	
Characteristics	Air exchange of 100h⁻¹ in layer 15	
U-value In W/(m² K)	VIP 20mm	0.164
	VIP 30mm	0.116
	VIP 40mm	0.090

Table 35: Interdependency between exterior and interior climate for normal and high moisture load according to EN 15026:2007.

Interior temperature as a function of exterior temperature for normal and high moisture load	Interior relative humidity as a function of exterior tempearture for normal moisture load	Interior relative humidity as a function of exterior tempearture for high moisture load
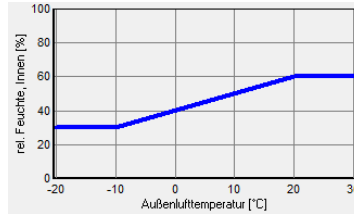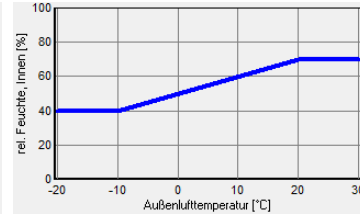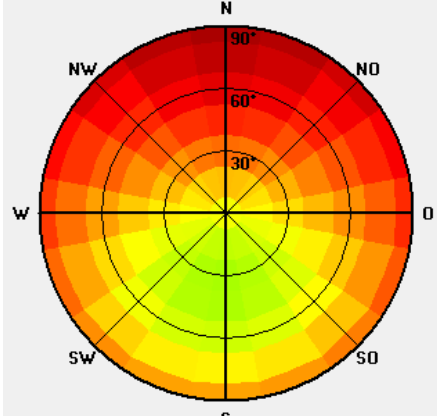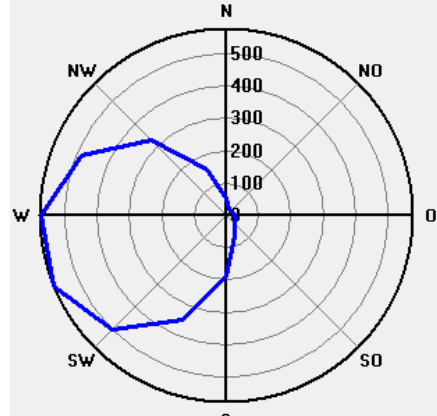
The interior climate is modelled according to EN 15026:2007 that assumes interdependency between interior and exterior temperature and relative humidity according to Table 35.

Table 36: Summarized exterior climatic analysis of the location Freiburg (WUFI®).

Mean temperature in °C:	10.4	**Mean relative humidity** in %:	74
Max. temperature in °C:	32.5	**Max. relative humidity** in %:	100
Min. temperature in °C:	-10.7	**Min. relative humidity** in %:	12
Downward terrestrial radiation in kWh/(m^2 a):	2431.3	**Mean windspeed** in m/s:	2.77
Mean degree of overclouding [-]:	0.65	**Normal rain sum** in mm/a:	940
Sum of solar radiation in kWh/(m^2 a)		**Sum of driving rain** in mm/a	

Table 37:   Summarized exterior climatic analysis of the location Holzkirchen (WUFI®).

Mean temperature in °C:	6.6	Mean relative humidity in %:	81
Max. temperature in °C:	32.1	Max. relative humidity in %:	98
Min. temperature in °C:	-20.1	Min. relative humidity in %:	24
Downward terrestrial radiation in kWh/(m² a):	2668.4	Mean windspeed in m/s:	2.33
Mean degree of overclouding [-]:	-	Normal rain sum in mm/a:	1185
Sum of solar radiation in kWh/(m² a)		Sum of driving rain in mm/a	

While Freiburg offers a higher mean temperature, Holzkirchen is characterised by higher hygric stress offering a higher relative humidity and more (driving) rain that leads especially for west-oriented building elements to a significantly higher humid stress acting on the building material.

5.2.3 Determination of internal pressure increase rates as a function of temperature and relative humidity

For the combined research approach consisting of lab-based investigation of ageing behaviour and appliance of hygro-thermal modelling, the 40 VIP panels in a thickness of 15mm produced in one batch of production were provided by a manufacturer. The thickness of 15mm was chosen to evoke a significant increase of internal pressure by time. Thicker panels with a higher volume need more time to show recordable increases of internal pressure.

The storage of the real panels in several climates ensures a realistic ageing of the panels. For this reason, nine climate steps with temperature in between 23°C and ca. 70°C and relative humidity starting with dry conditions of around 10% RH, ending up in around 90% RH were chosen. To ensure a consistent storage the panels were kept in transparent boxes including saturated salt solutions that guarantee a defined relative humidity when stored at a certain temperature. In each climate step four VIPs were stored for up to nine months.

Table 38:   Climate conditions for artificial ageing of VIP.

Salt	Climate @23°C	Climate @ ca. 45°C	Climate @ca. 70°C
LiCl	23°C / 11% RH	42°C / 11% RH	70°C / 11% RH
NaBr	23°C / 57% RH	45°C / 51% RH	69°C / 45% RH
K_2SO_4	23°C / 97% RH	46°C / 96% RH	71°C / 95% RH

The internal pressure inside the VIP is the sum of the partial pressure from dry air gases and water vapour. Both partial pressures are measured when the lift-off method according to Chapter 2.3 is applied.

To develop a model for the increase of thermal conductivity by time it is essential to have differentiated information about the permeation of dry gases and the permeation of water vapour. These values can be derived from experimental data about internal pressure at different temperature levels. The calculation is described in Kraus et al., 2005 as was conducted in this study similarly, using ca. 20°C and 40°C.

The results for the total pressure increase by time and the different climatic steps are plotted in Figure 91. The derived partial pressure of dry air gases and water vapour show a similar behaviour.
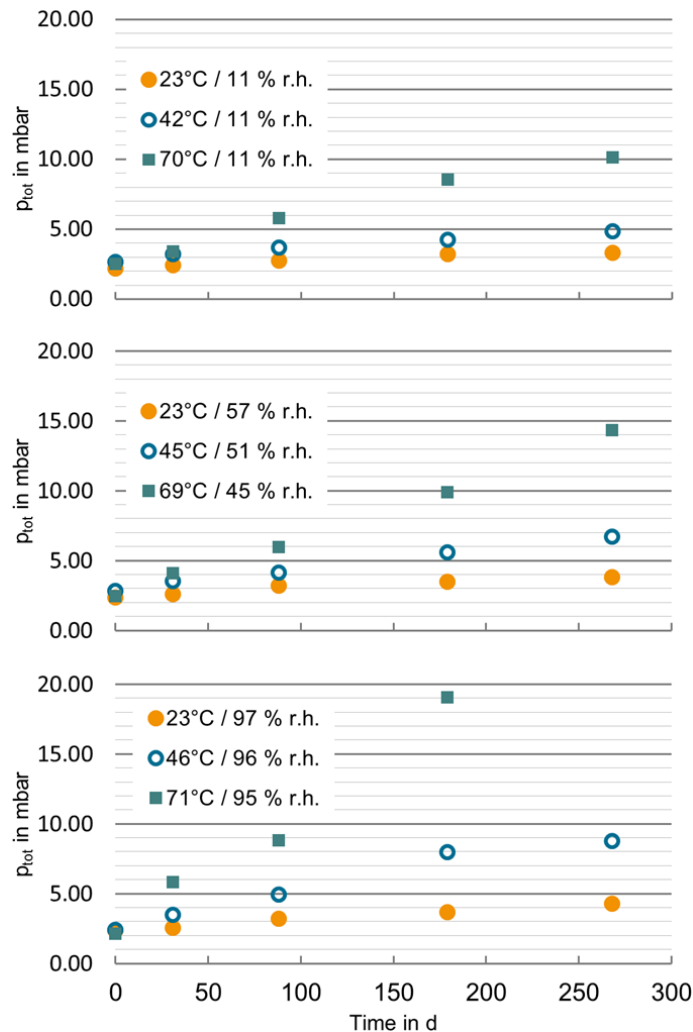
Figure 91: Increase of total internal pressure of the observed VIP by time in different climatic steps (Sprengard et al., 2016).

From Figure 91, increase rates of total and partial pressure in mbar per year (mbar/a) are calculated using linear regression for the obtained data rows over time. This is performed for the total pressure increase as well as the partial pressure of dry air gases and water vapour. Directly after the production, an increased rate of internal-pressure is observed due to outgassing of the silica-based core and the foil barrier. This initial pressure increase can be neglected. As the panels were kept in laboratory conditions for about half a year before the measurement was started, the obtained fresh values of internal pressure were not influenced by the described effect.

Figure 92 shows the calculated pressure increase rates (p_{inc}) grouped for the mean relative humidity of approximately 11%, 50% and 96%, respectively plotted over the temperature. It is obvious that an exponential shaped curve is obtained that way.
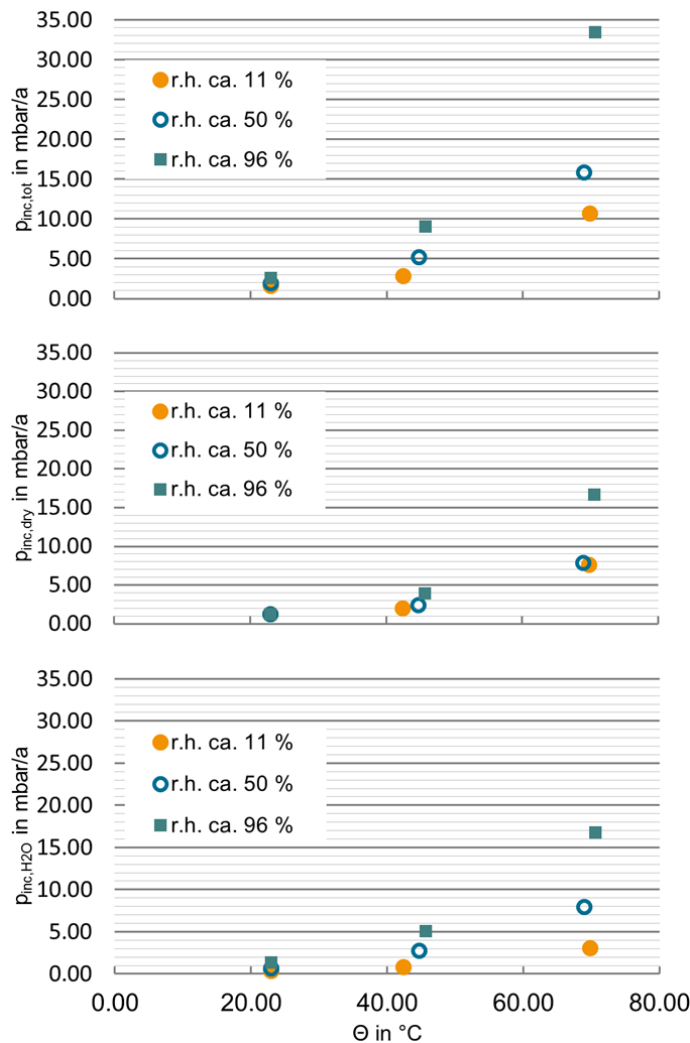
Figure 92: Pressure increase rates (p_{inc}) at different levels of mean relative humidity as a function of the storage temperature in °C. Top plot: total pressure increase; middle plot: dry air gases; bottom plot: water vapour (Sprengard et al., 2016).

The mentioned exponential shaped regression of pressure-increase rates by the temperature in °C is typical for Arrhenius behaviour of the observed measurements. To prove the Arrhenius behaviour ageing, the logarithm of the pressure increase rate is plotted over the reciprocal of the absolute temperature in Kelvin (Figure 93).

For the water vapour pressure increase (bottom plot in Figure 93) the obtained linear curves are clearly separated while the differentiation for the dry air pressure increase (middle plot in Figure 93) is not very significant because pressure increase rates of dry air gases are only affected in case of very high relative humidities.This is also visible in the middle plot of Figure 92. However, as relative humidities of >70-80% are reached by the mean values of the exterior climate in Freiburg and Holzkirchen, it makes sense to differentiate between dry air gases to describe the pressure increase by time.
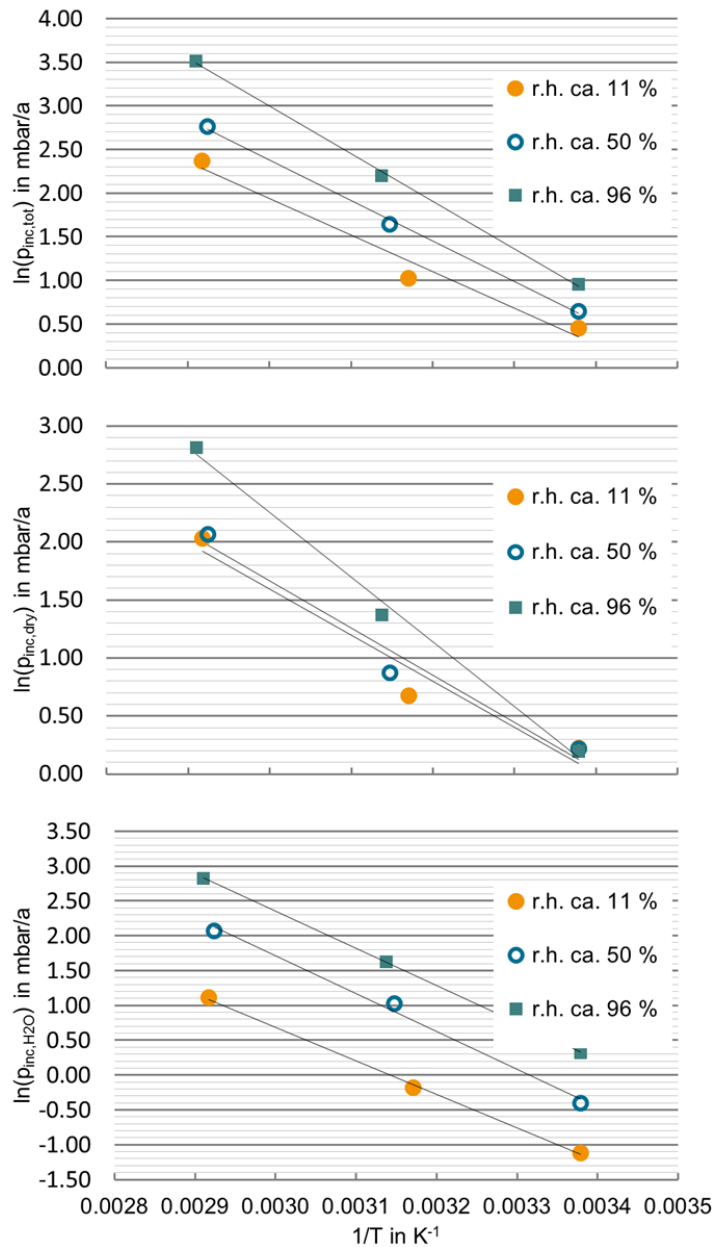
Figure 93: Logarithm of the pressure increase rate by the reciprocal of the absolute storage temperature in Kelvin. Top plot: total pressure increase; middle plot: dry air gases; bottom plot: water vapour (Sprengard et al., 2016).

To describe the (partial) pressure increase as a function of temperature and relative humidity, the data points included in Figure 93 are used to approximate a linear surface equation to the approach:

$$ln\left(p_{inc,tot}\right) = a \cdot T^{-1} + b \cdot \varphi + c \tag{34}$$

Via back-transformation the pressure increase can be plotted directly as a function of temperature in °C and relative humidity in % (Figure 94).
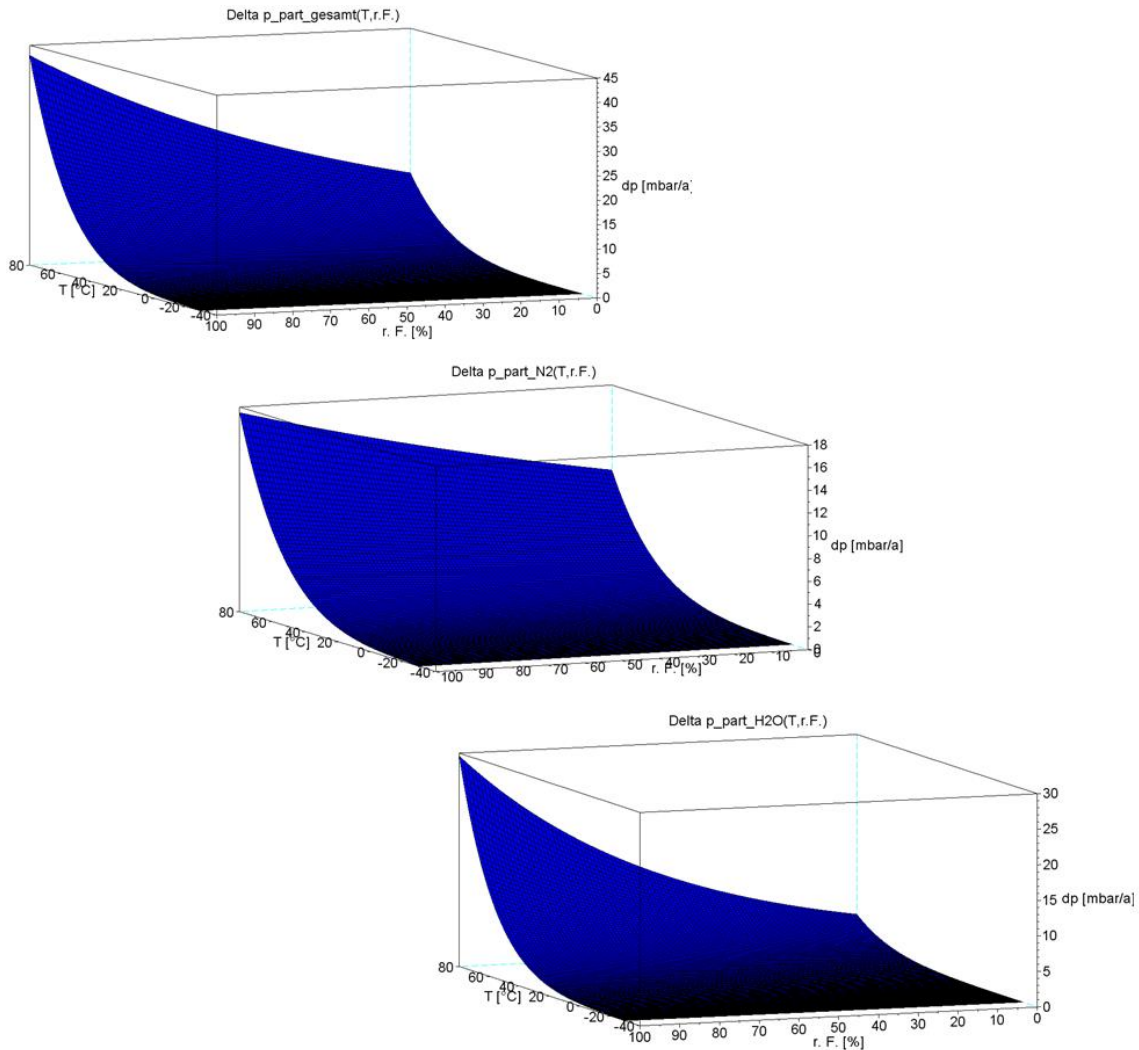
Figure 94: Pressure increase rates in mbar/a as a function of temperature in °C and relative humidity in %. Top plot: total pressure increase; middle plot: dry air gases; bottom plot: water vapour (Sprengard et al., 2016).

For storage of VIP in constant climate conditions the corresponding pressure increase by time can be directly calculated using the function of the curves plotted in Figure 94.

5.2.4 *Development of a model to describe the internal pressure increase in a certain building application*

To apply the determined functionalities of internal-pressure-increase as a function of temperature and relative humidity on real applications, hygro-thermal simulation was conducted on the constructions described in Chapter 5.2.2. The simulation was undertaken with the hygrothermal software package WUFI®. The observed time frame was three years and only values of the third year were considered for the subsequent calculations.

The calculation of the yearly pressure increase (separated for the dry air gases and water vapour) is taken out by inserting the hourly WUFI® obtained values of temperature and relative humidity (see Figure 95, for example) into the equations according to Figure 94.

As the laboratory experiment was conducted on VIP with 15mm thickness, the modelled pressure increases were converted to a panel thickness of 20, 30 and 40 mm, assuming the ideal gas equation.
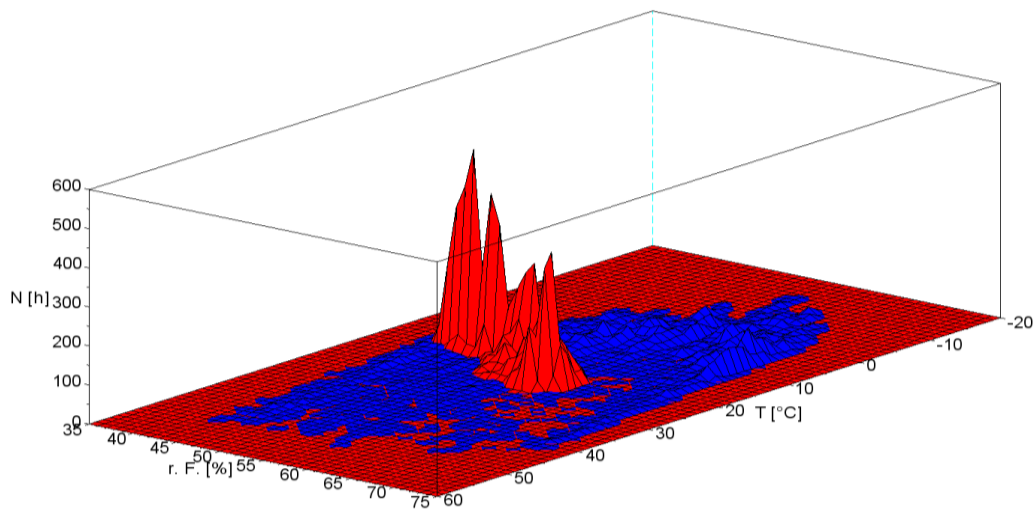
Figure 95: Distribution of hourly obtained values of temperature and relative humidity on the boundary layer of a VIP with 20mm in the application of a pitched roof, extruded polystyrene foam (XPS) cladding, located in Freiburg, normal internal moisture load and south orientation (Sprengard et al., 2016).

The sum of the hourly calculated pressure-increase then characterises the increase of the partial pressure of VIP in the first year of exposition in a specific application $p_{inc}(t = 0)$.

As there are different climatic conditions on the warm- and cold side of the VIP the calculation was performed separately, and the mean value is considered as the representative value for the subsequent calculations.

To calculate the long-time behaviour of the partial-pressure-increase, the value $p_{inc}(t = 0)$ is integrated in a saturation function to the approach:

$$p(t) = (p_{end} - p_0) \cdot \left(1 - e^{\left(\frac{-t}{\tau}\right)}\right) + p_o \tag{35}$$

The necessary assumptions for the ratio between dry air gases and water vapour was considered with 85% of the internal pressure being dry air gases and 15% being water vapour.

p_{end} (Partial-) pressure for t → infinity
              For dry air gases: 1013.25mbar
              For water vapour: according to the mean climate,

p_0 Initial pressure at the beginning of investigated time-frame:
              2.5mbar (total internal pressure)
              2.125mbar (internal pressure of dry air gases)
              0.375mbar (internal pressure of water vapour),

τ Damping constant

$$(p_{end} - p_0)/p_{inc}(t = 0).$$

The methodology for the modelling of internal pressure increase by time in a certain application is illustrated in Figure 96.
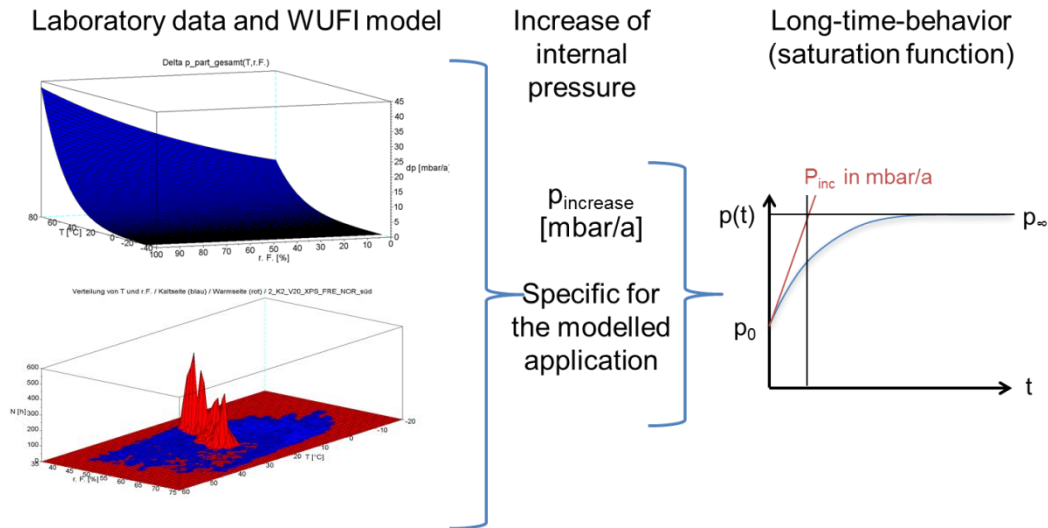
Figure 96: Methodology for calculation of internal pressure increase by time (Sprengard et al., 2016).

Applying this methodology to the climate data sets obtained for the different applications specified in Chapter 5.2.1, the results can be plotted e.g. for 50 years of use.

In Figure 97 the calculation for a VIP with 20mm thickness and XPS cladding in the application of a south-oriented pitched roof, located in Freiburg with normal internal moisture load is show to be effective. It becomes obvious that the partial pressure increase of water vapour decreases over the observed time period. In the actual application the mean climate is 16.4°C and 53.7% RH. This leads to a mean partial pressure of water vapour of 9.98mbar. This value is nearly reached after the 50 year timeframe.

On the other hand, the increase of dry air gases shows no such deterioration. This can be explained by the much higher value of end pressure for dry air gases with 1013.25mbar.

The sum of the partial pressure of dry air gases and water vapour is the total internal pressure increase that is characterised by a slight decreased trend.
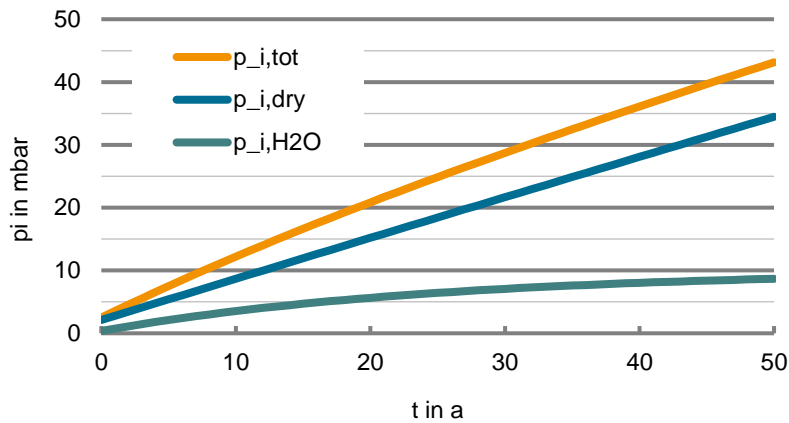
Figure 97: Result of the simulation of pressure increase by time over a period of 50 years; application of a 20mm VIP with XPS cladding in the construction of a pitched roof, located in Freiburg, normal internal moisture load and south orientation (Sprengard et al., 2016).

5.2.5 Calculation of thermal conductivity based on knowledge about partial pressure of dry air gases and water vapour and internal moisture content of the core material

The calculation of thermal conductivity of the VIP by time is based on the assumption of a starting value and subsequent increase of this value. The increase rate is based on the changes of gas thermal conductivity as well as thermal conductivity of the solid due to an increase of the moisture content.

The gas thermal conductivity is calculated taking into account the half-life gas pressure $p_{1/2,Gas}$ and thermal conductivity of the free gas, $\lambda_{Gas,free}$ according to Schwaab, 2004:

$$\lambda_{Gas}(p_{Gas,part}) = \frac{\lambda_{Gas,free}}{1 + \dfrac{p_{1/2}}{p_{Gas,part}}} \tag{36}$$

The required parameter $p_{1/2,Gas}$ und $\lambda_{Gas,free}$ are given in Table 39. For dry air gases nitrogen N_2 is considered.

Table 39: Parameter for calculation of thermal conductivity of the gas.

Gas	$\lambda_{Gas,frei}$ in mW/(m K)	$p_{1/2}$ in mbar
N_2	25.6	600
H_2O	18.2	240

The increase of thermal conductivity due to increase of the moisture content of the core material is considered assuming a linear relation that results in a factor C:

$$C = \frac{\Delta\lambda}{\Delta X_{w,m}} \tag{37}$$

121

The required moisture content of the core is calculated based on the sorption behaviour and the known partial water vapour pressure. As limited literature information is available, the factor C was determined by calibration measurement using measurement values of the characterisation of the artificial aged panels. The achieved conformance of the model with the measurements gives satisfying accuracy (Figure 98).
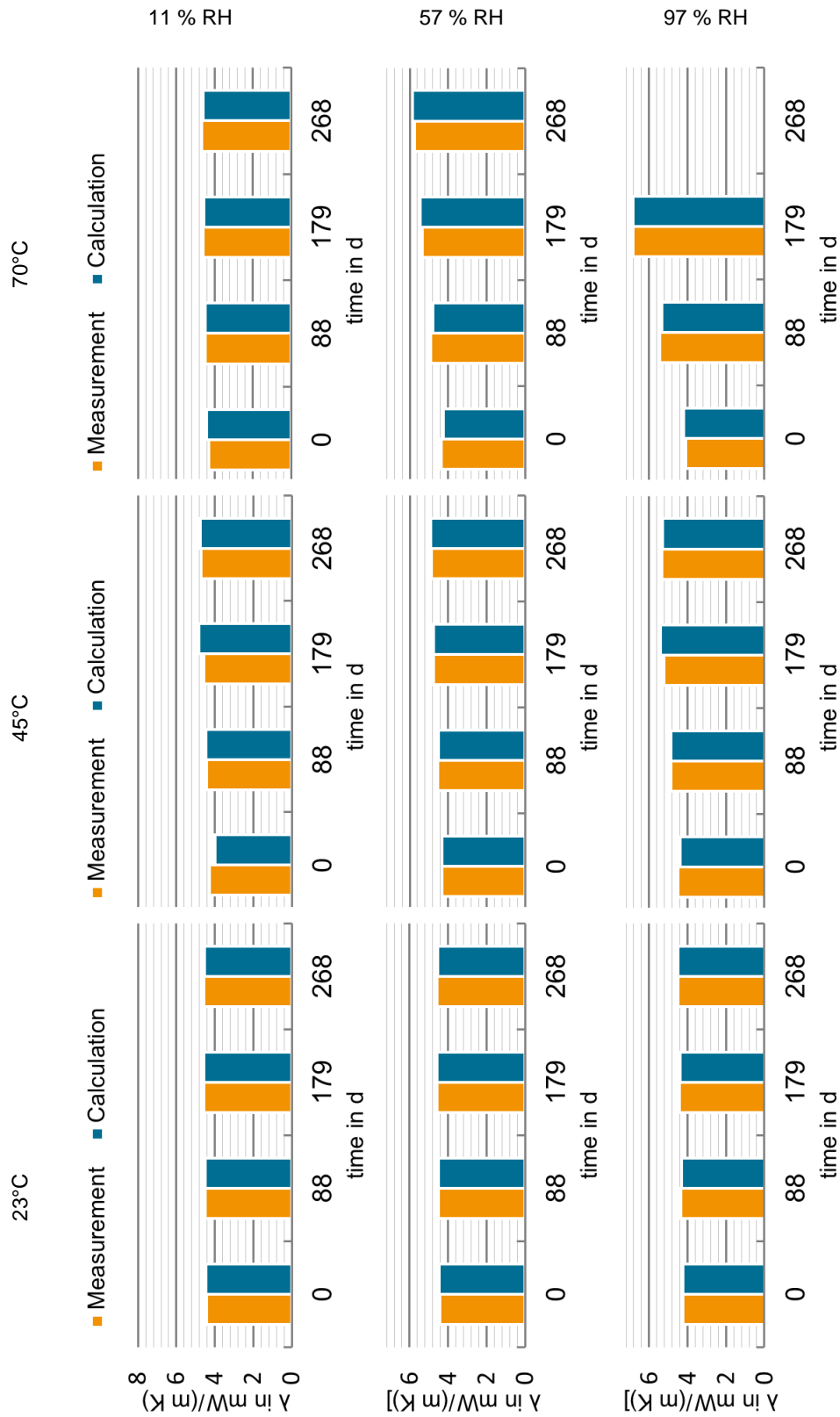
Figure 98: Comparison of thermal conductivity as measured in the lab during ageing of the panels to determine the internal pressure increase. Calculation based on internal pressure increase and increased moisture content of the core (Sprengard et al., 2016).

5.2.6 Simulation of long-time behaviour of thermal conductivity for different examples applications in Germany

According to the data of temperature and relative humidity derived from the WUFI® calculation for the warm- and cold side of the VIP, the evolution of the internal pressure and subsequent evolution of thermal conductivity by time was calculated, using the parameters according to Table 40.

Table 40: Parameter for the simulation of increase of thermal conductivity of VIP.

Parameter		Unit	Value
Thickness	d	mm	20, 30, 40
Internal pressure (initial)	p_{tot}	mbar	2.5
Partial pressure dry air (initial)	p_{dry}	mbar	2.125
Partial pressure water vapour (initial)	p_{H2O}	mbar	0.375
Thermal conductivity (initial)	λ_0	W/(m K)	0.004
Slope of sorption isotherm (0-60% RH)	α	m-%/% r. F.	0.0188
Therm. cond. / moisture content core	C	W/(m K)/m-%	0.00278

In all calculated constructions the VIP show a descendent functionality of thermal conductivity by time. The differences between the constructions and climatic impact due to external and internal moisture and temperature loads are specific. In particular, the constructions C3 (ETICS) and C5 (ventilated façade) show individual behaviour that will be discussed later in detail.
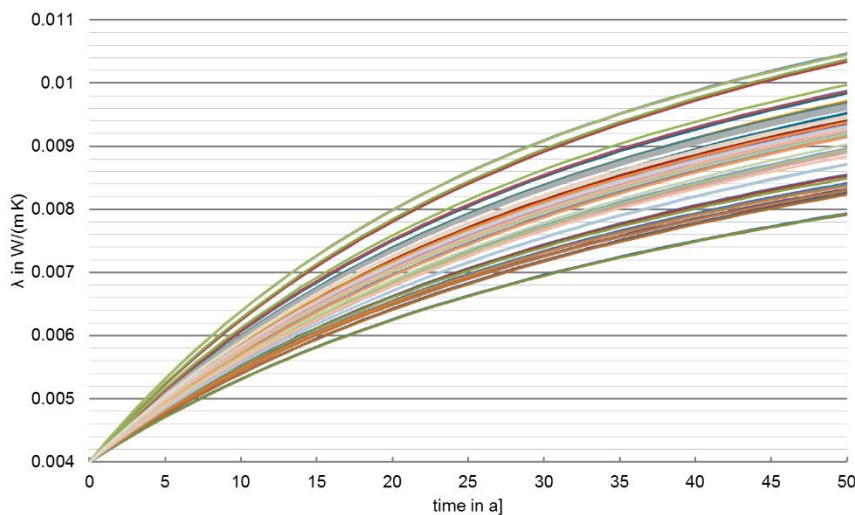
Figure 99: Time dependent behaviour of thermal conductivity of 20mm thick VIP panels in the observed constructions C1 – C5, assuming variation of cladding, location and orientation of the building element and internal moisture loads (Sprengard et al., 2016).

For comparison, in the following charts the mean thermal conductivity in the first 25 years of use is chosen. This is consistent with the actual draft of the product standard for VIP which recommends the mean thermal conductivity in the first 25 years of use as a rated value. In the first half of the use the rated value of thermal conductivity overestimates the

real value, conversely in the second half of use the value is underestimated. It will be discussed later how this influences the total heat loss balance.

For each case several statistical parameters are given in the charts that describe the climate impact and the ageing behaviour:

T_{mean} mean temperature on the boundary layer of the VIP,

$T_{effektiv}$ effective mean temperature on the boundary layer of the VIP,

φ_{mean} mean relative humidity on the boundary layer of the VIP,

$\varphi_{effektiv}$ effective mean relative humidity on the boundary layer of the VIP,

$p_{inc,dry}$ partial pressure increase of dry air gases in the VIP in the first year,

$p_{inc,H2O}$ partial pressure increase of water vapour in the VIP in the first year,

$p_{end,H2O}$ partial pressure increase of water vapour in the VIP after t →∞.

The effective mean temperature and relative humidity represents a constant climate that would causes the same ageing effect as the calculation based on observed transient climates. The difference to the mean temperature and relative humidity is due to the exponential weighting of the functionalities used to describe the influence of temperature and relative humidity on the internal pressure increase. Therefore, as a tendency, the effective mean temperature and relative humidity increasing.

The calculation of the effective values was taken out as described in the following. The equation to describe the partial water vapour pressure increases as a function of temperature and relative humidity.

$$ln\left(p_{a,H2O}\right) = \frac{a_{H2O}}{T_{eff}} + b_{H2O} \cdot \varphi_{eff} + c_{H2O} \tag{38}$$

is re-arranged to

$$T_{eff} = \frac{a_{H2O}}{ln(p_{H2O}) - b_{H2O} \cdot \varphi_{eff} - c_{H2O}} \tag{39}$$

The equation to describe the partial dry air gases pressure increase as a function of temperature and relative humidity

$$ln\left(p_{a,dry}\right) = \frac{a_{dry}}{T_{eff}} + b_{dry} \cdot \varphi_{eff} + c_{dry} \tag{40}$$

is re-arranged to φ_{eff} and the equation for T_{eff} is inserted

$$\varphi_{eff} = \frac{a_{H2O} \cdot ln\left(p_{dry}\right) - a_{H2O} \cdot c_{dry} - a_{dry} \cdot ln(p_{H2O}) + a_{dry} \cdot c_{H2O}}{a_{H2O} \cdot b_{dry} - a_{dry} \cdot b_{H2O}} \tag{41}$$

By inserting equation (21) in equation (19) T_{eff} is calculated.

In the application as flat roof / roof terrace (Figure 100) no variation of the orientation of the building element is considered due to the horizontal mounting orientation. The

influence of varying cladding on the mean temperatures is of low impact. The difference between the mean and effective temperatures is significant with 1.5°C higher effective temperatures.

The small but visible differentiation of the variation of cladding on the mean thermal conductivity correlates with the additional diffusion resistance. This is visible in lower mean and effective relative humidities and subsequent lower increase rates for partial water vapour pressure, as seen with XPS or GRP cladding. The increase of partial pressure of dry air gases is not very sensitive to variations of relative humidity, therefore the differences are lower in this case.

Assuming identical orientation and internal moisture loads, the influence of the location is negligible even though there are significant differences of mean temperature and relative humidity in between Holzkirchen and Freiburg. Again, due to the exponential weighting these differences become smaller or even negligible for the effective climate.

Significant influence is visible for the variation of internal moisture loads. An increase of the internal moisture load affects the increase rates of partial water vapour pressure in the VIP.

T_{mean} [°C]	15.5	15.5	15.5	14.6	14.7	14.6	14.6	14.7	14.6			
T_{eff} [°C]	16.7	16.8	16.8	16.2	16.2	16.3	16.3	16.3	16.4			
φ_{mean}[%]	79.1	76.4	75.8	77.7	75.2	74.6	81.5	79.2	78.8			
φ_{eff}[%]	80.6	77.6	76.7	80.7	77.6	76.4	83.4	80.9	80.0			
$p_{inc,dry}$ [mbar/a]	0.691	0.682	0.681	0.672	0.662	0.661	0.686	0.677	0.677			
$p_{inc,H2O}$ [mbar/a]	0.553	0.524	0.517	0.535	0.506	0.498	0.568	0.542	0.535			
$p_{end,H2O}$ [mbar]	13.9	13.4	13.3	12.9	12.5	12.4	13.5	13.2	13.1			
cladding	NC	XPS	GRP	NC	XPS	GRP	NC	XPS	GRP	-	-	-
room climate	Norm. moist. load			Norm. moist. load			Incr. moist. load			-		
orientation	-			-			-			-		
location	D-Freiburg			D-Holzkirchen			D-Holzkirchen			-		

Figure 100: Mean thermal conductivity of 20mm thick VIP during the first 25 years of use for the construction C1 – Flat roof / roof terrace with variation of location and orientation of the building, varying cladding and internal moisture loads (Sprengard et al., 2016).

Figure 101 summarises the results for the application pitched roof. Compared to the flat roof / roof terrace the mean thermal conductivity in the first 25 years of use is generally on a lower level. This can be explained with the lower adjacent relative humidity (mean values of 50-60% RH).

Differences between the locations with otherwise identical parameters are again lower than expected with respect to the variation of climate between Freiburg and Holzkirchen.

The inter-connections are comparable to the discussed behaviour of the flat roof / roof terrace. The effective mean temperatures become more or less equal. The lower mean relative humidity in Holzkirchen leads to lower increase rates for partial pressure of water vapour.

The variations with increased internal moisture load evoke a slightly higher level of thermal conductivity depending on the orientation of the building from South to West. The big difference between the heavy rain sums of the climate data when varying the orientation does not have a significant impact on the thermal conductivity because the moisture input into the construction is observed by air infiltration.

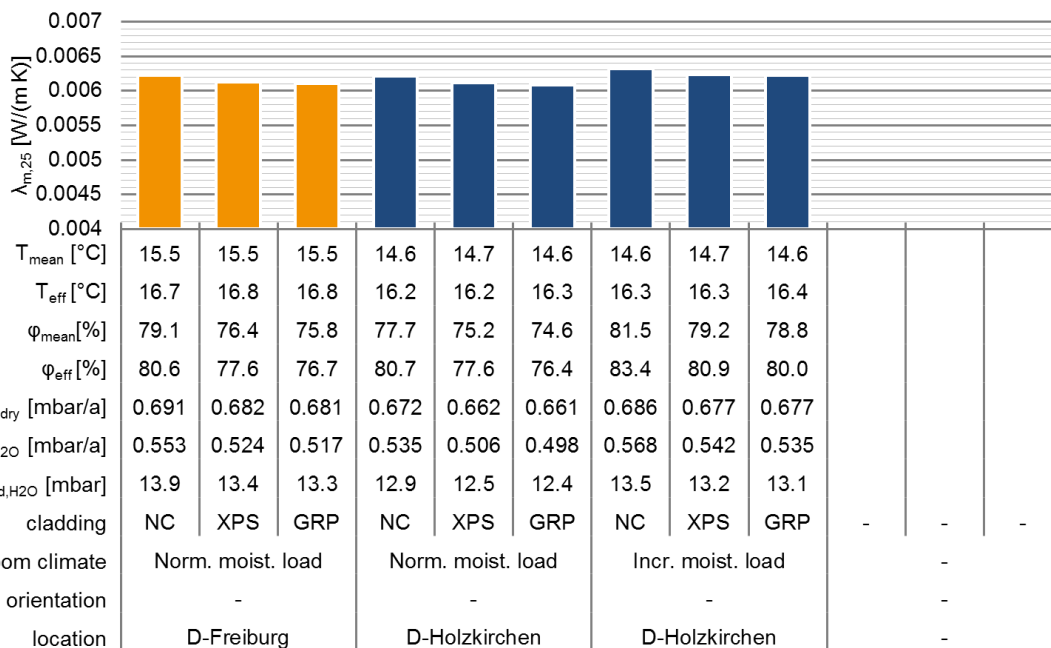| T_{mean} [°C]	16.4	16.4	16.4	15.8	15.8	15.8	15.8	15.8	15.8	14.6	14.7	14.6	15.3	15.3	15.3
T_{eff} [°C]	18.2	18.1	18.1	18.3	18.2	18.1	18.2	18.1	18.1	16.6	16.5	16.5	17.5	17.5	17.4
φ_{mean}[%]	54.2	54.0	53.7	48.5	48.2	48.4	54.6	54.4	54.3	61.7	61.3	60.3	57.5	57.2	56.7
φ_{eff} [%]	55.6	55.8	55.7	50.5	50.7	50.7	57.2	57.4	57.3	62.9	63.0	62.8	59.5	59.7	59.6
$p_{inc,dry}$ [mbar/a]	0.661	0.658	0.658	0.645	0.642	0.641	0.666	0.663	0.662	0.627	0.625	0.625	0.649	0.647	0.646
$p_{inc,H2O}$ [mbar/a]	0.384	0.383	0.383	0.350	0.350	0.349	0.396	0.395	0.393	0.396	0.395	0.394	0.395	0.394	0.393
$p_{end,H2O}$ [mbar]	10.1	10.1	10.0	8.7	8.7	8.7	9.8	9.8	9.7	10.3	10.2	10.0	10.0	9.9	9.8
cladding	NC	XPS	GRP	NC	XPS	GRP	NC	XPS	GRP	NC	XPS	GRP	NC	XPS	GRP
room climate	Norm. moist. load			Norm. moist. load			Incr. moist. load			Incr. moist. load			Incr. moist. load		
orientation	South			South			South			North			West		
location	D-Freiburg			D-Holzkirchen			D-Holzkirchen			D-Holzkirchen			D-Holzkirchen		

Figure 101:   Mean thermal conductivity of 20mm thick VIP during the first 25 years of use for the construction C2 – Pitched roof with variation of location and orientation of the building, varying cladding and internal moisture loads (Sprengard et al., 2016).

Figure 102 includes the result for the application of VIP as ETICS. Compared to the previous discussed applications, the mean thermal conductivity in the first 25 years of use is higher and shows more differentiation between the varying location and orientation of the building.

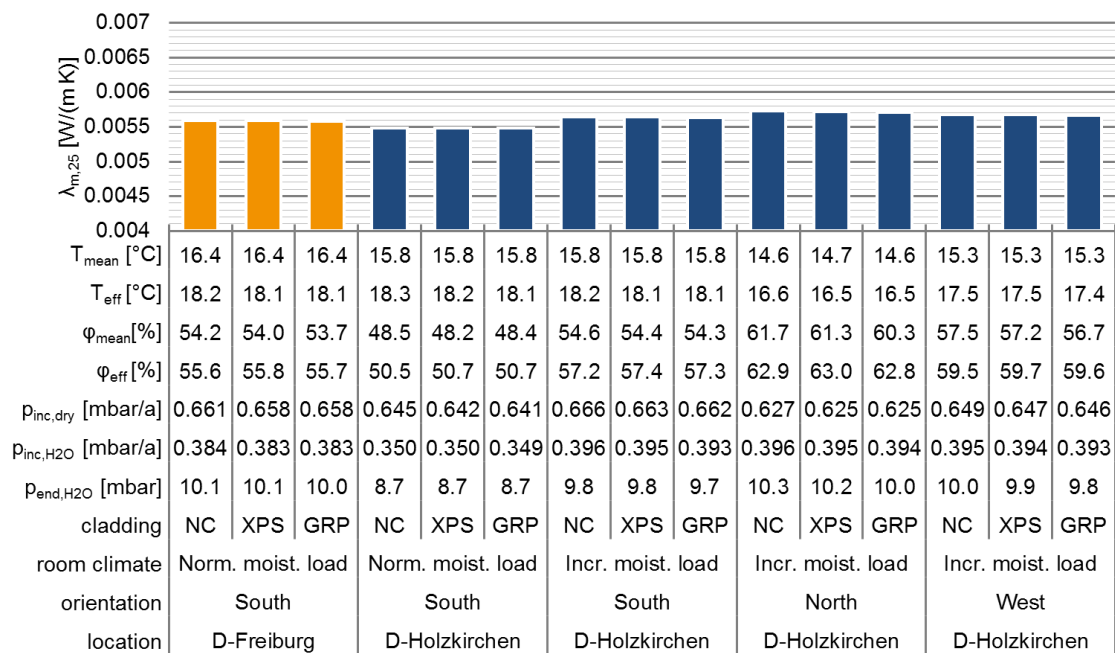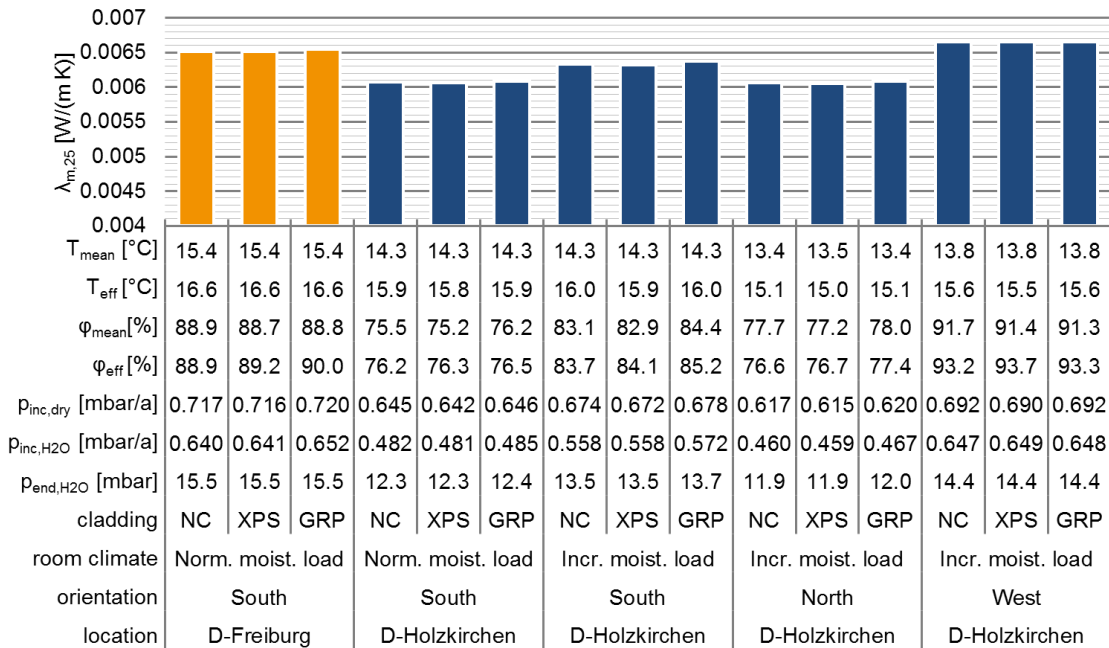|	South D-Freiburg Norm. moist. load			South D-Holzkirchen Norm. moist. load			South D-Holzkirchen Incr. moist. load			North D-Holzkirchen Incr. moist. load			West D-Holzkirchen Incr. moist. load		
T_{mean} [°C]	15.4	15.4	15.4	14.3	14.3	14.3	14.3	14.3	14.3	13.4	13.5	13.4	13.8	13.8	13.8
T_{eff} [°C]	16.6	16.6	16.6	15.9	15.8	15.9	16.0	15.9	16.0	15.1	15.0	15.1	15.6	15.5	15.6
φ_{mean} [%]	88.9	88.7	88.8	75.5	75.2	76.2	83.1	82.9	84.4	77.7	77.2	78.0	91.7	91.4	91.3
φ_{eff} [%]	88.9	89.2	90.0	76.2	76.3	76.5	83.7	84.1	85.2	76.6	76.7	77.4	93.2	93.7	93.3
$p_{inc,dry}$ [mbar/a]	0.717	0.716	0.720	0.645	0.642	0.646	0.674	0.672	0.678	0.617	0.615	0.620	0.692	0.690	0.692
$p_{inc,H2O}$ [mbar/a]	0.640	0.641	0.652	0.482	0.481	0.485	0.558	0.558	0.572	0.460	0.459	0.467	0.647	0.649	0.648
$p_{end,H2O}$ [mbar]	15.5	15.5	15.5	12.3	12.3	12.4	13.5	13.5	13.7	11.9	11.9	12.0	14.4	14.4	14.4
cladding	NC	XPS	GRP	NC	XPS	GRP	NC	XPS	GRP	NC	XPS	GRP	NC	XPS	GRP
room climate	Norm. moist. load			Norm. moist. load			Incr. moist. load			Incr. moist. load			Incr. moist. load		
orientation	South			South			South			North			West		
location	D-Freiburg			D-Holzkirchen			D-Holzkirchen			D-Holzkirchen			D-Holzkirchen		

Figure 102: Mean thermal conductivity of 20mm thick VIP during the first 25 years of use for the construction C3 – ETICS with variation of location and orientation of the building, varying cladding and internal moisture loads (Sprengard et al., 2016).

The climate in Holzkirchen is characterised by colder temperatures than Freiburg and at least in the south orientation shows lower relative humidity. Therefore, the pressure-increase rates both, for dry gases and water vapour are lower compared to Freiburg.

By increasing the internal moisture load, the adjacent relative humidity increases, too. This leads to an increased rate of the internal partial water vapour pressure.

With the application of ETICS, the orientation of the building has a significant impact. This can be explained by the influence of heavy rain on the moisture uptake of the building. The WUFI® model considers a moisture spring of 1% behind the exterior plaster of the wall with heavy rain. The direction the rain arrives from in Holzkirchen is oriented from west to south-west. If the orientation switches from south to north, the mean effective temperature is around 1°C lower and the relative humidity is around 7% lower on the boundary layer of the VIP. A building with a westward orientation raises the temperature and provides a high moisture impact on the VIP due to the increased heavy rain. The best-case scenario in Holzkirchen is a normal internal moisture load and a south orientated building while an increased internal moisture load with a west-oriented building is the worst case scenario. The difference is approximately 0.6mW.

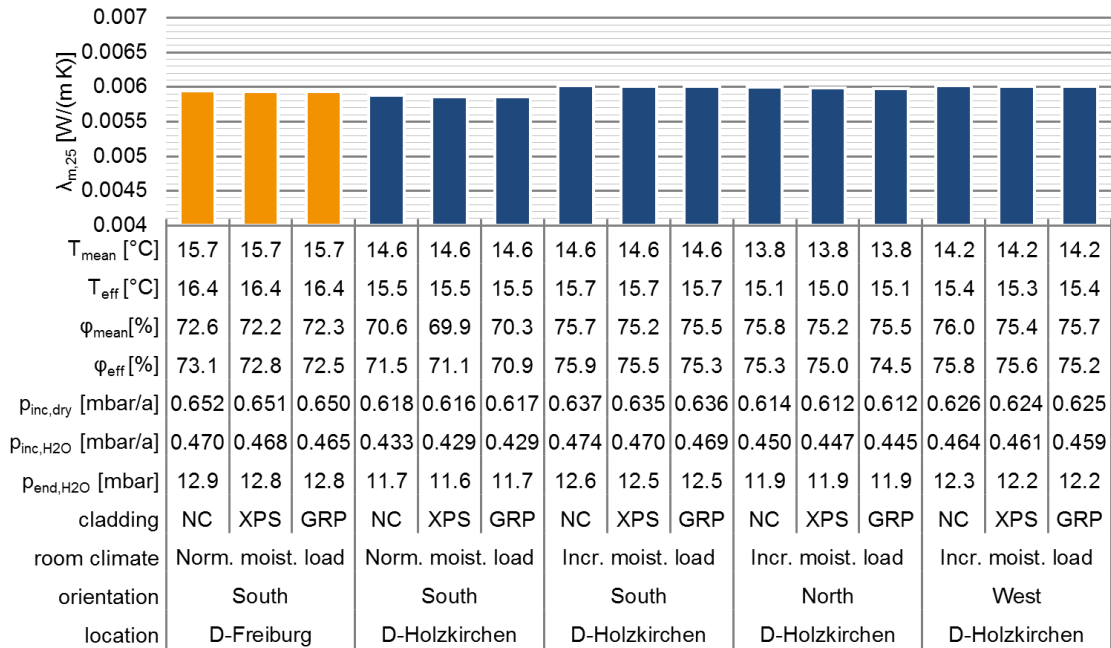| $\lambda_{m,25}$ [W/(m K)]															
T_{mean} [°C]	15.7	15.7	15.7	14.6	14.6	14.6	14.6	14.6	14.6	13.8	13.8	13.8	14.2	14.2	14.2
T_{eff} [°C]	16.4	16.4	16.4	15.5	15.5	15.5	15.7	15.7	15.7	15.1	15.0	15.1	15.4	15.3	15.4
φ_{mean}[%]	72.6	72.2	72.3	70.6	69.9	70.3	75.7	75.2	75.5	75.8	75.2	75.5	76.0	75.4	75.7
φ_{eff} [%]	73.1	72.8	72.5	71.5	71.1	70.9	75.9	75.5	75.3	75.3	75.0	74.5	75.8	75.6	75.2
$p_{inc,dry}$ [mbar/a]	0.652	0.651	0.650	0.618	0.616	0.617	0.637	0.635	0.636	0.614	0.612	0.612	0.626	0.624	0.625
$p_{inc,H2O}$ [mbar/a]	0.470	0.468	0.465	0.433	0.429	0.429	0.474	0.470	0.469	0.450	0.447	0.445	0.464	0.461	0.459
$p_{end,H2O}$ [mbar]	12.9	12.8	12.8	11.7	11.6	11.7	12.6	12.5	12.5	11.9	11.9	11.9	12.3	12.2	12.2
cladding	NC	XPS	GRP	NC	XPS	GRP	NC	XPS	GRP	NC	XPS	GRP	NC	XPS	GRP
room climate	Norm. moist. load			Norm. moist. load			Incr. moist. load			Incr. moist. load			Incr. moist. load		
orientation	South			South			South			North			West		
location	D-Freiburg			D-Holzkirchen			D-Holzkirchen			D-Holzkirchen			D-Holzkirchen		

Figure 103:   Mean thermal conductivity of 20mm thick VIP during the first 25 years of use for the construction C4 – Internal insulation with variation of location and orientation of the building, varying cladding and internal moisture loads (Sprengard et al., 2016).

In Figure 103 the results for the application of internal insulation are summarised. Compared to ETICS, the values of mean thermal conductivity lower and show less variation between the observed cases.

The reason for this unspecific behaviour is due to the fact that as the VIP is situated on the warm side of the construction, impacts from temperature and humidity peaks caused by exterior climate and the heavy rain are decreased.

With increasing internal moisture loads the relative humidity increases which in turn leased to higher values of water vapour partial pressure.

The results for the construction type ventilated façade are summarised in Figure 104. The interdependencies between the adjacent climate conditions caused by exterior weather impact and internal moisture loads are in line with the previous findings.

However, it is remarkable that there are significant differences in between the effective mean temperature of Freiburg and Holzkirchen, the mean thermal conductivity remains more or less the same. On the other hand, the impact of increased internal moisture loads leads to a differentiation.

Also for the ventilated façade the influence of the humidity has a greater impact on the development of thermal conductivity than the temperature.
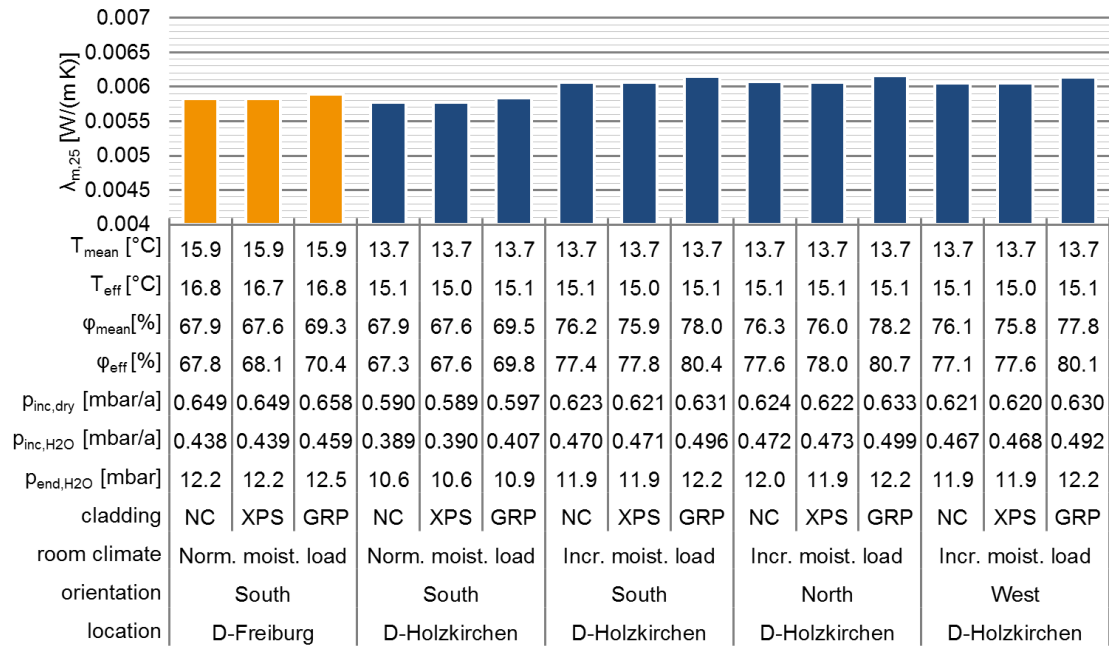
T_{mean} [°C]	15.9	15.9	15.9	13.7	13.7	13.7	13.7	13.7	13.7	13.7	13.7	13.7	13.7	13.7	13.7
T_{eff} [°C]	16.8	16.7	16.8	15.1	15.0	15.1	15.1	15.0	15.1	15.1	15.1	15.1	15.1	15.0	15.1
φ_{mean} [%]	67.9	67.6	69.3	67.9	67.6	69.5	76.2	75.9	78.0	76.3	76.0	78.2	76.1	75.8	77.8
φ_{eff} [%]	67.8	68.1	70.4	67.3	67.6	69.8	77.4	77.8	80.4	77.6	78.0	80.7	77.1	77.6	80.1
$p_{inc,dry}$ [mbar/a]	0.649	0.649	0.658	0.590	0.589	0.597	0.623	0.621	0.631	0.624	0.622	0.633	0.621	0.620	0.630
$p_{inc,H2O}$ [mbar/a]	0.438	0.439	0.459	0.389	0.390	0.407	0.470	0.471	0.496	0.472	0.473	0.499	0.467	0.468	0.492
$p_{end,H2O}$ [mbar]	12.2	12.2	12.5	10.6	10.6	10.9	11.9	11.9	12.2	12.0	11.9	12.2	11.9	11.9	12.2
cladding	NC	XPS	GRP	NC	XPS	GRP	NC	XPS	GRP	NC	XPS	GRP	NC	XPS	GRP
room climate	Norm. moist. load			Norm. moist. load			Incr. moist. load			Incr. moist. load			Incr. moist. load		
orientation	South			South			South			North			West		
location	D-Freiburg			D-Holzkirchen			D-Holzkirchen			D-Holzkirchen			D-Holzkirchen		

Figure 104: Mean thermal conductivity of 20mm thick VIP during the first 25 years of use for the construction C5 – Ventilated façade with variation of location and orientation of the building, varying cladding and internal moisture loads (Sprengard et al., 2016).

Up to now only results for VIP with a thickness of 20mm were discussed. Figure 105 shows the influence of increased VIP thickness for example cases of ETICS in Holzkirchen.

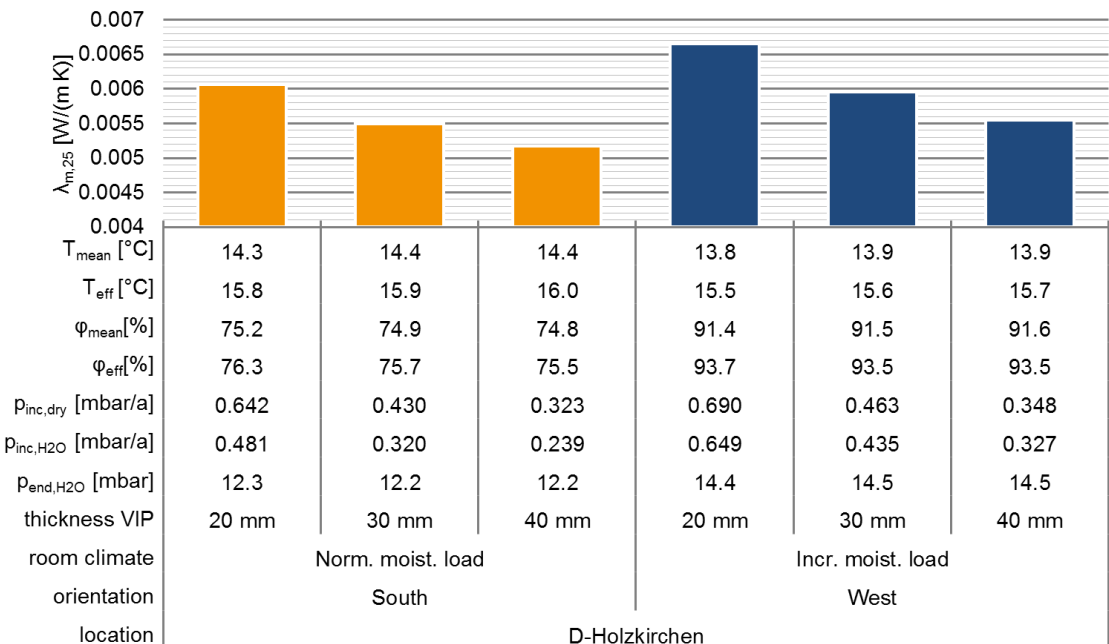|						
T_{mean} [°C]	14.3	14.4	14.4	13.8	13.9	13.9
T_{eff} [°C]	15.8	15.9	16.0	15.5	15.6	15.7
φ_{mean} [%]	75.2	74.9	74.8	91.4	91.5	91.6
φ_{eff} [%]	76.3	75.7	75.5	93.7	93.5	93.5
$p_{inc,dry}$ [mbar/a]	0.642	0.430	0.323	0.690	0.463	0.348
$p_{inc,H2O}$ [mbar/a]	0.481	0.320	0.239	0.649	0.435	0.327
$p_{end,H2O}$ [mbar]	12.3	12.2	12.2	14.4	14.5	14.5
thickness VIP	20 mm	30 mm	40 mm	20 mm	30 mm	40 mm
room climate	Norm. moist. load			Incr. moist. load		
orientation	South			West		
location	D-Holzkirchen					

Figure 105: Influence of thickness of VIP on the mean thermal conductivity over the first 25 years of use, ETICS in D-Holzkirchen (Sprengard et al., 2016).

The application of ETICS was determined as the application, connected to high hygric stress due to the consideration of moisture uptake dependent on the rain. In Figure 105, the best-case and worst-case scenario of the ETICS application at Holzkirchen are re-calculated assuming a varying thickness of the VIP with 20, 30 and 40mm.

Even if the effective climate conditions are not significantly affected by the changing thickness of the insulation layer, the greater volume of the VIP core with increasing thickness has significant impact on the correlated increase of internal pressure. In effect, the thicker the panels are, the lower the increase rates of dry air gases and water vapour.

5.2.7 *Summary on life expectancy estimation*

The durability of VIPs is influenced by several factors. Firstly, the production is crucial, especially with respect to the welding of the barrier foils. Secondly, careful handling during transport and installing of the VIP is imperative to ensure the barrier foil is not penetrated. The handling of the panels can be improved, for example, by utilising cladding consisting of rigid foam, GRP or metal.

The internal pressure of VIP will increase with time due to the unavoidable permeation of dry gases and water vapour. This couples with an increase of the thermal conductivity of the panels. A general finding of the investigation is that, besides the literature documented influence of temperature, the relative humidity and moisture loads are of significant impact on the performance of the panel. The humidity impact does not only lead to an increase of internal pressure, but also increases the moisture content of the core material which influences the thermal conductivity.

The described dependencies cause a descendent functional behaviour of the thermal conductivity by time. To compare different scenarios, the mean thermal conductivity $\lambda_{m,25}$ is used. This value is also used in the actual draft for the product standard of VIP. Thus, compared to the declared values, the customer gets lower values of thermal conductivity at the beginning of the life-time and higher values at the end.

5.2.7.1 *Influence of location, orientation and internal moisture load*

The biggest influence on the evolution of $\lambda_{m,25}$ are identified for the location and orientation of the building. However, these effects are specific to the constructions. E.g. a VIP in an ETICS at the location of Freiburg, south oriented has a of $\lambda_{m,25}$ ca. 6.5mW/(m K) which is around 0.5mW/(m K) higher than for the similar construction and orientation at the location of Holzkirchen ($\lambda_{m,25}$ = ca. 6.0mW/(m K)). If the orientation at the location of Holzkirchen switches to the main direction of heavy rain (west oriented), the value of $\lambda_{m,25}$ increases to 6.6mW/(m K). Between the best and the worst scenarios around ± 5% of variation can be obtained.

Significantly lower variation is considered for the internal insulation options. Here the best case (Holzkirchen, south oriented, normal internal moisture load) has a $\lambda_{m,25}$ of around 5.85mW/(m K) and the worst case (Holzkirchen, south oriented, increased

internal moisture load) ca. 6.0mW/(m K). The variation in this case is ± 1.25% and therefore much lower than the ETICS. This behaviour is logical, because the VIP is situated on the warm side of the construction.

The other cases are in between these extremes. Overall, the maximum variation of the values of $\lambda_{m,25}$ is in between 0.0055-0.0067W/(m K).

5.2.7.2   Influence of panel thickness

With increasing panel thickness, the area of the barrier foil increases only slightly, while on the other side the volume of the panel increases proportional to the thickness of the panel. Due to this effect, the increase of internal pressure by time is minimised. E.g. the increase of thermal conductivity of the VIPs in the worst-case scenario for the ETICS in Holzkirchen with a west orientation and increased internal moisture load is eased by the increased thickness of the panels. The obtained values drop from 6.6mW/(m K) (20mm panel thickness) to 5.9mW/(m K) (30mm panel thickness) and 5.5mW/(m K) (40mm panel thickness).

For the other observed cases the gradation is comparable. With respect to the ageing effects, the thicker panels are significantly non-problematic compared to thinner panels, if the dimension of the panel and therefore the ratio between welding seams and area of the panels remain the same.

5.2.7.3   General conclusion

As a general conclusion it is considered that VIPs that are produced under up to date production techniques can guarantee a useful lifetime with unrivalled low thermal conductivity between 25-50 years.

For the constructions and locations in Germany that were sampled, the following values of thermal conductivity can be estimated.

During the first 25 years of life-time, the mean thermal conductivity is in the range of ca. 0.0055-0.0067W/(m K) and for the first 50 years in the range of ca. 0.0064-0.0081W/(m K).

The thermal conductivity after 25 years of use is in the range of ca. 0.006-0.0086W/(m K) and after 50 years in the range of ca. 0.0079-0.0105W/(m K).

6 Error calculation for thermal conductivity measurement

In the following chapter some general information about the error calculation and examples for models used to calculate the error of GHP and HFM method are given. To help labs choose the right methods, sensitivity analysis is taken out showing the influence of individual measurement parameter errors on the result of the thermal conductivity.

6.1 Uncertainty estimation: type A and type B

All measurements are subject to uncertainty. In fact the word uncertainty means doubt, thus it expresses a lack of exact information about the measurement that was carried out. For this reason, every result should be expressed with a quantitative indication of its reliability and quality. The uncertainty depends on several factors like the type of specimen used, the resolution of the instrumentation, the skill of the operator, the effects of environmental conditions, the simplified assumptions of the method and procedure and other effects. Because of this, the measured value is always an estimate. As described in the standard GUM "Evaluation of measurement data – Guide to the expression of Uncertainty in Measurement", the uncertainty may be evaluated in two different ways: type A, a method of evaluation by the statistical analysis of series of observations, and type B, a method of evaluation by means other than the statistical analysis of series of observation.

Type A may be used when the magnitude Y is determined experimentally through a set of measurements carried out in the laboratory. In this method the uncertainty is calculated with information obtained directly from the experiment. The measurements are repeated n-times in a controlled environment in which all known parameters are kept constant. In this case, the uncertainty is expressed as statistical distribution, characterised by standard deviations.

When it is not possible to take repeated observations of the magnitude, the standard suggests defining the uncertainty of the measurements with type B. In this case, the uncertainty is obtained from the pool of the available information on the possible variability of the value. This pool of information is based on experience and general knowledge and may include: previous measurement data, manufacturer's specifications, uncertainties taken from handbook, experience and knowledge of behavior and properties of the materials and instruments.

Regardless, if uncertainties type A or type B are considered, these values always refer to a specific measurement gauge. Therefore the level of uncertainty for the evaluation of required parameters will vary from lab to lab. To achieve consistency a sensitivity study

is carried out using standard reference uncertainties taken from the standards EN 1946-2:1999 and EN 1946-3:1999, for GHP and HFM respectively (uncertainty analysis type B). These standards contain technical criteria and definitions about minimum requirements on measurement uncertainty for the measurement of thermal conductivity according to EN 12664:2001 and EN 12667:2001.

6.2 Uncertainty analysis for GHP

For the determination of thermal conductivity with the GHP method, the measurement area (A), temperature difference (ΔT), the electrical power (P) and the thickness of the sample (d) have to be considered.

Thus, the thermal conductivity for a 2-specimens apparatus is given as a function of four different parameters P, ΔT, A and t.

$$\lambda = \frac{1}{2} \frac{P \cdot d}{A \cdot \Delta T} \tag{22}$$

where

λ	centre of panel thermal conductivity in W/m K,
P	average power supplied to the metering section of the heating unit in W,
A	metering area in m^2,
ΔT	temperature difference between the plates in K,
d	average specimen(s) thickness in m.

For different example types of equipment, the standard EN 1946-2:1999 contains maximum probable errors for each of the parameters.

To consider geometrical aspects and general quality of the specific apparatus that influences the uncertainty of the result several additional parameters of uncertainty are considered by the standard. These can be included in the formula of thermal conductivity by adding them as factors of 1.0 and with a certain relative error in the calculation. The parameters are:

$\Delta\lambda_{R,E}$	imbalance and edge heat loss (dimensionless),
$\Delta\lambda_O$	imperfect contact (dimensionless),
$\Delta\lambda_S$	asymmetrical conditions (dimensionless).

Adding these parameters to the already given formula of thermal conductivity the equation is extended.

$$\lambda = \frac{1}{2} \frac{P \cdot d}{A \cdot \Delta T} \cdot \Delta\lambda_{R,E} \cdot \Delta\lambda_O \cdot \Delta\lambda_S \tag{23}$$

As already mentioned the standard EN 1946-2:1999 includes maximum probable errors for different type of equipment. The main difference is the metering area: $150^2 mm^2$ (equipment A), $250^2 mm^2$ (equipment B) and $500^2 mm^2$ (equipment C).

Table 41 includes the maximum relative errors by percentage for the required parameters of equation (16) to calculate the thermal conductivity for equipment A, B and C.

Table 41:   Equipment A, B and C according to EN 1946-2:1999 and maximum probable relative errors $u(x_i)$.

Relative errors in %	Abbr.	Unit	A	B	C
Imbalance and edge heat loss	$u(\Delta\lambda_{R,E})$	%	0.5	0.5	0.5
Imperfect contact	$u(\Delta\lambda_O)$	%	0.5	0.5	0.5
Non symmetrical condition	$u(\Delta\lambda_S)$	%	0.1	0.1	0.1
Electrical power	$u(P)$	%	0.1	0.1	0.1
Specimen thickness	$u(d)$	%	0.5	0.5	0.5
Metering section	$u(A)$	%	0.37	0.34	0.26
Temperature difference	$u(\Delta T)$	%	1.0	1.0	1.0

Limitations to a range of thickness and a range of thermal conductivity are specified so the total combined uncertainty is not increased (Table 42). The minimum and maximum specimen thicknesses are connected in geometrical aspects to the gap width between the metering area and the guard ring and will influence the errors due to the edge heat loss, the thickness determination and the electrical power.

Table 42:   Overall size and limitations of specimen thickness and range of thermal conductivity according to EN 1946-2:1999.

Equipment	Abbr.	Unit	A	B	C
Overall size	A_{tot}	mm^2	300^2	500^2	800^2
Metering section	A_{met}	mm^2	150^2	250^2	500^2
Min. gap width	w_g	mm	2	3	4
Min. specimen thickness	$d_{s,min}$	mm	20	30	40
Max. specimen thickness	$d_{s,max}$	mm	45	75	100
Min. therm. Conductivity	λ_{min}	W/(m K)	0.015	0.015	0.015
Max. therm. Conductivity	λ_{max}	W/(m K)	1.5	1.5	1.5

Commercially available measurement equipment for determination of thermal conductivity will usually meet the values in the standard EN 1946-2:1999. Considering a constant error for a parameter, the relative error of this parameter will increase with decreasing observed values. For the measuring of superinsulation materials like APM and VIP much lower values of thermal conductivity are likely to occur, going down to 0.002W/(m K) for fibre core based VIP. Therefore it is questionable how the combined uncertainty of thermal conductivity $u_c(\lambda)$ will develop with decreasing thermal conductivity and varying thickness of the specimen.

To investigate the evolution of $u_c(\lambda)$ in this manner, the first step is to create absolute errors of all necessary parameters by applying the maximum relative errors according to the standard on a set of data. As the relative errors are maximum relative errors, the set of data shall consider the minimum thickness and the minimum electrical power according to the specifications in equipment A, B and C (Table 43).

Table 43: Set of data for calculation of combined uncertainty of thermal conductivity $u_c(\lambda)$.

Set of data	Abbr.	Unit	A	B	C
Min. therm. conductivity	λ_{min}	W/(m K)	0.015	0.015	0.015
Electrical power	P	W	0.15	0.25	0.75
Min. specimen thickness	$d_{s,min}$	m	0.02	0.03	0.04
Metering section	A	m^2	0.0225	0.0625	0.25
Minimum temperature difference through the specimen	ΔT_{min}	K	10	10	10

Applying the maximum probable relative errors according to Table 41 on the set of data according to Table 43, absolute errors for further calculation of combined uncertainty of thermal conductivity according to Table 44 are obtained.

The Guide to Uncertainty of Measurement (GUM) describes how to calculate the combined uncertainty of a value that is functional dependent on a couple of measurands. The uncertainty of each measurand necessary to calculate the required value shall be determined according to type A or type B. Further explanations about uncertainty estimation for a couple of parameters necessary for calculation of thermal conductivity are discussed later. Up to now we assume an absolute error according to Table 44.

Table 44: Absolute errors for parameters for calculation of thermal conductivity for different type of equipment (A, B, C) according to EN 1946-2:1999.

Absolute errors for calc.	Abbr.	Unit	A	B	C
Imbalance and edge heat loss	u($\lambda_{R,E}$)	W/(m K)	0.000075	0.000075	0.000075
Imperfect contact	u(λ_O)	W/(m K)	0.000075	0.000075	0.000075
Non-symmetrical condition	u(λ_S)	W/(m K)	0.000015	0.000015	0.000015
Electrical power	u(P)	W	0.00015	0.00025	0.00075
Specimen thickness	u(d)	m	0.0001	0.00015	0.0002
Metering section	u(A)	m^2	0.00008325	0.0002125	0.00065
Temperature difference	u(ΔT)	K	0.10	0.10	0.10

The squares of the known uncertainties $u(x_i)$ are multiplied with the squares of the associated differential quotient.

The differential quotient represents the first partial derivative of the thermal conductivity with respect to the observed measurand parameter. In this manner it is representative for the sensitivity of the function of thermal conductivity for changes of the observed parameter. The combination of the uncertainty with the sensitivity is important because it includes the severity of changes of the observed parameter on the calculated result.

The differential quotients in the case of the calculation of thermal conductivity are:

$$\frac{\delta(\lambda)}{\delta(P)} = \frac{d}{2 \cdot A \cdot \Delta T} \tag{24}$$

$$\frac{\delta(\lambda)}{\delta(d)} = \frac{P}{2 \cdot A \cdot \Delta T} \tag{25}$$

$$\frac{\delta(\lambda)}{\delta(A)} = -\frac{1}{A^2} \cdot \frac{P \cdot d}{2 \cdot \Delta T} \tag{26}$$

$$\frac{\delta(\lambda)}{\delta(\Delta T)} = -\frac{1}{\Delta T^2} \cdot \frac{P \cdot d}{2 \cdot A} \tag{27}$$

$$\frac{\delta(\lambda)}{\delta(\lambda_{R,E})} = \lambda \tag{28}$$

$$\frac{\delta(\lambda)}{\delta(\lambda_O)} = \lambda \tag{29}$$

$$\frac{\delta(\lambda)}{\delta(\lambda_S)} = \lambda \tag{30}$$

All calculated products of the squared absolute uncertainty and the squared differential quotients are then summed and represent the square of the combined uncertainty of the calculated value of thermal conductivity. The principle equation is given as follows:

$$u_c(y)^2 = \sum_{i=1}^{n} u(x_i)^2 \cdot \left(\frac{\delta(y)}{\delta(x_i)}\right)^2 \tag{31}$$

Referring the combined uncertainty $u_c(\lambda)$ to the calculated value of λ the combined relative uncertainty is expressed by:

$$u_c(\lambda)[\%] = \frac{u_c(\lambda)}{\lambda} \cdot 100 \tag{32}$$

6.3 Sensitivity analysis for GHP

As explained before, the relative uncertainty of thermal conductivity is influenced by the uncertainty of the involved measurands and the differential quotients as well as by the level of thermal conductivity. The determination of most measurands becomes more uncertain the lower the value is, respectively the relative error increases.

To check the suitability of applying the common method for determination of thermal conductivity for super insulation materials, a sensitivity analysis is carried out and presented in the following. Variation is applied to the type of equipment (A, B and C according to EN 1946-2:1999), the value of thermal conductivity representing fibre based VIP (0.002W/(m K)), fumed silica core VIP (0.004W/(m K)), aged VIP (0.008W/(m K)) and APM (0.016W/(m K)/ 0.02W/(m K)). Since the maximum thermal conductivity of SIMs is assumed to be equal to 0.02 W/(m K), no higher values are analysed.

6.3.1 Influence of thickness and temperature difference for different levels of thermal conductivity, assuming maximum probable errors according to EN 1946-2:1999

Figure 106 - Figure 109 include the results for the calculation of the combined relative uncertainty for the thermal conductivity, dependent from the thickness of the specimen and the temperature difference. The results are arranged for each observed specimen thickness from 10mm to 80mm accordingly.

Figure 106 shows the results for the 10mm thick specimen.

First of all it becomes obvious that the relative uncertainty for a defined temperature difference is not significantly affected by the decreasing values of thermal conductivity from 0.02-0.002W/(m K).

As a general trend for all observed cases the huge difference of the combined uncertainty between 5 and 10K temperature difference is visible. Decreasing the temperature also causes proportionally decreasing electrical power. Therefore for both parameters the error increases. The difference from 5-10K is dramatic and gets lower for higher temperatures. However, increasing the temperature difference to e.g. 15K offers some potential to lower the uncertainty significantly.

The next noticeable effect is the general increase of the level of uncertainty while varying equipment A – C. On the first view this seems surprising, as the increasing measurement area leads to increases electrical heating power meaning a less relative uncertainty and also less uncertainty for the determination of the measurement area. Both effects would decrease the relative uncertainty for the thermal conductivity. However these effects are overcompensated by the increasing absolute uncertainty for the thickness determination. According to Table 44 the absolute uncertainty for the thickness determination of equipment A to C varies from u(t) = 0.1mm for equipment A to u(t) = 0.2mm for equipment C. This is plausible, as the variation of thickness gets higher for an increasing metering area.
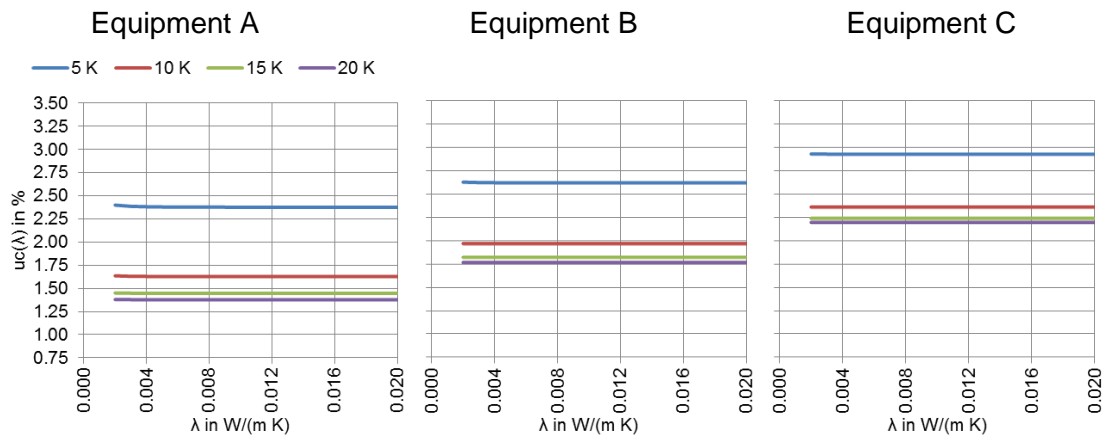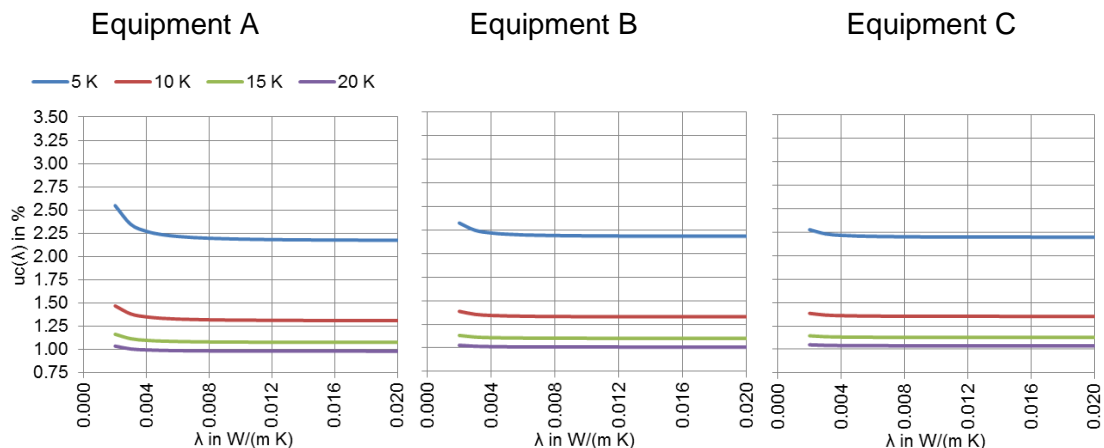

Figure 106:   Combined relative uncertainty as a function of thermal conductivity for a panel thickness of 10mm for the exemplary equipment A, B and C according to EN 1946-2:1999 with varying temperature difference.

The results for the specimen thickness of 20mm are included in Figure 107.

Again, the results are not, or only slightly affected by the thermal conductivity if a constant temperature difference is assumed. Only for very low thermal conductivity and small size of the apparatus a certain effect on the relative uncertainty is visible. This effect is explained by the lower electrical power due to the decreasing metering area from apparatus C – A and therefore increasing relative uncertainty for the low values of thermal conductivity.

As a general conclusion for all apparatus the values of the relative uncertainty are decreasing with increasing thickness of the specimen. This effect is especially pronounced for equipment B and C with bigger metering areas and can be explained especially with the improvement of relative uncertainty for the thickness determination with increasing thickness.
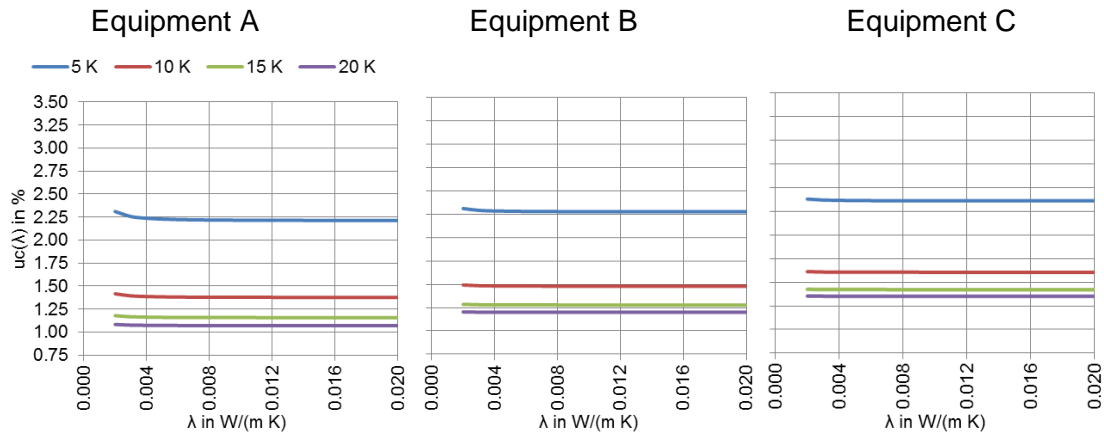
Figure 107:   Combined relative uncertainty as a function of thermal conductivity for a panel thickness of 20mm for the exemplary equipment A, B and C according to EN 1946-2:1999 with varying temperature difference.

The results for increasing specimen thickness up to 40mm (Figure 108) and 80mm (Figure 109) show similar, but more pronounced effects as explained before. With increasing thickness the thermal resistance gets higher and therefore, especially for the smaller apparatus, the relative uncertainty for the electrical power determination increases dramatically. This effect can be compensated using equipment with a larger metering area. For a specimen thickness of 40mm the relative uncertainty is not affected down to 0.004W/(m K) for equipment B. For increasing specimen thickness up to 80mm, an apparatus of type C is recommendable to ensure no influence of the combined relative uncertainty even for very low values of thermal conductivity.

Figure 108:   Combined relative uncertainty as a function of thermal conductivity for a panel thickness of 40mm for the example equipment A, B and C according to EN 1946-2:1999 with varying temperature difference.

Equipment A   Equipment B   Equipment C
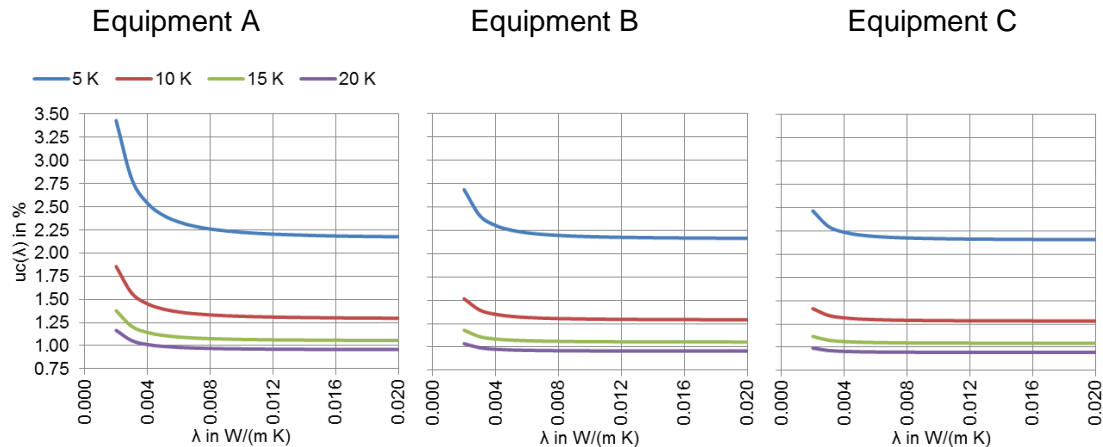
Figure 109:   Combined relative uncertainty as a function of thermal conductivity for a panel thickness of 80mm for the example equipment A, B and C according to EN 1946-2:1999 with varying temperature difference.

The performed sensitivity analysis assumes uncertainties for the measurands according to the standard EN 1946-2:1999. Therefore, the recommendations and conclusions are based on theoretical assumptions and may be influenced in practical applications by varying uncertainties specific to the equipment and limitations by applying common methods of lab-handling.

However, the following general recommendations can be concluded:

- the higher the temperature difference is, the lower the combined relative uncertainty occurs. For this reason, a minimum temperature difference of 10K is required. As a recommendation the temperature difference should be increased to 15K,
- the lower the thickness of the specimen the smaller the metering area of the apparatus should be. This is explained by the increasing relative uncertainty for small thickness and large metering areas. The following recommendations can be derived:
    - for thicknesses d < 20mm use a metering area of around $150^2 mm^2$,
    - for thicknesses $20 < d <$ 40mm use a metering area of around $250^2 mm^2$,
    - for thicknesses d > 40mm use a metering area of around $500^2 mm^2$,
- using the GHP method, for theoretical reasons a combined relative standard uncertainty of thermal conductivity of around 1.0-1.7% can be achieved when the right equipment is used.

6.3.2 Isolines of uncertainty as a function of thickness and temperature difference

A different type of drawing the data from Chapter 6.3.1 is shown as an example for equipment B in Figure 110. The graphic shows isolines for a constant level of combined relative uncertainty of thermal conductivity in the reticule of specimen thickness (ordinate) and temperature difference (abscissae). Therefore the graphic displays the top view of the 3-dimensional function $u_c(λ) = f(\Delta T, d)$.

The range of thickness and temperature according to the definitions in EN 1946-2:1999 for equipment B is shown in form of the greyed box. It becomes obvious that the intentionally described boundary conditions during the measurement are in a region where the impact of potential changes of one of the parameters thickness and temperature difference is of low impact on the resulting relative uncertainty of the thermal conductivity. Beginning with temperature differences smaller than 10K the distance between the isolines becomes smaller and the same happens for a specimen thickness smaller than 15mm.

The influence of decreasing thermal conductivity on the position of the isolines is visible by comparing the different style of lines within one colour. It becomes obvious that especially for values of thermal conductivity higher than 0.008W/(m K) the position of the isolines remains more or less constant. However, for lower values there is a certain influence visible that affects the results slightly as discussed before.
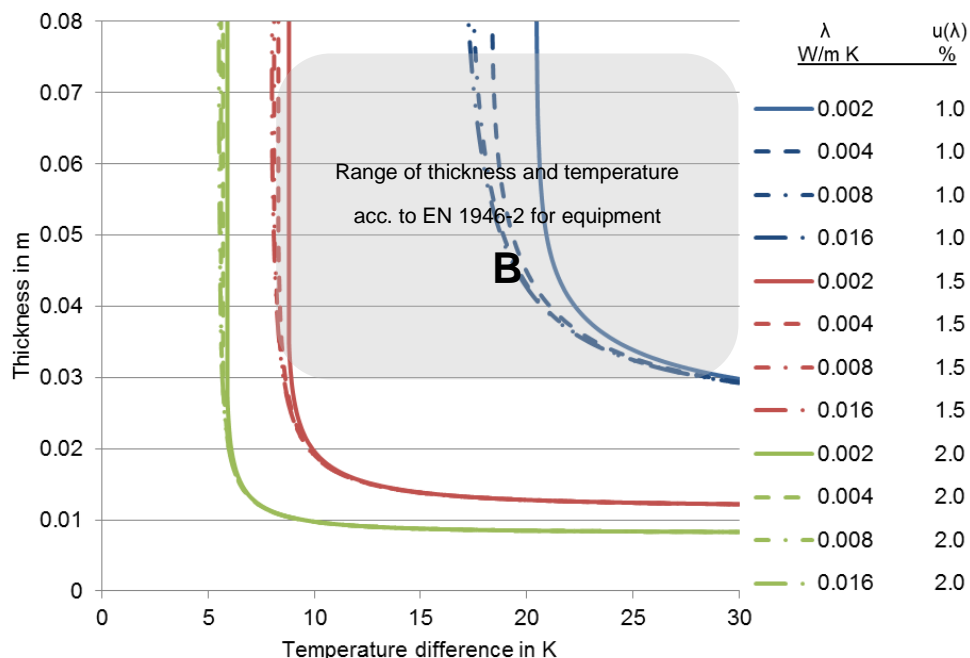
Figure 110: Isolines of levels of uncertainty $u_c(λ)$ = 1.0-2.0% for varying levels of λ = 0.004-0.016W/(m K) dependent on temperature difference ΔT in K and thickness of the specimen t in m, assuming the maximum uncertainty according to EN 1946-2:1999, equipment B with a measuring area of $250^2 mm^2$.

6.3.3 Sensitivity of increasing error of single parameters on the combined uncertainty of thermal conductivity

Up to now a constant uncertainty for the determination of the required parameters, according to EN 1946-2:1999 was considered. Besides the sensitivity analysis of varying the involved parameters, it is of interest to discuss the influence of varying uncertainties for the most important parameters.

Therefore Figure 111 compares the changes of isolines of the relative uncertainty of the thermal conductivity if one of the parameters electrical power (Figure 111, top right), thickness (Figure 111, bottom left) or temperature difference (Figure 111, bottom right) are increasing by a factor of two, compared to the relative uncertainty assuming the absolute uncertainties for all parameters according to EN 1946-2:1999 (Figure 111, top left). The effects are discussed separately in detail.

Starting with the doubled uncertainty for the electrical power determination (Figure 111, top right), it becomes visible that the isolines are spread, compared to the standard case. Especially for cases with low thermal conductivity this will lead to an increasing combined relative uncertainty. However, the isolines are not shifted dramatically, which means that the effect can be compensated easily by an increased temperature difference.

The increasing error of the thickness determination (Figure 111, bottom left) also leads to a certain spreading of the isolines, but also shifts the isolines upwards. Especially for low thicknesses of the specimen it is hard to compensate this by an increased temperature difference.

The increase of uncertainty of determination of the temperature difference (Figure 111, bottom left) cannot be compensated by increased temperature difference in a reasonable temperature range.
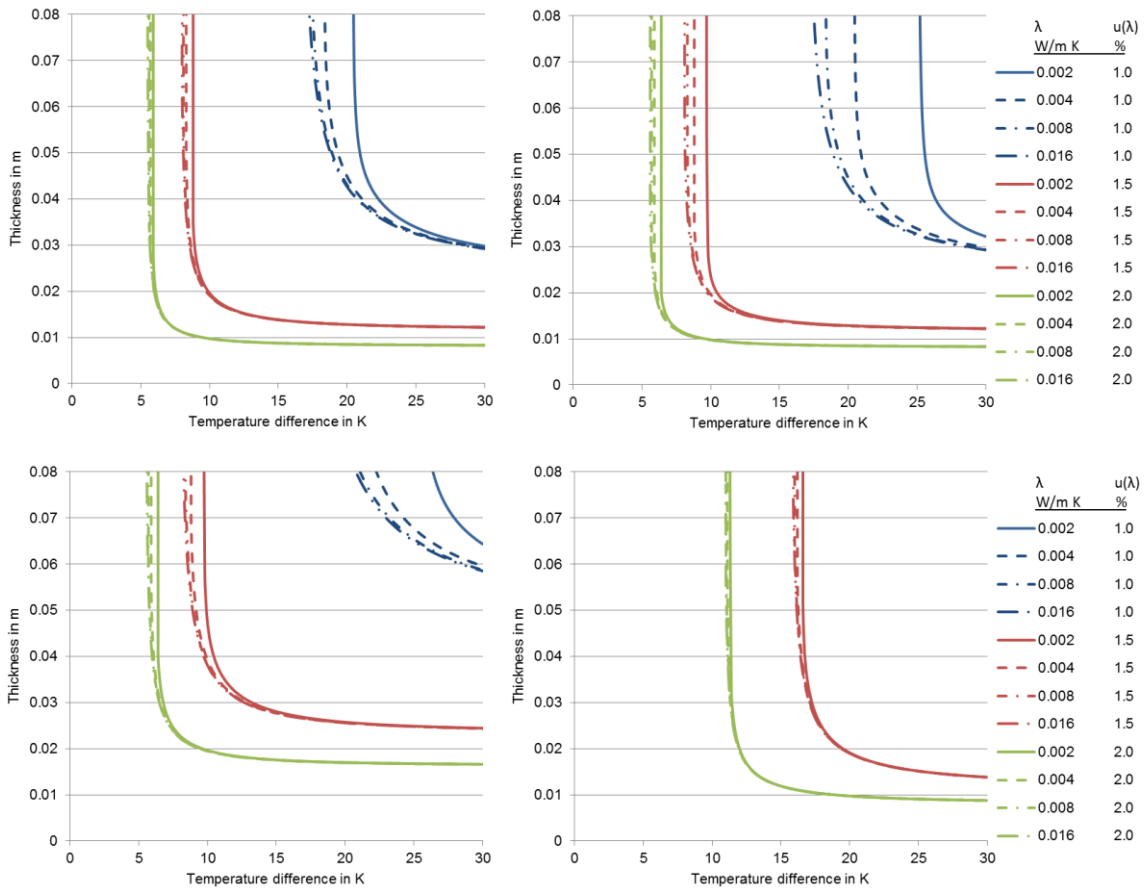
Figure 111: Isolines of levels of uncertainty $u_c(\lambda)$ = 1.0-2.0% for varying levels of λ = 0.004-0.016W/(m K) dependent on temperature difference ΔT in K and thickness of the specimen t in m,
top left: assuming the maximum uncertainty according to EN 1946-2:1999, equipment B with a measuring area of 250^2mm^2 ,
top right: by increasing the error of the electrical power by a factor of 2,
bottom left: by increasing the error of the thickness determination by a factor of 2,
bottom right: by increasing the error of the determination of ΔT by a factor of 2.

6.4 Uncertainty analysis of HFM

The assessment of the thermal conductivity with the HFM method is based on the measurement of the electrical signal (E), the temperature difference (ΔT), the thickness of the sample (s), and on the value of the calibration factor $f_{cal}(T)$ in W/m²µV, that should be referred to the transducers actual temperatures and represent a characteristic of the device.

$$\lambda_{test} = \frac{f_{cal}(T) \cdot e \cdot d}{\Delta T} = \frac{q \cdot d}{\Delta T} \tag{33}$$

where

λ	centre of panel thermal conductivity in W/m K,
e	electric signal from the transducer in µV,
ΔT	temperature difference between the plates in K,
d	average specimen(s) thickness in m,
$f_{cal}(T)$	calibration factor in W/m²µV,
q	specific heat flux through the sample in W/(m²).

Since each plate has its own temperature, the calibration factors should be calculated for each plate's actual temperature, obtaining two values of thermal conductivity: the result of thermal conductivity test is obtained by averaging these two values.

For different example types of equipment, the standard EN 1946-3:1999 contains maximum probable errors for each of the parameters.

As well as the GHP method, in order to consider geometrical aspects and general quality of the specific apparatus that influences the uncertainty of the result several additional parameters of uncertainty are considered by the standard. These parameters can be included in the formula of thermal conductivity by adding them as factors of 1.0 and with a certain relative error in the calculation. The parameters are:

$\Delta\lambda_E$	edge heat loss (dimensionless),
$\Delta\lambda_O$	imperfect contact (dimensionless).

Moreover, the specific heat flux (q) is affected by some factor regarding the calibration factor ($f_{cal}(T)$) of the instrument and the measured electrical signal (e). If these two quantities (measurands and uncertainties) are unknown, it is possible to consider the following errors, directly for the evaluation of the specific heat flux (q):

$\Delta\lambda_K$	calibration accuracy of the specimen (dimensionless),
$\Delta\lambda_L$	maximum permissible non-linearity of the calibration (dimensionless),
$\Delta\lambda_g$	maximum permissible calibrating drift (dimensionless).

These parameters can be included in the formula of the specific heat flux by adding them as factors of 1.0 and with a certain relative error in the calculation.

Adding these parameters to the already given formula of specific heat flux and thermal conductivity the equations are extended.

$$q = q_{value} \cdot \Delta\lambda_K \cdot \Delta\lambda_L \cdot \Delta\lambda_g \tag{34}$$

$$\lambda_{test} = \frac{q \cdot d}{\Delta T} \cdot \Delta\lambda_E \cdot \Delta\lambda_O = \frac{(q_{value} \cdot \Delta\lambda_K \cdot \Delta\lambda_L \cdot \Delta\lambda_g) \cdot d}{\Delta T} \cdot \Delta\lambda_E \cdot \Delta\lambda_O \tag{35}$$

As already mentioned the standard EN 1946-3 includes maximum probable errors for different type of equipment. Main difference is the metering area that varies by $150^2 mm^2$ (equipment A), $200^2 mm^2$ (equipment B) and $300^2 mm^2$ (equipment C).

Table 45: Equipment A, B and C according to EN 1946-3:1999 and maximum probable relative errors $u(x_i)$.

Relative errors in %	Abbr.	Unit	A	B	C
Edge heat loss	$u(\lambda_E)$	%	0.5	0.5	0.5
Imperfect contact	$u(\lambda_O)$	%	0.5	0.5	0.5
Specimen thickness	$u(d)$	%	0.5	0.5	0.5
Temperature difference	$u(\Delta T)$	%	1.0	1.0	1.0
Calibration accuracy of the specimen	$u(\lambda_K)$	%	1.5	1.5	1.5
Maximum permissible non-linearity of the calibration	$u(\lambda_L)$	%	1.0	1.0	1.0
Maximum permissible calibrating drift	$u(\lambda_q)$	%	1.0	1.0	1.0

Limitations to a range of thickness and a range of thermal conductivity are specified so the total combined uncertainty is not increased. The minimum and maximum specimen thicknesses are connected in geometrical aspects to the gap width between the metering area and the guard ring and will influence the errors due to the edge heat loss, the thickness determination and the electrical power.

Table 46: Overall size and limitations of specimen thickness and range of thermal conductivity according to EN 1946-3:1999.

Equipment	Abbr.	Unit	A	B	C
Overall apparatus size	A_{tot}	mm	300	500	600
Metering section width	A_{met}	mm	150	200	300
Min. specimen thickness	$d_{s,min}$	mm	15	25	30
Max. specimen thickness	$d_{s,max}$	mm	50	140	100
Min. thermal conductivity	λ_{min}	W/(m K)	0.015	0.015	0.015
Max. thermal conductivity	λ_{max}	W/(m K)	0.4	0.4	0.4
Minimum temperature difference through the specimen	ΔT_{min}	K	10	10	10

It is possible to assume that commercially available measurement equipment for determination of thermal conductivity will stick, more or less, to the values in the standard EN 1946-3:1999. Considering a constant error for a parameter, the relative error of this parameter will increase with the decreasing of the values that are observed.

As already explained, the first thing to do is to define the absolute errors of all necessary parameters by applying the maximum relative errors according to the standard on a set of data. As the relative errors are maximum relative errors, the set of data shall consider the minimum thickness and the minimum electrical power according to the specifications in equipment A, B and C.

Table 47: Set of data for calculation of combined uncertainty of thermal conductivity $u_c(\lambda)$.

Set of data	Abbr.	Unit	A	B	C
Min. thermal conductivity	λ_{min}	W/(m K)	0.015	0.015	0.015
Heat flux	q	W/m^2	3.0	1.1	1.5
Min. specimen thickness	$d_{s,min}$	m	0.015	0.025	0.03
Temperature difference	ΔT	K	10	10	10

Applying the maximum probable relative errors according to Table 45 on the set of data according to Table 47, absolute errors for further calculation of combined uncertainty of thermal conductivity according to Table 48 are obtained.

Table 48: Absolute errors for parameters for calculation of thermal conductivity for different type of equipment (A, B, C) according to EN 1946-3:1999.

Absolute errors for calcolation	Abbr.	Unit	A	B	C
Edge heat loss	$u(\lambda_E)$	W/(m K)	0.000075	0.000075	0.000075
Imperfect contact	$u(\lambda_O)$	W/(m K)	0.000075	0.000075	0.000075
Specimen thickness	$u(d)$	m	0.000075	0.000125	0.00015
Temperature difference	$u(\Delta T)$	K	0.1	0.1	0.1
Calibration accuracy of the specimen	$u(\lambda_K)$	W/m^2	0.045	0.016	0.023
Maximum permissible non-linearity of the calibration	$u(\lambda_L)$	W/m^2	0.03	0.01	0.02
Maximum permissible calibrating drift	$u(\lambda_q)$	W/m^2	0.03	0.01	0.02

The squares of the known uncertainties $u(x_i)$ are multiplied with the squares of the associated differential quotient.

The differential quotients in the case of the calculation of thermal conductivity are:

$$\frac{\delta(\lambda)}{\delta(q)} = \frac{d}{\Delta T} \tag{36}$$

$$\frac{\delta(\lambda)}{\delta(d)} = \frac{q}{\Delta T} \tag{37}$$

$$\frac{\delta(\lambda)}{\delta(\Delta T)} = \frac{q \cdot d}{\Delta T^2} \tag{38}$$

$$\frac{\delta(q)}{\delta(\lambda_K)} = q \tag{39}$$

$$\frac{\delta(q)}{\delta(\lambda_L)} = q \qquad (40)$$

$$\frac{\delta(q)}{\delta(\lambda_g)} = q \qquad (41)$$

$$\frac{\delta(\lambda)}{\delta(\lambda_E)} = \lambda \qquad (42)$$

$$\frac{\delta(\lambda)}{\delta(\lambda_O)} = \lambda \qquad (43)$$

All calculated products are then summed and represent the square of the combined uncertainty of the calculated value of thermal conductivity (equation (24)). Referring the combined uncertainty $u_c(\lambda)$ to the calculated value of λ the combined relative uncertainty is expressed by equation (25).

6.5 Sensitivity analysis for HFM

In order to check the suitability of applying the HFM method for the assessment of super insulation materials thermal conductivity, a sensitivity analysis is carried out and hereinafter presented. The three types of equipment (A, B and C according to EN 1946-3:1999) are considered, and the value of thermal conductivity represent fibre based VIP (0.002W/(m K)), fumed silica core VIP (0.004W/(m K)), aged VIP (0.008W/(m K) and APM (0.016W/(m K)/0.020W/(m K)). Since the maximum thermal conductivity of SIMs is assumed to be equal to 0.02W/(m K), no higher values are analysed.

6.5.1 Influence of thickness and temperature difference for different levels of thermal conductivity, assuming maximum probable errors according to EN 1946-3:1999

If compared to traditional insulating material, the heat flux through the specimens during a HFM test is sensibly reduced in case of super insulating material because of their thermal conductivity: the lower the heat flux, the highest sensitivity of the heat flux meter must be used. The two main factors that influenced the heat flux through the sample are: the sample thickness (which defines its thermal resistance), and the temperature difference between the HFM plates during the tests.

For this reason a sensitivity analysis is performed, in order to evaluate the effects on the combined measurement uncertainty $u_c(\lambda)$ of four different sample thicknesses (0.01, 0.02, 0.04 and 0.08m) and four different temperature differences ΔT (5, 10, 15 and 20K), considering a thermal conductivity range of the specimen between 0.002 and 0.02W/(m K), as mentioned before.

Figure 112 to Figure 115 show, for each thickness, the effect of the different temperature difference on $u_c(\lambda)$, and the most relevant results are summarised in Table 49 to Table 51.
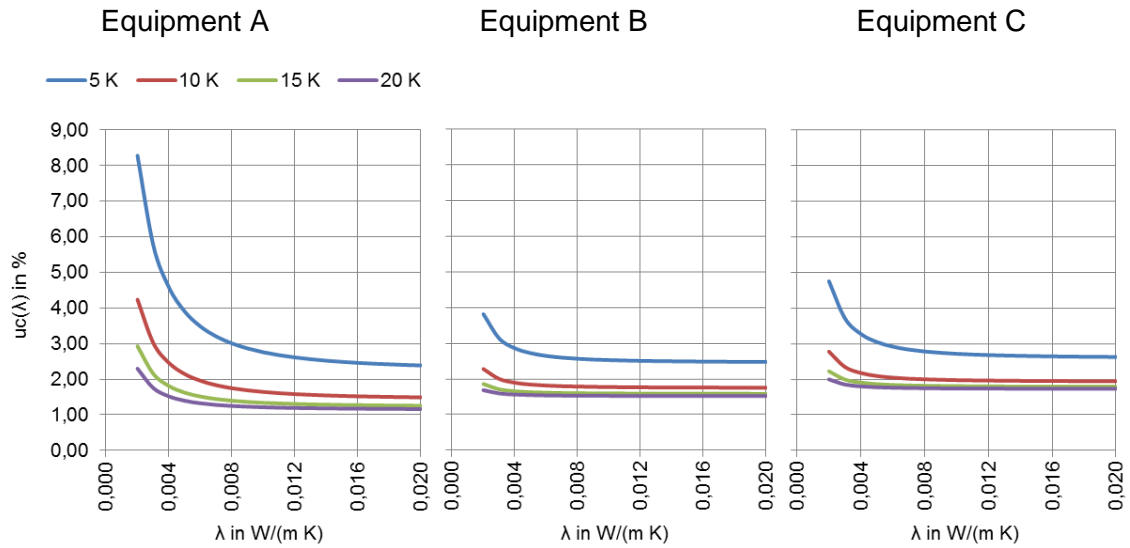

Figure 112: Combined relative uncertainty as a function of thermal conductivity for a panel thickness of 10mm for the example equipment A, B and C according to EN 1946-3:1999 with varying temperature difference.
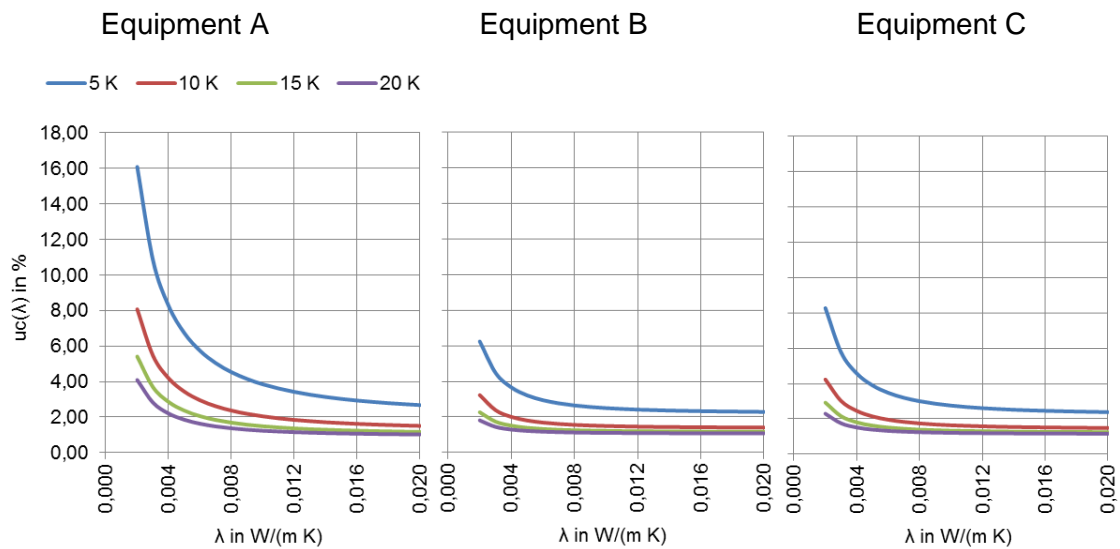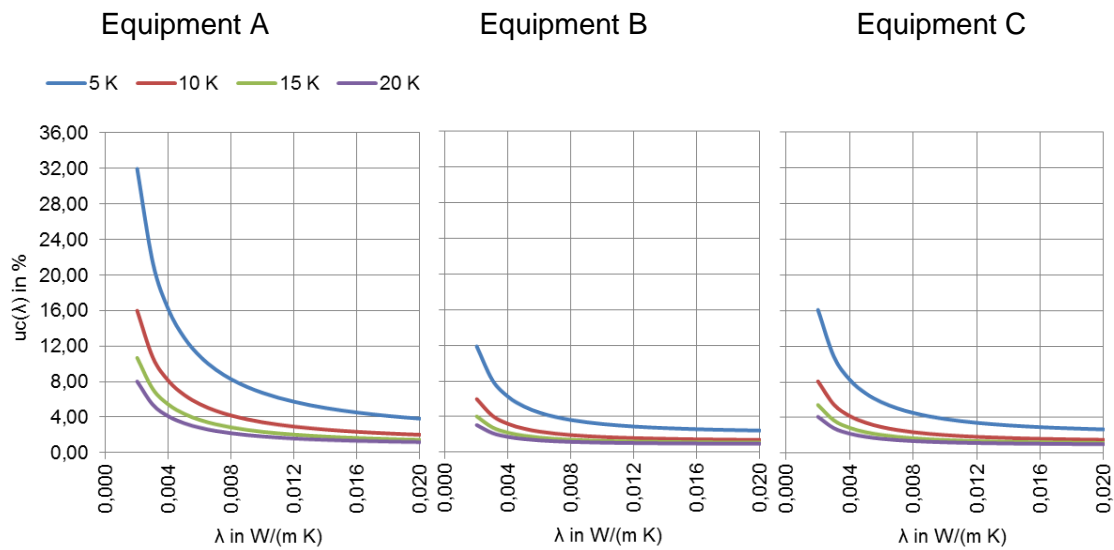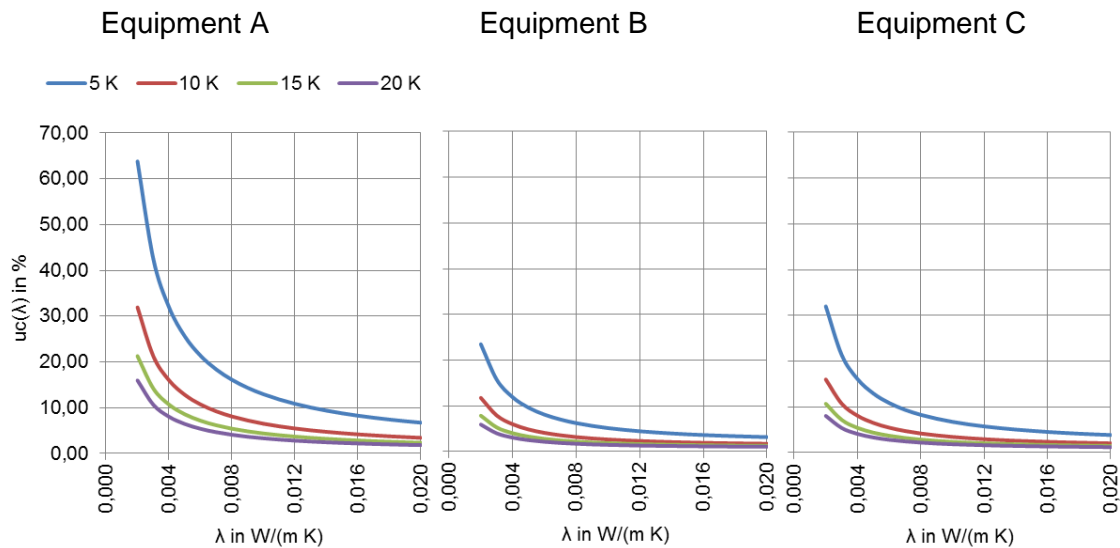

Figure 113: Combined relative uncertainty as a function of thermal conductivity for a panel thickness of 20mm for the example equipment A, B and C according to EN 1946-3:1999 with varying temperature difference.

Equipment A   Equipment B   Equipment C

Figure 114:   Combined relative uncertainty as a function of thermal conductivity for a panel thickness of 40mm for the example equipment A, B and C according to EN 1946-3:1999 with varying temperature difference.

Equipment A   Equipment B   Equipment C

Figure 115:   Combined relative uncertainty as a function of thermal conductivity for a panel thickness of 80mm for the example equipment A, B and C according to EN 1946-3:1999 with varying temperature difference.

Differently from GHP, for HFM the different equipment used strongly influences the obtainable uncertainty level: single-specimen symmetrical configuration, with higher maximum available thickness representing the best solution.

After that it is possible to observe that the measurement uncertainties of lower thermal conductivities are more influenced by the applied temperature difference. Increasing the thermal conductivity, the $u_c(\lambda)$ tends to similar values for each ΔT considered (except for

ΔT = 5K, which is always characterised by higher uncertainty values, especially for thinner samples).

Moreover, the thermal conductivity measurement uncertainty is often higher than the expected value proposed by the standard EN 12667:2001, equal to 3% (Table 49).

Once the thermal and geometrical properties of the analysed panel are known, and a certain expectancy level of the measurement uncertainty is defined, it is possible to define the adequate testing temperature difference.

Table 49: Combined uncertainty $u_c(\lambda)$ in % as a function of λ (equal to 0.002, 0.002, 0.008 and 0.02W/(m K)) with varying temperature difference ΔT in K and (for each chart) constant thickness t in mm, assuming maximum the maximum uncertainty according to EN 1946-3:1999, equipment A with a measuring area of 150^2 mm^2.

Thickness in m	ΔT in K / λ in W/mK	5	10	15	20
0.01	0.002	8.28	4.24	2.93	2.30
	0.004	4.58	2.46	1.81	1.52
	0.008	3.01	1.75	1.40	1.25
	0.016	2.46	1.52	1.27	1.17
	0.020	2.39	1.49	1.26	1.16
0.02	0.002	16.09	8.07	5.42	4.10
	0.004	8.26	4.19	2.85	2.21
	0.008	4.53	2.37	1.69	1.37
	0.016	2.93	1.62	1.24	1.07
	0.020	2.68	1.51	1.17	1.02
0.04	0.002	31.96	15.99	10.68	8.02
	0.004	16.09	8.07	5.41	4.08
	0.008	8.25	4.17	2.84	2.18
	0.016	4.52	2.35	1.66	1.33
	0.020	3.83	2.02	1.45	1.19
0.08	0.002	63.82	31.91	21.28	15.97
	0.004	31.96	15.99	10.67	8.02
	0.008	16.09	8.07	5.40	4.08
	0.016	8.25	4.17	2.83	2.18
	0.020	6.72	3.42	2.34	1.82

Giving an overview of the table, the general trend of the uncertainties is observable. They increase with the increasing of the thickness, and the decreasing of both temperature difference and thermal conductivity.

Going deeper, it is possible to define the minimum testing temperature difference for each panel thickness, to reach a defined uncertainty value, considering the different thermal conductivity of the sample. The EN 12667:2001 standard defines as expected value of HFM uncertainty equal to 3% (while for the GHP apparatus this value is 2%). The light grey highlighted values in the table define the minimum temperature difference

(between those analysed) that guarantees $u_c(\lambda) < 3\%$, while the dark grey values correspond to the minimum ΔT to obtain $u_c(\lambda) < 2\%$ (to have results as reliable as those obtained with the GHP method). For example, a 20mm thick fumed silica based VIP (λ = 0.004W/(m K)) needs a ΔT_{min} = 15°C to obtain a $u_c(\lambda) < 3\%$, and a $\Delta T_{min} > 20$°C to obtain a $u_c(\lambda) < 2\%$. On the contrary, a fibre-based VIP with the same thickness needs a $\Delta T_{min} > 20$°C for both 3% and 2% of uncertainty.

The same analysis is performed considering the equipment B and C (EN 1946-3:1999), and similar behaviours are observed, with a lower uncertainty levels (especially for apparatus B).

Table 50: Combined uncertainty $u_c(\lambda)$ in % as a function of λ (equal to 0.002, 0.002, 0.008 and 0.02W/(m K)) with varying temperature difference ΔT in K and (for each chart) constant thickness t in mm, assuming maximum the maximum uncertainty according to EN 1946-3:1999, equipment B with a measuring area of $250^2 mm^2$.

Thickness in m	ΔT in K λ in W/mK	5	10	15	20
0.01	0.002	3.82	2.28	1.86	1.69
	0.004	2.86	1.90	1.66	1.56
	0.008	2.57	1.79	1.60	1.53
	0.016	2.49	1.76	1.59	1.52
	0.020	2.48	1.76	1.59	1.52
0.02	0.002	6.25	3.23	2.27	1.81
	0.004	3.67	2.01	1.51	1.29
	0.008	2.65	1.56	1.25	1.13
	0.016	2.33	1.42	1.18	1.08
	0.020	2.29	1.41	1.17	1.08
0.04	0.002	11.89	5.98	4.03	3.06
	0.004	6.23	3.18	2.20	1.73
	0.008	3.63	1.93	1.41	1.18
	0.016	2.60	1.46	1.13	0.99
	0.020	2.44	1.39	1.09	0.97
0.08	0.002	23.48	11.76	7.86	5.91
	0.004	11.89	5.98	4.02	3.05
	0.008	6.22	3.17	2.18	1.71
	0.016	3.62	1.91	1.39	1.14
	0.020	3.16	1.70	1.26	1.06

Also in this case, a 20mm thick fumed silica based VIP (λ = 0.004W/(m K)) needs a ΔT_{min} = 10°C to obtain a $u_c(\lambda)$ around 2%, while a fibre based VIP with the same thickness needs a ΔT_{min} = 15°C for 3% of uncertainty and ΔT_{min} = 20°C for 2%.

Table 51: Combined uncertainty $u_c(\lambda)$ in % as a function of λ (equal to 0.002, 0.002, 0.008 and 0.02W/(m K)) with varying temperature difference ΔT in K and (for each chart) constant thickness t in mm, assuming maximum the maximum uncertainty according to EN 1946-3:1999, equipment C with a measuring area of $500^2 mm^2$.

Thickness in m	ΔT in K / λ in W/mK	5	10	15	20
0.01	0.002	4.76	2.78	2.23	2.00
	0.004	3.27	2.18	1.91	1.80
	0.008	2.78	2.00	1.82	1.75
	0.016	2.65	1.95	1.80	1.74
	0.020	2.63	1.95	1.79	1.73
0.02	0.002	8.28	4.24	2.93	2.30
	0.004	4.58	2.46	1.81	1.52
	0.008	3.01	1.75	1.40	1.25
	0.016	2.46	1.52	1.27	1.17
	0.020	2.39	1.49	1.26	1.16
0.04	0.002	16.09	8.07	5.42	4.10
	0.004	8.26	4.19	2.85	2.21
	0.008	4.53	2.37	1.69	1.37
	0.016	2.93	1.62	1.24	1.07
	0.020	2.68	1.51	1.17	1.02
0.08	0.002	31.96	15.99	10.68	8.02
	0.004	16.09	8.07	5.41	4.08
	0.008	8.25	4.17	2.84	2.18
	0.016	4.52	2.35	1.66	1.33
	0.020	3.83	2.02	1.45	1.19

For equipment C, the same fumed silica based VIP ($\lambda = 0.004$W/(m K), d = 20mm) needs a ΔT_{min} = 10°C or 15°C to obtain a $u_c(\lambda)$ around 3% and 2% respectively, while a fibre based VIP with the same thickness needs a ΔT_{min} = 15°C for 3% of uncertainty and ΔT_{min} > 20°C for 2%.

However, the following general recommendations can be concluded:

- the higher the temperature difference is, the lower the combined relative uncertainty occurs. For this reason, a minimum temperature difference of 15K is required, in order to obtain $u_c(\lambda)$ < 3% for all the three apparatus. As a recommendation the temperature difference should be increased to 20K, to reach the same uncertainty limit for GHP equal to 2%,
- the higher the measurable thickness of the specimen, the lower the combined uncertainty: therefore single-specimen symmetrical configuration, with high maximum available thickness are suggested,

- using the HFM method, for theoretical reasons a combined relative standard uncertainty of thermal conductivity lower than 2.0% can be achieved when the right equipment is used, except for thick specimens (more than 40mm) with thermal conductivity equal to 0.004W/(m K) or 0.002W/(m K): in this case a ΔT_{min} > 20°C is required.

Moreover, it is important to highlight that the so defined uncertainties are represented by theoretical values (obtained considering the minimum uncertainty of the heat flux measurement). During real measurements, the combined uncertainty values could be higher (Lorenzati et al., 2015), and therefore higher temperature differences could be required.

6.5.2 Isolines of uncertainty as a function of thickness and temperature difference

Another way to show the combined effects of sample thickness and temperature difference on the uncertainty level is through the isolines curves, for each analysed thermal conductivity (see Chapter 0). For sake of brevity only the results about apparatus B are shown (Figure 116). The thickness and temperature according to the definitions in EN 1946-3:1999 for equipment B is shown in form of the greyed box.

The curves referred to uncertainty $u_c(\lambda)$ = 1% are shown only in case of thermal conductivity higher than 0.008 W/(m K), ΔT > 20K ,and thickness higher than 0.02m (see previous chapter). Moreover, samples with λ equal to 0.004W/(m K) and 0.002W/(m K) could be affected by a minimum level of $u_c(\lambda)$ equal to 1.5%. The influence of decreasing thermal conductivity on the position of the isolines is visible by comparing the different style of lines within one colour.

Differently from the GHP, the spread between the curves is far wider, but it remains the fact that with temperature differences smaller than 10K the distance between the isolines becomes smaller and the same happens for a specimen thickness lower than 10mm.

Generally, considering a fixed thickness, high variations in temperature difference are necessary for their uncertainty reduction (especially for the lowest thermal conductivities and desired uncertainty value). Otherwise, for a defined value of ΔT a lower variation in thickness is required for the uncertainty improvement.

As mentioned before, thicker panels have higher values of uncertainty, especially for very low thermal conductivities. This is due to the strong reduction of the heat flux through the sample because of the high thermal resistance of the samples.
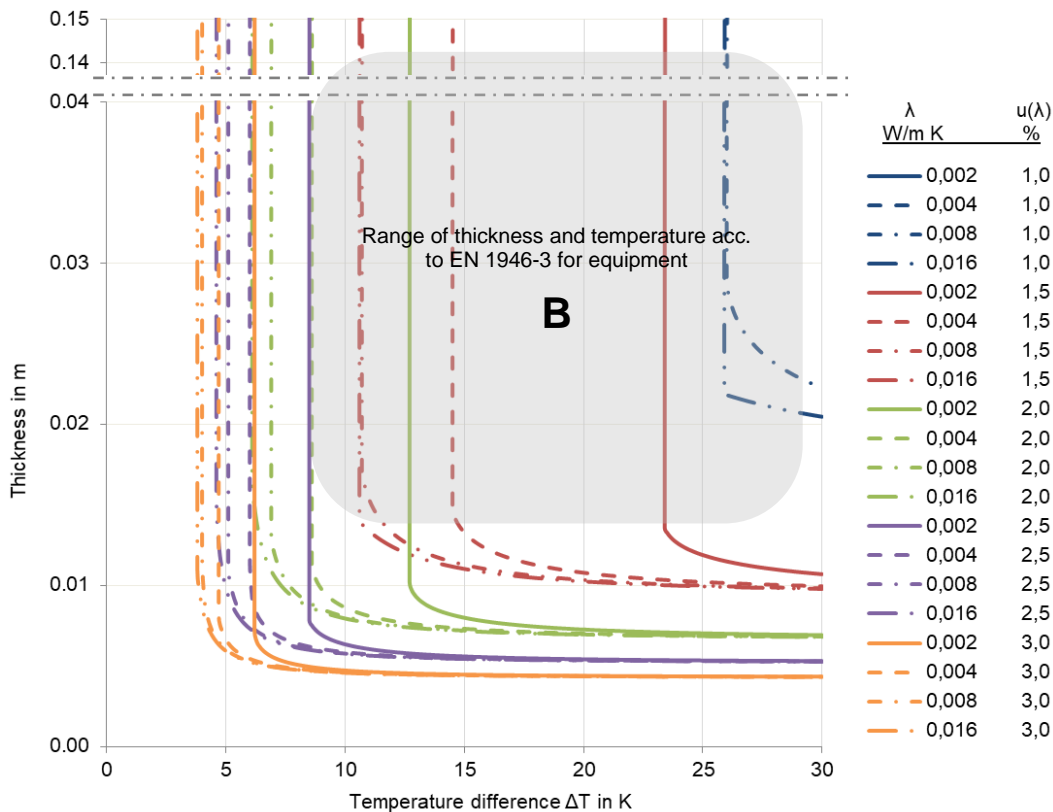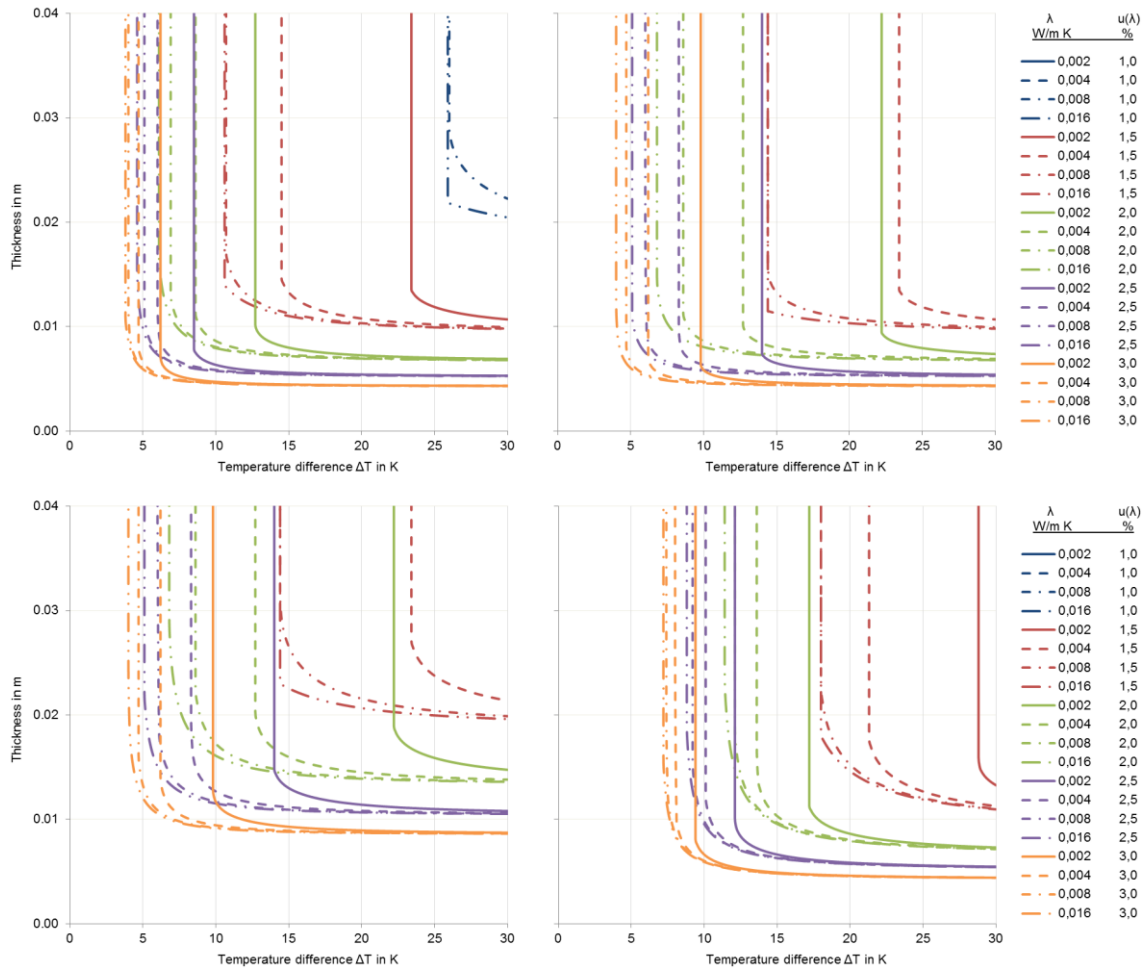
Figure 116: Isolines of levels of uncertainty $u_c(\lambda)$ = 1.0-3.0% for varying levels of λ = 0.004-0.016W/(m K) dependent on temperature difference ΔT in K and thickness of the specimen t in m, assuming the maximum uncertainty according to EN 1946-3:1999, equipment B with a measuring area of $250^2 mm^2$.

6.5.3 Sensitivity of increasing error of single parameters on the combined uncertainty of thermal conductivity

A sensitivity analysis is carried out to identify the more influencing parameters involved in the uncertainty evaluation: in case of HFM the temperature difference, the sample thickness and the heat flux through the specimens have to be considered. This is useful to quantify the variation of the $u_c(\lambda)$ as a function of the singles uncertainty contributes. Moreover, if one of the sensors uncertainties is not declared, this analysis shows how much this unknown could affect the final combined uncertainty (the considered variable errors are about the measurement of heat flux, thickness and temperature difference).

In case of commercial measurement devices usually the unique parameter that can be changed by the operator is the set point temperature and consequently the temperature difference. This kind of survey is useful to estimate if the temperatures change is enough to compensate the uncertainty increasing of the other parameters.

Figure 117 compares the changes of isolines of the relative uncertainty of the thermal conductivity if one of the parameters heat flux (Figure 117, top right), thickness (Figure 117, bottom left) or temperature difference (Figure 117, bottom right) are increasing by

a factor of two, compared to the relative uncertainty assuming the absolute uncertainties for all parameters according to EN 1946-3:1999 (Figure 117, top left).

As observable from Figure 117 (top right), the effects of a doubled value of heat flux uncertainty causes a right shifting and a larger spread of all the curves, compared to the standard case, depending on the thermal conductivity and of the expected combined uncertainty. For instance, fibre core VIP could reach minimum values of uncertainty equal to 1.5% (in the considered range of ΔT < 30K) using a temperature difference higher than around 23K (instead of around 14K). Otherwise, for lower uncertainty expectancy or thermal conductivities higher than 0.002W/(m K), is possible to compensate the increasing of u(q) by the increase of ΔT.

The increasing error of the thickness determination (Figure 117, bottom left) has the same effects of the heat flux increased error (right shifting and a larger spread), but also shifts the isolines upwards. This effect is hard to compensate by an increased temperature difference. For any values of ΔT, 10mm thick specimens could reach uncertainty values not lower than 3%, while $u_c(\lambda) = 1.5\%$ is available only for thicknesses higher than 20mm.

The method is less sensible to a variation of temperature uncertainty. Indeed, an error of the determination of ΔT increased by a factor of 2 causes a shorter right shifting of the curves if compared with the previous. The same $u_c(\lambda)$ level is still possible also simply by increasing the temperature difference of around 5-7K (except for $u_c(\lambda) = 1\%$, for which ΔT > 30K are required).

Figure 117:   Isolines of levels of uncertainty $u_c(\lambda)$ = 1.0-3.0% for varying levels of λ = 0.004-0.016W/(m K) dependent on temperature difference ΔT in K and thickness of the specimen t in m,
top left: assuming the maximum uncertainty according to EN 1946-3:1999, equipment B with a measuring area of 250^2mm^2 (Top left),
top right: increasing the error of the heat flux by a factor of 2,
bottom left: increasing the error of the thickness determination a factor of 2,
bottom right: increasing the error of the determination of ΔT by a factor of 2.

6.6 Uncertainty evaluation of selected parameters

In Chapter 6.3 and 6.5 a sensitivity analysis was carried out for GHP and HFM apparatus about the dependence of the combined relative uncertainty from the different measurands necessary to calculate the thermal conductivity. As explained therein, to obtain results that are universally valid, the calculations are based on assumptions about uncertainty for the measurands based on information in EN 1946-2/-3:1999.

Most commercially available apparatus meet the values of uncertainty claimed in EN 1946-2/-3:1999. However, some parameters require special attention to be in the required specifications. For super insulation materials especially, the thickness determination and the heat flux plate calibration are of interest in this manner.

While the thickness determination, using standard measurement gauges may be problematic, especially for VIP with partly curvature surfaces, the heat flux calibration requires special attention. The determination of heating power and temperature difference is not that different in comparison to the required setup for standard insulation materials.

The following analyses are performed considering single-specimen apparatus: in case of double specimen it will be necessary to proceed with the combined uncertainty evaluation.

6.6.1 *Uncertainty of thickness determination (GHP and HFM)*

The uncertainty of thickness determination is of great influence on the combined relative uncertainty of the calculated thermal conductivity. Therefore, an investigation on the thickness assessment is performed. Three specimens of VIP taken from the market from different manufacturers with equal dimension of 0.6x0.5m and a thickness of 10 and 30mm were chosen (Table 52). The thicknesses are determined with different equipment, on different positions on the panel surface, respectively the edge and by different users.

Table 52: VIP specimen chosen for determination of uncertainty of thickness determination.

Specimen	L in m	W in m	d in mm	Visible curvature
A	~ 0.6	~ 0.5	~ 10	flat
B	~ 0.6	~ 0.5	~ 10	curved
C	~ 0.6	~ 0.5	~ 30	flat
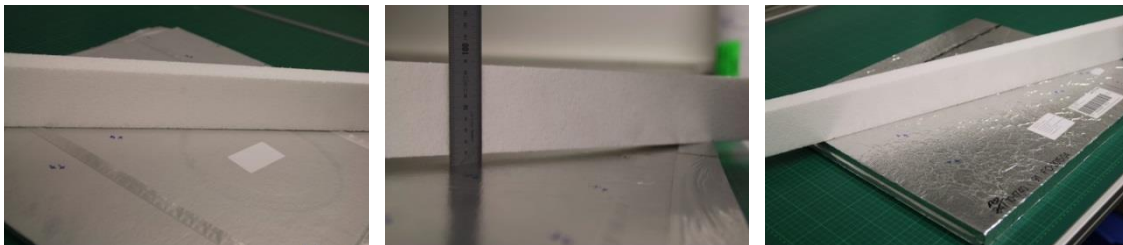
Figure 118: Left: specimen A, 10mm, flat; middle: specimen B, 10mm, curved; right: specimen C, 30mm, flat. (FIW München)

Even if the conducted measurements do not represent a detailed repeatability and reproducibility study, some conclusions about useful methods and differences in the results can be derived.

The measurements are taken out with different equipment. Measurement equipment 1 (ME 1) represents a special equipment for thickness determination from (0) – 300mm with a resolution of 0.001mm and an uncertainty type B of $0.0025\,mm + d\,[mm]\,/\,175\,[mm]$. The ME 1 is positioned beneath a measurement table that ensures a stable and flat support of the sample. Before the sample is measured, the equipment is manually referenced to zero. The panel is then positioned on the measurement table and pressed down by hand around the measurement tip before the measurement is

obtained. This is to ensure the best possible contact between the specimen and the reference plane of the measurement table, even if the panel has a certain curvature. The length of the measurement allows a positioning of the measurement tip in between 215mm away from the edge of the panel (Figure 119).

Figure 119:   Setup for thickness determination on VIP with ME 1. Source: FIW München.

Measurement equipment 2 (ME 2) is a standard calliper with a measurement range of (0) to 150mm with a resolution of 0.01mm and an uncertainty type B of 0.02mm.

The short length of the measurement axes prevents a measurement in the middle of the panel. Therefore, only measurement at the edge of the panel could be conducted. Figure 120 shows the setup of the equipment.

Figure 120:   Setup for thickness determination on VIP with ME 2. Source: FIW München.

The obtained relative errors for different specimen thicknesses in between 1 and 80mm are displayed in Figure 121 in comparison to the values referring to the standard EN 1946-2/-3:1999 for different equipment of type A, B and C.
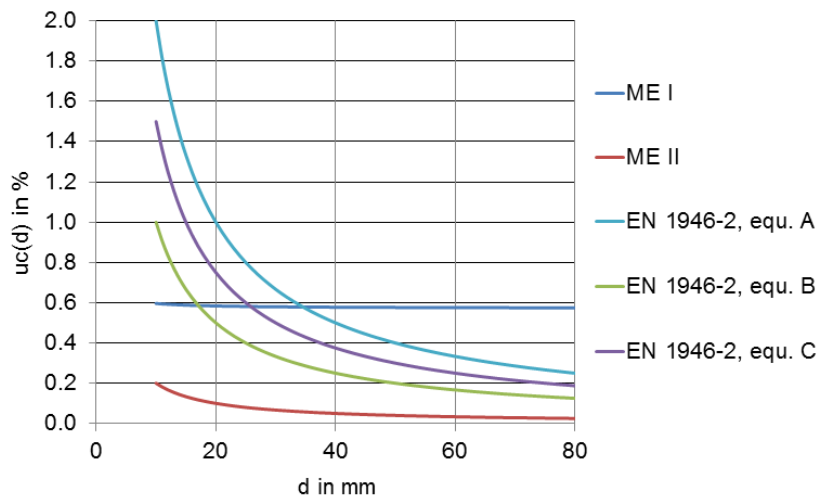
Figure 121: Relative uncertainty type B for different equipment used in the lab (ME 1, ME 2) in comparison to the errors according to the standard EN 1946-2/-3:1999.

The special equipment for thickness determination offers a quite stable performance over the observed range of thicknesses. However, the standard calliper gives more accurate results. The assumed standard uncertainty for equipment A – C according to EN 1946-2/-3:1999 overestimates the error for small thicknesses and underestimates the error for higher values, compared to the example equipment ME 1 and ME 2.

For comparison reasons, also an estimation of uncertainty type A was taken out, using the equipment ME 1 and ME 2 on the panels according to Table 52. Table 53 contains information about the variation of conducted measurement in order to clarify the general repeatability and reproducibility, investigating the potential influence of the operator and of the number of measurement points on the results and data spreading.

Table 53: Variation of conducted measurement to investigate the repeatability and reproducibility with varying number of measurement points.

Measurement series	N_{Op}	N_{MP}	Specimen
Repeatability	1	3, 5, 9	A, B, C
Reproducibility	5	3, 5, 9	A, B, C

The absolute uncertainty u(d) was calculated by

$$u(d) = \frac{1}{\sqrt{n}} \cdot s \tag{44}$$

with:

$$s = \sqrt{\frac{(x_i - x_m)^2}{(n-1)}} \tag{45}$$

where

x_i individual measurement point,

x_m arithmetic mean of the measurement points,

n number of individual measurement points.

The results of the repeatability study are summarised in Table 54. The specimens A, B and C were positioned on the measurement table and pressed flat by hand to avoid the influence of any curvature on the results by imperfect contact of the specimen with the measurement table.

Table 54: Results of repeatability study (one operator), measurement equipment 1 (ME 1), specimen A, specimen B, specimen C.

		Specimen A			Specimen B			Specimen C		
N_{MP}		3	5	9	3	5	9	3	5	9
x_m	in mm	10.60	10.45	10.52	10.86	10.88	10.80	29.39	29.38	29.38
s	in mm	0.2402	0.1661	0.1970	0.2857	0.2309	0.1995	0.2014	0.1858	0.1750
$u(d)$	in mm	0.044	0.023	0.021	0.052	0.033	0.021	0.037	0.026	0.018
$u(d)$	in %	0.41	0.22	0.20	0.48	0.30	0.19	0.13	0.09	0.06

Generally, the higher the number of points taken to perform the measurements, the greater the accuracy that is obtained. Therefore, the thickness measurement performed with nine measuring points is the most precise, as happens in the specimens B and C. In specimen A, the standard uncertainty of the thickness measurement considering five measuring points is lower compared to nine measuring points. The reason for this may be found in VIP configuration. During the measurement of the thickness, a pressure is applied to avoid any curve between the panel and the measurement table influences the measure. As the pressure is not kept perfectly constant, the thickness measures of nine points differ more. However, the calculated uncertainty is lower for nine measuring points. Furthermore, from the chart, it is possible to see that the mean thickness value of the specimen C (d = 30mm) is almost constant.
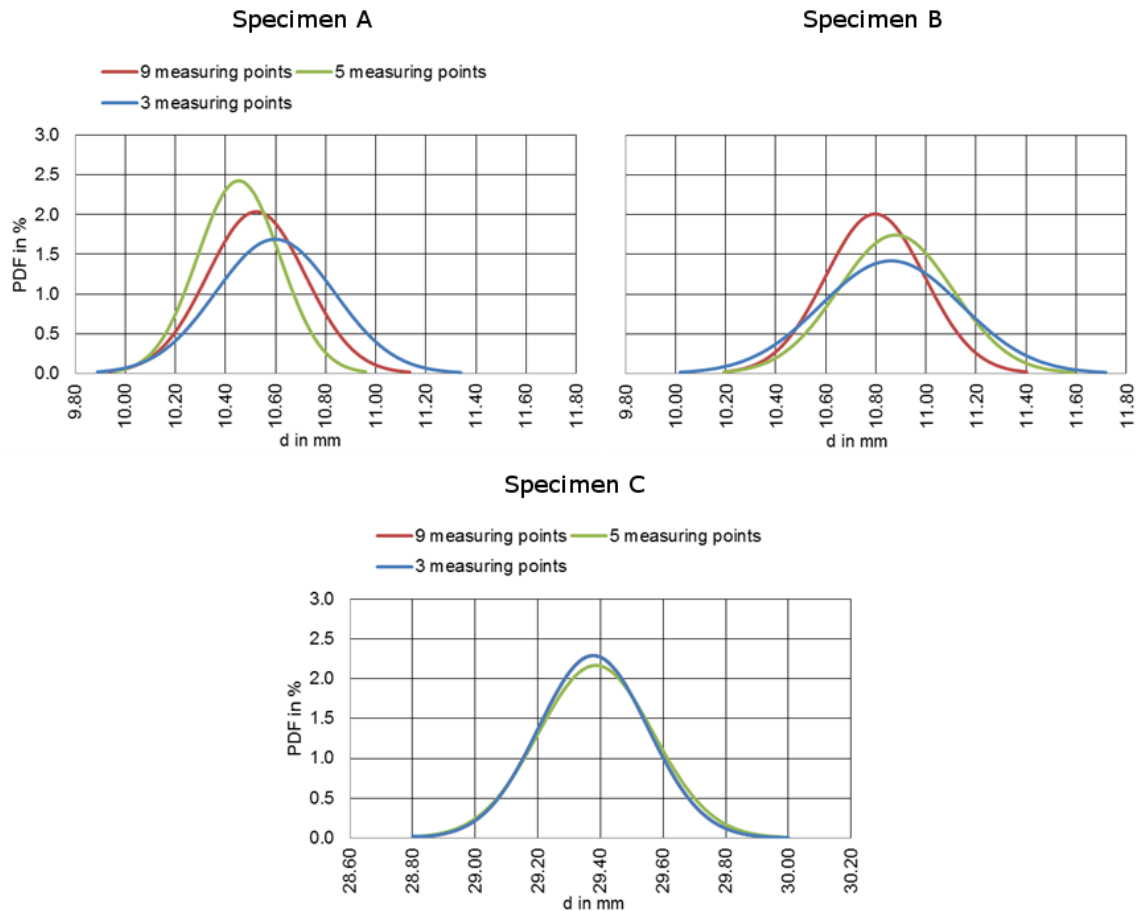
Figure 122: Comparison of Gaussian distributions of the three cases considered with 3, 5, 9 measuring points, measurement equipment 1 (ME 1), specimen A, specimen B, specimen C. (The obtained PDF from 9 measuring points coincides with the one obtained from 3 measuring points).

The results of the reproducibility study are summarised in Table 55. The specimens A, B and C were positioned on the measurement table and pressed flat by hand to avoid the influence of any curvature on the results by imperfect contact of the specimen with the measurement table as much as possible. In the same way the measure was repeated by five different operators.

The obtained results from five operators are compared with the results from one operator (Table 54) taking nine measuring points from each specimen.

Keeping the same surrounding conditions during the thickness measurement and changing only the operator who performs the measurement, it was possible to observe how this change affects the uncertainty of the measurement. The result shows that the value obtained with only one operator is more precise than the mean value obtained by different operators. This is because the panel is not rigid: to guarantee an ideal contact between the sample and the measuring table, some pressure is applied with the hand. Therefore, this different pressure influences the uncertainty of the measurement.

Table 55: Comparison between results of repeatability study (one operator) and results of reproducibility study (five operators), measurement equipment 1 (ME1), specimen A, specimen B, specimen C.

		Specimen A		Specimen B		Specimen C	
N_{Op}		1	5	1	5	1	5
N_{MP}		9	9	9	9	9	9
x_m	in mm	10.52	10.56	10.80	10.83	29.38	29.41
s	in mm	0.1970	0.2097	0.1995	0.2532	0.1750	0.2314
$u(d)$	in mm	0.021	0.031	0.021	0.038	0.018	0.034
$u(d)$	in %	0.20	0.30	0.19	0.35	0.06	0.12
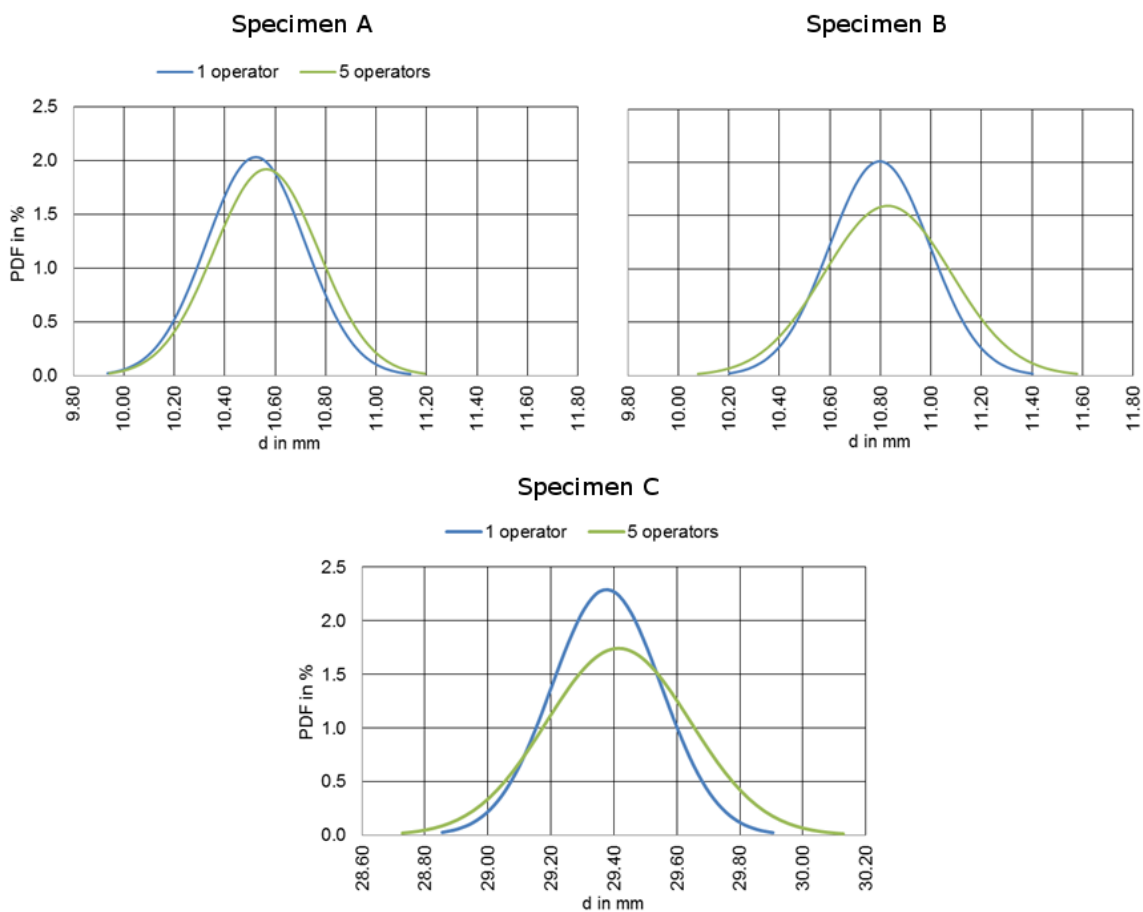
Figure 123: Comparison of Gaussian distributions between measures taken by one operator and five operators, measurement equipment 1 (ME 1), specimen A, specimen B, specimen C, 9 measuring points.

To determine the influence of the measurement equipment and the sensitivity to the position of the measurement points on the panel surface on the measurement uncertainty, another study is performed. Considering six points on the edge, the thickness was measured both with the calliper and with the measurement table. These values were compared with each other and with the corresponding measure of six measurement points at the centre of the panel. Results are summarized in Table 56.

Table 56: Results of repeatability study (one operator), measurement equipment 1 (ME 1) in the centre, measurement equipment 1 (ME 1) on the edge, measurement equipment 2 (ME 2) on the edge specimen A, specimen B, specimen C, 6 measuring points.

Measurement	Specimen A			Specimen B			Specimen C		
	Centre ME 1	Edge ME 1	Edge ME 2	Centre ME 1	Edge ME 1	Edge ME 2	Centre ME 1	Edge ME 1	Edge ME 2
x_m in mm	10.55	10.44	10.09	10.77	10.80	10.32	29.37	29.36	28.85
s in mm	0.232	0.365	0.452	0.310	0.413	0.157	0.173	0.316	0.321
$u(d)$ in mm	0.030	0.047	0.058	0.017	0.053	0.020	0.022	0.041	0.041
$u(d)$ in %	0.28	0.45	0.58	0.16	0.49	0.20	0.08	0.14	0.14

As the edge of the specimen has more irregularities such as folds, from the comparison of the thickness measurements performed it comes out that the measurement in the centre of the sample has a lower uncertainty than the measurement performed at the edge, either the latter is measured with the calliper or with the measuring table.

Comparing the two measurements performed to the edge of the sample, the measurement table has a lower uncertainty than the calliper. This is verified for specimens A and B. For specimen C, both measurement equipment at the edge have the same uncertainty that is even lower than the uncertainty determined for the measurement in the centre of the panel for specimen A and B.

The lower uncertainty for ME 2 compared to ME 1, determined on the edge of specimen B, may depend on the more curved specimen; therefore, the use of the measuring table to measure the thickness at the edge of the specimen is less accurate because it is difficult to apply a constant pressure to avoid the influence of the curvature.

From Figure 124, it is possible to see how the mean value of the thickness remains almost constant for the measurement performed at the edge and the centre of the panel with the same instrument but it changes for the measurement performed with the calliper. The most likely reason for this behaviour is the pressure applied by hand, using the calliper that leads to a higher pressure compared to the measuring table.
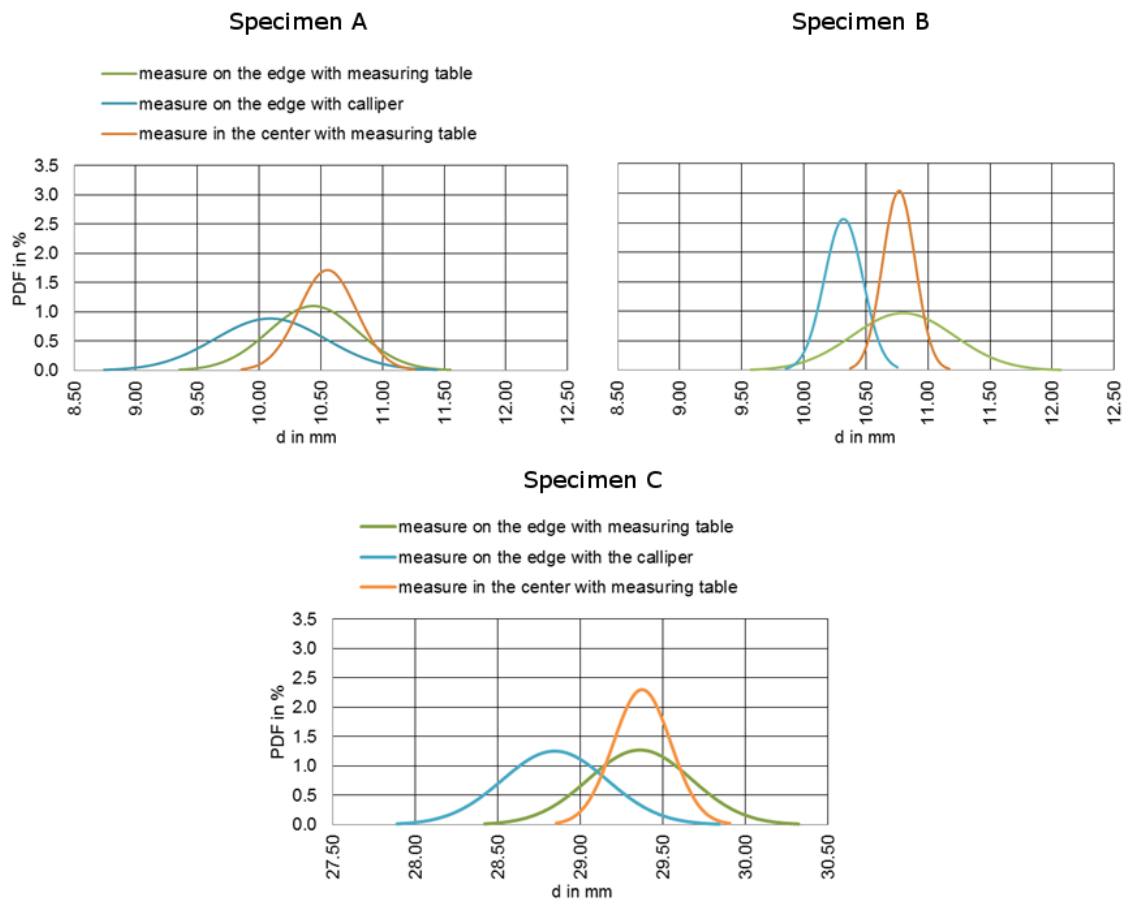
Figure 124: Comparison of Gaussian distributions between centre panel measurements with measurement equipment 1 (ME 1) and edge panel measurement with measurement equipment 1 (ME 1) and 2 (ME 2), specimen A, specimen B, specimen C, 6 measuring points.

6.6.2 Uncertainty of determination of temperature difference (GHP and HFM)

The temperature difference ($ΔT$) is calculated by the difference between the temperature of the hot and cold plate ($ΔT = T_h - T_c$).

Hot (T_h) and cold temperature (T_c) are calculated as the mean value of the temperatures measured by the thermocouples.

$$T_{h/c} = \frac{\sum_{i=1}^{m} T_i}{m} \qquad (46)$$

where

T_i individual measured temperature in Celsius degree [°C],

m number of measured temperatures.

Different types of thermocouples are available in the market, and they are distinguished by the metal that constitutes their two electrical conductors. ISO 8302:1991 provides the uncertainty for any thermocouple divided into standard and special. The difference between them is the degree of precision: special thermocouples have a lower uncertainty

than standard thermocouples, and for this they are used more frequently. Thermocouple features are summarised in Table 57.

Table 57: Type, material and limit error of thermocouples according to ISO 8302:1991.

Type	Material	Temperature range in °C (above 0°C)	Limits of error	
			Standard	Special
T	Cu-CuNi	0 to 350 °C	$\pm\,1\,°C$ or $\pm\,0.75\,\% \cdot |T|$	$\pm\,0.5\,°C$ or $\pm\,0.4\,\% \cdot |T|$
J	Fe/CuNi	0 to 750 °C	$\pm\,2.2\,°C$ or $\pm\,0.75\,\% \cdot |T|$	$\pm\,1.1\,°C$ or $\pm\,0.4\,\% \cdot |T|$
E	NiCr-CuNi	0 to 900 °C	$\pm\,1.7\,°C$ or $\pm\,0.5\,\% \cdot |T|$	$\pm\,1\,°C$ or $\pm\,0.4\,\% \cdot |T|$
K	NiCr-Ni	0 to 1250 °C	$\pm\,2.2\,°C$ or $\pm\,0.75\,\% \cdot |T|$	$\pm\,1.1\,°C$ or $\pm\,0.4\,\% \cdot |T|$
R or S	Pt13Rh-Pt Pt10Rh-Pt	0 to 1450 °C	$\pm\,1.5\,°C$ or $\pm\,0.25\,\% \cdot |T|$	$\pm\,0.6\,°C$ or $\pm\,0.1\,\% \cdot |T|$
B	Pt30Rh-Pt6Rh	800 to 1700 °C	$\pm\,0.5\,\% \cdot |T|$	/

The standard provides, as limit of error, two parameters: one absolute value and one relative value. The uncertainty that has to be assigned to the measured temperature shall be the higher value between the two factors.

As the number of thermocouples used during the test is a choice of the operator, it the influence of the number of thermocouples on the uncertainty of the temperature difference was analysed. Two examples are analysed: one with five thermocouples between the specimen and the hot plate and five between the specimen and the cold plate with a total of ten thermocouples; the other with ten thermocouples used in both sides of the specimen with a total of twenty thermocouples. The calculation of the uncertainty was carried out for a temperature difference range from 5 to 50°C but, for the analysis, the range from 10 to 40°C was taken into account because these are the temperatures set as minimum and maximum limits by EN 1946-2/3:1999. The calculation is repeated for both standard and special thermocouples.

The combined standard uncertainty for the temperature difference is calculated by:

$$u_n\bigl(T_{h/c}\bigr) = \frac{\sqrt{u\bigl(T_{h/c}\bigr)^2 \cdot n}}{n} \tag{47}$$

$$u(\Delta T) = \sqrt{u_n(T_{h/c})^2 + u_n(T_{h/c})^2} \tag{48}$$

where

$u(T_{h/c})$ uncertainty of one temperature given by ISO 8302:1991,

$u_n(T_{h/c})$ uncertainty of n temperatures,

n number of thermocouples used during the test.

Figure 125 shows that for both, standard and special thermocouples a relative uncertainty value less than 1% (value set by ISO 1946:1999 for the temperature difference) is never reached for low temperature using the uncertainty of EN 8302:1991, except for the thermocouple B which, however, produces the same potential difference for temperature from 0 to 42°C and therefore is not used below 50°C.
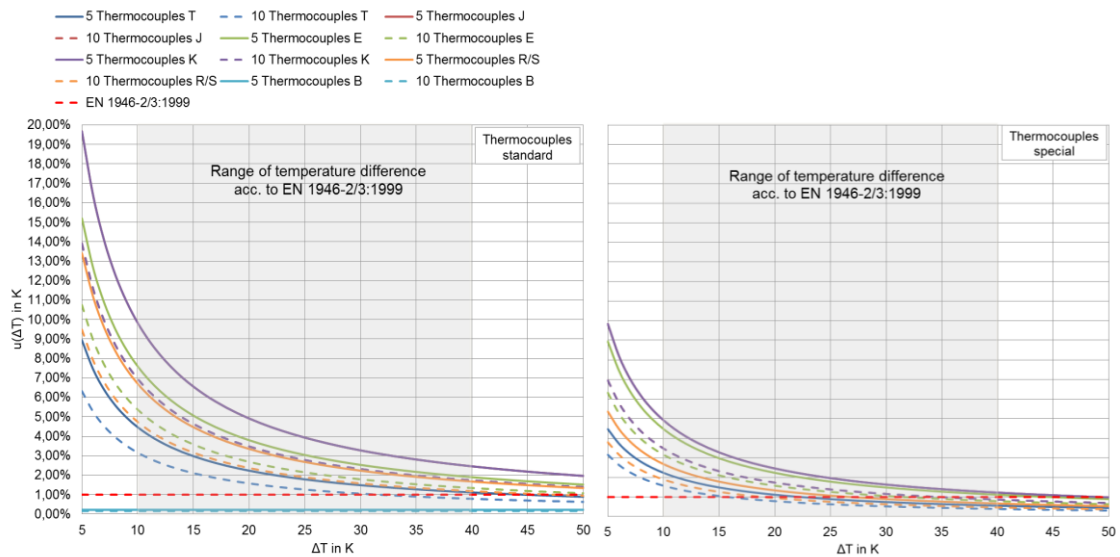
Figure 125:   Relative uncertainty of the temperature difference between 5-50°C with 5 and 10 thermocouples. Left: Standard thermocouple; right: Special Thermocouple.

Because of the results obtained with the temperature uncertainty of the standard, the same study is conducted using the uncertainty value obtained by calibration summarized in Table 58. The laboratory, from which the values are taken, uses T and N thermocouples, so only these thermocouples are analysed.

Table 58:   Type, material and limit of error of thermocouples calibrated.

Thermocouple Type	Material	Temperature range in °C	Error limit
T	Cu-CuNi	- 40 to 40°C	± 0.25°C
N	NiCrSi-NISi	0 to 375°C	± 1.7°C

Through equation (41), the relative uncertainties obtained for a total of 10 and 20 thermocouples T and N, is shown in Figure 126. As N thermocouples are used for high temperatures, at low temperatures the relative uncertainty is higher than 1% set from the standard. This is different to the results obtained for T thermocouples that are used for low temperatures. Indeed, at low temperature the relative error is less than 1%. However for temperature difference around 10°C, the relative uncertainty does not follow the limit imposed by the standard (Table 59). This means that it is necessary to increase the number of thermocouples used because the relative uncertainty then decreases.

Table 59:   Relative uncertainty for 10 and 20 thermocouples T at the temperature between 10°C to 16°C. The grey highlighted values do not respect the standard limit.

Number of thermocouples	10	20
ΔT in K	u(ΔT) in %	
10	1.58%	1.12%
11	1.44%	1.02%
12	1.32%	0.93%
13	1.22%	0.86%
14	1.13%	0.80%
15	1.05%	0.75%
16	0.99%	0.70%
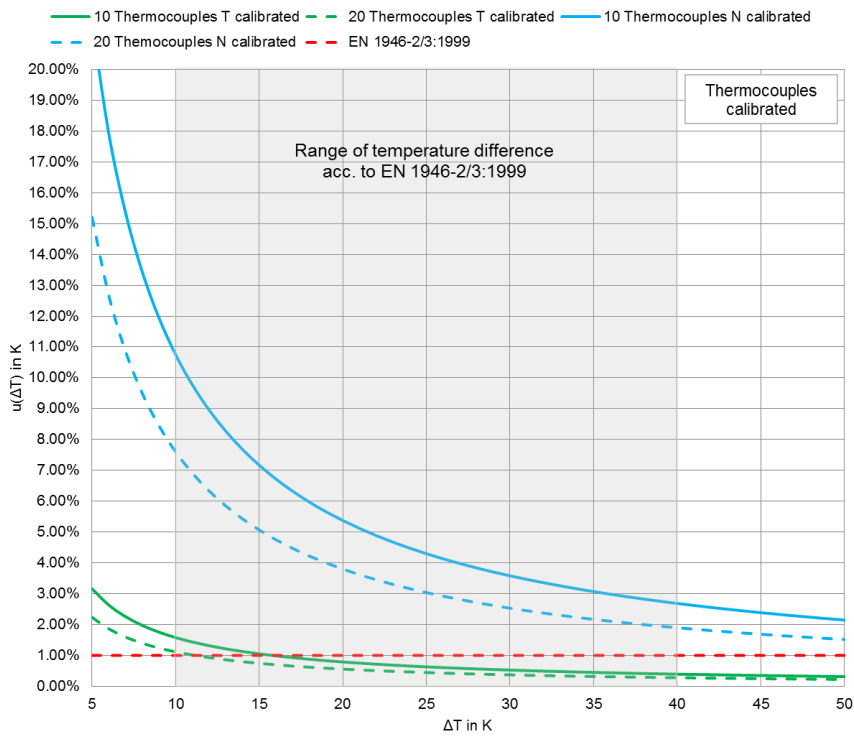
Figure 126:   Relative uncertainty of the temperature difference between 5-50 °C with 10 and 20 calibrated thermocouples.

6.6.3 Uncertainty of determination of heating power (GHP)

The electrical heating power (P) in Watt (W) is calculated by the product of the voltage (U) in Volt (V) and the current (I) in Ampere (A):

$$P = U \cdot I \tag{49}$$

Both measurands can be determined with standard measurement equipment. The measurement of the voltage normally has a lower uncertainty compared to the measurement of the current. The reason for this is that for the permanent measurement of the current an additional resistance R has to be implemented.

Dependent on the measured material and the expected thermal conductivity from 0.002-0.020W/(m K) for SIMs together with the range of specimen thickness a wide range of electrical power values can be obtained. In the performed sensitivity study a range of electrical power was from 0.006W (0.002W/(m K), 0.08m) to 20W (0.020W/(m K), 0.01m). Thus, the uncertainty of electrical power determination will also vary in a broad range.

The combined uncertainty for the electrical power is calculated according to:

$$u(P)^2 = \left(\frac{\delta P}{\delta U} \cdot u(U) \right)^2 + \left(\frac{\delta P}{\delta I} \cdot u(I) \right)^2 \tag{50}$$

with the differential operators:

$$\frac{\delta P}{\delta U} = I \tag{51}$$

$$\frac{\delta P}{\delta I} = U \tag{52}$$

and uncertainties $u(U)$ and $u(I)$ according to Table 60.

Table 60:   Measurement range and related uncertainties of voltage (V) and current (I).

Measurement range in V		u(U)	u(U$_{min}$)
U$_{min}$	U$_{max}$	in V	in %
0.07	0.7	0.0000084	0.012
0.7	7	0.000084	0.012
7	70	0.00084	0.012

Measurement range in A		u(I)	u(I$_{min}$)
I$_{min}$	I$_{max}$	in A	in %
0.003	0.03	0.0000072	0.24
0.03	0.3	0.000072	0.24
0.3	3	0.00072	0.24

The given relative uncertainties $u(U)$ and $u(I)$ reflect typical values. However it has to be taken into account that the measurement range normally incorporates values in the range of a factor of 10. Thus, for the calculation of the relative uncertainty of electrical power the range of values for the voltage and current has to be calculated first. The heating elements contain filaments that have a certain electrical resistance. By controlling the voltage, the current is set to a certain level according to the Ohm's law:

$$R = \frac{U}{I} \tag{53}$$

For the sensitivity study the equations (42) and (46) are used to calculate the associated values of voltage and current for the range of values in between 0.005-20W, assuming an electrical resistance for the heating element of equipment A, B and C according to EN 1946-2:1999 (Table 61). The electrical resistance depends more on the material and dimension of the filament. However, the size is somehow correlated, which is why an increasing electrical resistance was chosen correlating to the size of the heating element.

Table 61: Electrical resistance R related to the size of the heating element according to equipment A, B and C according to EN 1946-2:1999.

Equipment	Edge length of heating element in mm	R in Ω
A	150	47
B	250	54
C	500	71

Figure 127 shows the results of the calculated combined relative uncertainty of electrical power as a function of the electrical power. Several steps with increasing relative uncertainties of electrical power ($u_c(P)$) are visible for all type of equipment. This is always related to a change of the measurement range for determination of voltage and current.

The expected values of $u_c(P)$ will not exceed 0.24% even in the worst case. However, compared to the value of 0.1% according to the standard in some cases this value is excelled by a factor of two.

An improvement could be achieved by the definition of individual measurement ranges or enhanced calibration of the equipment in the transition zone between two measurement ranges.
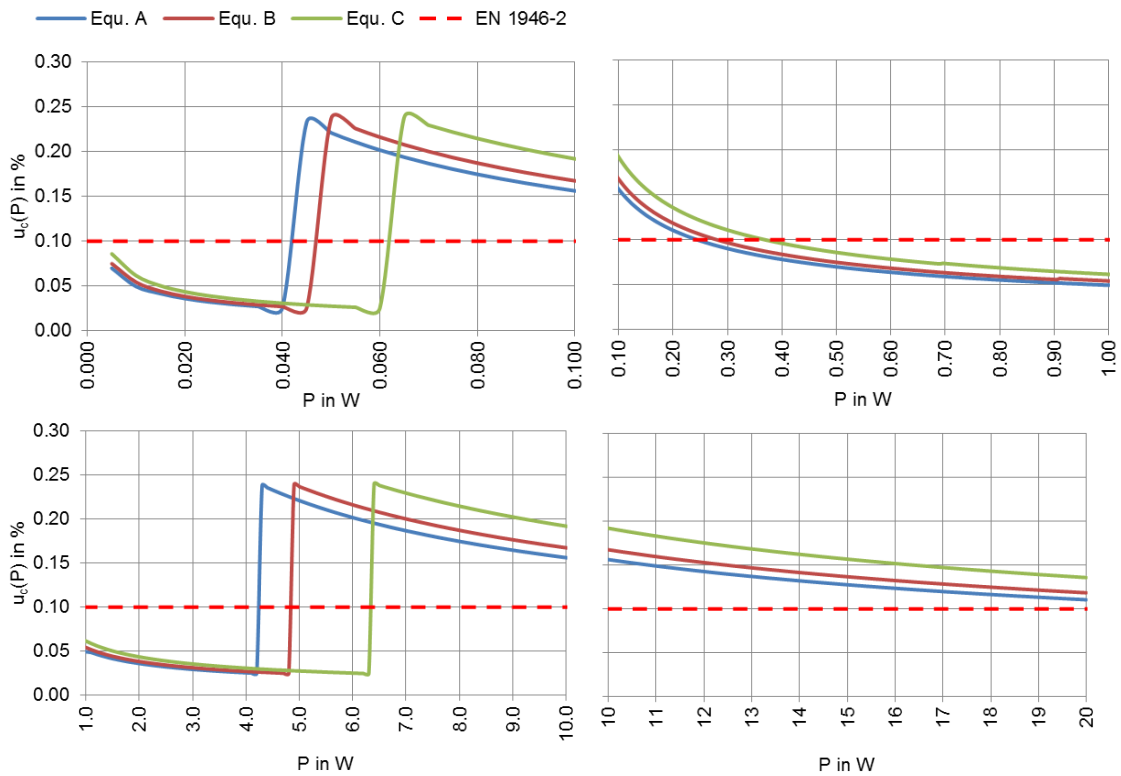
Figure 127:Combined uncertainty of the electrical power in between 0.005-20W assuming measurement uncertainty of voltage and current according to Table 60, top left: P = 0.005-0.100W; top right: P = 0.10-1.0W; bottom left: P = 1.0-10W; bottom right: P = 10-20W.

6.6.4 Uncertainty of heat flux plate calibration (HFM)

As opposed to the GHP method, the HFM method is not a direct measurement but requires a special equipment to measure the heat flux (q in W/m²). Together with the thickness of the specimen (d) and the temperature difference (ΔT), the thermal conductivity (λ) can be calculated.

$$\lambda = \frac{q \cdot d}{\Delta T} \tag{54}$$

The equipment to measure the heat flux consists of a thermocouple chain embedded in a polymer matrix. If a temperature difference is applied on both sides, the grid of thermocouples generates a signal of voltage in mV (e) that is proportional to the heat flux by the factor $f_{cal}(T)$ in W/(m² mV)

$$q = e \cdot f_{cal}(T) \tag{55}$$

The factor $f_{cal}(T)$ is temperature dependent and therefore shall be determined for every heat flux plate by calibration in the required temperature range (Figure 128).
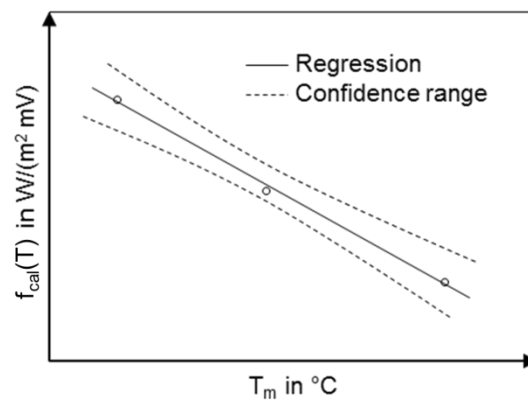
Figure 128:   Temperature dependence of $f_{cal}(T)$.

The accuracy of the heat flux plate is dependent on the quality of the calibration curve of $f_{cal}(T)$ expressed by a confidence range. In this context several methods can be applied.

One possibility is to use an adequate reference material in the apparatus that has a stable and known temperature dependent thermal conductivity. Knowing the temperature difference, the associated heat flux can be calculated and used for calibration of the curve of $f_{cal}(T)$. While this method is easy to perform, the accuracy may not be that high, because unavoidable variations in the thermal conductivity of the reference material will influence the accuracy of the results.

Therefore, the preferable method is the calibration of the heat flux plate in a GHP apparatus. Figure 129 shows a possible setup of the configuration. Therefore the heat flux plate is positioned in between a hot plate and a cold plate. The lower plate has temperature guard below that is controlled to isothermal conditions. In this configuration the electrical power of the heating plate nearby the heat flux plate is going unidirectional through the heat flux plate. The known methods for calculation of heat flux based on the electrical power of the heating plate, the temperature difference and the measurement are used to calculate *q*.
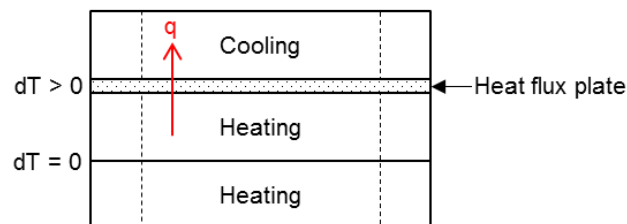
Figure 129:Setup for calibration of a heat flux plate in the GHP apparatus. Source: FIW   München.

To determine the confidence range of the regression $f_{cal}(T) = f(T_m)$, both, type A and type B uncertainty have to be considered. As an example

172

Table 62 contains a possible result considering three data points from the calibration of the $f_{cal}(T)$.

Table 62:   Example data from calibration of $f_{cal}(T)$.

x	y
Tₘ in °C	$\boldsymbol{f_{cal}(T)}$ in W/(m² mV)
6.2	6.24
25.8	6.08
48.5	5.88

For the type A uncertainty, the linear regression and the associated 95% confidence range is calculated first.

The linear regression is fitted to the equation

$$\hat{y} = m \cdot x + b \tag{56}$$

According to Sachs, 1984, the following prediction interval for future obtained values of $f_{cal}(T)$ at a certain temperature T_m is chosen.

$$\hat{y} \mp t_{(n-2)} \cdot s_{\hat{y}} \tag{57}$$

While $\hat{y}$ represents the regression value of $f_{cal}(T)$ and $t_{(n-2)}$ is derived from tabled values for t-distribution, the standard deviation $s_{\hat{y}}$ represents the standard deviation for a predicted single value of $\hat{y}$ at a certain temperature T_m expressed by:

$$s_{\hat{y}} = s_{y \cdot x} \cdot \sqrt{1 + \frac{1}{n} + \frac{(x - \bar{x})^2}{Q_x}} \tag{58}$$

with:

$$s_{y \cdot x} = \sqrt{\frac{\sum(y - \hat{y})^2}{n - 2}} \tag{59}$$

$$Q_x = \sum(x - \bar{x})^2 \tag{60}$$

where

$\bar{x}$ arithmetic mean of the observed values of x,
n number of observations.

Applying this to the values according to

Table 62 a regression and confidence range type A (dashed line) as shown in Figure 130 is achieved.
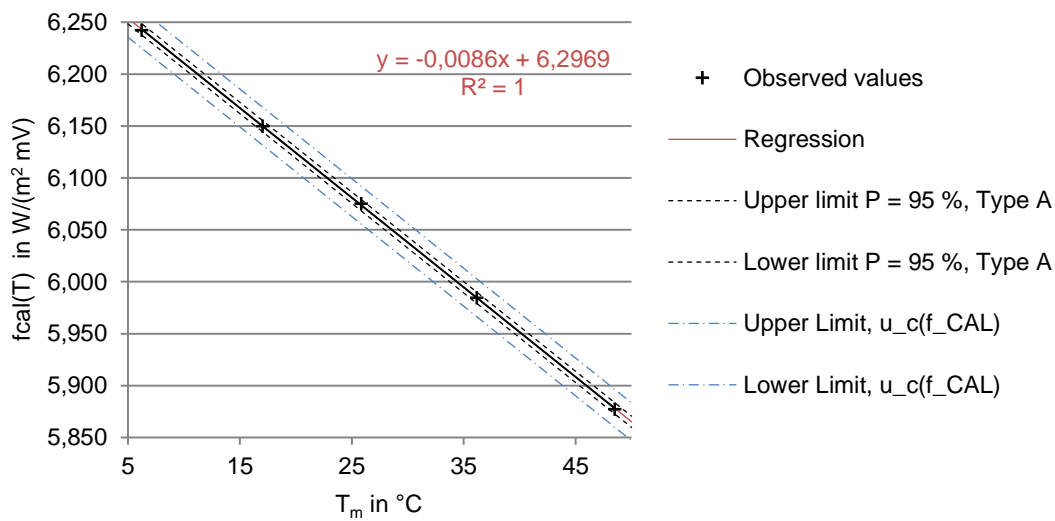
Figure 130: Observed values, regression and confidence range for P = 95% (type A) (dashed line) and combined uncertainty $u_c(f_{cal}(T))$ (chain line).

The confidence range for P = 95% is highly dependent on the number of data points. In the given example five data points are considered. This leads to a $t_{(n-2)}$ factor of 3.182. If less data points are considered the spreading of the confidence range gets significantly higher due to increasing value of $t_{(n-2)}$. In such case it has to be decided wether it is useful to consider the type A uncertainty or not.

For determination of error type B, the measurement uncertainty for calculation of the mean temperature and the $f_{cal}(T)$ signal have to be calculated separately.

Starting with the error for the determination of the mean temperature the equations according to Chapter 0 can be applied. In the example given, an uncertainty for the mean temperature of $u(T_m)$ = 0.074K is considered.

The combined uncertainty for the determination of $f_{cal}(T)$ is calculated assuming the errors of the obtained electrical power (*P*) in W, measuring area (*A*) and the voltage in mV (*e*) based on the equation:

$$f_{cal}(T) = \frac{P}{A \cdot e} \tag{61}$$

For the example, given a combined uncertainty $u(f_{cal}(T))$ = 0.0174W/(m^2 mV) is assessed. Thus the combined uncertainty type B for the curve of $f_{cal}(T)$ as a function of the mean temperature is given by:

$$u(f_{cal}(T)) = \sqrt{\left(\frac{u(T_m) \cdot \frac{\delta f_{cal}(T)}{\delta T_m}}{f_{cal}(T)}\right)^2 + \left(\frac{u(f_{cal}(T))}{f_{cal}(T)}\right)^2} \cdot f_{cal}(T) \tag{62}$$

The calculation of the combined uncertainty of type A and type B is performed in the same way as described before and is shown in Figure 130 (chain line).

6.7 Comparison of GHP and HFM method

In order to compare GHP with HFM, the thermal conductivity uncertainty was calculated for both of the methods, GHP and HFM, using the combined standard uncertainty (Chapter 6.2 for GHP and Chapter 0 for HFM). The calculation was performed again considering different levels of thermal conductivity in between 0.002-0.016W/(m K). The value of thickness was chosen with 0.02m, because it is commonly used for VIP. The temperature difference is assumed to be 15K. At this temperature difference the uncertainty limit imposed by EN 1946-2/3:1999 is achieved with five calibrated thermocouples of type T. The value of the electrical power (P) for GHP and heat flux (q) for HFM were calculated.

$$P = \frac{\lambda \cdot A \cdot \Delta T}{d} \tag{63}$$

With the value of the metering area (A) was assumed equal to 0.09015m^2.

$$q = \frac{\lambda \cdot \Delta T}{d} \tag{64}$$

To the set of data the absolute uncertainties derived from the analyses carried out in the previous chapters are applied.

For the thickness the absolute uncertainty equal to 0.000021m obtained through the thickness measurement with one operator, measurement equipment 1 (ME1 = measuring table), in 9 measuring point (Chapter 6.6.1); for the temperature difference an uncertainty equal to 0.158K (Chapter 6.6.2) and for the metering area an uncertainty of 0.16% was assumed. The uncertainty of the electrical power (u(P)) and heat flux (u(q)) was calculated by:

$$u_P = \sqrt{\left(\frac{\delta\lambda}{\delta U}\right)^2 u_U{}^2 + \left(\frac{\delta\lambda}{\delta I}\right)^2 u_I{}^2} \tag{65}$$

$$u_q = \sqrt{\left(\frac{\delta\lambda}{\delta f_{cal}(T)}\right)^2 u_{fcal(T)}{}^2 + \left(\frac{\delta\lambda}{\delta e}\right)^2 u_e{}^2} \tag{66}$$

Through different assumptions the value of voltage (U), current (I) and heat flow meter (e) were determined, and their respective uncertainties were calculated from the typical values of uncertainty (Chapter 0 and 6.6.4). For the calculation of the value and uncertainty of calibration factor ($f_{cal}(T)$) the graphic of temperature dependence of $f_{cal}(T)$ after the assumption of the mean temperature of the heat flux plate is used (Chapter 0). The analysis was performed considering an equipment B for both the

methods. The set of data and the uncertainties are summarised in Table 63 and Table 64.

Table 63: Set of data and assumed uncertainties for calculation of combined uncertainty of thermal conductivity $u_c(\lambda)$.

Set of data	Abbr.	Unit	B	Uncertainty
Specimen thickness	d	m	0.02	0.000021
Temperature difference	ΔT	K	15	0.158
Metering area	A	m^2	0.09015	0.000144
Calibration factor	$f_{cal}(T)$	W/(m^2 mV)	~ 6.147	0.035

Table 64: Uncertainty of the voltage (U), current (I) and heat flow meter (e).

Measurement range in V		u(U) in V
U_{min}	U_{max}	
0.7	7	0.000084
7	70	0.00084
Measurement range in A		u(I) in A
I_{min}	I_{max}	
0.03	0.3	0.000072

Table 65 and Table 66 show the thermal conductivity uncertainty of GHP and HFM. The combined relative uncertainty obtained with GHP is lower than the one obtained with HFM.

Table 65: Absolute and relative uncertainty of thermal conductivity for GHP with d = 0.02m; ΔT = 15K and uncertainty known.

λ in W/(m K)	$u_c(\lambda)$ in W/(m K)	$u_c(\lambda)$ in %
0.0020	0.0000259	1.29
0.0040	0.0000516	1.29
0.0080	0.000103	1.29
0.0160	0.000206	1.29

Table 66: Absolute and relative uncertainty of thermal conductivity for HFM with d = 0.02m; ΔT = 15K and uncertainty known.

λ in W/(m K)	$u_c(\lambda)$ in W/(m K)	$u_c(\lambda)$ in %
0.0020	0.0000279	1.39
0.0040	0.0000558	1.39
0.0080	0.000112	1.39
0.0160	0.000223	1.39

The same calculation was also performed using the same set of data but with the uncertainties provided by EN 1946-2/3:1999. The results are summarised in Table 67 and Table 68.

Table 67: Absolute and relative uncertainty of thermal conductivity for GHP with d = 0.02m; ΔT = 15K and uncertainty of EN 1946-2:1999.

λ in W/(m K)	$u_c(λ)$ in W/(m K)	$u_c(λ)$ in %
0.0020	0.0000275	1.37
0.0040	0.0000549	1.37
0.0080	0.00011	1.37
0.0160	0.00022	1.37

Table 68: Absolute and relative uncertainty of thermal conductivity for HFM with d = 0.02m; ΔT = 15K and uncertainty of EN 1946-3:1999.

λ in W/(m K)	$u_c(λ)$ in W/(m K)	$u_c(λ)$ in %
0.0020	0.000049	2.45
0.0040	0.000098	2.45
0.0080	0.000196	2.45
0.0160	0.000392	2.45

To see the influence of factors on the thermal conductivity uncertainty for each parameter the uncertainty contribution was calculated. Therefore the product of the standard uncertainty with the sensitivity was expressed as a percentage of the combined uncertainty:

$$u_i(\lambda) \ in \ \% = \frac{u_i(\lambda)}{\sum u_i(\lambda)}$$

(67)

The term $u_i(\lambda)$ represents the value of the uncertainty contribution of the analysed parameter. The calculation was performed for both the uncertainty as determined in the previous chapters for selected parameters under lab conditions and the uncertainty according to EN 1946-2/3:1999.

Using the uncertainty known for GHP, Figure 131 shows that the most influential parameter is the temperature difference with a percentage of 41.1%. Using the uncertainty values provided by the standard, all the parameters have a relative influence except the heating power (P) and the error due to non-symmetrical condition ($\Delta\lambda_S$). Even in this case the temperature difference is the most influential.
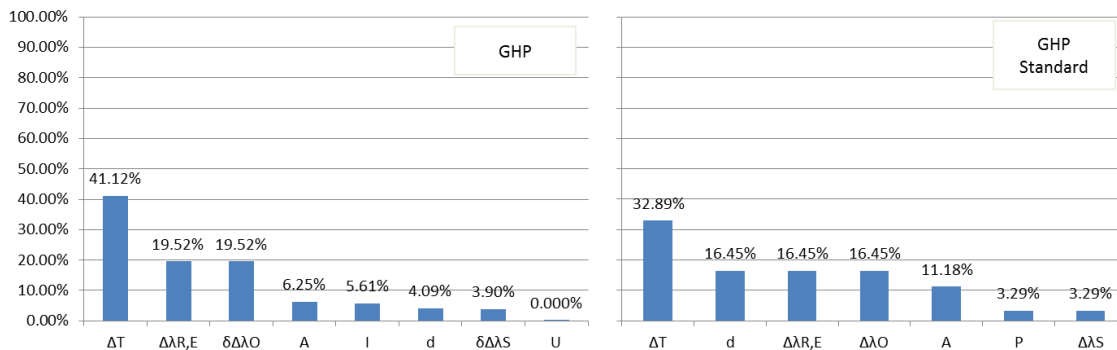
Figure 131:   Influence of each factor on thermal conductivity uncertainty for GHP. Left: uncertainty known; right: uncertainty of EN 1946-2:1999.

Figure 132 shows that for both cases for the HFM the temperature difference (ΔT) and the heat flux (q) are the more influential parameters on the final result.
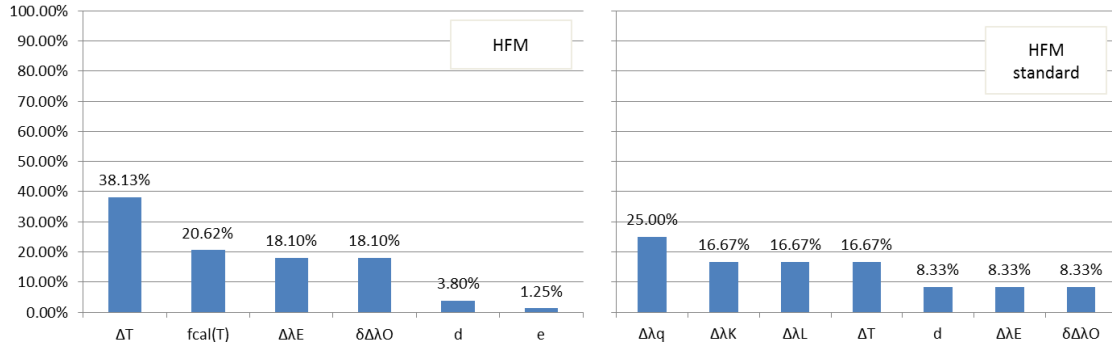

Figure 132:   Influence of each factor on thermal conductivity uncertainty for HFM. Left: uncertainty known; right: uncertainty of EN 1946-3:1999.

7 Recommendations

The defined aim of Subtask 2 is to investigate whether the common methods for thermal characterisation, especially thermal conductivity, provide sufficient accuracy for the determination of material properties of super insulation materials. Due to the very low thermal conductivity, uneven shape of the panels (especially for VIPs) and still missing product standards for VIPs and APMs that would provide information about handling and useful adaptions of existing test standards, the serviceability of the standards methods must be investigated.

Based on the performed tests, several recommendations to improve the quality of measurement on SIMs can be derived. The following conclusion is not structured according to the table of content but tries to summarise and cross-link the findings from different views on the topic.

7.1 Lab Handling

Starting with recommendations for lab handling, the very first thing to consider is the general material characteristic. In this context, SIMs can consist of loose fill granulate (e.g. loose Aerogel particles), flexible mats (e.g. fibre mats with aerogels inside) or rigid boards (e.g. nano-structured rigid foams or VIPs). Each mechanical characteristic requires special attention, starting with the handling, the determination of the geometrical properties and the installation in the measurement equipment.

7.1.1 Loose filled material

Starting with loose fill material in any case a cavity is required to limit and to hold a volume that is then filled with the material. For testing purposes, this means a frame is required to generate a test specimen with a defined thickness that can be installed in the test apparatus. In this manner, the thickness is not defined by the product itself, but by the thickness (the height) of the test frame. To determine correct values of thermal conductivity the right raw density, according to the specifications of the manufacturer, must be installed. Especially when the material shall be compressed a stable frame is necessary to avoid bulging of the sides of the frame when the material is pressed inside the frame. In this manner the utilisation of EPS frames might not be the most appropriate because the material is not rigid and furthermore, granulate can be pressed inside the soft foam which also influences the raw density. Another problem with soft and compressible frames is the possibility that the test frame is compressed to a lower thickness when installed inside the apparatus. Even though modern apparatus offer a monitoring of the distance between the measuring plates, the agreed thickness should not be changed too much because this again influences the raw density.

A recommendation for a suitable test frame would be "duroplastic", plastics that provide a stable construction. Wood based materials would also provide a stable frame but have

the problem of hygroscopic behaviour. To document drying or moisture uptake during testing, the frame together with the installed material needs to be weighed before and after the testing. Using a wooden test-frame the hygroscopic behaviour of the test frame would influence the result of the mass determination.

Before installation of the test specimen the required mass must be calculated considering the volume of the test frame and the raw density, referring to an agreed moisture content if the material is hygroscopic.

When filling the material in the test frame it must be ensured that one homogeneous layer of material with constant raw density over the measurement zone and over the thickness of the sample is achieved. In this manner two things must be considered. If the material must be compressed somehow to achieve the required raw density in the installed case – e.g. when the bulk density is lower than the installed density – it is recommendable to use an extension of the frame to enable filling in with vertical exaggeration. The material can then be compressed using a stamp. Compared to a procedure of interspersing the material layer-wise this guarantees a homogeneous layer over the height of the sample with a lower risk of having formation of separated layers with differing density.

If the density of the material is in the range of the bulk density, it also has to be considered that settling phenomena could occur due to mechanical impacts during handling and also due to thermal and hygric stress whilst testing. Therefore, after testing, it should carefully be checked if any gap between the surface of the specimen and the heating or cooling plate has occurred as this would influence the achieved thermal conductivity.

As for all products, a good thermal coupling of the heating and cooling plates with the specimen, respectively the testing frame should be achieved. Therefore, the test frame should also offer precisely aligned sides.

7.1.2 Flexible products

For flexible products the thickness determination and the pressure force of the measuring plates require special attention.

Many measuring gauges for thickness determination provide a specific pressure to guarantee a good contact of the measuring tip with the surface of the specimen and to guarantee enough contact of the specimen with the supporting measurement table.

For flexible products the measuring force must be adjusted, so the material is not compressed in an unintended way. In the same connection, the pressure force of the measuring plates in the apparatus should not lead to a compression that changes the structural characteristic of the material.

Again, the task is to install the material to ensure a good thermal contact between the heating and cooling plates is guaranteed. If there is data from the manufacturer about

the declared thickness, these values can be considered for orientation. However, the installation in the apparatus must be set up carefully.

7.1.3 Rigid boards

For rigid boards it is more a question of determining the correct thickness and ensuring a good thermal contact between the heating/cooling plates rather than having the risk of influencing the structure of the material during measurement.

Especially for VIPs the welding seams on the panel surface are problematic. In this context the utilization of thin sheets of foam (e.g. made from silicone or rubber) in between the panel surface and the heating/cooling plates are recommended.

The already described approach of using thicker sheets of material with a high thermal conductivity on both sides of the VIP installed in the apparatus to increase the thermal conductivity of the package with the aim to be in the specifications of the apparatus used, may cause problems. On the one hand, the thermal cross-conduction in the extra layer may increase the error due to lateral heat flux and edge losses; on the other hand the heat flux becomes even lower. Therefore, in any case the uncertainty of the heat flux plate or the uncertainty of the determination of electrical power will increase. Anyway, if it is not possible to use a different apparatus, this approach could be helpful, with the following suggestions. The rubber elements (or a different high conductivity material) must have the dimensions equal to the measuring area of the apparatus and need to be surrounded by a soft sample frame, slightly thicker than the sample. Moreover, if required by the device configuration, the "sandwich sample" in this way obtained could also be included into a second insulating mask (Figure 133). In this way, at least the lateral heat losses are reduced.
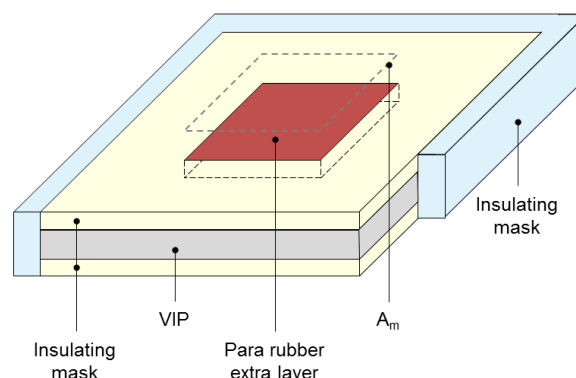

Figure 133:Adoption of thick rubber extra layer.

Crucial for rigid boards, especially for VIP is the determination of the correct thickness. As described, oftentimes standard measurement equipment is used in this context.

Common is the use of a stable measuring table and a dial gauge fixed on a gantry portal. With such equipment the thickness in the centre of the specimen can be determined, depending on the overhang of the gantry portal.

Compared to the use of standard calliper this setup has advantages and disadvantages. The considered heat flux is measured as the mean heat flux inside the measurement zone. Therefore, the thickness should also refer to the thickness of the measurement zone. If bulk materials are compressed, as for VIP core materials, oftentimes the edges get more compression than the middle. As the leg length of the standard calliper only makes it possible to measure at the edge of the panels it is questionable if these results are characteristic for the centre of panel also.

However, in some cases the measurement at the edges using a calliper may be preferable, especially when the panels are curved. In this case it can become difficult to ensure enough contact of the panel with the measurement table as the pressure applied by hand varies from user to user.

An appropriate measurement setup using a table support and an optical measurement system from above and below could solve the described problems (Figure 134). If a pressure force is needed, mechanical driven measurement tips could be used.
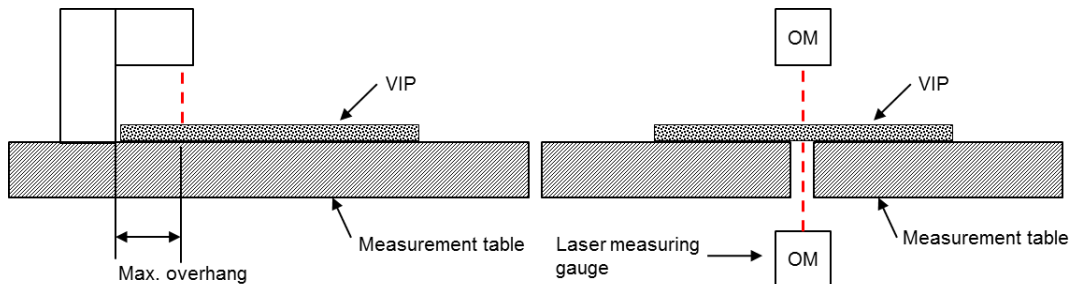
Figure 134:Left: standard equipment for thickness determination with limited possibilities to measure the thickness in the measurement area; right: alternative setup of measurement equipment for thickness determination of VIP allowing a thickness determination on any position.

The advantage of the proposed equipment is that the thickness of the VIP can be measured inside the measuring zone on many points by moving the panels over the measurement zone and calculating the mean thickness. Also, big panels can be measured directly in the middle of the specimen, not being influenced by limitations of the overhang of the gantry portal. The measurement from above and below avoids the imperfect contact problem between the measurement table and the specimen when the specimen has a curved surface.

7.1.4   General recommendations for thermal conductivity measurement

Due to the low thermal conductivity the testing time of SIMs is likely to be higher than for conventional insulation materials. The time frame for settling may be longer, until a steady state thermal condition over the thickness of the panel is reached. It should also be checked carefully if there is any time limitation for the settling time implemented in the test program that could lead to unexpected changes of the test procedure.

A main recommendation of the performed uncertainty analysis is the use of adequate temperature difference, both for GHP and HFM apparatus. In this context a minimum temperature difference of 15K seems recommendable.

If the material is hygroscopic the specimen should be dried to obtain a value of thermal conductivity that is not influenced by differing moisture content. Especially for quality check purposes this is recommendable to achieve constant material dependent values not affected by possible varying temperatures and climate conditions in summer and winter scenarios. The thermal conductivity measurement is influenced besides the moisture content itself, also by the migration of the moisture according to the temperature gradient over the panel thickness. This effect complicates the measurement procedure and enlarges the testing time. The heat carried by the moisture molecules during their diffusion in the panel influences the different thermal transport phenomena as well as latent heat effects and ad- and desorption occur. These phenomena affect the measure of the heat flux and therefore the thermal conductivity measure.

Thus, an extended analysis of the time dependent fade characteristic of the measured heat flux is necessary to isolate the mentioned effects from the general requirements to proof the steady state temperature conditions.

For drying of building materials, a material-adjusted temperature range has to be used. As SIMs are relatively new insulation materials no such recommendation exists in the relevant standards for drying, e.g. EN 12570. If in doubt, the manufacturer should be contacted to avoid a temperature stress on the panel that potentially influences the material structure or provokes ageing effects that are not common for the use during the life time.

After the drying is finished, the material shall be prevented from further moisture uptake during testing.

A temperature related issue during testing is also the possible condensation phenomena, both, on the surface of the panel and inside the material structure. Applying temperatures that are too far below the dew point of the actual water vapour pressure means there is risk of condensation occurring. If this occurs on the surface of the specimen, for example, in small air gaps between the surface and the cooling plate, the thermal resistance in this area is lowered – however, the results should not be influenced too much. More severe effects may occur with condensation inside the material structure. If this happens, the condensed moisture can be absorbed by the material, thus provoking a rise of the moisture content with effects on the thermal conductivity. The condensed humidity may affect the internal partial water vapour pressure inside the structure of VIP – again with effects on the corresponding thermal conductivity.

A very general question is the decision for a one-specimen or two-specimen apparatus. This requires a different discussion for GHP and HFM apparatus. In the case of a two-specimen GHP apparatus, the electrical power from the heating plate is used to keep up the temperature difference for both specimen, but can only be measured as a whole.

Therefore, half of the measured heating power is considered for the calculation of the thermal conductivity of the upper specimen, and half of the heating power for the lower specimen. The thermal conductivity of the upper and lower specimen will always vary in a certain range – even for conventional insulation materials that are not produced batch-wise but are cut from a continuous production line. For some APMs (e.g. aerogel granular or nano-structured rigid foams) the case may be closer to conventional insulation materials, but for VIPs it must be considered that each panel is an individual component whose thickness and internal pressure may vary. Therefore, it may be recommendable to use single-specimen apparatus rather than two-specimen apparatus to get a more precise result. For HFM this is not as important as the heat flux plates measure the heat flux separately for the upper and lower panel. Therefore, two individual results will always obtained.

7.1.5   Determination of linear thermal bridges

The common exercise results about the evaluation of the linear thermal transmittance in case of coupled VIPs, highlight the importance of well-defined measurement boundary conditions to obtain reliable and comparable values of each individual test. There are many influencing factors which can affect the result of a ψ-value measurement (e.g. the panel thickness, the gap width, the core material, the foil material). Even small deviations can lead to inaccuracies. Therefore, the following suggestion should help to carry out measurements of the ψ -value with the guarded hot plate (GHP) or the heat flow meter (HFM) as uniformly as possible increasing the comparability and the significance of the results.

Define the testing criteria.

- Define the aspired goals of the measurements (e.g. aspired definition target and accuracy, considering all the factors that can affect the result).

- Define an appropriate panel size. The pair of samples must adequately cover the existing metering area to ensure a stationary heat flow in the measuring range (the centre of panel - COP areas of the VIPs must be inside of the apparatus metering area). Areas affected by edge effects must not lie within the metering area (Figure 4). The areas which are influenced by edge effects depend on the panel properties and must be determined in advance (using numerical simulations). The length of the joint must cover the existing metering area.

- Define appropriate mean temperatures for the heating- and cooling plates, which could depend on the actual panel applications. It makes sense to define three or more mean temperatures to represent the dependence of the ψ-value on the temperature.

- Consider the shape of the panel edges and the edge design to define the best coupling method. If the design of the edges is not rectangular and, for example, have a slight trapezoidal shape, the orientation of the panels relative to one another can influence the ψ-value (Figure 53). Moreover, the ψ -value depends on the type of edge design: therefore it is important to observe whether the joint assembly has a single or a multilayered edge.

- Define the number and position of external thermocouples (if any). A uniform distribution of the thermocouples must be determined so that the inhomogeneous temperatures can be recorded on the panel surface. As shown in Lorenzati et al., 2016, reliable data can also be obtained by means of a commercial device without the adoption of external thermocouples. This must be verified in advance.

Determining the experimental setup.

- Before measuring the ψ -value, the λ_{COP}-values of the involved VIPs must be determined in a separate measurement. This could be performed through the same apparatus (if the samples are large enough) to avoid lateral heat losses, or through an apparatus with a smaller metering area.

- To obtain comparable measurement results for all measurements of a test series, it is important to draw the positions of the thermocouples (if any) and the marking of the metering area on the test specimens. The marking of the metering area could also simplify the installation of the test specimens in the measuring instrument.

- Pay attention to the exact position of thermocouples, especially in case of air thin joints (thermocouple must be exactly in the middle of the joint).

- For an accurate measurement, and for an easier installation and removal of the sample, it is important to couple the panels well together (Figure 135). For this, an adhesive and tear-resistant tape is advantageous. It must be ensured that the adhesive tape can be removed again after the measurement without damaging the sensitive VIP envelope.
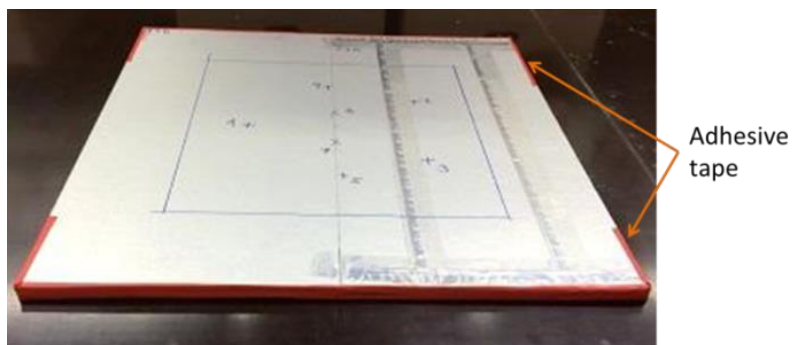

Adhesive tape

Figure 135:Adhesive tape (red) for the fixing of the panels. Source: FIW München.

- The use of spacers (e.g. plastic-spacers) is strongly recommended, in order to measure a defined joint width. The spacers must be installed outside the metering area between the VIPs (Figure 136).
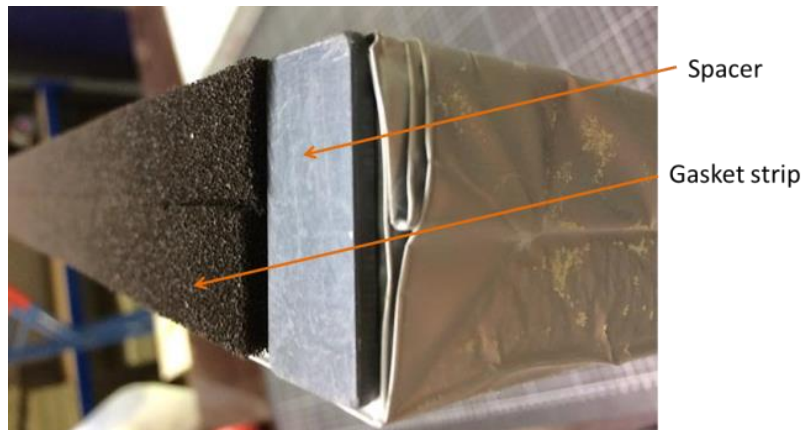

Figure 136: Assembly with a gasket strip as the joint filler material and a plastic-spacer to ensure the correct joint width. Source: FIW München.

A crack width template is suitable for the depiction of the joint widths (Figure 137).
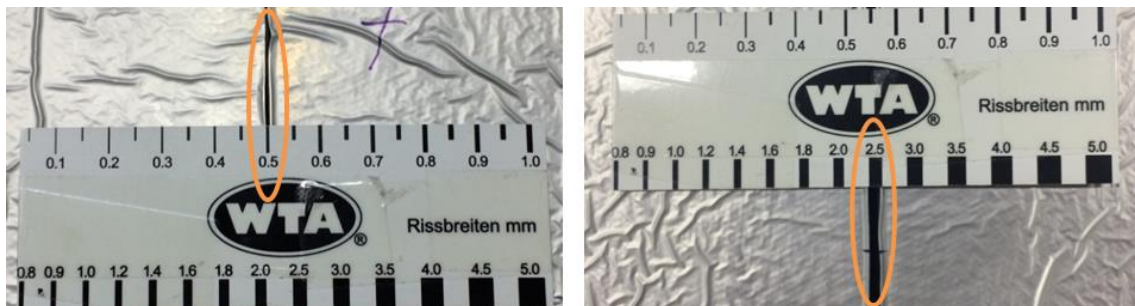

Figure 137:Depiction of the joint width with a crack width template. Source: FIW München.

- If some repeatability and reproducibility tests (or inter-laboratory comparison) were to be performed, it is crucial to define at least one reference sample joint, with well-defined thermal and geometrical characteristics.

- Follow the same suggestions about the λ_{COP} measurements for the installation of the sample (flexible insulating mask around the samples and best possible contact between samples and plates).

As the assessment of thermal bridges is extremely sensitive to numerous factors, for practical reasons it could be most useful (especially for designers) to deal directly with their numerical simulations. The modelling of the air present in the cavity of the envelope flaps and in the joints as well as the modelling of the envelope itself are aspects that require special attention. Lorenzati et al., 2016, demonstrates that numerical models are sufficiently reliable for the analysis of structural joints, especially when the thermal resistance of the joint is higher than 0.100(m^2 K)/W, while their performances may vary significantly when they are applied to an air joints study. Moreover, when the VIPs are

applied to some structures, there are always some extra layers (with extra thermal resistance) which obviously affect the thermal bridging effects: these extra layers can be easily modelled, but not always measured through experimental apparatus. Isaia et al., 2016, proposed a simple empirical model for the estimation of the linear thermal transmittance values, based on the total thermal resistance of the boundary layers and the thermal resistance of joint material, assuming a fixed width of the joint. This model must be extended and generalised, but it could be considered as a guideline for the thermal-bridges assessment procedure.

7.2 Measurement uncertainty

Concerning the investigation on measurement uncertainty the study contains detailed information on sensitivities of the relevant parameters on the obtained combined standard uncertainty of thermal conductivity measurement.

Important parameters for both GHP and HFM are the temperature difference and the thickness determination. For HFM also the calibration factor for the heat flux is of importance.

A comparison of the combined relative uncertainty for GHP and HFM under lab conditions with the values derived applying the maximum uncertainties for the parameters, according to the standards EN 1946-2/-3 show that the impact of the different measurands on the measurement uncertainty can vary.

7.3 Ageing conditions

The agreed ageing conditions were 50°C / 70% RH for VIPs and 80°C / 60% RH for the APMs. The VIPs were mostly stored in the agreed climate of 50/70, however the APM were stored partly in 50/70 and partly in 80/60. The differences in the effect of the differing climates on the thermal conductivity of the APM were statistically not significant. In general, APM was not affected by the applied climate conditions. Thus, no conclusion if one climate or the other is more severe can be derived.

For the aged VIPs, the applied climate of 50°C and 70% RH reflects the current state of work in the draft product standard for VIPs. Depending on the individual material distinct differences in the impact of the ageing on the thermal properties were recognized. For the silica core based materials under the applied ageing conditions a yearly increase rate of around 0.8-3.9mW/(m K a) was calculated from the lab data, dependent on the material with huge differences according to the applied mean temperature during measurement of thermal conductivity (10°C and 23°C). For VIP 1 the increase rate at 23°C mean temperature was higher, for the VIP 3, 4 and 6 the increase rate was lower at a mean temperature of 23°C. It is not clear from the data if the observed effect of lower increase rates at higher mean test temperature for characterisation is significant.

However, a possible explanation could be based on the already described effect of condensation phenomena at lower temperatures. If a temperature difference of 15K is applied, in the case of 10°C mean temperature the cold plate has a temperature of 2.5°C, while a cold plate temperature of 15.5°C is reached for the case of a mean temperature of 23°C.

Even if this explanation cannot be proven with the available data, the described differences in the cold side temperature could lead to condensation inside the panel and on the surface of the material, thus influencing the obtained results in the observed direction.

To come to conclusions about adequate reference conditions for ageing of the panels two things must be considered. Firstly, an adequate ageing procedure that reflects the impacts of natural ageing (when the material is applied to a certain construction during use) must be defined. In the case of building constructions, mainly temperature and relative humidity will stress the material. Secondly, the impact during artificial ageing should not exceed physical limitations that would lead to an unintended change of structure or could damage the material. For VIP, the temperature is mainly significant in this manner. By defining 50°C as the ageing temperature an adequate acceleration of the permeation rates is achieved, without being in the range of the softening temperature of the thermoplastic welding.

The accelerated impact on the relevant properties obtained with artificial ageing then must be referred to reference conditions that are representative for a certain application. The reference conditions under real climatic exposure are highly dependent on the location and orientation of the building element and the specific construction.

By comparison of different constructions at the same location it becomes obvious that the relative humidity acts on the boundary layer between the VIP and the adjacent air, respectively building material is more affected from the construction than the effective temperature. The specific input of moisture due to heavy rain is important in this instance.

In Figure 138 the effective climate combinations according to the constructions and locations observed in Chapter 5.2 are shown (typical for Germany in example constructions using VIP as thermal insulation). The blue and green line represent equivalent climate conditions to 23°C and 50% RH (blue line) and 23°C and 80% RH (green line) that will cause the same effect on the increase of total internal pressure of VIP.
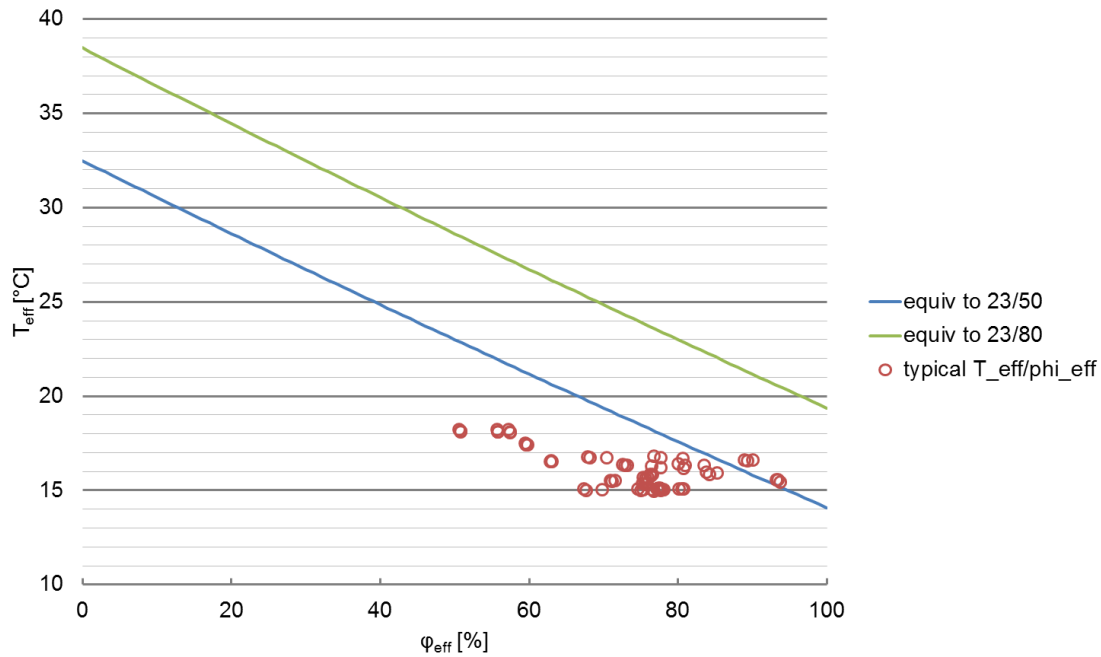
Figure 138 Effective climate as combinations of temperature in °C and relative humidity in % as derived from the calculations according to Chapter 5.2 (representative for Germany in example constructions using VIP)

It is visible that the observed effective climates are in most cases below the line of equivalent climate combinations to 23°C and 50% RH. All the typical constructions using VIP investigated are below the reference climate of 23°C and 80% RH, so that will mean that the observed increase rates of internal pressure will be also lower if this reference climate is chosen.

For this reason, a reference climate in between 23°C and 50-80% RH seems favourable. However, an additional important ageing effect on the increase of thermal conductivity is the moisture increase of the core materials so further comparison is necessary. For this reason in Figure 139 the time dependent increase of thermal conductivity is calculated for the cases shown in Figure 138.

A significant effort is necessary to develop a precise (degressive) model for increase of thermal conductivity that considers detailed dependence of thermal conductivity from internal pressure increase of dry air gases and water vapour and moisture uptake in the core material. Thus, a linearisation of the increase rates of thermal conductivity derived from the first year of storage are favourable for practical reasons.
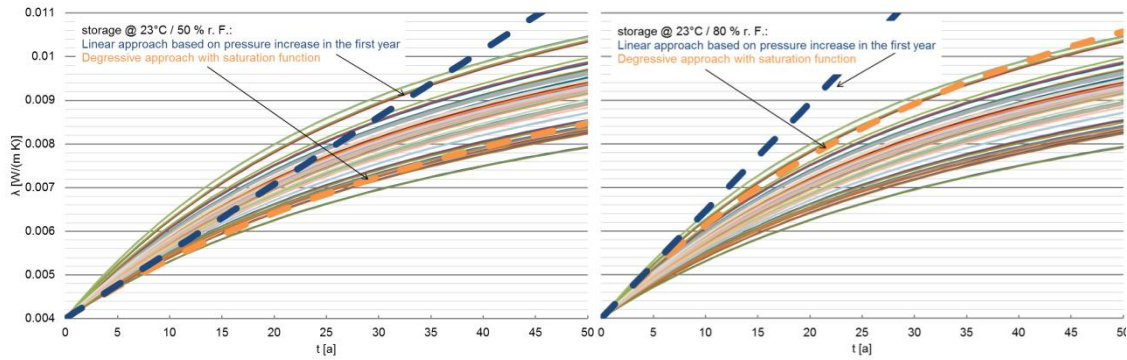
Figure 139 Comparison of evolution of values of thermal conductivity based on a simplified linear (blue dotted line) and degressive approach (orange dotted line) in comparison with the increase of the observed reference cases in Germany (array of curves). Left: reference climate 23°C/50% RH; right: reference climate 23°C/80% RH

A comparison of these two possibilities is shown in Figure 139. On the left hand-side, the case for a reference climate at 23°C and 50% RH is shown, while the case for a reference climate of 23°C and 80% RH is drawn on the right hand side. The values are compared with the range of observed increase curves associated to the constructions and locations in Germany.

It becomes obvious that the linear model in the case of 23°C/50% RH underestimates the development of the values during the first 25 years. Also, the mean thermal conductivity in the first 25 years underestimates the simulated value in many cases. The linear approach based on the reference climate of 23°C/80% RH on the other hand overestimates the thermal conductivity of the simulated values. The degressive approach considering 23°C/80% RH seems to be the most realistic case up to now.

References

Affinito, J., Hilliard, D. (2004). A New Class of Ultra-Barrier Materials. In: 47th Annual Technical Conference Proceedings, Society of Vacuum Coaters, 563-593.

ASTM. (2012). C687 - 12. Standard Practice for Determination of Thermal Resistance of Loose-Fill Building Insulation.

ASTM. (2013). C1045-07(2013). Standard Practice for Calculating Thermal Transmission Properties Under Steady-State Conditions.

ASTM. (2013). C177-13. Standard Test Method for Steady-State Heat Flux measurements and Thermal Transmission Properties by Means of the Guarded-Hot-Plate Apparatus.

ASTM. (2013). C1045-07(2013). Standard Practice for Calculating Thermal Transmission Properties Under Steady-State Conditions.

ASTM. (2015). C518-15. Standard Test Method for Steady-State Thermal Transmission Properties by Means of the Heat Flow Meter Apparatus.

ASTM. (2015). C1667-15. Standard Test Method for Using Heat Flow Meter Apparatus to Measure the Center-of-Panel Thermal Resistivity of Vacuum Panels.

Batard, A., Planes, E., Duforestel, T., Flandin, L., Yrieux, B. (2017): Water vapour permeation through high barrier materials: numerical simulation and comparison to experiments. Publication project for Journal of Materials Science.

Brunner, S., Gasser, P., Simmler, H., Ghazi Wakili, K. (2006): Investigation of multilayered aluminium-coated polymer laminates by focused ion beam (FIB) etching, Surface & Coatings Technology, 200, 5908-5914.

Crank, J. (1975): The Mathematics of Diffusion, London, Oxford University Press

DIN. (2009-10). 16269-6:2009-10. Statistische Auswertung von Daten - Teil 6: Ermittlung von statistischen Anteilsbereichen (ISO 16269-6:2005).

DIN EN ISO. (2005). 15106-3:2005. Kunststoffe - Folien und Flächengebilde - Bestimmung der Wasserdampfdurchlässigkeit - Teil 3: Elektrolytnachweis-Sensorverfahren

EN. (1999). 1946-2:1999. Thermal performance of building products and components. Specific criteria for the assessment of laboratories measuring heat transfer properties. Measurements by guarded hot plate method.

EN. (1999). 1946-3:1999. Thermal performance of building products and components. Specific criteria for the assessment of laboratories measuring heat transfer properties. Measurements by heat flow meter method.

EN. (2001). 12664:2001. Thermal performance of building materials and products - Determination of thermal resistance by means of guarded hot plate and heat flow meter methods - Dry and moist products of medium and low thermal resistance.

EN. (2001). 12667:2001. Thermal performance of building materials and products. Determination of thermal resistance by means of guarded hot plate and heat flow meter methods. Products of high and medium thermal resistance.

EN. (2007). 15026:2007. Hygrothermal performance of building components and building elements. Assessment of moisture transfer by numerical simulation.

Garnier, G., Yrieix, B., Brechet, Y., Flandin, L. (2010). Influence of structural feature of aluminum coatings on mechanical and water barrier properties of metallized pet films, Journal of Applied Polymer Science 115 (5) 3110-3119. doi:10.1002/app.31372.

Graff, G. L., Williford, R. E., Burrows, P. E. (2004): Mechanisms of vapor permeation through multilayer barrier films: Lag time versus equilibrium permeation, Journal of Applied Physics 96 (4), 1840-1849.

Hanika, M. (2004). Zur permeation durch aluminiumbedampfte polypropylen- und polyethylenterephtalatfolien, Ph.D. thesis.

He, W., Lv, W., Dickerson, J. H.. (2014). Gas Dffusion Mechanisms and Models, Springer International Publishing, Cham. doi:10.1007/978-3-319-09737-4_2.

Hopfenberg, H. B., Stannett, V. (1973): The Diffusion and Sorption of Gases and Vapours in Glassy Polymers, Springer Netherlands, Dordrecht.

ISO. (1991). 8301:1991. Thermal insulation -- Determination of steady-state thermal resistance and related properties -- Heat flow meter apparatus.

ISO. (1991). 8302:1991. Thermal insulation -- Determination of steady-state thermal resistance and related properties -- Guarded hot plate apparatus.

ISO. (2007). 10211:2007. Thermal bridges in building construction -- Heat flows and surface temperatures -- Detailed calculations.

ISO. (2015). 22007-2:2015. Plastics -- Determination of thermal conductivity and thermal diffusivity -- Part 2: Transient plane heat source (hot disc) method.

Isaia, F., Fantucci, S., Capozzoli, A., & Perino, M. (2016). Thermal bridges in vacuum insulation panels at building scale. Engineering Sustainability, 170, 47-60. http://dx.doi.org/10.1680/jensu.15.00057

Kiese, S., Kücükpinar, E., Reinelt, M., Miesbauer, O., Ewender, J., Langowski, H.-C. (2017): A systematic approach for the accurate and rapid measurement of water vapor transmission through ultra-high barrier films, Review of Scientific Instruments 88, 025108-1-025108-7.

Klopffer, M. H., Flaconneche, B. (2001). Transport properdines of gases in polymers: Bibliographic review, Oil & Gas Science and Technology 56 (3) 223-244. Doi :10.2516/ogst:2001021.

Kraus, D., Büttner, D., Heinemann, U., Fricke, J. (2005): Non-destructive Method to Determine the Water Vapour Pressure in Vacuum Insulation Panels (VIP), Bavarian Centre for Applied Energy Research (ZAE Bayern) 2005

Langowski, H.-C. (2008): Permeation of Gases and Condensable Substances Through Monolayer and Multilayer Structures. In: Piringer, O. G. (Ed.), Baner, A. L. (Ed.): Plastic Packaging - Interactions with Food and Pharmaceuticals, Second edition, Weinheim, Wiley-VCH, 2008, 297-347

Lorenzati, A., Fantucci, S., Capozzoli, A., & Perino, M. (2015). VIPs Thermal Conductivity Measurement: Test Methods, Limits and Uncertainty. Energy Procedia, 78, 418-423. https://doi.org/10.1016/j.egypro.2015.11.686

Lorenzati, A., Fantucci, S., Capozzoli, A., & Perino, M. (2016). Experimental and numerical investigation of thermal bridging effects of jointed Vacuum Insulation Panels. Energy and Buildings, 111, 164-175.
https://doi.org/10.1016/j.enbuild.2015.11.026.

Miesbauer, O. (2017): Analytische und numerische Berechnungen zur Barrierewirkung von Mehrschichtstrukturen, Dissertation, submitted to the Technische Universität München.

Mocon. (2014). Aquatran_ Model 1 Operator's Manual – Revision D, http://www.mocon.com/distributor/pdfmanuals/Aquatran%20-%20d.pdf.

NanoInsulate. (2013). Development of Nanotechnology-based High-performance Opaque & Transparent Insulation Systems for Energy-efficient Buildings, funded by the European Union Seventh Framework Programme (FP7/2007 – 2013) under grant agreement no. NMP4-SL-2010-260086. Retrieved from http://cordis.europa.eu/result/rcn/172099_en.html

Pons, E., Yrieix, B., Heymans, L., Dubelley, F., & Planes, E. (2014). Permeation of water vapor through high performance laminates for VIPs and physical characterization of sorption and diffusion phenomena. *Energy and Buildings, 85*, 604-616. doi:http://dx.doi.org/10.1016/j.enbuild.2014.08.032

Regauer, S.(2017):Validierung des Folienabhebeverfahrens zur Innendruckmessung von Vakuumisolationspaneelen. Bestimmung des Innendrucks von Vakuumisolationspaneelen (VIP) mit Kieselsäurekern mittels direktem und indirektem Messverfahren. Technische Universität München, Master-Thesis

Rogers, C. E. (1985): Permeation of Gases and Vapours in Polymers. In: Comyn, J. (Ed.): Polymer Permeability, London, Chapman & Hall, 11-73.

Reichenauer, G., Heinemann, U., & Ebert, H. P. (2007). Relationship between pore size and the gas pressure dependence of the gaseous thermal conductivity. *Colloids and Surfaces a-Physicochemical and Engineering Aspects, 300*(1-2), 204-210. doi:10.1016/j.colsurfa.2007.01.020

Sachs, L. (1984): Angewandte Statistik. Anwendung statistischer Methoden. 6. Auflage, Springer Verlag

Schwaab, H. (2004): Vakuumisolationspaneele - Gas- und Feuchteeintrag sowie Feuchte- und Wärmetransport. Dissertation, Julius-Maximilian-Universität, Würzburg

Shufer, E. (2017). Hanita Methodology for Testing VIPs. Retrieved from http://www.hanitacoatings.com/energy/images/energy/files/tech/Hanita_Testing_Methodology_for_VIPs_Ed_C.pdf

Simmler, H., & Brunner, S. (2005). Vacuum insulation panels for building application. Basic properties, aging mechanisms and service live, Energy and Buildings 37 (2005) 1122-1131. doi:10.1016/j.enbuild.2005.06.015

Sprengard, C. (2016): Determination of linear thermal transmittance of vacuum insulation panels by measurement in a guarded hot-plate apparatus or a heat-flow meter apparatus. Buildings XIII Conference of the Oakridge National Laboratory in Clearwater, Florida, December 5th 2016

Sprengard, C., & Holm, A. H. (2014). Numerical examination of thermal bridging effects at the edges of vacuum-insulation-panels (VIP) in various constructions. Energy and Buildings, 85, 638-643. doi:http://dx.doi.org/10.1016/j.enbuild.2014.03.027

Sprengard, C.; Treml, S.; Engelhardt, M.; Simon, H.; Kagerer, F. (2016): Vakuum-Isolations-Paneele (VIP) in der Bauanwendung: vom Dämmstoff zum Dämmsystem. Verarbeitung, Befestigung, Dauerhaftigkeit. Abschlussbericht FO-2012/08, IRB Verlag

Stannett, V. (1968). Simple gases, in diffusion in polymers, Crank, J.and Park. 41-73.

Yrieix, B., Morel, B., & Pons, E. (2014). VIP service life assessment: Interactions between barrier laminates and core material, and significance of silica core ageing. Energy and Buildings, 85, 617-630. doi:10.1016/j.enbuild.2014.07.035

www.iea-ebc.org